Cellular Mechanisms and Function of Hippocampal Gamma Oscillations



Pantelis Antonoudiou

New College

University of Oxford

A thesis submitted for the degree of

Doctor of Philosophy

HILARY 2018

Abstract

Gamma oscillations (30 - 120 Hz) are a common feature of active cortical networks and changes in these rhythms can act as a useful marker of circuit dysfunction in psychiatric disorders and neurological disease. While their function remains debated, there has been converging evidence regarding their mechanism of generation. These rhythms depend upon the spiking of inhibitory interneurons, which synchronise the firing of excitatory pyramidal cells via fast synaptic inhibition. Specifically, parvalbumin-expressing interneurons, which target the perisomatic domain of pyramidal neurons, are thought to play the key role in generating and maintaining gamma oscillations in the brain. However, it was recently demonstrated that somatostatin-expressing interneurons, which target the dendritic domains of pyramidal neurons, are responsible for the generation of low-frequency gamma oscillations in the primary visual cortex of awake mice. It is not yet known if the involvement of somatostatin-expressing interneurons in gamma rhythmogenesis is specific to visually-induced oscillations in V1, or if it is general phenomenon that occurs across brain areas. Here, we took advantage of optogenetic techniques to test the involvement of parvalbumin- and somatostatin-expressing interneurons in a well studied model of carbachol-induced gamma oscillations in the hippocampal CA3 *in vitro*. For both classes of interneurons, we found that rhythmic photo-activation was sufficient to entrain ongoing gamma oscillations, and that the predominant effect of sustained photo-activation was to decrease the power and increase the frequency of gamma oscillations. Importantly, there was a functional distinction between the interneuronal classes. While photo-inhibition of parvalbumin-expressing interneurons decreased the oscillation power,

photo-inhibition of somatostatin-expressing interneurons both decreased the oscillation power and increased its frequency. These experiments suggest that the activity of both interneuron classes are important for carbachol-induced oscillations in hippocampal area CA3. They also indicate that somatostatin-expressing interneurons may have a more intimate role in the control of gamma oscillation frequency. Interestingly, sustained photo-activation of somatostatin-expressing interneurons was sufficient to induce *de novo* high-frequency gamma oscillations. Our experiments reveal that the *de novo* gamma oscillations may have different properties than cch-induced oscillations, but may also depend on synaptic excitation.

Our data suggest that several different interneuronal subtypes may be necessary to generate and/or maintain oscillations across the gamma range, but are also consistent with the idea that rhythmic perisomatic inhibition is a critical feature of low-frequency gamma oscillations in the hippocampus. In order to further understand the function of rhythmic perisomatic inhibition, we used dynamic clamp to inject inhibitory conductance trains into pyramidal neurons, and examined the effects of disturbing rhythmicity and/or synchrony on pyramidal cell spiking. Previous evidence using this approach has highlighted a role for gamma frequency synchronisation of excitatory inputs in multiplicative gain enhancement of principal cell output. Here, we show that rhythmic inhibition can also induce multiplicative increases in the gain of principal cell output. Moreover, we found that reductions in either rhythmicity or synchrony of the input trains impaired that multiplicative gain enhancement in principal cells. These experiments suggest that inputs at gamma frequency are ideally suited for multiplicatively enhancing gain, and highlight an important implication for gamma oscillations at the single cell level.

Statement of Originality

I declare that the work in this thesis is entirely my own and where others have contributed is clearly acknowledged. This work has not been submitted for any qualification or degree at this or any other institutions.

Acknowledgements

The completion of this thesis is the culmination of my efforts during the last four years in Oxford and it signifies the end of an important period in my life. These past few years have been challenging and frustrating but also fun and rewarding due to the encouragement from my mentors, colleagues, friends and family.

Foremost, I would like to express my utmost gratitude to my supervisor Dr. Ed Mann for his support throughout these last four years. This project would have not been possible without his help and guidance. Thank you for welcoming me to the lab and making me a better scientist. I would also like thank Dr. Louise Upton for teaching me how to perform viral injections and for her helpful advice.

Special thanks to my first student Yulin Tan who performed the initial photoinhibition experiments. Many thanks to Georgina Kontou who performed the biocytin labelling and confocal imaging. I am also grateful to Dr. Alexandru Calin for kindly providing the SST-cre and PV-cre mouse colonies.

Furthermore, I would like to extend my thanks to all Mann lab members Julian, Antonia, Martin, Matthew, Sofia, Michael and Sonia for their help and for making my time in the lab and Oxford enjoyable. I would like to give special thanks to Dr. Antonia Langfelder for demonstrating the use of perforate patch and other helpful advice. I would especially like to thank Martin Kahn, Yves Weissenberger and Lev Tankelevitch because we have embarked on this trip together and helped each other along the way. I would also like to thank Martin and Yves for some unforgettable gaming nights with dominos pizza! Many thanks to Michele, Josep, Jacobo, Federico, Elias and all my other friends in UK and Cyprus for their support.

Moreover, I would like to thank the DPAG administrative team, DPAG workshop and BSB staff for their for their help and support. I would also like to thank the

MRC for funding this project.

Finally, I would like to give special thanks to my sister Christiana, my parents Stella and Michael, and my “giagia” Stavroulla who have always supported me throughout my studies and life. I would especially like to thank my parents who have always put our education above everything else. It is because of your support and encouragement that I am here today. I will always be grateful.

Above all, I would like to thank my girlfriend and fellow scientist Georgina. Your constant support and strong motivation have always been a driving force that helped me overcome even the most difficult challenges. Your help, patience, and faith in me have been the cornerstone of my DPhil studies and the production of this thesis. Thank you for always being there for me.

ども ありがとう ございました.

Contents

1 Introduction **1**

1.1 WHAT ARE BRAIN OSCILLATIONS? 1

1.2 RHYTHMIC OSCILLATIONS IN THE GAMMA BAND RANGE . . 3

1.3 GAMMA OSCILLATIONS AND COGNITION 5

1.3.1 GAMMA SYNCHRONISATION IN VISUAL ATTENTION . 5

1.3.2 GAMMA SYNCHRONISATION IN MEMORY 7

1.4 DOES THE GAMMA RHYTHM CONTRIBUTE TO INFORMATION TRANSMISSION IN THE BRAIN? 9

1.4.1 GAMMA OSCILLATIONS AND LOCAL NETWORK SIGNALLING 10

1.4.2 GAMMA OSCILLATIONS AND LONG-RANGE SYNCHRONISATION 12

1.5 MECHANISMS OF GAMMA OSCILLATION GENERATION 14

1.5.1 EXCITATION, INHIBITION AND GAMMA RHYTHMOGENESIS 16

1.5.2 GAMMA OSCILLATIONS *IN VIVO* 18

1.5.3 INHIBITORY INTERNEURONS AND GAMMA OSCILLATIONS 20

1.5.3.1 PERISOMATIC - TARGETING INTERNEURONS 22

1.5.3.2 DENDRITE - TARGETING INTERNEURONS . . . 24

1.6 GAMMA OSCILLATIONS IN DISEASE 28

1.7 COMBINING MECHANISM AND FUNCTION: A WINDOW IN BRAIN COMPUTATIONS 31
1.8 THESIS OBJECTIVES 34

2 Materials and Methods **35**
2.1 ANIMALS 35
2.2 VIRAL INJECTIONS PROCEDURES 35
2.3 *EX VIVO* BRAIN SLICE PREPARATION 36
2.3.1 CONSTRUCT EXPRESSION 37
2.4 ELECTROPHYSIOLOGY 38
2.4.1 EXTRACELLULAR RECORDINGS 38
2.4.2 LOCAL FIELD POTENTIAL RECORDINGS 38
2.4.3 MULTI - ELECTRODE RECORDINGS 39
2.4.4 LIGHT DELIVERY 39
2.5 INTRACELLULAR RECORDINGS 41
2.6 DYNAMIC CLAMP 42
2.7 IMAGING 44
2.7.1 BIOCYTIN LABELLING 44
2.7.2 FLUORESCENCE IMAGING 44
2.7.3 CONFOCAL IMAGING 44
2.8 DATA ANALYSIS 45
2.8.1 GAMMA OSCILLATION ANALYSIS 45
2.8.2 UNIT DETECTION AND CLUSTERING 46
2.9 STATISTICS 47

3 The Role of Parvalbumin - Expressing Interneurons in Hippocampal Gamma Oscillations **48**
3.1 INTRODUCTION 48
3.2 INDUCING GAMMA OSCILLATIONS IN THE CA3 HIPPOCAMPAL SUBFIELD 50

3.3 VIRAL EXPRESSION OF OPTOGENETIC CONSTRUCTS 52
3.4 RHYTHMIC PHOTO-STIMULATION OF PV+ INTERNEURONS DURING GAMMA OSCILLATIONS 57
3.5 SUSTAINED PHOTO-ACTIVATION OF PV+ INTERNEURONS . 59
3.6 THETA PHOTO-ACTIVATION OF PV+ INTERNEURONS DURING GAMMA OSCILLATIONS 65
3.7 MULTI-ELECTRODE ARRAY RECORDINGS DURING PV+ INTERNEURON PHOTO-ACTIVATION 67
3.8 PHOTO-INHIBITION OF PV+ INTERNEURONS DURING GAMMA OSCILLATIONS 71
3.9 PHOTO-INHIBITION OF PV+ INTERNEURONS WITH LASER ILLUMINATION 75
3.10 SUPPLEMENTARY INFORMATION 79
3.11 DISCUSSION 81
3.11.1 MECHANISMS GOVERNING HIPPOCAMPAL NETWORK MODULATION DURING PV+ INTERNEURON PHOTO-ACTIVATION 82
3.11.1.1 CELLULAR DISINHIBITION THROUGH DEPOLARISATION BLOCK 82
3.11.1.2 DIRECT PV+ INTERNEURON EXCITATION DURING PHOTO-STIMULATION 83
3.11.2 MECHANISMS GOVERNING HIPPOCAMPAL NETWORK MODULATION DURING PV+ INTERNEURON PHOTO-INHIBITION 84

4 The Role of Somatostatin - Expressing Interneurons in Hippocampal Gamma Oscillations 87

4.1 INTRODUCTION 87
4.2 RHYTHMIC PHOTO-STIMULATION OF SST+ INTERNEURONS 89

4.3 SUSTAINED PHOTO-EXCITATION OF SST+ INTERNEURONS DURING GAMMA OSCILLATIONS 94
4.4 SST+ INTERNEURON PHOTO-ACTIVATION CAN GENERATE *DE NOVO* GAMMA OSCILLATIONS 99
4.5 MECHANISMS OF GENERATION OF SST-INDUCED *DE NOVO* GAMMA OSCILLATIONS 103
4.5.1 *DE NOVO* OSCILLATIONS DEPEND ON SYNAPTIC EXCITATION AND INHIBITION 103
4.5.2 SINGLE CELL ACTIVITY DURING SST+ INTERNEURON PHOTO-ACTIVATION 105
4.6 MULTI-ELECTRODE ARRAY RECORDINGS DURING *DE NOVO* OSCILLATIONS 112
4.7 PHOTO-INHIBITION OF SST+ INTERNEURONS DURING GAMMA ACTIVITY 114
4.8 SUPPLEMENTARY INFORMATION 121
4.9 DISCUSSION 123
4.9.1 MECHANISMS GOVERNING HIPPOCAMPAL NETWORK MODULATION DURING SST+ INTERNEURON PHOTO-ACTIVATION 123
4.9.2 MECHANISMS OF *DE NOVO* OSCILLATION GENERATION 125
4.9.2.1 GENERATION OF NETWORK EXCITATION DURING SST+ INTERNEURON PHOTO-ACTIVATION 125
4.9.2.2 SYNAPTIC INHIBITION AS THE MAIN INGREDIENT 127
4.9.3 SST+ INTERNEURONS ARE NECESSARY FOR HIPPOCAMPAL GAMMA OSCILLATIONS 128

4.9.3.1 MECHANISMS GOVERNING HIPPOCAMPAL NETWORK MODULATION DURING SST+ INTERNEURON PHOTO-INHIBITION 129

5 Effect Of Gamma Rhythm and Synchrony On Cell Input-Output Properties 131

5.1 INTRODUCTION 131

5.2 INPUT RESISTANCE AND STABILITY 134

5.3 EXPERIMENTAL PROTOCOL AND INPUT GENERATION . . . 134

5.4 EFFECTS OF EXCITATORY GAMMA RHYTHM ON PRINCIPAL CELL GAIN IN S1 139

5.5 EFFECTS OF EXCITATORY GAMMA RHYTHM ON PRINCIPAL CELL GAIN IN CA1 142

5.6 EFFECTS OF INHIBITORY GAMMA RHYTHM ON PRINCIPAL CELL GAIN 145

5.7 EFFECTS OF SYNCHRONY ON PRINCIPAL CELL GAIN 148

5.8 GAMMA POWER, VARIABILITY AND GAIN 150

5.9 GAMMA OSCILLATIONS, VARIABILITY AND SPIKE FIDELITY 153

5.10 SUPPLEMENTARY INFORMATION 158

5.11 DISCUSSION 161

5.11.1 GAMMA OSCILLATIONS PRODUCE MULTIPLICATIVE INCREASES IN PRINCIPAL CELL GAIN 162

5.11.2 RHYTHMIC EXCITATION VS. RHYTHMIC INHIBITION 163

5.11.3 VARIABILITY IN GAIN ENHANCEMENT OF INHIBITORY GAMMA TRAINS 164

5.11.4 GAMMA POWER, VARIABILITY AND SPIKE FIDELITY 164

6 General Discussion 166

6.1 INVESTIGATING GAMMA OSCILLATIONS IN ACUTE SLICES . 169

6.2 CELL SPECIFICITY AND TARGETING EFFICIENCY 170

6.3 RHYTHMIC INHIBITORY GAMMA OSCILLATION INPUTS IN PYRAMIDAL CELLS 172
6.4 MECHANISMS OF GAMMA OSCILLATION GENERATION IN HIPPOCAMPAL AREA CA3 172
6.5 GAMMA OSCILLATIONS INDUCE MULTIPLICATIVE GAIN ENHANCEMENT IN PRINCIPAL CELLS 177

Bibliography **179**

List of Figures

2.1 LFP recordings and light delivery in the interface chamber 40

3.1 Carbachol induced γ oscillations in the interface chamber 51
3.2 Expression of ChR2 in PV-cre mice 53
3.3 ChR2 is expressed in fast-spiking perisomatic interneurons 54
3.4 Pyramidal cell inhibition by PV+IN photo-activation 56
3.5 Rhythmic photo-stimulation of PV+INs entrains ongoing γ oscillations 58
3.6 Sustained photo-activation of PV+INs decreases the power and increases the frequency of γ oscillations 60
3.7 Peak power is directly proportional to power area 61
3.8 γ power decrease and peak frequency increase are proportional to light intensity 62
3.9 Strong photo-activation of PV+IN abolishes γ oscillations 64
3.10 Strong photo-activation of PV+IN during spontaneous activity does not increase the local field potential 64
3.11 Theta photo-activation of PV+INs modulates γ oscillation amplitude 66
3.12 PV+IN photo-activation decreases unit activity during cch γ oscillations 69
3.13 Example of a PV+IN photo-activated unit 70
3.14 Functional expression of Arch in PV+INs 71
3.15 Sustained LED photo-inhibition of PV+INs produces inconsistent responses in γ oscillation power and frequency 73
3.16 Sustained LED photo-inhibition of PV+INs elicits changes in power that are negatively correlated to differences in peak frequency 74

3.17 Sustained photo-inhibition of PV+INs using laser illumination suppresses γ power. 77
3.18 Light intensity correlates negatively with γ oscillation power 78
3.19 Laser illumination in PV+INs expressing tdTomato is not sufficient to alter γpower 80

4.1 Expression of ChR2-mCherry in SST+INs 90
4.2 Rhythmic excitation of SST+INs entrains ongoing γ oscillations . . . 92
4.3 Possible non-specific effects of transient SST+IN activation 93
4.4 Sustained photo-activation of SST+INs decreases the power and increases the frequency of γ oscillations 95
4.5 γ power decrease and peak frequency increase are correlated to light intensity 96
4.6 SST+IN strong photo-activation elicits variable responses 98
4.7 Photo-activation of SST+INs induces *de novo* γ oscillations 101
4.8 Effects of light power on γ oscillations induced by theta photo-activation of SST+INs 102
4.9 *De novo* high-frequency oscillations require fast synaptic excitation and inhibition 104
4.10 Current clamp recording of an SST+IN 106
4.11 Cellular responses of non-opsin expressing cells to SST+IN photo-activation 108
4.12 Inhibition prevails during SST+IN activation 110
4.13 Dendritic GABAergic transmission is inhibitory 111
4.14 SST+IN photo-activation increases unit activity 113
4.15 Functional expression of Arch in SST+INs 116
4.16 Sustained LED photo-inhibition of SST+INs consistently decreases the power and increases the frequency of cch-induced γ oscillations . 117

4.17 Sustained photo-inhibition of SST+INs using laser illumination suppresses γ power and increases frequency 119
4.18 Light intensity correlates negatively with γ oscillation power but not frequency 120
4.19 Sustained photo-inhibition of SST+INs is not sufficient to induce γ oscillations 122

5.1 Input resistance and cell stability 135
5.2 Generation of γ oscillation inputs 137
5.3 Experimental Protocol. 138
5.4 Rhythmic and arrhythmic 40 Hz excitation lead to multiplicative enhancement of gain in cortical area S1 141
5.5 Reducing rhythmicity at 40 Hz decreases gain divisively in hippocampal area CA1 144
5.6 Dynamic Clamp Configuration 145
5.7 Impaired inhibitory rhythmicity produces divisive decreases and additive increases in gain 147
5.8 Impaired synchrony produces divisive and subtractive decreases in gain 149
5.9 Increasing γ oscillation power, while conserving variability, produces multiplicative increases in gain 152
5.10 Arrhythmic excitatory input at 40 Hz increases spike fidelity in S1 . . 156
5.11 Spike time fidelity does not correlate with γ power 157
5.12 Slope correlation with input parameters 159

6.1 Role of PV+ and SST+ interneurons in hippocampal γ oscillations . 168

List Of Abbreviations

AAV, adeno-associated virus

aCSF, artificial cerebrospinal fluid

Arch, archaerhodopsin

CA1, Cornu Ammonis 1

CA3, Cornu Ammonis 1

cch, carbachol

ChR2, channel rhodopsin

CV, coefficient of variation

DMSO, Dimethyl sulfoxide

DG, dentate gyrus

EPSC, excitatory post-synaptic current

f-i, firing rate versus input

FFT, fast Fourier Transform

FS, fast spiking

IC, current clamp

IN, interneuron

IPSC, inhibitory post-synaptic current

IPSG, inhibitory post-synaptic conductance

ISI, inter synchronous interval

ITR, inverted terminal repeats

LFP, local field potential

MCI, mean correlation index

MEA, multi electrode array

P2T, peak to trough

pA, polyadenylation signal

PV+, parvalbumin

Pyr, pydamidale

Rad, radiadum

Ri, input resistance

rmANOVA, repeated measures analysis of variance

RMSD, root mean square devation

RS, regular spiking

S1, primary somatosensory cortex

SEM, standard error of the mean

sr., stratum

SST+, somatostatin

V1, primary visual cortex

V4, extrastriate visual area 4

VC, voltage clamp

Vm, membrane potential

WPRE, woodchuck hepatitis virus post-transcriptional regulatory element

Chapter 1

Introduction

1.1 WHAT ARE BRAIN OSCILLATIONS?

Brain oscillations are rhythmic patterns of neuronal activity. On a temporal scale they can range from slow changes in excitability across the sleep - wake cycle to the millisecond synchronisation of spike timing (Buzsáki et al. 2004; Cardin et al. 2009; Gentet et al. 2012; Harris et al. 2003; Sohal et al. 2009; Steriade et al. 1993; Vyazovskiy et al. 2013). On a spatial scale they can take place from the single cell level to large and extended brain networks (Buzsáki et al. 2004; Steriade et al. 1993; Vyazovskiy et al. 2013). Brain oscillations that take place on a timescale relevant for neuronal communication were first characterised in humans by Hans Berger using electroencephalography (EEG) based on Richard Caton's earlier discoveries (Ahmed et al. 2013; Berger 1929; Caton 1875). These oscillations, termed as the "alpha" rhythm, appeared as electrical waves (with a frequency around 10 Hz) in the EEG when human subjects closed their eyes (Ahmed et al. 2013; Berger 1929). Alpha rhythmic oscillations were subsequently confirmed in the local field potential (LFP) of animal brains by Lord Adrian and Matthews (Adrian et al. 1934). The EEG and/or LFP remain until this day the standard approach to analysing oscillatory activity in neuronal networks (Buzsáki et al. 2004, 2012; Uhlhaas et al. 2006). Using these techniques, oscillations of different frequency bands have been discovered and were accordingly labelled after letters of the Greek alphabet. Specifically, oscillations have a frequency range of delta (δ) 0.5 - 4 Hz, theta (θ) 4 - 8 Hz, alpha (α) 8 -12 Hz,

beta (β) 12 - 30 Hz and gamma (γ) > 30 Hz (Buzsáki et al. 2004). The boundaries of different oscillations are somewhat arbitrary, and thus may not match specific network functions and their associated brain states (Cole et al. 2017; Womelsdorf et al. 2014). Indeed, γ oscillations in the hippocampal area CA1 have been further divided in three different frequency bands (Lasztóczi et al. 2016; Schomburg et al. 2014). As will be discussed later, these three frequency bands are believed to reflect the participation of distinct microcircuits (Section 1.5.2).

An important observation is that different oscillations dominate during distinct brain states (Buzsáki et al. 2004; Poulet et al. 2008; Steriade et al. 1993). Perhaps, one of the most obvious examples of brain states and their accompanying oscillations is the distinction between non - rapid eye movement (REM) sleep and active awake states. That is, an animal brain in non - REM sleep is dominated by high - amplitude slow oscillations (Steriade et al. 1993; Vyazovskiy et al. 2013), whereas an animal brain in an awake and active state is dominated by low - amplitude fast oscillations (Bragin et al. 1995; Buzsáki 2002; Fries et al. 2001). The read-out of these distinct rhythmic activities can enable specific assumptions to be made about the signalling of neuronal networks. For example, there are biophysical constraints on the ability of brain circuits to synchronise large numbers of neurons at high frequencies mainly due to the limited speed of action potential propagation and synaptic transmission (P. Andersen et al. 1978; Bastos et al. 2015; Bibbig et al. 2002; Buzsaki 2006; Murakoshi et al. 1993; Traub et al. 1996a). Therefore, slow waves with a large cycle duration allow more neurons in one area to synchronise and fire together in that time period. This could indicate that slower oscillations are more important in global coordination of neuronal networks and mediate processes with longer integration epochs (Buzsaki 2006). On the other hand, faster oscillations could be more important in local networks and mediate processes that require precise integration of synaptic inputs (Buzsaki 2006). However, these restraints do not exclude a role of faster oscillations in long-range synchronisation between specific circuits (Fries 2015).

Moreover, these oscillations sometimes co-exist together, with the smaller and faster oscillations usually nested in larger and slower oscillations (Bragin et al. 1995; Buzsáki et al. 2004). It has been suggested that oscillations of different frequencies could interact together and could also act as separate channels that multiplex information in the temporal domain (Akam et al. 2010; Buzsáki et al. 2004; Sohal 2016). Therefore, understanding the mechanisms that give rise to brain oscillations, and the interactions between them, may lead to insights into the function of their associated brain state.

1.2 RHYTHMIC OSCILLATIONS IN THE GAMMA BAND RANGE

γ oscillations can be defined as rhythmic activity with frequencies ranging between 30 - 120 Hz. However, the upper and lower limits of the oscillation frequency are still debated (Buzsáki et al. 2012; Cardin 2016; Sohal 2016). γ oscillations were discovered in the first half of the 20th century by Lord Adrian and gained a lot of interest after the seminal discoveries of Singer and colleagues in 1989 (Adrian 1942; Gray et al. 1989). Specifically, Singer and colleagues proposed that γ oscillations could provide a solution for the perceptual binding problem (Buzsaki 2006; Gray et al. 1989; Singer 1993). The perceptual binding problem is a class of problems concerned with the mechanisms that the brain uses to combine the separate features of the environment into a single percept (Malsburg 1999; Milner 1974; Roskies 1999; Treisman 1996). In particular, their experiment showed that presentation of a visual stimulus in anaesthetised cats induces γ oscillations in different areas of the visual cortex (tuned to that stimulus) that are synchronised together in time (Gray et al. 1989). This suggested that separate features can be bound together by synchrony (binding by synchrony or "BBS", Singer 1993). The role of γ oscillations in solving the binding problem remains controversial due to fact that the expected changes in synchrony are not observed consistently across conditions (Lamme et al. 1998; Ray et al. 2010; Roelfsema et al. 2004; Thiele et al. 2003). Moreover, a mechanism is

lacking for the communication of distant areas with zero-phase lag at fast time scales, and it is not yet clear how such synchrony could be maintained (Bastos et al. 2015; Dong et al. 2008; Ray et al. 2015). Another more functional hypothesis, which is also highly debated, was put forward by Pascal Fries and is known as communication through coherence (CTC) hypothesis (Bastos et al. 2015; Fries 2005, 2015; Ray et al. 2015). This hypothesis centres around the proposition that groups of neurons communicate with higher efficiency when they are coherently oscillating together. Furthermore, many studies emerged showing that γ oscillations are associated with a variety of brain operations such as sensory binding, attention, memory recall and spatial navigation (Bosman et al. 2012; Fell et al. 2001; Fries et al. 2001; Montgomery et al. 2007; Tallon-Baudry et al. 1999).

When examining the evidence for the functional role of γ oscillations, it is inherently difficult to resolve whether oscillatory activity supports neuronal communication, or is an artefact of this process. Active networks tend to display γ oscillations, with changes in frequency/amplitude of γ oscillations modulated by excitatory drive (Adesnik et al. 2010; Butler et al. 2018; Ni et al. 2016), and thus one would expect changes in effective bottom-up and top-down drive to impact the local properties of γ oscillations and their long-range synchronisation. However, this does not preclude a role for rhythmic synchronisation within γ band in enhancing communication, and competing out distractors (Cardin 2016; Merker 2013; Ray et al. 2015; Sohal 2016). Bearing these caveats in mind, the next section focuses on visual attention and memory processes, as they have been extensively studied in the context of γ oscillations. Additionally, by understanding how γ oscillations can affect signal processing in visual circuits some of their basic mechanisms/functions could be generalised to other cortical circuits. Moreover, memory processes involve the hippocampal area, where the mechanisms of γ oscillations have been explored in great detail and our study takes place.

1.3 GAMMA OSCILLATIONS AND COGNITION

1.3.1 GAMMA SYNCHRONISATION IN VISUAL ATTENTION

The visual environment contains a vast amount of information that can not be processed simultaneously by the brain (Awh et al. 2012; Moore et al. 2017; Reynolds et al. 2004). Attention allows the allocation of limited brain resources to the relevant subset of information in the visual space (Awh et al. 2012; Moore et al. 2017; Womelsdorf et al. 2015). Interestingly, it has been observed that there is a strong link between attentional processes and γ-band activity. Specifically, Fries and colleagues recorded multi-unit activity (MUA) and the local field potential (LFP) from extrastriate visual area 4 (V4) of monkeys during a visual attention task (Fries et al. 2001). They demonstrated that the spike coherence increased specifically with high-frequency oscillations in the γ-band range. This occurred when the monkey attended the stimulus inside the receptive field (RF) of the recorded neurons (Fries et al. 2001). On the other hand, the firing rate of the recorded neurons was not different when stimuli were attended inside or outside their receptive fields (RFs) (Fries et al. 2001). Therefore, it seems that visual attention causes a selective increase in γ frequency synchronisation, but not overall spike rates in a local V4 circuit. Furthermore, it was shown that when monkeys have to detect a change in visual stimulus properties, γ synchronisation could predict the monkey's speed of detection (Womelsdorf et al. 2006). In particular, γ synchronisation was higher in fast detection trials during a change of stimulus detection task in V4 (Womelsdorf et al. 2006). This happened only if the stimulus appeared within the RF of the recorded neurons (Womelsdorf et al. 2006). If the stimulus was presented outside the RF of the recorded neurons, γ synchronisation was lower during fast detection trials (Womelsdorf et al. 2006). This indicates that increased arousal or alertness cannot explain the changes in γ synchronisation. Therefore, γ synchronisation dur-

ing attention may allow amplification of behaviourally relevant signals (Fries et al. 2001).

However, the increase in local γ synchrony is not consistent across visual areas. Particularly, it was shown that visual attention decreased (Chalk et al. 2010) or did not change strongly (Buffalo et al. 2011) γ synchronisation in primary visual cortex area, V1. Therefore, γ synchronisation increase during visual attention is not a general phenomenon and is restricted to particular cortical circuits (Buffalo et al. 2011; Chalk et al. 2010; Womelsdorf et al. 2006). Interestingly, it has been shown that if two visual stimuli activate two different visual fields in monkey primary visual cortex (V1) but the same extrastriate V4 site, γ synchronisation between V1 and V4 sites only emerges when the relevant stimulus is attended (Bosman et al. 2012; Grothe et al. 2012). Both relevant and distractor stimuli drove equally strongly the γ oscillations in V1 (Bosman et al. 2012). Furthermore, the change in γ synchronisation was not depended on the amplitude of V1 γ oscillations (Grothe et al. 2012). Therefore, γ synchronisation during attention could promote communication only with the behaviourally relevant stimulus. In addition, during visual attention, the frontal eye field synchronises with the visual area V4 in the γ-band range (Gregoriou et al. 2009). These results suggest that synchronisation by γ oscillations may promote dynamic functional coupling between different cortical areas during attention by enhancing the effectiveness of the relevant input.

However, it is important to emphasise that in the studies mentioned above, artificial visual stimuli were used. When natural stimuli were employed, contrasting results were generated about γ synchronisation (Brunet et al. 2015; Martin et al. 2016; Ray et al. 2015). Therefore, further investigation is required to understand the contribution of γ oscillations during naturalistic sensory input. It is also worth noting that the analyses in many of these studies begin 200 - 300 ms after cue onset (Ray et al. 2015). This could indicate that γ oscillations do not play a role in initial processing like attention shift. On the other hand, this does not preclude a role for γ oscillations in functional coupling during attention maintenance.

1.3.2 GAMMA SYNCHRONISATION IN MEMORY

The coupling between different brain areas at γ frequencies is not only evident in visual attention tasks. Specifically, it was demonstrated that γ synchronisation between rhinal - hippocampal areas was associated with subsequent successful, but not unsuccessful, memory recall (Fell et al. 2001). Interestingly, γ oscillation power in rhinal cortex and hippocampus was reduced during unsuccessful memory when compared to successful memory recall (Fell et al. 2001). Thus, γ synchronisation could also promote functional coupling in memory processes. Whether the increase in γ synchronisation is also mediated by attention required for the memory formation or is part of the information transfer was not determined (Fell et al. 2001). Furthermore, γ oscillations have also been implicated in working memory. Working memory is the temporary storage used in order to achieve short-term goals (Atkinson et al. 1968; Baddeley 1992). Specifically, elevated working memory load was found to increase γ power (Basar-Eroglu et al. 2007; Howard et al. 2003; Roux et al. 2012). These findings suggest that γ oscillations are associated with distinct, but multiple cognitive processes including attention and memory.

In addition, it was demonstrated that γ power increased and coherence was found in CA3 and CA1 of rats during a delayed spatial alternation task (Montgomery et al. 2007). This increase in power and γ coherence were specific to the time when the rats were in the centre of the maze, a phase thought to correlate with retrieval of spatial cues of the previous trial (Montgomery et al. 2007). The γ synchronisation between CA3 and CA1 was specific to the mnemonic demands of the delayed spatial alternation task as other similar tasks with no mnemonic demands did not cause a change in γ synchronisation between these two areas (Montgomery et al. 2007). Furthermore, γ power only weakly related to other variables such as running speed and acceleration (Montgomery et al. 2007). This means that the characteristic change in γ power was not caused by motor activity. Therefore, increased γ synchronisation between CA3 and CA1 hippocampal regions may strengthen the functional coupling

between these regions during memory recall. However, the γ power was not different between correct and incorrect trials (Montgomery et al. 2007) which signified that it could not be used as a reliable marker for task performance.

Moreover, it was demonstrated that disruption of synaptic transmission from medial entorhinal cortex (mEC) to CA1 impairs mice performance during (DNMP) T-maze task, which is used to assess spatial working memory (Suh et al. 2011; J. Yamamoto et al. 2014). This suggests that mEC - CA1 communication is important for correct functioning of spatial working memory in mice. Interestingly, it was also shown that only high-γ power (but not low γ or θ) was suppressed when the mEC to CA1 transmission was disrupted in these mice (J. Yamamoto et al. 2014). In support of this, mice with no disruptions in mEC to CA1 transmission exhibited increased high-γ power (65 – 120 Hz) in CA1 when the mice were at close proximity to the T-junction (J. Yamamoto et al. 2014). This correlates to the recall of spatial working memory. At the same time, it was observed that γ synchrony increased between mEC and CA1 only in the correct trials (J. Yamamoto et al. 2014). Therefore, increases in γ power in CA1 and coherence between mEC and CA1 are correlated with the successful execution of spatial working memories. Interestingly, in some trials animals first entered the wrong arm and then changed direction towards the correct arm (J. Yamamoto et al. 2014). In those trials it was seen that γ synchrony was shifted right before the direction change (200 ms) (J. Yamamoto et al. 2014). Since the γ oscillations became synchronised before the animal makes the decision, the synchronisation observed may promote correct decision making rather than being a consequence of their choice (J. Yamamoto et al. 2014). This evidence reinforces the close association between mEC-CA1 γ synchrony with successful execution of working memory. In support of this, optogenetic inhibition of mEC terminals on CA1 reduced mEC - CA1γ synchrony and decreased task performance, but also inhibited spike rates (J. Yamamoto et al. 2014). Consequently, high γ synchrony between mEC and CA1 could signal successful working memory function in mice.

Additionally, photo-inhibition of CA1 hippocampal terminals in medial prefrontal cortex (mPFC) impaired task performance of mice during the DNMP sampling phase (Spellman et al. 2015). This suggested that input from the CA1 area to mPFC is critical for encoding of spatial cues with temporal proximity (Spellman et al. 2015). Interestingly, a subset of mPFC units was phase-locked to the CA1 γ oscillation and the greatest number of units phase-locked on times at which CA1 γ preceded (Spellman et al. 2015). This directionality in coupling was specific to γ oscillations as it was not reflected on the θ rhythm (Spellman et al. 2015). These findings indicate that CA1 γ oscillation input could promote the coupling between CA1 and mPFC during spatial working memory encoding. In support of this, the phase-locking to γ but not θ oscillations was disrupted when CA1 terminals were photo-inhibited (Spellman et al. 2015). Furthermore, the phase-locking of mPFC cells was greater during spatial encoding phase and was stronger in correct trials (Spellman et al. 2015). These findings could suggest that γ oscillation inputs from CA1 could affect spike-timing of mPFC cells that is required during successful spatial working memory encoding. Therefore, it seems that γ synchrony may be promoting functional coupling between brain regions required for distinct cognitive processes.

1.4 DOES THE GAMMA RHYTHM CONTRIBUTE TO INFORMATION TRANSMISSION IN THE BRAIN?

As discussed above, there are converging evidence pointing towards a role for γ oscillations as a useful and specific marker during particular cognitive functions (Bosman et al. 2012; Grothe et al. 2012; Montgomery et al. 2007; Roux et al. 2012; J. Yamamoto et al. 2014). Consequently, by understanding how distinct γ oscillations are generated during particular cognitive functions, insights could be gained about the mechanistic operations of those functions. On the other hand, despite all the above evidence, there is still no causal proof that γ oscillations contribute to information processing. This partly arises due to the fact that γ oscillations emerge

from the inherent properties of brain networks (Cardin 2016; Sohal 2016). Therefore, changes in γ oscillations and synchrony must be driven by changing inputs, and γ oscillations can not be selectively affected without altering the signalling properties of the underlying circuit that generates them. This gives rise to the crucial question: do γ oscillations play any functional role in the cognitive operations they are associated with or are they an inevitable byproduct of the underlying network signalling that occurs during those processes?

1.4.1 GAMMA OSCILLATIONS AND LOCAL NETWORK SIGNALLING

The presence of γ oscillations on participating local networks can give rise to some unavoidable consequences on information transmission.

Firstly, rhythmic synaptic input at γ frequencies is capable of altering pyramidal cell input-output properties. This does not require long-range synchronisation between different areas because the population of pyramidal cells that is involved in γ oscillation generation will be receiving synaptic inputs at γ frequencies. This γ input unavoidably biases their input-output properties. How can γ oscillation input alter the input-output properties of pyramidal cells in the brain? Interestingly, it has been demonstrated that fast changes in the membrane potential (Vm) of pyramidal cells *in vivo* lower the action potential threshold (AP threshold) whereas slow membrane depolarisation increases the AP threshold (Azouz et al. 2000, 2003; Henze et al. 2001). This means that faster Vm fluctuations occurring during γ oscillations are very effective in evoking AP firing in pyramidal cells. The effectiveness in spike initiation is believed to occur due to the efficient recruitment of active sodium channels (Azouz et al. 2000). This happens because prolonged depolarisations such as slow Vm changes decrease sodium channel conductance (Bean 2007; Hodgkin et al. 1952; Noble et al. 1966). In support of this, principal cells receiving rhythmic inhibition at 40 Hz experience a multiplicative gain in their output firing rate in contrast to asynchronous activity (Sohal et al. 2009). Rhythmic activity at lower frequen-

cies (8 Hz) was not sufficient to induce this multiplicative gain enhancement (Sohal et al. 2009). Furthermore, it was demonstrated that the size of neuronal responses could be modulated by the γ cycle phase in area V4 of awake monkeys (Ni et al. 2016) in agreement with previous experimental and modelling studies (Börgers et al. 2008; Cardin et al. 2009; Siegle et al. 2014). Specifically, cycle phases corresponding to lower inhibition produced a high gain in the multi-unit responses (induced by stimulus change) (Ni et al. 2016). Interestingly, α oscillations that were larger in amplitude caused similar but slightly lower gain when compared to γ oscillations (Ni et al. 2016). These findings suggest that fast oscillations at γ frequencies could be ideally suited in enhancing gain in cortical circuits.

Moreover, the increased effectiveness of rapid fluctuations in evoking action potentials can also affect when they occur in time. In support of this, rapid membrane potential fluctuations elicit action potentials with higher temporal fidelity than constant excitatory input (Mainen et al. 1995). Synaptic input during γ oscillations could instruct when the spikes occur in pyramidal cells because i) there are narrow time points of low inhibition in the γ cycle where cells can fire with less excitation and ii) during γ oscillations the synaptic inputs causes rapid membrane voltage fluctuations that can evoke effectively action potentials. In support of this, 40 Hz rhythmic input in pyramidal cells decreases response variability in contrast to asynchronous input (Sohal et al. 2009). Therefore, rhythmic synaptic input at 40 Hz can reduce spike variability and also increase multiplicative gain. Unlike the differences observed in gain, 8 Hz rhythmic input can also decrease spike variability to a similar extent. Furthermore, an upstream area generating γ oscillations will send γ rhythmic inputs to a downstream area and if strongly connected it can also alter their input-output properties (Sohal 2016).

In addition, the presence of γ oscillations is thought to promote the generation of local cell assemblies (Buzsáki et al. 2012; Harris et al. 2003). This is because transient partnerships between neurons are believed to form best during periods of 25 ms corresponding to the duration of a γ cycle (Harris et al. 2003). In agreement

to this, only a subset of pyramidal cells (from the local population) fire at each γ cycle (Csicsvari et al. 2003; Hajos 2004; Senior et al. 2008). Furthermore, during γ oscillations only cells that reach threshold at close temporal proximity (when inhibition is low) can fire in each cycle (Almeida et al. 2009; Brunel et al. 2003; Traub et al. 2000). This indicates that γ oscillations also promote segregation of cell assemblies by selecting groups of neurons with similar excitation levels. Therefore, the presence of γ oscillations in a local circuit may produce particular constraints on the signalling of the participating cells.

1.4.2 GAMMA OSCILLATIONS AND LONG-RANGE SYNCHRONISATION

There are several ways in which γ oscillations can contribute to information transmission in the brain, which have long-range synchronisation as a common element. Firstly, γ oscillations have been proposed to bind distributed brain areas by synchrony (Singer 1993). According to this proposal, neurons that participate together in one representation must have synchronised spike timing at zero-phase lags. γ oscillations are believed to act as a means of synchronising these neurons across different areas in time. In addition, it was postulated that γ oscillations can act like a reference clock, where information is encoded by the γ phase at which spikes occur (Fries et al. 2007). To this day, the validity of these hypotheses are still hotly debated (Fries 2015; Ray et al. 2015; Sohal 2016). To begin with, for any oscillation to act like a clock it requires a stable frequency across time. In contrast, γ oscillation frequency has been reported to be highly variable and unstable (Burns et al. 2011; Cardin 2016; Ray et al. 2015). In addition, γ oscillation frequency is modulated by altering low-level stimulus properties (Cardin 2016; Ray et al. 2010, 2015). Importantly, zero phase lag is difficult to achieve at γ frequencies (Bastos et al. 2015; Ray et al. 2015). This evidence argues against these γ functions by long-range synchronisation.

A similar but distinct function of γ oscillations was put forward through the

CTC hypothesis. The CTC hypothesis states that two brain areas communicate more effectively when coherently oscillating together (Fries 2005). This effect occurs because the upstream area sends information with a conduction delay, which arrives to the downstream area, at the trough of γ cycle, when inhibition is lower. Therefore, the frequency of γ oscillations along with the anatomical delays can allow efficient coupling between two brain areas. The CTC hypothesis does not require stable frequency but it does require stable coherence between the two regions to maintain phase relationships. Therefore, the CTC hypothesis has been extended to incorporate inter-areal delays and time-lag between γ communicating regions (Bastos et al. 2015; Fries 2015). Under this regime, the γ oscillations of the downstream area shift with a similar time as the conduction delay allowing excitation from the upstream area to arrive at phases of low inhibition. This shift has been observed to occur across inter-laminar areas which produces a systematic increase in γ delay across cortical layers (Bastos et al. 2015). Therefore, γ oscillations could promote effective coupling though CTC even in non-zero lag communication.

On the other hand, it was recently shown that synchronisation between areas occurred more reliably at θ and β than γ bands (Vinck et al. 2016), in support of previous findings (Bibbig et al. 2002; Fries 2015; Stein et al. 2000). Slower oscillations could better couple areas as they provide a wider time window for synchronisation of distant areas in each oscillation cycle (Buzsaki 2006). Similarly, a number of concerns exist regarding the communication of different areas through γ oscillation coherence. Firstly, many of the studies are using the LFP to compare the coherence between different areas. The LFP is believed to reflect mostly the synaptic input to the area measured (Buzsáki et al. 2015; Haider et al. 2016; Perrenoud et al. 2016). Therefore, synchronous LFP oscillatory activity between two brain regions reflects synchronous inputs (Buzsáki et al. 2015). Moreover, volume conduction from strong γ generators, recurrent connections, synaptic delays and poor site localisation complicate the interpretation of the results (Buzsáki et al. 2015; Ray et al. 2015). For accurate measurement of input-output coherence the spikes from

the somatic layer of the upstream region have to be correlated to the LFP from the dendritic layer of the downstream (Buzsáki et al. 2015). One study used such recordings with accurate localisation analysis. The study showed that there was poor coupling between EC γ oscillations and CA1 spike output (Schomburg et al. 2014). Instead, CA1 spikes were phase-locked to the locally generated γ oscillation (Schomburg et al. 2014). This indicates that EC γ oscillations did not manage to effectively synchronise many pyramidal cells in CA1. Therefore, it is unclear if γ oscillations can effectively achieve global long-range synchronisation. Research methodologies allowing unit sampling of larger neuronal population may be able to delineate this in the future. Furthermore, exploring the mechanisms of γ generation may allow a better understanding on the ways in which γ oscillations contribute to information transmission in the brain. There are converging evidence associating γ oscillations to multiple but distinct cognitive functions. This could allow their activity to be used as a read-out during those functions. An examination of this read-out may allow us to get deeper insights into the signalling mechanisms and information transmission of participating microcircuits.

1.5 MECHANISMS OF GAMMA OSCILLATION GENERATION

The γ oscillation frequency range is broad (30 - 120 Hz). It has been shown that in this frequency range more than one "type" of γ oscillation exists (Bragin et al. 1995; Colgin et al. 2009; Csicsvari et al. 2003; Lasztóczi et al. 2016; Schomburg et al. 2014). The different γ oscillations could arise from distinct mechanisms in different brain areas (with different wiring properties) (Cardin 2016). In addition, spontaneously occurring oscillations could engage different network dynamics than oscillations arising upon stimulus presentation (Cardin 2016). In this section we are going to discuss what mechanisms are responsible for the rhythmic synchronisation of neuronal populations in the γ-band range. Interestingly, despite the variability in γ oscillation mechanisms some underlying principles emerge.

The mechanisms of γ generation in local cortical circuits have been extensively studied using brain slice preparations. γ oscillations in brain slices can be induced by application of a number of pharmacological agents such as carbachol, kainate, metabotropic glutamate receptor (mGluR) agonists and elevated potassium (Bartos et al. 2007; Cardin 2016). It has also been reported that γ oscillations can arise spontaneously in some preparations (Jackson et al. 2011; Pietersen et al. 2009). Interestingly, in all manipulations tested, synaptic inhibition is required for oscillation maintenance as $GABA_A$ receptor ($GABA_AR$) antagonists impair oscillation generation (Bartos et al. 2007; Cardin 2016). Furthermore, prolonging the inhibitory post synaptic current (IPSC) duration using barbiturates reduces the frequency of the oscillations (E. H. Buhl et al. 1998; Fisahn et al. 1998, 2004; Oke et al. 2010; Pietersen et al. 2009). These findings suggest that synaptic inhibition directly affects the frequency of the observed oscillation. Furthermore, genetic removal of connexin 36, the major gap junction protein that electrically links inhibitory neurons, decreases the amplitude of γ oscillations (Bartos et al. 2007; D. L. Buhl et al. 2003; Hormuzdi et al. 2001). Thus, it seems that the presence of gap junctions could increase γ power by strengthening the synchronisation within inhibitory neuron networks (Buzsáki et al. 2012; Whittington et al. 2000). In addition, inhibition is believed be critical to the synchronisation of principal cell assemblies during γ-band activity (Cardin et al. 2009; Cobb et al. 1995; Sohal et al. 2009). Consequently, inhibition seems to be an essential driving force required in the generation of γ oscillations. In contrast, the reliance on synaptic/phasic excitation differs depending on the pharmacological agent and brain region used (Bartos et al. 2007; Cardin 2016). Thus, two theoretical models have been proposed where inhibition is responsible for synchronising principal cells, with or without the requirement for synaptic/phasic excitation. The first model is the interneuron network gamma model (ING) where a network of inhibitory interneurons is sufficient for generation of oscillations. Tonic input to inhibitory interneurons underlies the generation of γ oscillations in this model. The second model is the pyramidal - interneuron network gamma model (PING) where

phasic excitation is a requirement for oscillation generation (Buzsáki et al. 2012; Whittington et al. 2000).

1.5.1 EXCITATION, INHIBITION AND GAMMA RHYTHMOGENESIS

In this section we review how these models fit with the mechanism of γ generation in different *in vitro* manipulations and then compare their properties to γ oscillations occurring *in vivo*. There are some evidence that oscillatory activity in the γ-band range can arise from ING mechanisms. Particularly, γ oscillations induced by elevated potassium oscillations in CA3/CA1 and transient metabotropic glutamate receptor activation in CA1 survive in the presence of AMPA/Kainate glutamate receptor (GluR) blockers (LeBeau et al. 2002; Whittington et al. 1995). Furthermore, γ oscillations induced by puffs of kainate are not blocked during photo-inhibition of pyramidal cells in the CA1 area of the hippocampus (Craig et al. 2015). Additionally, spontaneously occurring fast - γ oscillations are not impaired by AMPA/Kainate antagonists in the subiculum (Jackson et al. 2011). Therefore, it is possible that interneuron networks alone can generate and impose the γ rhythm in some cases.

On the other hand, the mechanism of kainate induced γ oscillations in CA3 is less straightforward. Specifically, AMPAR antagonists do not fully abolish, but strongly attenuate kainate induced oscillations in CA3 (Fisahn et al. 2004; Pietersen et al. 2009). It was therefore proposed that kainate could induce γ oscillations generated through ING mechanisms. However, γ oscillations induced by puffs of kainate in CA3 are abolished when photo-inhibiting pyramidal cells (Craig et al. 2015). It should be noted though that the oscillations may not have been detected in the field because of pyramidal cell membrane hyperpolarisation (discussed below). Therefore, it seems that phasic excitation is at least partly required for the generation of kainate γ oscillations in CA3.

In contrast, there are converging evidence showing that carbachol induced oscillations, at least in the hippocampus, arise due to PING mechanisms. To begin

with, oscillations induced using carbachol in CA3, CA1 and cortex are abolished by AMPA receptor (AMPAR) and AMPA/Kainate antagonists implicating fast synaptic excitation as an integral part of this oscillation (Fisahn et al. 1998; Mann et al. 2005b; Pietersen et al. 2014). In addition, carbachol induced γ oscillations recorded in CA3 area have been shown to reflect alternating somatic inhibitory and excitatory voltage fluctuations in the pyramidal cell layer (Mann et al. 2005b). In further support of this, the dominant phasic input to pyramidal cells is inhibitory and the dominant phasic input to fast-spiking inhibitory neurons is often excitatory (Oren et al. 2006). Importantly, as predicted by the PING mechanism pyramidal cells fire earlier in the γ cycle than interneurons with monosynaptic delays (Hajos 2004; Mann et al. 2005b). Therefore, carbachol induced γ oscillations seem to be generated by phasic excitation with feedback inhibition supporting generation through the PING model.

It is important to emphasise that the carbachol induced oscillations may be undetectable in the LFP upon AMPA/Kainate blockage, but can nevertheless still be present. This is because IPSCs, which are thought to generate the γ LFP, decrease in size during AMPA/Kainate blockage. IPSCs are thought to generate the γ LFP because the i) activation of single inhibitory but not excitatory neurons is able to generate a detectable LFP / electric field response in the hippocampus (Bazelot et al. 2010; Glickfeld et al. 2009) and ii) perisomatic IPSCs are most correlated to fluctuations of the LFP during γ activity in the pyramidal cell layer, where γ power is the highest (Mann et al. 2005b; Oren et al. 2010). The decrease in IPSC size is caused by the hyperpolarisation of pyramidal cells, which causes their membrane voltage to approach GABA reversal potential. To test whether the oscillation was still present, Mann and colleagues recorded synaptic potentials and showed that AMPAR antagonist application abolished the LFP, along with inhibitory (and excitatory) synaptic currents when the cells were held at -70 mV (Mann et al. 2005b). This evidence supports that phasic excitation is important for carbachol induced oscillations in the hippocampus, reinforcing PING mechanisms.

Lastly, γ oscillations have been also induced in brain slices by photo-activating excitatory cells across different brain areas and species (Adesnik et al. 2010; Akam et al. 2012; Betterton et al. 2017; Butler et al. 2016, 2018). This observation demonstrates that excitation to a group of pyramidal cells at the same time is sufficient for γ oscillation induction in cortical circuits (with feedback inhibition). These oscillations have also been shown to be of the PING type as fast synaptic excitation and inhibition need to be intact for oscillation maintenance (Adesnik et al. 2010; Betterton et al. 2017; Butler et al. 2016, 2018). In addition, pyramidal cells fire earlier than interneurons with monosynaptic delays in CA1 (Butler et al. 2016). These results demonstrate that both PING and ING mechanisms can occur in different *in vitro* manipulations. The above results also demonstrate that PING mechanisms require phasic excitation whereas ING mechanisms only require tonic excitation.

1.5.2 GAMMA OSCILLATIONS *IN VIVO*

γ oscillations are observed in the hippocampus nested within slower θ cycles and occur during exploration, sniffing and REM sleep (Bragin et al. 1995). Initially, two separate γ oscillations were discovered. A fast γ oscillation that disappeared upon removal of entorhinal cortex and a slow γ oscillation that emerged in CA3-CA1 region (Bragin et al. 1995). It was shown that the current generators for fast and slow γ were arising from dentate gyrus (depending on entorhinal cortex input) and CA3 respectively (Csicsvari et al. 2003). These fast and slow γ oscillations were found to be coupled to different phases of the theta rhythm in CA1 (Colgin et al. 2009). The phase separation of different γ oscillations indicates that CA1 pyramidal cells receive information from CA3 and entorhinal cortex at different time points. Thus, studying θ - γ coupling during spatial exploration revealed that CA1 pyramidal cells receive spatial information from CA3 and entorhinal cortex with temporal segregation. Recently, more detailed recordings revealed that there are three γ oscillations experienced by CA1 pyramidal cells. A slow γ oscillation in stratum radiatum that originates from CA3, a slightly faster γ oscillation in stratum lacunosum-moleculare

originating from entrohinal cortex and a very fast γ oscillation in stratum pyramidale generated locally in CA1 (Lasztóczi et al. 2016; Schomburg et al. 2014). In agreement with this, all three regions can generate γ oscillations in isolation (Butler et al. 2018; Cunningham et al. 2003; Fisahn et al. 1998; Pietersen et al. 2014). Moreover, the CA3 subfield generates slower frequency oscillations than CA1 and EC (Butler et al. 2018). Hence, there are at least three distinct γ generators that interact in the hippocampal area CA1. An exploration of the interactions between different oscillators may uncover a more detailed temporal communication between the three different areas. In addition, the oscillations observed *in vivo* seem to support mainly pyramidal-interneuron interactions as a mechanism for γ-oscillation generation. Firstly, as in acute slices, photo-activation of pyramidal cells *in vivo*, is sufficient to generate γ oscillations possibly through PING mechanisms (Adesnik et al. 2010; Butler et al. 2018). This means that if a big enough group of pyramidal cells receives strong excitation of sufficient duration, a cortical circuit *in vivo* will resonate with PING oscillations. More importantly, the spiking of pyramidal cells precedes the spiking of fast-spiking interneurons (Csicsvari et al. 2003; Hájos et al. 2009; Hasenstaub et al. 2005; Senior et al. 2008; Tukker et al. 2007; Vinck et al. 2013) and IPSCs follow EPSCs with monosynaptic delays (Atallah et al. 2009). Moreover, the current source density profiles are similar with the carbachol induced oscillations in CA3, supporting a similar mechanism of generation (Csicsvari et al. 2003; Hájos et al. 2009). Finally, even oscillations induced by rhythmic excitation of inhibitory interneurons, require excitation from pyramidal cells (Cardin et al. 2009). This shows that the PING mechanism is strongly supported *in vivo* and that induction of oscillations via carbachol application is a suitable (and simplified) model for investigating γ oscillation mechanisms. Carbachol application also mimics high cholinergic activity which is thought to promote γ oscillations *in vivo* (Howe et al. 2017; Rodriguez et al. 2004; Teles-Grilo Ruivo et al. 2017; Weber et al. 2016).

On the other hand, there are also evidence for ING mechanisms *in vivo*. It was recently observed, that pyramidal cells fire earlier than fast-spiking interneurons

during visually γ, supporting PING mechanisms. However, during the prestimulus cue-period only fast-spiking interneurons were strongly synchronised to the γ oscillation in the LFP, supporting ING mechanisms (Vinck et al. 2013). Similarly, it was shown that pyramidal cells phase-lock to visually induced but not spontaneously occurring γ oscillations in V1 (Perrenoud et al. 2016). These data indicate that some types of γ oscillation may be preferentially generated though ING mechanisms. Recent studies also found little average phase difference between pyramidal and fast-spiking interneurons during some forms of γ oscillation (Cardin 2016; Vinck et al. 2016). These results are further complicated by the participation of multiple cell populations (H. Kim et al. 2016; Vinck et al. 2016). For example, Vinck and colleagues demonstrated that one group of fast-spiking cells fired earlier and another group fired later than principal excitatory cells (Vinck et al. 2016). Therefore, it was suggested that the early group is involved in ING oscillations and the late group is involved in PING oscillations. It should be mentioned though that phase relationships may be determined by whether the circuit is generating or following the oscillation, as can be seen in CA3 versus CA1 hippocampal subfields (Csicsvari et al. 2003). Consequently, additional investigation is required in order to delineate the diversity of γ oscillation generation mechanisms in the brain. In conclusion, it seems that there is strong evidence for the existence of PING mechanisms with possible participation of ING mechanisms. Given that the cortical circuit architecture is able to support both PING and ING (see perisomatic interneuron section below), it is possible that they are differentially recruited depending on particular brain area and specific input.

1.5.3 INHIBITORY INTERNEURONS AND GAMMA OSCILLATIONS

Inhibition is critical for the emergence of oscillations in the γ-band range (Buzsáki et al. 2012; Cardin 2016; Hájos et al. 2009; Mann et al. 2007; Sohal 2016). The cells in the brain that apply inhibition, the inhibitory interneurons, are a diverse

group of neurons that have been classified according to electrophysiological properties, axon innervation pattern on principal cell sub-cellular domains and molecular expression profile (Freund et al. 1996; Somogyi et al. 2005). More than a total of 15 classes of interneurons have been identified in cortical brain circuits (Gelman et al. 2010; Somogyi et al. 2005). Despite this diversity, inhibitory interneurons can be roughly classified into three functional categories based on their axonal projection patterns. These three classes are i) perisomatc-targeting, ii) dendritic-targeting, and iii) interneuron-selective interneurons.

Perisomatic-targeting interneurons mainly consist of basket cells that target the soma along with the proximal dendrites and axo-axonic (chandelier) cells that target exclusively the axon initial segment (Freund et al. 1996; Hua Hu et al. 2014; Somogyi et al. 2005). The basket cells are further divided into neurons that express the calcium-binding protein parvalbumin (PV+) and neurons that express the neuropeptide cholecystokinin (CCK+) (Bartos et al. 2012; Somogyi et al. 2005). Axo-axonic cells selectively express the PV protein (Somogyi et al. 2005). PV+ interneurons are the classical fast-spiking cells with narrow action potential waveforms and high-frequency spiking activity (Bartos et al. 2012; Hua Hu et al. 2014). PV+ interneurons comprise about a third of the interneuron population in the brain (Hua Hu et al. 2014; Pfeffer et al. 2013. On the other hand, CCK+ cells are a smaller group of neurons that have regular and accommodating spiking phenotypes (Bartos et al. 2012).

Dendrite-targeting interneurons mainly consist of cells that express the neuropeptide somatostatin (SST+) and have heterogeneous characteristics comprising both fast and regular spiking phenotypes (Ma et al. 2006; Maccaferri et al. 2000; Muller et al. 2014; Urban-Ciecko et al. 2016). Like PV+ cells, SST+ interneurons also constitute about a third of the interneuron population in the brain (Pfeffer et al. 2013; Urban-Ciecko et al. 2016). In the hippocampus, the OLM cells which target the apical tufts of principal cells and the bistratified cells which target the proximal and distal dendritic regions are two major classes of SST+ interneurons (Somogyi et al.

2005). In addition, the Martinotti cell in the cortex is the major SST+ interneuron which locally projects to pyramidal cell dendrites (Urban-Ciecko et al. 2016).

Interneuron-selective interneurons inhibit predominately other interneurons, as their name suggests and mainly consist of cells expressing the vasoactive intestinal peptide (VIP+) and calretinin (CR+) protein (Pelkey et al. 2017; Pfeffer et al. 2013; Somogyi et al. 2005). Due to the use of transgenic cre driver lines to record and manipulate interneuronal subtypes, distinctions based on molecular expression have become increasingly employed (eg. PV+, SOM+, VIP+). This classification may include distinct and functionally unrelated interneurons. In the next section we are going to focus on PV+ perisomatic interneurons because of their importance in γ oscillations. We will then describe new evidence suggesting that dendrite-targeting interneurons may also contribute to the generation of γ rhythmic activities.

1.5.3.1 PERISOMATIC - TARGETING INTERNEURONS

A few classes of inhibitory interneurons have been implicated in γ oscillation generation, but the one that has been shown to contribute the most is the classical fast-spiking PV+ interneuron (Cardin 2016; Hájos et al. 2009). As mentioned earlier, it has been demonstrated that the main inhibitory currents during γ oscillation generation in the hippocampus arise in the pyramidal cell layer (Mann et al. 2005b; Oren et al. 2010). Both, PV+ and CCK+ interneurons target the perisomatic region and can contribute to this perisomatic current generation. In addition, both neurons can control pyramidal cell output effectively because they apply inhibition close to the action potential generation site (Cobb et al. 1995). Importantly, somatic inhibition is not filtered as much as dendritic inhibition and therefore permits higher frequencies to affect the spike timing in target cells (Buzsáki et al. 2015). Indeed, it has been demonstrated that somatic inhibition can allow for the control of pyramidal cell action potentials with millisecond precision (Pouille et al. 2001). However, CCK+ interneurons have slow and weak signalling properties and therefore do not probably participate in fast oscillations directly (Bartos et al. 2012; Kohus et al.

2016). On the other hand, PV+ interneurons act as rapid signalling devices that are able to transmit high-frequency inhibition reliably and respond readily to excitation (Bartos et al. 2012; Kohus et al. 2016). Indeed, PV+ interneurons fire action potentials at high-frequency and can sustain synaptic transmission at γ frequencies (Bartos et al. 2012; Kohus et al. 2016). On the other hand, CCK+ cells fire trains of accommodating action potentials at low-frequency and cannot sustain γ frequency synaptic inhibition on pyramidal cells (Bartos et al. 2012; Kohus et al. 2016). Furthermore, PV+ interneurons have a shorter membrane time constant than CCK+ cells allowing them to respond faster to excitation (Bartos et al. 2012; Kohus et al. 2016). PV+ interneurons also apply stronger synaptic inhibition on pyramidal cells than CCK+ interneurons (Bartos et al. 2012; Kohus et al. 2016). Lastly, PV+ interneurons have intrinsic sub- and suprathreshold resonance within γ frequencies, allowing them to fire optimally in response to fast rhythmic input (Pike et al. 2000). Consistent with this finding, driving them in a range of frequencies selectively amplifies the LFP in the γ-band range (Cardin et al. 2009; G. Chen et al. 2017). These properties make the PV+ interneuron ideal for synchronising neighbouring cells at high frequencies (Bartos et al. 2012; Hua Hu et al. 2014).

Furthermore, during γ oscillations the participating network has to be silenced uniformly on a short time scale. In agreement to this, PV+ interneurons densely innervate the local pyramidal cell network homogeneously (Packer et al. 2011; Pelkey et al. 2017). Therefore, they can apply strong inhibition that synchronously silences the local pyramidal cell population. Interestingly, PV+ interneurons are strongly connected by both chemical and electrical synapses (Bartos et al. 2002; Takaichi Fukuda et al. 2006; T. Fukuda et al. 2003; Gibson et al. 1999; Kohus et al. 2016; Pfeffer et al. 2013; Tamás et al. 2000). The strong coupling by electrical synapses allows PV+ interneurons to form a mutually connected network allowing for greater synchronisation between them (Bartos et al. 2007; Wang et al. 1996; Whittington et al. 2000). In addition, PV+ interneurons apply even stronger inhibition to other PV+ interneurons than excitatory principal cells or other interneurons (Bartos et

al. 2002; Kohus et al. 2016; Oren et al. 2006; Pfeffer et al. 2013). These connections make PV+ interneurons a suitable candidate for the ING model also, as tonic excitation to models of mutually interconnected interneurons allows for γ oscillation generation (Buzsáki et al. 2012; Traub et al. 1996a; Whittington et al. 2000). However, many of the functional studies investigating electrical connections via gap junctions in PV+ interneurons have been made in developing animals. Since, gap junction strength decreases during development, the contribution of electrical coupling is also reduced in adulthood (Galarreta et al. 2002; Meyer et al. 2002). On the other hand, it was demonstrated that inhibitory synaptic coupling is sufficient to generate synchrony between strongly connected cells (Hang Hu et al. 2011; Wang 2010). This could indicate that PV+ interneurons could still be synchronised in response to tonic input via mutual and strong chemical (GABAergic) synapses.

These evidence collectively suggest that PV+ interneurons have clock-work properties allowing them to participate in fast-rhythms and apply fast inhibition to quickly synchronise principal cell assemblies during each γ-cycle. Importantly, PV+ basket cells participate in almost every γ cycle during kainate and carbachol induced oscillations (Gloveli et al. 2005; Gulyás et al. 2010; Hajos 2004). Furthermore, PV+ fast-spiking interneurons *in vivo* are strongly phase-locked to γ oscillations (G. Chen et al. 2017; Csicsvari et al. 2003; Hasenstaub et al. 2005; Lasztóczi et al. 2014; Perrenoud et al. 2016; Vinck et al. 2013). In addition, decreasing excitation on fast-spiking interneurons reduces the power of kainate induced γ oscillations (Fuchs et al. 2007). Furthermore, inhibiting PV+ neurons in the cortex of anaesthetised mice decreases the power of γ oscillations (Sohal et al. 2009). Thus, PV+ interneurons have properties tuned for fast rhythms and directly contribute to γ oscillation generation in the brain.

1.5.3.2 DENDRITE - TARGETING INTERNEURONS

Even though PV+ interneurons are critical for γ oscillations in the brain, it is likely that other interneuron classes contribute directly or indirectly to γ generation

(Cardin 2016; Sohal 2016). It is also possible that some interneurons participate but do not generate observable electric fields due irregular positioning in brain circuits. Recently, SST+ interneurons have been directly implicated in the generation of γ oscillations (G. Chen et al. 2017; Veit et al. 2017; Vinck et al. 2016). SST+ interneurons consist of cell populations that can be either fast-spiking or regular-spiking with varied IPSC kinetics, and have been reported to have high levels of spontaneous activity (Muller et al. 2014; Urban-Ciecko et al. 2016; Vinck et al. 2016). It has also been shown that SST+ neurons in the cortex densely innervate local pyramidal cells (Fino et al. 2011). It is thus possible that a subset of these cells have sufficiently fast signalling capabilities to participate in γ rhythms. In agreement to this, fast-spiking cells in barrel cortex were separated into two groups, which fired on average at different γ phases (Vinck et al. 2016). These two groups of cells have been hypothesised to belong to PV+ and SST+ GABAergic interneuron classes.

Furthermore, it was shown that SST+ and PV+ interneurons were phase-locked to the visually induced γ oscillations in the V1 of awake mice (Veit et al. 2017). On single trials, the spike rates of SST+ cells were correlated with the low-frequency visually-induced γ (Veit et al. 2017). On the contrary, PV+ spike rates were anti-correlated with the low-frequency visually-induced γ (Veit et al. 2017). Accordingly, optogenetic suppression of SST+ interneurons reduced γ power and long-range γ coherence (Veit et al. 2017). The γ power reduction was correlated with light levels when photo-inhibiting SST+ interneurons, whereas photo-inhibition of PV+ cells with only very strong light intensities was able to block the oscillations. However, strong photo-inhibition of PV+ interneurons also resulted in the induction of seizure activity (Veit et al. 2017). Thus, it was proposed that SST+ interneurons are important for the generation of the low-frequency γ oscillations in V1, whereas PV+ interneurons are important for maintaining excitation-inhibition balance (Veit et al. 2017). In addition, like PV+ interneurons, activation of SST+ at different frequencies selectively amplified the LFP in γ-band range (this range is actually in

the low γ to high β range in awake animals for both PV+ and SST+ cells) and a pyramidal cell - SST+ feedback circuit was sufficient to generate γ oscillations in a V1 cortical slice (Veit et al. 2017). SST+ interneurons fired on average after regular-spiking putative pyramidal cells and PV+ interneurons fired at the same phase as putative pyramidal cells (Veit et al. 2017). Thus, SST+ interneurons are necessary and sufficient in generating low frequency γ oscillations in V1 of awake mice, probably through PING mechanisms.

The importance of SST+ interneurons in visually induced γ oscillations in V1 was also confirmed by a subsequent study (G. Chen et al. 2017). In this study it was demonstrated that SST+ interneuron spiking is most strongly correlated with the low-frequency visually-induced γ oscillations (G. Chen et al. 2017). SST+ cells increased their firing rate as the stimulus size increased and photo-inhibition of SST+ cells decreased low-frequency γ power (G. Chen et al. 2017). It is important to note that the authors refer to the low-γ frequency as β, but the frequency range is very similar with the previous study (G. Chen et al. 2017; Veit et al. 2017). In contrast, it was shown that PV+ interneuron activity was most strongly correlated to high-frequency γ oscillations which occurred spontaneously during running and visual stimulus presentation (G. Chen et al. 2017). Photo-inhibition of PV+ interneurons caused seizure like activity signifying again the importance of PV+ interneurons in maintaining excitation-inhibition balance (G. Chen et al. 2017). However, it is difficult to understand if PV+ activity suppression directly affected the generation of high-frequency γ oscillations from this experiment. Despite this, it was also shown that PV+ IPSCs decay faster than SST+ IPSCs (G. Chen et al. 2017). This is in agreement with previous findings and suggests that PV+ interneurons are better suited for high-frequency inhibition (Bartos et al. 2012; G. Chen et al. 2017). Furthermore, driving PV+ and SST+ interneurons across different frequencies showed that PV+ interneurons increase the LFP with a wider range centred at high frequencies (G. Chen et al. 2017). In contrast, SST+ interneurons increased the LFP

at lower frequencies (G. Chen et al. 2017). This evidence suggests that PV+ interneurons can be involved in higher frequency oscillations than SST+ cells and powerfully apply inhibition to prevent rampant activity. In the two studies the LFP power ratio for the two interneurons were different (G. Chen et al. 2017; Veit et al. 2017). It is possible that this effect was caused by the different light intensities used.

Other dendrite-targeting interneurons have also been implicated in *in vitro* γ oscillations. Trilaminar and bistratified interneurons fire in almost every cycle and strongly phase-lock to kainate - induced γ oscillations (Craig et al. 2015; Gloveli et al. 2005). Bistratified interneurons are hippocampal cells that target the proximal and distal dendrites of neighbouring neurons. Trilaminar interneurons neurons target mainly the dendrites but they also project to perisomatic regions and have an extended axon that targets downstream areas and thus implicating them in long-range synchronisation (Gloveli et al. 2005; Somogyi et al. 2005). In addition, it has been also demonstrated that bistratified cells have the strongest correlation to γ oscillations in anaesthetised rats (Tukker et al. 2007). In contrast, high acetylcholine levels, which often coincide with γ oscillation presence *in vivo* (Teles-Grilo Ruivo et al. 2017; Weber et al. 2016) seem to inhibit or have little effect on bistratified interneurons (Gulyás et al. 2010; Lovett-Barron et al. 2014; Muller et al. 2014). On the other hand, high cholinergic tone increases the firing O-LM cells and cortical SST+ cells (N. Chen et al. 2015; Lovett-Barron et al. 2014; Muller et al. 2014). But, O-LM cells are thought to weakly participate in γ oscillations and better support the generation of θ oscillations (Gloveli et al. 2005; Gulyás et al. 2010; Klausberger et al. 2008). In conclusion, there are sufficient evidence now to show that dendrite-targeting interneurons contribute to some forms of γ oscillation. More experiments are required to delineate the contribution of distinct interneuron classes. Consequently, exploring different interneuron contributions to oscillatory activities may allow us to understand how network activity is orchestrated during distinct brain states.

1.6 GAMMA OSCILLATIONS IN DISEASE

Impairment of γ oscillations has been observed in a number psychiatric and neurological disorders such autism, schizophrenia, epilepsy and Alzheimer's Disease (Herrmann et al. 2005; Uhlhaas et al. 2006). Several alterations in γ oscillation properties have been observed in patients diagnosed with schizophrenia (Uhlhaas et al. 2010). Firstly, steady state responses evoked by stimulating the auditory system evokes γ oscillations with decreased power in schizophrenia patients compared to controls (Light et al. 2006; Uhlhaas et al. 2010). Steady state responses represent the ability of the cortical networks to support synchronisation at γ frequencies (Uhlhaas et al. 2010). Therefore, impairments in steady state responses at γ frequencies could signify that the cortical circuits of schizophrenic patients can not properly synchronise at high frequencies within the γ-band range. Furthermore, it has been demonstrated that γ oscillation power increases with working memory load in humans, and this task-relevant increase is disrupted in schizophrenia patients along with task performance (Basar-Eroglu et al. 2007; Howard et al. 2003). Therefore, γ oscillations could be utilised as a biomarker capable of diagnosing synchrony abnormalities in schizophrenia patients. On the other hand, alterations in γ oscillations of schizophrenia patients have produced mixed results across studies (Herrmann et al. 2005; Uhlhaas et al. 2010). Schizophrenia is a disorder characterised with heterogeneous symptoms that vary between patients (Minzenberg et al. 2012; Uhlhaas et al. 2010). Therefore, there is a large difference in the observed symptoms among patients (Minzenberg et al. 2012) that undoubtedly leads to large variability in the underlying causes. Chronic drug intake affecting the brain neurotransmission complicates interpretations even further (Uhlhaas et al. 2010). Nevertheless, it is thought that the core symptom of schizophrenia patients is the cognitive dysfunction (Lesh et al. 2011; Minzenberg et al. 2012). On the other hand, animal models of schizophrenia are only able to model a subset of dysfunctions observed in human schizophrenia patients, albeit with more specificity. Hence, it is possible to understand how specific cognit-

ive processes are impaired by linking cellular dysfunction to altered network activity in these models. In particular, it was observed that schizophrenia patients were impaired in a cognitive control task when compared to control participants (R. Y. Cho et al. 2006). Higher γ activity in frontal areas was associated with higher cognitive control for healthy participants but not patients (R. Y. Cho et al. 2006). Accordingly, mouse models (Dl5/6$^{+/-}$) with impaired development of medial ganglionic eminence (MGE) derived interneurons exhibit decreased cognitive flexibility after adolescence (K. K. Cho et al. 2015). The impaired cognitive flexibility was accompanied by abnormal function in fast-spiking interneurons (ie PV+ interneurons), reduced inhibition, and altered γ oscillation properties in prefrontal cortex (K. K. Cho et al. 2015). Indeed, photo-inhibition of inhibitory neurons in the prefrontal cortex of wild-type mice replicated the behavioural deficits observed in the Dl5/6$^{+/-}$ mice (K. K. Cho et al. 2015). Furthermore, pharmacological enhancement of fast GABAergic signalling restored the behavioural deficit observed and restored high - frequency γ oscillations in Dl5/6$^{+/-}$ mice (K. K. Cho et al. 2015). Therefore, it is possible that fast-spiking inhibitory interneuron synchronisation at γ frequencies is important for cognitive flexibility tasks which depend on prefrontal cortex. In agreement to this, photo-activation of inhibitory interneurons only at 40 or 60 Hz but not 12.5 Hz rescued the behavioural deficit with a long-lasting effect (K. K. Cho et al. 2015). Thus, synchronisation of GABAergic interneurons (including PV+) in prefrontal cortex at γ frequencies is sufficient in rescuing cognitive inflexibility. It is important to note that even if high-power γ (62 - 120 Hz) was decreased in the Dl5/6$^{+/-}$ mice during task performance, the low-power γ (30 - 58 Hz) was significantly increased (K. K. Cho et al. 2015). Therefore, the pro-cognitive effect could occur from stronger entrainment of PV+ interneurons when stimulated at 40/60 Hz rather than a mechanistic role of γ synchronisation.

Alterations in synchronisation of neuronal populations at γ frequency have also been observed in individuals with neurodegenerative disorders such as Alzheimer's disease (Herrmann et al. 2005; Uhlhaas et al. 2006). The primary pathological

symptom of patients with Alzheimer's disease is increased burden of amyloid-beta ($\alpha\beta$) plaques in the brain (Hardy et al. 2002; Masters et al. 2015). Accordingly, a mouse of model of Alzheimer's disease with progressive increase in $\alpha\beta$ plaque load is accompanied by a reduction in γ power and PV+ interneuron dysfunction (Verret et al. 2012). In addition, the mouse exhibited epileptiform activity that was associated with bouts of low - power γ activity (Verret et al. 2012). Therefore, it was hypothesised that impaired inhibition from PV+ interneurons altered network activities during high $\alpha\beta$ plaque burden. Restoring inhibition by the introduction of an interneuron specific sodium channel increased γ power, reduced epileptiform activity, reduced memory deficits and prevented early mortality (Verret et al. 2012). In addition, aged mice with knock-in of apolipoprotein E4 (ApoE4), the biggest genetic risk factor in Alzheimer's disease, have reduced low-frequency γ oscillations (30 - 50 Hz) during sharp wave ripples (SWRs) (Gillespie et al. 2016). Removal of ApoE4 from GABAergic interneurons rescued the γ oscillation impairment and prevented behavioural deficits in aged ApoE4 mice (Gillespie et al. 2016; Knoferle et al. 2014). The decrease in low-frequency γ power was also observed in an Alzheimer mouse model with increased $\alpha\beta$ plaque deposition (Iaccarino et al. 2016). Surprisingly, photo-activation of PV+ interneurons at 40 Hz and not other frequencies reduced plaque load (Iaccarino et al. 2016). Interestingly, this effect could not be replicated by pyramidal cell photo-activation at any frequency (Iaccarino et al. 2016). The PV+ induced γ oscillations could have partly caused this effect by effectively activating microglia that cleared $\alpha\beta$ plaque accumulation. The decrease in $\alpha\beta$ plaque levels was replicated by stimulating the visual cortex with only 40 Hz visual stimulation (Iaccarino et al. 2016). This effect was dependent on inhibition as GABAergic blocker application prevented plaque reduction (Iaccarino et al. 2016). Lastly, visual stimulation reduced phosphorylated tau, another major pathological feature of Alzheimer's disease, in a taupathy mouse model (Iaccarino et al. 2016). Therefore, research in γ oscillations does not only enable us to further

explore cognitive operations but also to understand and maybe even treat brain disorders. Consequently, exploring the mechanisms that enable rhythmic oscillations to emerge may help us understand how oscillations recorded in humans reflect participating microcircuits, and provide insights into which neuronal computations are disrupted in cognitive disorders.

1.7 COMBINING MECHANISM AND FUNCTION: A WINDOW IN BRAIN COMPUTATIONS

The work mentioned previously is pivotal to our understanding of brain rhythms, their importance in cognition, and the underlying mechanisms that generate them. Furthermore, the aforementioned work has shown that despite some general principles in γ oscillations, there are also significant differences. It is now clear that γ oscillations are generated in several regions of the brain and could involve different mechanisms that are state-dependent. Thus, it seems that a deeper understanding of cognitive operations can be gained by relating specific network activities to their associated brain state. This window to brain computations can be provided though rhythmic activity, which enables linking single-cell signalling to distinct cognitive functions.

Controlling the activity of specific interneuron classes, using mouse genetics, is a powerful way of connecting single cell function to specific cognitive processes through oscillatory activity. In particular, it was shown that 40 Hz photo-activation of PV+ interneurons induced oscillatory activity in the γ-band range (Cardin et al. 2009). Whisker stimulation during PV+ photo-activation resulted in enhanced neuronal responses and spike precision (Cardin et al. 2009). This enhancement occurred only in particular phases of the γ cycle where inhibition from PV+ cells was the smallest (Cardin et al. 2009). Therefore, PV+ induced γ oscillations increase temporal precision of sensory - evoked responses. Interestingly, peristimulus increase in endogenous γ oscillation power predicted correct detection of less salient stimuli

in primary somatosensory cortex, S1 (Siegle et al. 2014). In agreement to this, 40 Hz photo-activation of PV+ interneurons enhanced detection of less salient stimuli, but also impaired detection of more salient stimuli (Siegle et al. 2014). It was further demonstrated that the enhancement in detection of less salient stimuli occurred only during specific phases of the γ oscillation corresponding to reduced inhibition (Siegle et al. 2014). In all other phases, behavioural performance was unaltered or decreased (Siegle et al. 2014). These results show that synchronous firing of PV+ cells at 40 Hz improves sensitivity of difficult-to-detect stimuli. In addition, they demonstrate that the potentiation in sensitivity was due to synchronisation of neuronal populations at 40 Hz and not due to non-specific general inhibition or arousal effects.

Furthermore, it was also shown that fast-spiking PV+ activity closely correlated with attentional processes in medial prefrontal cortex (H. Kim et al. 2016). During periods of putative high attention, PV+ interneuron activity, γ oscillation power, and phase-locking of neuronal populations was higher during correct trials (H. Kim et al. 2016). Photo-inhibition of PV+ interneurons during high attention increased the error rate of mice (H. Kim et al. 2016). Thus, high PV+ interneuron activity and increased γ synchronisation could be required for attentional allocation leading to successful task execution. Moreover, PV+ photo-activation at 40 Hz reduced error rates whereas other frequencies had no effect or increased error rates (H. Kim et al. 2016). Motor coordination or arousal could not explain the findings as there were no changes in reaction times during light stimulation (H. Kim et al. 2016). These findings suggest that selective circuit synchronisation at specific frequencies enhances distinct cognitive operations, whilst impairing others. Therefore, linking cellular changes through mesoscopic network activity to behaviour can be a powerful future approach that will allow us to gain deeper insights in cognitive computations.

However, in order to achieve this bridge between single cell function and cognition it is important to first understand the neural circuit components that are responsible for generating mesoscopic network activity. Since inhibition is critical for the generation of γ oscillations, selective manipulation of different inhibitory

interneurons can be a powerful method for dissecting the neuronal circuits involved in γ oscillation generation (Cardin et al. 2009; G. Chen et al. 2017; Sohal et al. 2009; Veit et al. 2017). Therefore, in our study we tried to dissect these circuits in a simplified *ex vivo* preparation of the hippocampus in the CA3 subfield, an area that has been studied in detail both in regards of interneuron anatomy and γ oscillation generation (Akam et al. 2012; Betterton et al. 2017; Butler et al. 2018; Freund et al. 1996; Gloveli et al. 2005; Hajos 2004; Mann et al. 2005a; Oren et al. 2006, 2010; Somogyi et al. 2005; Whittington et al. 1995). After investigating the γ oscillation mechanisms we then turned to examine some of the consequences of a circuit generating this particular network activity on principal cell function.

1.8 THESIS OBJECTIVES

In this project we aimed to investigate the mechanisms of γ oscillation generation in CA3 *in vitro* which are believed to have many similarities to *in vivo* γ oscillations. Furthermore, PV+ interneurons have been shown to contribute to the generation of γ oscillations in the brain by many studies (Section 1.5.3.1). Therefore, we studied in chapter 3 how optogenetic modulation of PV+ interneurons affects carbachol-induced γ oscillations in ventral CA3 subfield (positive control).

However, PV+ interneurons represents less than a third of the interneuron population in the hippocampus (Hua Hu et al. 2014; Pfeffer et al. 2013). It is therefore possible that other interneuron populations are involved in the generation of γ-band oscillations in CA3. Thus, in chapter 4 we examined how optogenetic modulation of another major class of interneurons, the SST+ interneurons, affects carbachol-induced γ oscillations in ventral CA3 subfield.

Our data reinforce the existing evidence which indicate that rhythmic perisomatic inhibition is a critical feature of low-frequency γ oscillations in the hippocampus. In order to further understand the function of rhythmic perisomatic inhibition, we used dynamic clamp to inject inhibitory conductance trains into pyramidal neurons, and examined the effects of disturbing rhythmicity and/or synchrony on pyramidal cell spiking. We address these issues in chapter 5 by applying simulated synaptic inputs in putative principal cells.

Chapter 2

Materials and Methods

2.1 ANIMALS

All procedures were performed according to the United Kingdom Animals Scientific Procedures Act (ASPA) 1986 and the University of Oxford guidelines. Adult PV-cre (B6;129P2-Pvalbtm1(cre)Arbr/J) and SST-cre mice (Sst tm2.1(cre)Zjh/J) were used for all experiments (unless clearly stated otherwise).

2.2 VIRAL INJECTIONS PROCEDURES

All viral constructs were acquired from Vector Core Facilities, Gene Therapy Centre (North Carolina, UNC). The viral constructs used the AAV5-EF1a-DIO-ChR2--mCherry, AAV5-EF1a-DIO-ChR2-eYFP, AAV-EF1a-DIO-Arch3.0-EYFP, pAAV--Ef1a-DIO-hChR2(E123T/T159C)-p2A-mCherry-WPRE (Dr. Karl Deisseroth) and AAV-CAG-FLEX-ArchT-GFP (Dr. Ed Boyden).

Anaesthesia was induced with 4% isoflurane/medical oxygen mixture at a rate of 2 L per min. The area around the head was shaved and cleaned in preparation for scalp incision. Anaesthesia was subsequently maintained using 1.5 - 2.5% isoflurane at a rate of 2 L per min. The breathing was continuously monitored ($\sim$ 1 Hz) and the level of isoflurane was adjusted to keep the depth of anaesthesia stable. Before the onset of the procedure a cocktail of systemic peri-operative analgesics (Metacam 1 mg/Kg and Vetergesic 0.1 mg/Kg) and a local analgesic (Marcaine 10mg/Kg) were administered subcutaneously (all drugs were purchased from Oxford University

Veterinary Services). Following, ChloraPrep antibiotic solution was applied on the head and an incision of the scalp was performed that allowed a small craniotomy to be made. A 33/34 gauge needle was attached on a Hamilton Microliter Syringe and used to inject the virus solution at a rate of $\sim$ 100 nL/min (viral concentration was on the order of 10^{12} genome copies per mL). The virus solution levels were continuously monitored during every injection to verify that the needle was not blocked and that the virus solution could exit the syringe. After every injection, the needle was left stationary for at least three minutes to allow diffusion of virus in the surrounding area.

HIPPOCAMPAL INJECTIONS: The virus solution was injected with the aid of a stereotaxic frame to ventral CA3 area of hippocampus (2.7 mm caudal and 2.75 mm lateral from Bregma). A total of 600 - 800 nL were injected at two depths (300 - 400 nL at 3.1 mm and 300 - 400 nL at 2.7 mm). Following the injection, local analgesic (Marcaine 10 mg/Kg) was applied on the incised scalp before it was sutured. The animals were then transferred in a heating chamber and allowed to recover. Subsequently, they were given a strawberry jelly containing 1.2 mg/Kg Metacam to consume overnight. The animals were monitored and welfare scored in the following days to ensure that they properly recovered after surgery. Injected mice were assessed for viral expression after a minimum of 3 weeks.

2.3 *EX VIVO* BRAIN SLICE PREPARATION

Brain extraction: Mice were anaesthetised using 4 % isoflurane (Oxford University Veterinary Services) and were sacrificed by decapitation after the pedal reflex was abolished.

Ventral hippocampus preparation-CA3 (Chapter 3-PV and Chapter 4-SST): Brains were extracted in warm sucrose solution ($30 - 35°C$) and transverse hippocampal slices of 350 μm thickness were cut using a Leica vibratome (VT 1200S). A warm sucrose preparation was used because it enabled robust network

activity and easier *in vitro* patch-clamp experimentation in hippocampal area CA3 (Huang et al. 2013).

Somatosensory cortex preparation-S1 (Chapter 5-Gain): Brains were extracted in cold aCSF solution ($0-4°C$) and coronal brain slices of 350 μm thickness were cut using a Leica vibratome (VT 1200S).

Ventral hippocampus preparation-CA1 (Chapter 5-Gain): Brains were extracted in cold aCSF solution ($0-4°C$) and transverse hippocampal slices of 350 μm thickness were cut using using a Leica vibratome (VT 1200S).

Slice recovery: Slices were then immediately placed in an interface storing chamber containing warm aCSF ($30-35°C$) at least one hour to equilibrate. The solutions were continuously bubbled with 95% O_2 and 5% CO_2 (carbogen gas) beginning 30 minutes before the procedure until the end of the experiment.

Sucrose solution: 40 mM NaCl, 3 mM KCL, 7.4 mM $MgSO_4.7H_2O$, 150 mM Sucrose, 1 mM $CaCl_2$, 1.25 mM NaH_2PO_4, 25 mM $NaHCO_3$ and 15 mM Glucose.
Osmolality: 300 +/- 10 mOsmol/Kg.

Artificial Cerebrospinal Fluid (aCSF): 126 mM NaCl, 3.5 mM KCl, 2 mM $MgSO_4$-$7H_2O$, 1.25 mM NaH_2PO_4, 24 mM $NaHCO_3$, 2 mM $CaCl_2$ and 10 mM Glucose.
Osmolality: 300 +/- 10 mOsmol/Kg.

2.3.1 CONSTRUCT EXPRESSION

Brain slices from injected mice were assessed for successful expression of the viral construct before the onset of electrophysiological recordings. Successful expression in slices was assessed by the presence of green or red fluorescence emission (according to the fluorophore type expressed). Before slices were used for electrophysiological experiments they were screened for appropriate viral expression that covered the CA3 hippocampal subfield. Slices were only used if there was an observable light-induced response during either extracellular or intracellular recordings in CA3.

2.4 ELECTROPHYSIOLOGY

2.4.1 EXTRACELLULAR RECORDINGS

Extracellular recordings were conducted in an interface recording chamber. The interface recording chamber was comprised of two sub-chambers. The top chamber was perfused with the aCSF and drugs or other solutions were added as required by the experiment. The bottom chamber was filled with distilled H_20 (18.2 MΩ) that was bubbled with carbogen gas and maintained at 33-34$°C$. This chamber served to heat the incoming aCSF, and provided an atmosphere of warm humidified carbogen for the top chamber. The slice was held at the interface between the aCSF and humidified carbogen, with conditions maintained by covering the top of the chamber. Visualisation of the slice and electrode placement was performed using a Wild Heerbrugg dissection microscope.

2.4.2 LOCAL FIELD POTENTIAL RECORDINGS

A borosilicate glass electrode (tip resistance = 1 - 5 $M\Omega$) was filled with aCSF and was inserted in CA3 in order to record local field potentials (LFPs) (Fig. 2.1). Data were acquired and amplified (x 10) by Axoclamp 2A (Molecular Devices). The signal was further amplified x 100 and low pass filtered at 1 KHz (LPBF-48DG, NPI Electronic). The signal was then digitised at 5000 samples per second by a data acquisition board (ITC-16, InstruTECH) and recorded from the IgorPro software (Wavemetrics). Gamma (γ) oscillations were induced by the application of 5 μM carbachol (cch). The LFP signal was quantified using real-time fast Fourier transform (FFT) analysis and γ oscillations were detected by a peak in the power spectrum at low γ-band frequencies (25 Hz - 49 Hz).

2.4.3 MULTI - ELECTRODE RECORDINGS

For unit recordings a linear 16 channel tungsten multi-electrode array (MEA; Micro-Probes) was lowered in the CA3 subfield. The array channels had 100 μm spacing to ensure full coverage of the hippocampus. The MEA was mounted on an RHD2132 Amplifier board and connected to the RHD2000 USB Interface Board (Intaan Technologies). Data were acquired at a rate of 20000 samples per second using the RHD2000 rhythm software (Intaan Technologies).

2.4.4 LIGHT DELIVERY

For photo-activation (ChR2) experiments, light illumination was delivered through a fibre optic using a blue LED (470 $\pm$ 20 nm, Thor labs, M470F3; max power at fibre optic tip = 10 mW). For photo-inhibition (Arch) experiments light illumination was delivered through a fibre optic by a green LED (530 $\pm$ 30 nm, Thor labs, M530F2; maximum power at fibre optic tip = 4.25 mW) and with an amber LED (595 $\pm$ 20 nm, Doric, maximum power at fibre optic tip = 5 mW). LED module output was controlled using the IgorPro software. Some photo-inhibition experiments were also performed with a green laser (MatchBox series, 532 $\pm$ 0.5 nm, maximum power at fibre optic that was used $\approx$ 40 mW). In these experiments the data were acquired at a rate of 10000 samples per second using IgorPro. The laser was operated manually and the light duration was detected using an Arduino Uno board that created a digital time stamp. Experiments were only included if the laser illumination duration was between $\approx$ 19.6 - 20.7 seconds. The area of light illumination was estimated to have a diameter of 1 - 2 mm and therefore for a power of 10 mW the area was between 0.8 - 3.2 mW / mm^2.

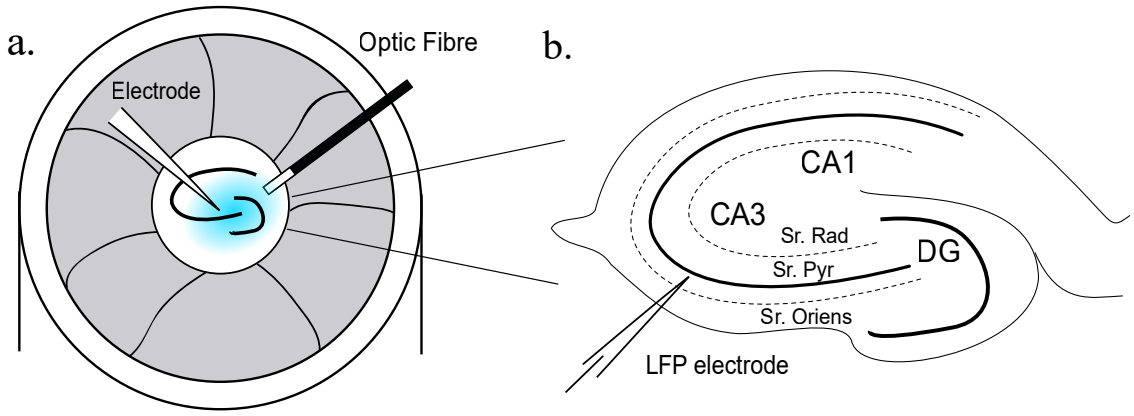


Figure 2.1: LFP recordings and light delivery in the interface chamber. a) Schematic diagram of an interface recording chamber illustrating LFP recordings by a glass electrode and light delivery through an optic fibre. b) Placement of electrode in the pyramidal cell area of hippocampal area CA3. CA3 = Cornu Ammonis 3, CA1 = Cornu Ammonis 1, DG = Dentate Gyrus, sr. Pyr. = stratum Pyramidale, sr. Rad. = stratum Radiatum, sr. Oriens = Stratum Oriens.

2.5 INTRACELLULAR RECORDINGS

Intracellular recordings were always conducted in a single submerged chamber ($\approx$ 28 - 32 $^{\circ}C$) using borosilicate glass pipettes (5-12 $M\Omega$). The signal was acquired through the MultiClamp 700B amplifier (Molecular Devices) and digitised at a rate of 10000 samples per second by a data acquisition board (ITC-18, InstruTECH) and was then recorded using the Igor Pro software. The signals were low pass filtered (Bessel) at 10 kHz for current clamp mode and 3 kHz for voltage clamp (VC) mode. Slice and cell visualisation was achieved using oblique illumination and monitored through a HAMATATSU ORCA - ER digital camera. Filtered white LED (460 $\pm$ 30 nm, 1.53 mW, Thor Labs) via epi-illumination was used to activate channel rhodopsin (ChR2). Filtered white LED (525 $\pm$ 20 nm, 1.45 mW, Thor Labs) via epi-illumination was used to activate archaerhodopsin (Arch). For a power of 1.5 mW, the illuminated area is 3.68 mW / mm^2 .

CELL - ATTACHED RECORDINGS: Cell attached recordings were performed in current clamp (IC) mode (Multiclamp software) using glass pipettes filled with aCSF.

WHOLE - CELL CURRENT CLAMP: For whole cell current clamp recordings pipettes were filled with internal solution containing 110 mM KGluconate, 40 mM HEPES, 2 mM ATP-Mg, 0.3 mM GTP-NaCl, 4 mM NaCl (pH 7.2-7.3; Osmolality 270-290 mOsmol/Kg. 3-4 mg/ml biocytin (Sigma) was added for visualisation of cell morphology. After break through the bridge balance was adjusted to compensate for electrode access. Hyperpolarising and depolarising square current pulses were applied in all cells in order to characterise the electrophysiological phenotype of the cell. All cells that depolarised strongly during the duration of experiments were excluded for analysis.

WHOLE - CELL VOLTAGE CLAMP: For whole cell voltage recordings pipettes were filled with internal solution containing 140 mM Cesium methanesulfonate, 5 mM NaCl, 10 mM HEPES, 0.2 mM EGTA, 2 mM ATP-Mg, 3 mM GTP-Na, 5 mM

QX-314. 3-4 mg/ml biocytin (Sigma) was added for visualisation of cell morphology. Series resistance compensation was not performed in all cells included for analysis. This should not affect the results presented in the current study as were only looking for qualitative differences within cells. Specifically, voltage-clamp recordings were used to assess the differences in magnitude between synaptic excitation and inhibition that each cell received. Since, series resistance compensation was the same for each cell, the interpretation of our results should not be affected.

PERFORATED PATCH RECORDINGS: For perforated patch recordings the tip of the pipette was filled with a KCl-containing solution (150 mM KCl and 10 mM HEPES, pH 7.2-7.3; Osmolality 300 mOsmol/Kg). The rest of the pipette was filled with the same KCl solution containing 5 μM gramicidin D (1:1000 DMSO dilution, Sigma) and 10 μM Fluorescein (Sigma) to visualise if there was spontaneous rupture of the membrane during patching experiments. A rupture of the membrane was also recognised by the sudden depolarisation in the cellular membrane voltage. All recordings after membrane rupture were excluded from further analysis. Positive pressure was applied to the pipette just before the slice was reached. This was made to ensure that the gramicidin did not reach the tip of the pipette when approaching the target cell. Following the formation of a gigaOhm seal, there was a waiting period of 15 - 30 minutes until the cell was perforated. This was assessed by applying short (20 ms) hyperpolarising pulses at 5 - 10 mV in voltage - clamp mode.

2.6 DYNAMIC CLAMP

Dynamic clamp was used to simulate perisomatic inhibition applied by GABAergic interneurons to pyramidal cells during γ oscillation activity. Dynamic clamp was performed using IgorPro and data were acquired at a rate of 8000 samples per second. Output currents updated at 50 KHz according to the equation: Iinj(t) = Itonic + GInh(t) $\times$ [EInh – Vm(t)]; where Iinj(t) = total current injected at each

time point (t), Itonic = excitatory tonic current, GInh = inhibitory conductance at time (t), EInh= reversal potential for inhibitory GABAergic synapses and Vm(t)= the mebranve voltage of the cell at time point (t). Therefore, dynamic clamp simulates synaptic currents when provided with a synaptic conductance input and a reversal potential value for the simulated receptor. Accordingly, synaptic conductance trains with a 2 second duration were created for GABAergic inhibitory synapses. This was achieved by first creating 1000 synchronous synaptic inputs that occurred rhythmically at 40 Hz (Fig.5.2a Top Left). These inputs were convolved by single inhibitory post synaptic conductance events (sIPSG = $(a^3 \times x \times e^{-ax}) * Iamp * (e/a)$; $a = 200$, $e = 2.71828$ and $Iamp = 5 \times 10^{-18}$ S) to generate inhibitory post synaptic conductance IPSG trains with 1.04 pS peak amplitude (Fig.5.2a Top Right).

The peak amplitude of the IPSG trains was varied in each experiment with the purpose of inducing a 5 mV fluctuation at action threshold (2 - 21 nS). In order to control rhythmicity of the 40 Hz trains the interval between synchronous events (inter synchronous interval = ISI) was varied (Fig. 5.2a Middle). ISI was varied by sampling from a γ distribution (Mean = ab; Variance = ab^2) with a mean of 25 ms, and a standard deviation of CV x 25ms, where CV is the coefficient of variation (CV = standard deviation/mean). CV = 0 for rhythmic trains; CV = 1 for Poisson trains. To control the synchrony of single synaptic inputs (SynTime) a noise component was added to the time of their occurrence relative to the synchronous event and was controlled by the "jitter" parameter (Fig. 5.2a Bottom). SynTime was varied by sampling from a flat distribution between $\pm$ jitter. A square inhibition conductance was created by averaging over the 2 second period of the rhythmic and synchronous (CV = 0, jitter=0) IPSG train. Furthermore, dynamic clamp experiments were performed in the the perforated patch configuration. The perforated patch configuration resulted in an increased offset error that hyperpolarised action potential thresholds close to Einh. In those cases the offset was changed until the threshold of the cell was set approximately at -50 mV.

2.7 IMAGING

After electrophysiological recordings, acute brain slices were fixed in 4% PFA overnight. Slices were kept in PBS (Phosphate Buffered Saline: 1.37 mM NaCl, 2.7 mM KCl, 10 mM Na_2HPO_4, 2 mM KH_2PO_4) at $4°C$ for short-term storage. Biocytin labelling and confocal imaging were performed by Georgina Kontou (Kittler Lab, University College London).

2.7.1 BIOCYTIN LABELLING

After intracellular recordings, the biocytin-filled slices were fixed in 4 % PFA overnight at $4°C$. The slices were washed with 1X PBS 3-4 times and permeabilised with freshly prepared 0.3 %-Triton 1X PBS for 4-5 hours. Streptavidin conjugated to Alexa Fluor^{TM} 488 (Invitrogen S32355) in PBS-T 0.3 % (1:500) was incubated overnight at $4°C$. The slices were then washed 4-5 times in PBS for 2 hours. Before mounting, the slices were checked under the confocal microscope using the 10x air objective in order to identify which side is accessible for imaging.

2.7.2 FLUORESCENCE IMAGING

The slices were placed on glass slides and a coverslip was mounted on top using a mounting medium. The fluorescence images were obtained using a fluorescence microscope and the images were acquired with Retiga R1 camera (Micro-Manager software).

2.7.3 CONFOCAL IMAGING

The slices were placed on glass slides and a coverslip was mounted on top using Dako Fluorescent (Dako S3023) mounting medium. Confocal images (1024 x 1024) were acquired on a Zeiss LSM700 upright confocal microscope using the 10x air, 20x water objective and digitally captured using the default LSM acquisition software. For neuronal reconstructions, confocal stacks of 1024 x 1024 pixels were acquired.

2.8 DATA ANALYSIS

2.8.1 GAMMA OSCILLATION ANALYSIS

In order to characterise and analyse the γ oscillations, a hanning window was applied and we calculated power spectra as the normalised magnitude square of the FFT (IgorPro). The 50 Hz and 100 Hz frequencies were not included in the analysis to exclude the mains noise and its harmonic component. The oscillation amplitude was quantified firstly by measuring the peak of the power spectrum termed as peak power and secondly by measuring the area below the power spectrum plot in the γ-band range (20 - 100 Hz) termed as power-area. The peak frequency of the oscillation was obtained by measuring the frequency at which the peak of the power spectrum occurred in the γ-band range. In the interface-conditions the power of cch-induced γ oscillations tends to increase slowly overtime. In the current study, the majority of the experiments were performed in a time period of 5 seconds where γ power does not significantly change ($F(2, 28) = 0.024$, $p = 0.98$, repeated measures ANOVA). Furthermore, the photo-inhibition experiments using laser illumination were performed on longer time scales (80 - 100 seconds), where increases in γ power are possible. However, it is unlikely that the slow increases in γ power could alter the interpretations of our experiments. As γ power was often suppressed in these experiments, γ power changes coincided with light onset and were usually reversed when the light was turned off.

In order to quantify when cch-induced oscillations where abolished upon light stimulation and to exclude the peak frequencies of those oscillations from further analysis one of the two criteria had to be met. Firstly, an auto-correlation of the oscillations was computed and was fitted with a Gabor function ($f(x) = (A \times cos\ (2\pi \times f \times x)) \times e^{-x^2\ /\ 2tau}$). The first criterion was met if the resulting Gabor fit had a linear correlation coefficient (r) > 0.7 and product of $\sqrt{f \times tau} > 0.1$ (> 0.15 for frequencies higher than 50 Hz). The second criterion was a power-area bigger than 200 μV^2 in the range of $\pm$ 3 Hz of the peak frequency. It was manually

confirmed that this criterion could identify whether oscillations were present. This was done to ensure that frequency quantification was accurate during cch-induced oscillations experiments. The power-area was always included in the analysis even if oscillations were abolished. For the laser and *de novo* γ experiments, the only criterion that had to met was power-area bigger than 40 μV^2 in the range of $\pm$ 7 Hz of the peak frequency. This was used in the aCSF experiments because we often used theta-photo-stimulation. For the laser experiments the Gabor fit was computationally expensive and the oscillations were rarely abolished. The conclusions in PV+ and SST+ experiments in cch were very similar if this criterion was used and did not change the interpretation of results. The power spectrum analysis in SST+ photo-excitation experiments in aCSF was extended to 149 Hz since the induced oscillations sometime exceeded the 100 Hz frequency band. For visualisation purposes the magnitude of the continuous wavelet transform was used (Morlet wavelet; non-dimensional frequency = 6). The magnitude of the continuous wavelet transform was then normalised by its maximum value. Hilbert transforms were used to obtain instantaneous γ magnitude.

2.8.2 UNIT DETECTION AND CLUSTERING

Unit detection was performed using custom-written procedures in MATLAB (Mathworks). Extracellular spikes from the 16 channel MEA were detected were detected as described before by Quiroga and colleagues (Quian Quiroga 2009; Quiroga et al. 2004). The MEA data were processed with an elliptical band-pass filter (for spike detection: 4th order, 300 - 3000 Hz, for spike sorting: 2nd order, 300 - 6000 Hz). Spikes were detected as signals exceeding 5 standard deviation (s.d.) of the noise ($5 \times \sigma n = \text{median}\{|x| \ / \ 0.6745\}$). Signals that exceeded 10 times the s.d. of the detected spikes were eliminated as artefacts/population spikes. Subsequently, spikes that had peaks occurring at the same time (< 0.1 ms) across channels were grouped together as one unit. This prevented detection of the same unit more than once.

Clustering of the detected spikes was performed using custom-written procedures in Igor Pro. A spike sorting procedure adapted from Fee et al. 1996 was used to explore whether neurons displaying specific spike waveforms were selectively recruited by optogenetic stimulation. Briefly, spike metrics were converted into z scores, over-clustered using an in-built k-means algorithm, and progressively aggregated if the intercluster distance was <2.5 and merging did not produce more violations of refractory period of 2 ms. Analysis was performed on the clustered spikes, with auto-correlation and cross-correlation plots used to validate the clustering procedure. Spike metrics from the average waveform for each cluster were used to identify different waveform types via a k-means algorithm. This clustering procedure is likely to be conservative, and underestimate the firing rate of individual neurons, but was deemed sufficiently robust to detect any bias in optogenetic recruitment. A single-unit cluster was identified if it i) had less than 1.4 % of its total spike waveforms within 2 ms of its refractory period and ii) consisted of more than 800 members. When a cluster did not obey this criteria, it was merged with other clusters that had similar action potential waveforms giving rise to a multi-unit cluster.

2.9 STATISTICS

Repeated measures ANOVA (rmANOVA) was performed in SPSS with Greenhouse-Geisser correction where required (i.e. significance in Mauchly's test for sphericity) and followed by Bonferroni-corrected post-hoc paired t-tests. Linear correlations, circular correlations, Bonferroni-corrected one sample t-tests were performed using Igor Pro. In all experiments, the bar charts display the average value and the error bars represent the standard error of the mean. Stars represent significance values where * is $p < 0.05$, ** is $p < 0.01$ and *** is $p < 0.001$.

Chapter 3

The Role of Parvalbumin - Expressing Interneurons in Hippocampal Gamma Oscillations

3.1 INTRODUCTION

The role and function of parvalbumin (PV+) interneurons has been studied extensively, and many lines of evidence have suggested that their activity is critical in the generation and maintenance of gamma (γ) oscillations across the brain (Bartos et al. 2007; G. Chen et al. 2017; Mann et al. 2005a; Sohal et al. 2009). In the current study, we wanted to test how direct modulation of the PV+ interneuron activity, using optogenetics, affects γ oscillation properties in the CA3 area of the ventral hippocampus. To achieve that, we injected PV-cre mice with the light-activatable protein, channelrhodopsin 2, and performed whole-cell recordings to confirm that we were indeed targeting and photo-activating PV+ interneurons. Since PV+ interneurons have been shown to be critical in the synchronisation of principal cells during γ oscillations we first tested how rhythmic photo-activation of PV+ interneurons at 40 Hz affects ongoing γ oscillations in the LFP. We then proceeded with testing how sustained up-regulation of PV+ interneuron activity (sustained photo-activation) can affect ongoing oscillations in the γ band range. γ oscillations that occur in vivo during exploration are usually nested in slower theta oscillations (8 - 12 Hz) (Bragin et al. 1995; Buzsáki 2002; Lisman et al. 2013). We thus examined how sinusoidal

modulation of PV+ interneurons, mimicking theta input drive, affects γ power. Finally, we tested if PV+ interneuron activity is necessary for the maintenance of ongoing γ oscillations. To achieve that, we selectively expressed the inhibitory light-activatable pump archaerhodopsin in PV+ interneurons and photo-inhibited them during carbachol-induced γ oscillations. Collectively, our results indicate that PV+ interneuron activity is important for the generation of γ oscillations in CA3 and that alterations in their function can lead to impaired rhythmogenesis.

3.2 INDUCING GAMMA OSCILLATIONS IN THE CA3 HIPPOCAMPAL SUBFIELD

The experiments were performed in the hippocampus due to its suitability for our study. Firstly, the properties of interneurons in the hippocampus, and especially fast-spiking PV+ interneurons (PV+INs), have been studied extensively in respect of anatomy, single cell physiology and activity during γ oscillations (Bartos et al. 2012; Hajos 2004; Somogyi et al. 2005). The CA3 subfield was chosen specifically because it is a γ generator, allowing it to sustain γ oscillations *in vivo* (Bragin et al. 1995) and *in vitro* even if isolated from other brain areas (Fisahn et al. 1998). We therefore recorded the local field potential (LFP) from the pyramidal cell layer of the ventral CA3 subfield (Fig. 3.1a) and induced γ oscillations by the application of 5 μM carbachol (cch) (Fig. 3.1b). This particular γ oscillation model was chosen since γ oscillations induced by cch application *in vitro* have many similarities with *in vivo* γ oscillations (Hájos et al. 2009). The cch-induced γ oscillations were rhythmic as demonstrated by the auto-correlation (Figure 3.1c). In order to characterise and analyse the LFPs, we calculated power spectra as the normalised magnitude square of the Fast Fourier Transform (FFT). The oscillation amplitude was quantified firstly by measuring the peak of the power spectrum, termed as peak power, and secondly by measuring the area below the power spectrum plot within the γ band range (20 - 100 Hz) termed as power-area (Fig. 3.1d). The peak frequency of the oscillation was obtained by measuring the frequency at which the peak of the power spectrum occurred within the γ band range (Fig. 3.1d). The cch-induced oscillation frequency was in the low γ band range centred around 30 - 40 Hz (Fig. 3.1d). Furthermore, all optogenetic experiments in the LFP were repeated at least 5 times per slice.

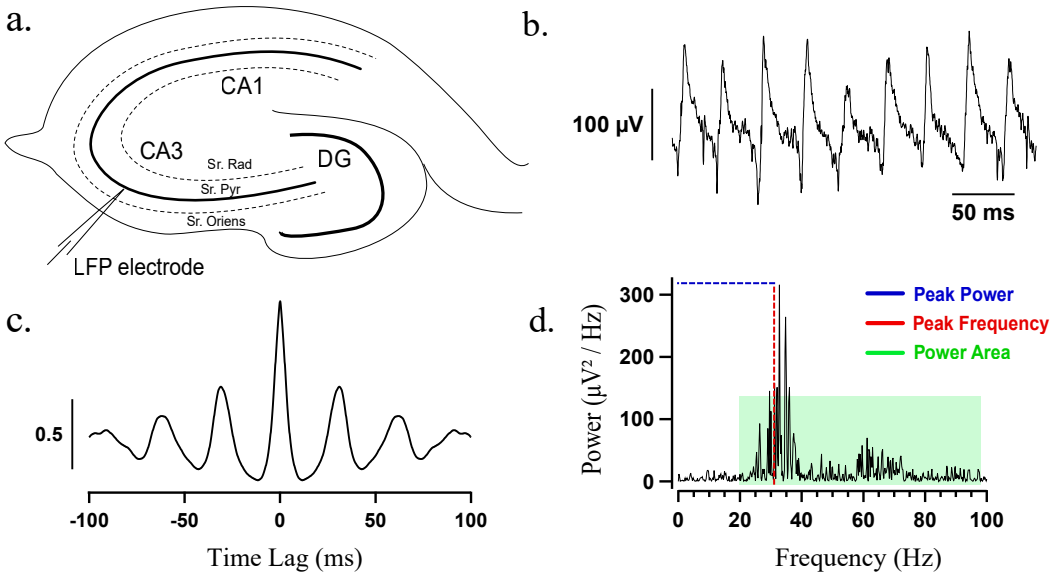


Figure 3.1: Carbachol γ oscillation induction in the interface chamber. a) Illustration of the electrophysiological setup used for field recordings. The LFP was recorded by inserting a glass electrode (1 - 5 MΩ) in the stratum pyramidale of the ventral CA3 subfield. The experiments were performed in an interface recording chamber which allowed robust γ oscillations to be induced by the application of 5 μM carbachol (cch) at 33 - 34°C. b) Representative LFP recording from the ventral CA3 area obtained by the application of 5 μM cch. c) Autocorrelogram of the recording in b) illustrating that the oscillation is rhythmic with a period of 31 ms. d) Power spectrum of the LFP recording from b). The oscillation had a peak power of 315.89 μV^2/ Hz with a peak frequency of 32.8 Hz and power-area of 1429.71 μV^2. DG: Dentate Gyrus, CA3 = Cornu Ammonis 3, CA1 = Cornu Ammonis 1, sr. Rad. = stratum Radiatum, sr. Pyr = stratum pyramidale, sr. Oriens = stratum Oriens.

3.3 VIRAL EXPRESSION OF OPTOGENETIC CONSTRUCTS

In order to study the role of parvalbumin positive interneurons (PV+INs) in γ oscillations, we wanted to directly manipulate their activity with temporal precision. To achieve that we used viral vectors containing optogenetic constructs and stereotaxically injected them in the CA3 ventral hippocampus of PV-cre mice (Methods, section 2.2). We first wanted to test how up-regulation of PV+IN activity affects the generation of γ oscillations. Therefore, we injected PV-cre mice with adeno-associated virus (AAV) carrying the light-gated ion channel, channelrhodopsin 2 (ChR2) (Nagel et al. 2003) fused with a fluorescent reporter (mCherry or eYFP) (Fig. 3.2a). Viral construct expression was allowed for at least three weeks before obtaining acute hippocampal slices for electrophysiological experiments. This induced robust expression of ChR2 as evidenced by the strong fluorescence signal that was restricted in the pyramidal layer of the hippocampus (Fig. 3.2b). The fluorescence in the pyramidal cell layer was diffuse, indicating that the signal mainly arises from ChR2 expression in perisomatic presynaptic terminals (Fig. 3.2c). This is in agreement with targeting basket and axo-axonic PV+INs, whose projections synapse at or near the soma of principal cells (Hua Hu et al. 2014; Somogyi et al. 2005). PV+ expression has also been observed in O-LM and bistratified interneurons that target the dendrites of pyramidal cells (Somogyi et al. 2005). However, the pattern of expression in our model suggests that the majority of the infected cells are perisomatic targeting PV+INs. We then performed whole-cell recordings in the current clamp configuration to verify the intrinsic properties and functional ChR2 expression in PV+INs. Current steps produced a typical fast-spiking phenotype with large after hyperpolarisation (Fig. 3.3ai, aii). All cells that could sustain more than 5 action potentials during the step had spike half-width between 0.26 to 0.35 ms with an average of 0.31 $\pm$ 0.016 ms (n = 5 of 6 cells).

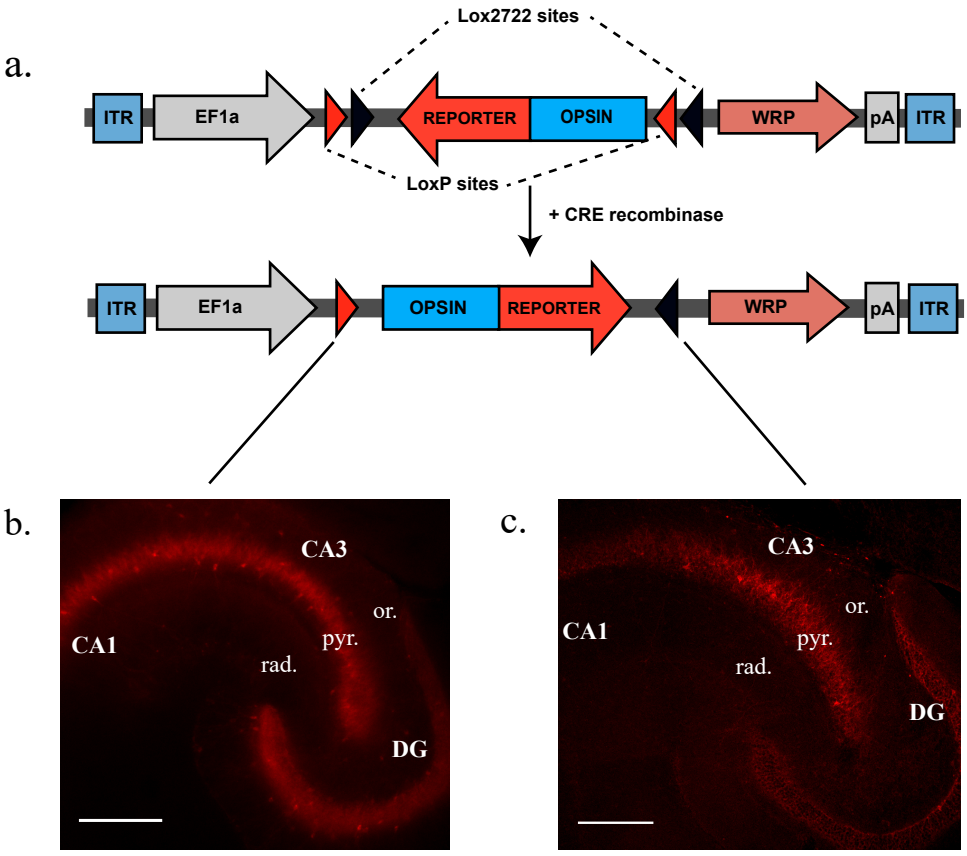


Figure 3.2: Expression of ChR2 in PV-cre mice. a) Schematic of optogenetic DNA construct carried in double-floxed AAV5 vector used to inject PV-cre mice. In Cre-expressing cells, the viral DNA is flipped in the sense orientation (Sohal et al. 2009). ITR = inverted terminal repeat, WPRE = woodchuck heptatitis virus post-transcriptional regulatory element, pA = polyadenylation signal. b) Fluorescence and c) Confocal image of ventral hippocampal slices (350 μm) from PV-cre mice showing the expression of mCherry-ChR2. Fluorescence signal from mCherry is mainly restricted to the pyramidal cell layer. CA3 = Cornu Ammonis 3, CA1 = Cornu Ammonis 1, DG = Dentate Gyrus, sr. Pyr. = stratum Pyramidale, sr. Rad. = stratum Radiatum, sr. Oriens = Stratum Oriens. Scale bar = 200 μm.

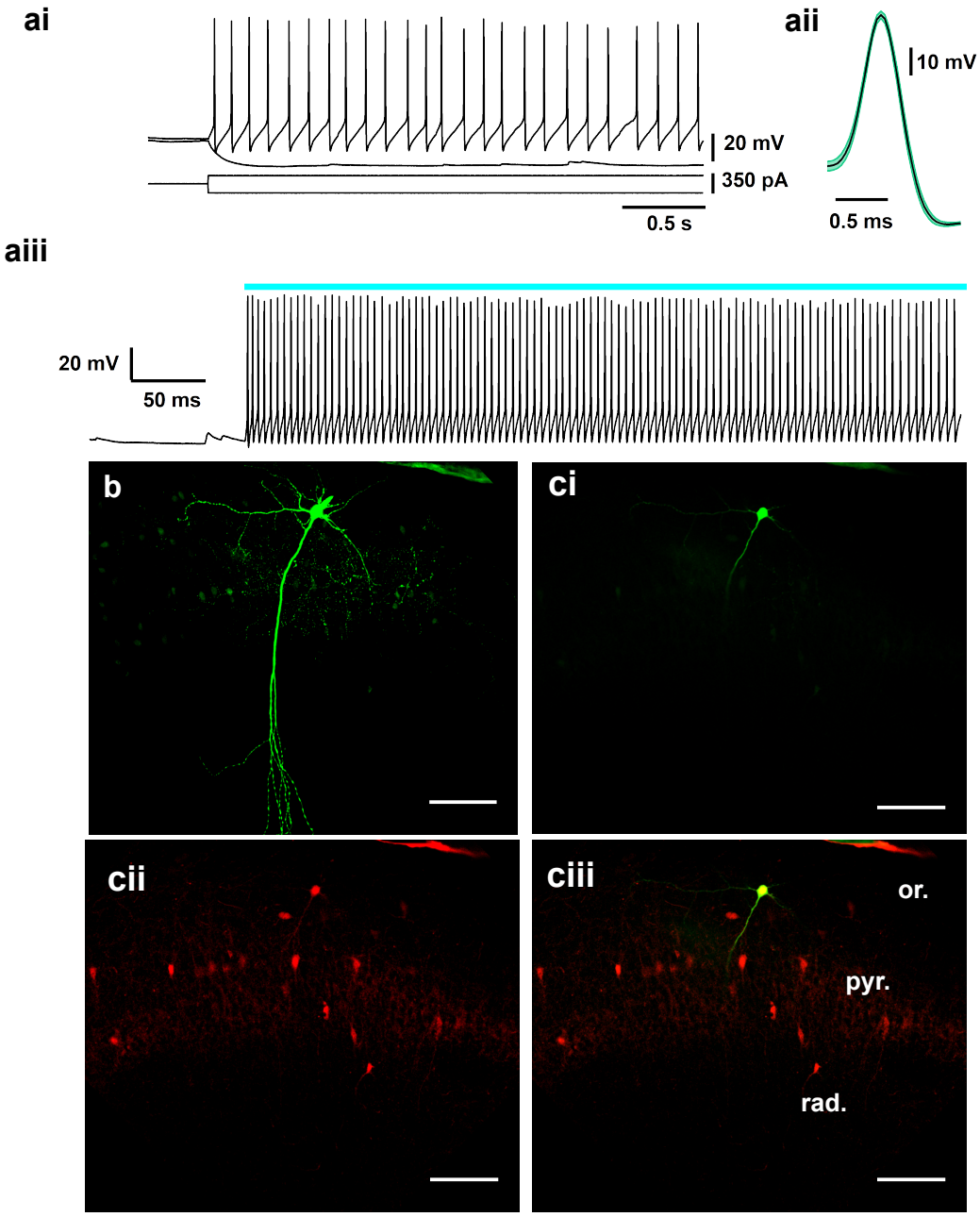


Figure 3.3: ChR2 is expressed in fast-spiking perisomatic interneuron. A PV-cre-Ai9 (PV-Cre x Gt ROSA (CAG-td Tomato) Hze/J) mouse was injected with AAV5-ChR2-eYFP. The PV-cre-Ai9 mouse expressed tdTomato reporter protein in PV+ cell bodies allowing easy identification. ai) Current clamp recording in a PV+IN from CA3 area in response to depolarising and hyperpolarising current injection. aii) Average waveform of the PV+IN obtained from responses to increasing levels of depolarising current injection. The green shaded area represents standard deviation. aiii) High-frequency action potential firing of a PV+IN in response to sustained blue light illumination (1.53 mW). b) Maximum intensity projection of the recorded cell filled with biocytin and visualised with Alexa Fluor 488. Confocal images that capture the fluorescence signal from ci) Alexa Fluor 488 cii) tdTomato and ciii) merged. This shows that the recorded neuron expressed parvalbumin and had axon terminals in the pyramidal cell layer. sr. Pyr. = stratum Pyramidale, sr. Rad. = stratum Radiatum, sr. Oriens = Stratum Oriens., scale bars = 100μm.

Four cells responded consistently during blue light illumination (at least 5 repetitions per cell) with high firing frequency of action potentials indicating that ChR2 expression was functional (Fig. 3.3aiii). One cell did not produce action potentials because it did not express high opsin levels (produced less than 50 pA of excitation when the cell was held at -65 mV using voltage clamp mode) and one cell did not fire any spikes because of depolarisation block. One of the recorded neurons was filled with biocytin and visualised (Fig. 3.2b, c), revealing that the axon was situated in the pyramidal cell layer (Fig. 3.2b, c). Together, this suggested that ChR2 was functional and was successfully expressed in PV+ fast-spiking perisomatic-targeting interneurons. To observe the effects of PV+IN optogenetic activation (photo-activation), we recorded from putative pyramidal cells. Putative pyramidal cells had regular-spiking phenotypes (Fig. 3.4a) with half-spike widths ranging from 0.64 to 0.90 ms with an average of 0.73 $\pm$ 0.06 ms (n = 4). The maximum spike rate of these cells did not exceed 20 action potentials per second, in agreement with their regular spiking behaviour. All of the putative pyramidal cells hyperpolarised during wide-field illumination with a two second light step (repeated at least 5 times per cell) with an average decrease of -4.05 $\pm$ 0.85 mV (Fig. 3.4d). This was sufficient to prevent spiking in a putative pyramidal cell during light activation of PV+INs (induced by 100 pA current injection; pyramidal cell hyperpolarised by an average of 2.25 mV Fig. 3.4e). As before, one of the patched cells was visualised and had a typical pyramidal cell morphology (Fig. 3.4c). Therefore, excitation of PV+ interneurons by ChR2 activation induces reliable inhibition in putative pyramidal cells that can suppress their spiking activity.

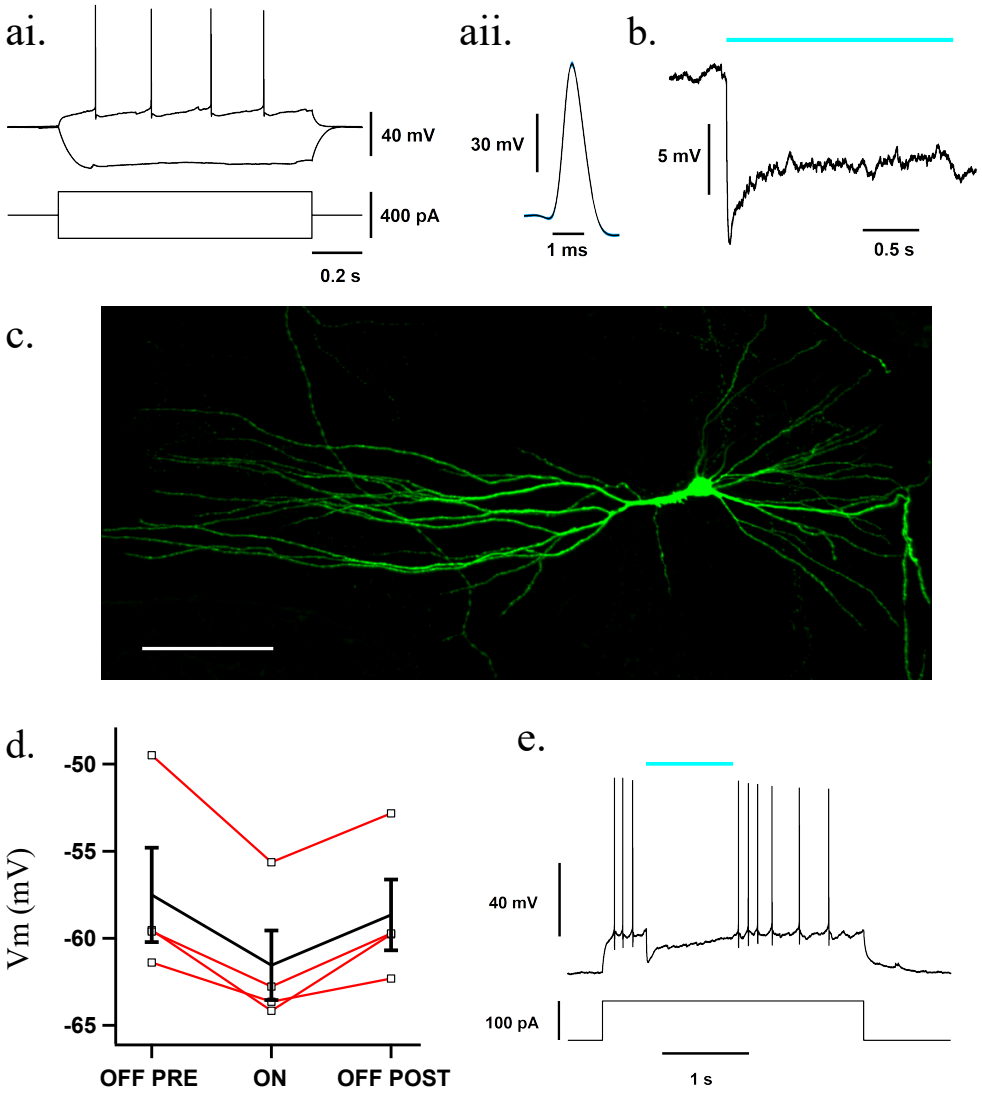


Figure 3.4: Pyramidal cell inhibition by PV+IN photo-activation. ai) Current clamp recording in a putative pyramidal cell from CA3 area in response to depolarising and hyperpolarising current injection. aii) Average waveform of the putative pyramidal cell obtained from responses to increasing levels of depolarising current injection, blue shaded area represents the standard deviation. b) hyperpolarisation of the recorded cell in response to blue light illumination (1.53 mW). c) Maximum projection of the recorded cell filled with biocytin and visualised with Alexa Fluor 488, indicating typical pyramidal cell morphology. Scale bar = 100 μm. d) hyperpolarising responses of putative pyramidal cells produced during PV+IN activation by two second constant blue light illumination (ON), when compared to the preceding 1 second baseline (OFF PRE). Light off period following light illumination (OFF POST). e) Action potential firing induced by 100 pA current injection is suppressed during PV+IN activation with a 1 second blue light illumination.

3.4 RHYTHMIC PHOTO-STIMULATION OF PV+ INTERNEURONS DURING GAMMA OSCILLATIONS

Phasic synchronisation of principal cell ensembles, arising from PV+INs, is believed to be critical for the generation of γ oscillations (Bartos et al. 2007; Mann et al. 2005a; Sohal et al. 2009). Here we wanted to test whether this can be confirmed using optogenetic approaches in the hippocampus. (n = 12 at 5.5 mW, n = 6 at 2.2 mW for 1 ms pulse width, and n = 7 at 5.5 mW, n = 6 at 2.2 mW for 5 ms pulse width; merged). Consistent with previous findings, photo-stimulation of ChR2-expressing PV+INs at 40 Hz (1 ms pulse width) was able to entrain ongoing γ oscillations in most experiments (14 / 18; Fig. 3.5a, ci). In 10 out of 18 experiments, rhythmic photo-activation of PV+IN was sufficient to shift the peak frequency to 40 Hz (Fig. 3.5bi, di). In 4 out of the 18 experiments, the ongoing oscillations were locked at 20 instead of 40 Hz (Fig. 3.5di). This occurred because the 40 Hz pulses phase locked the one cycle and abolished the following resulting in half of the total cycles (Fig. 3.5bii). In 4 out of 18 experiments the ongoing oscillations were not entrained (Fig. 3.5biii, di). This occurred because of low ChR2 expression, as pulses with 5 ms width were able to entrain the oscillation in the same experiments (Fig. 3.5dii). Rhythmic photo-activation of PV+INs at 40 Hz with 5ms pulse width entrained the ongoing oscillations in all experiments analysed (Fig. 3.5dii). The experiments that inhibited half of the cycles were not repeated with 5 ms pulse width, as preliminary experiments showed that this would increase synaptic inhibition and abolish more γ cycles. These experiments indicate that rhythmic photo-activation of PV+INs can successfully synchronise the hippocampal CA3 network and shift the frequency of cch-induced γ oscillations.

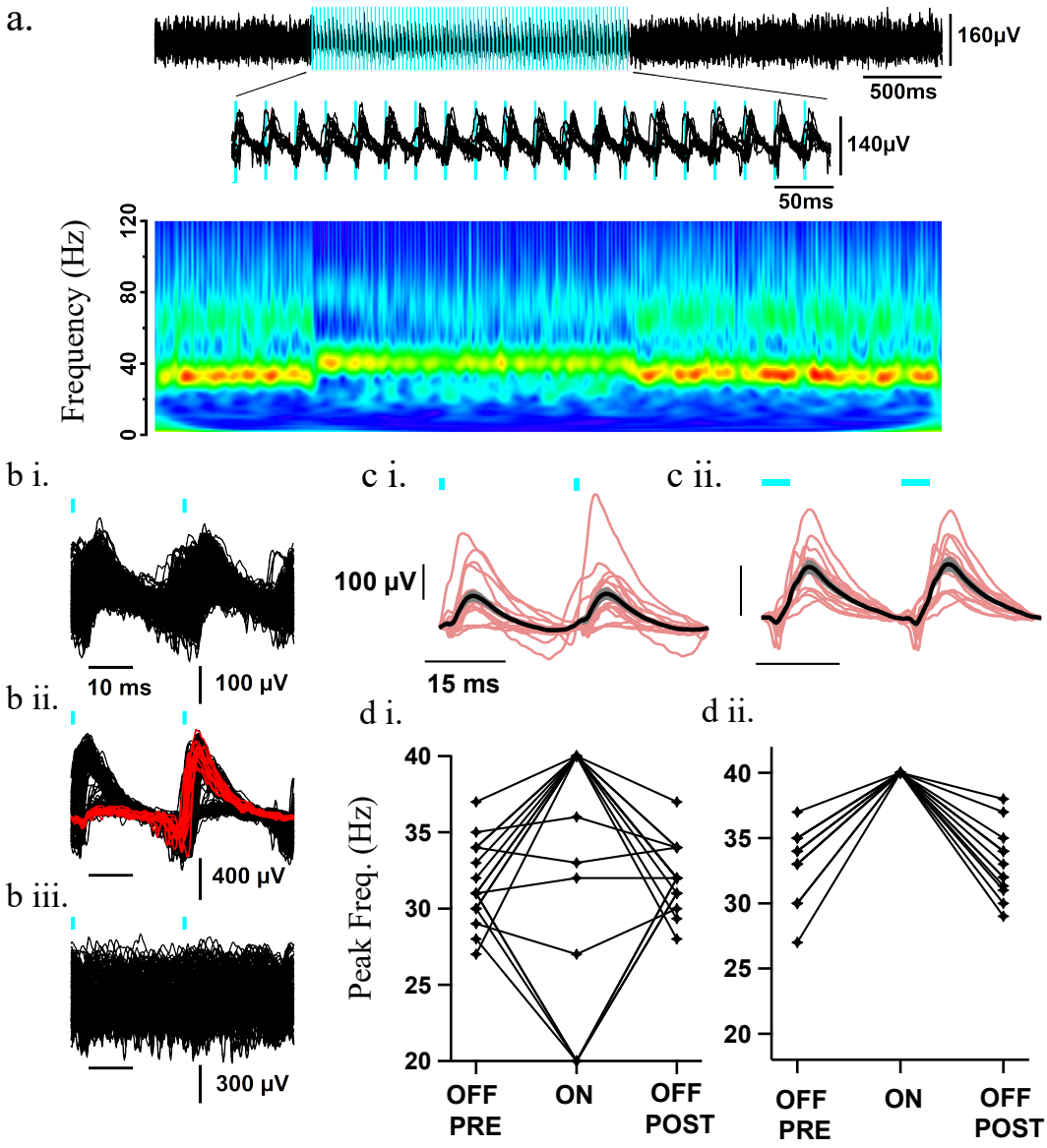


Figure 3.5: Rhythmic stimulation of PV+INs entrains ongoing γ oscillation. a) Top: Representative LFP recording from CA3 area illustrating the entrainment of cch-induced γ oscillations to 40 Hz light pulses with width of 1 ms (2 second train of blue light illumination, with peak power of approx. 2.2 mW). Middle: Zoomed recordings from a) during pulse stimulation. Bottom: Magnitude component of the wavelet transform normalised by its maximum value, brighter colours represent larger magnitude. b) Extracted waveforms following two consecutive pulses at 40 Hz from one experiment showing i) strong entrainment, ii) entrainment of half of the cycles and inhibition of the other half, and iii) no entrainment. Red lines represent a subset of extracted waveforms. c) Average waveform following two consecutive pulses at 40 Hz with pulse widths of i) 1 ms (n = 18) and ii) 5 ms (n = 13). d) Peak Frequency of oscillation before (OFF PRE), during (ON) and after (OFF POST) light stimulation at 40 Hz with pulse widths of i) 1ms (n = 18) and ii) 5 ms (n = 13). Note that the slices with 20 Hz induction were not tested with 5 ms pulse width. Black lines represent single experiments.

3.5 SUSTAINED PHOTO-ACTIVATION OF PV+ INTERNEURONS

We showed that PV+IN rhythmic photo-stimulation can reliably entrain the hippocampal network at γ frequencies. We then tested if increased PV+IN activity is also sufficient to modulate cch-induced γ oscillations in the hippocampus. To test that, we recorded the LFP whilst tonically driving PV+INs at increasing strengths during ongoing γ oscillations, by changing the levels of blue light illumination (10 - 5500 μW). The change in power-area between baseline and light activation period was measured at each light intensity level. We then obtained the response level at which the power-area changed by half of the maximum for each experiment (half-maximal response). The power-area was then normalised by dividing the 5 second trial with the 1 second baseline preceding light onset (Norm. Power). Photo-activation of PV+IN (2 seconds) consistently decreased the power-area when compared to baseline period (normalised half-maximal response: 0.52 ± 0.016, $p < 0.001$, one-sample t-test; Fig .3.6a,c and e). Interestingly, the power-area immediately recovered in the period following light activation (0.5 to 1.5 seconds after light stimulation) and was not different from the baseline (0.99 ± 0.017, $p < 0.001$, one-sample t-test; Fig .3.6a,c and e). In addition, the peak frequency significantly increased from 32.70 ± 0.793 Hz during baseline period to 38.76 ± 1.094 Hz during PV+IN photo-activation ($p < 0.001$, paired t-test; Fig .3.6b,d and f). As expected the peak frequency returned back to baseline in the period following light activation (33.49 ± 0.780 Hz, $p = 1.00$, paired t-test; Fig .3.6d and f). These results indicate that tonic up-regulation of PV+IN activity decreases the power and increases the peak frequency of cch-induced γ oscillations. Furthermore, the peak power had a strong positive correlation ($r = 0.75$) with power-area (Fig .3.7). Thus, in the following experiments only the power-area will be used to report γ power unless the conclusions changed with peak power as a measure.

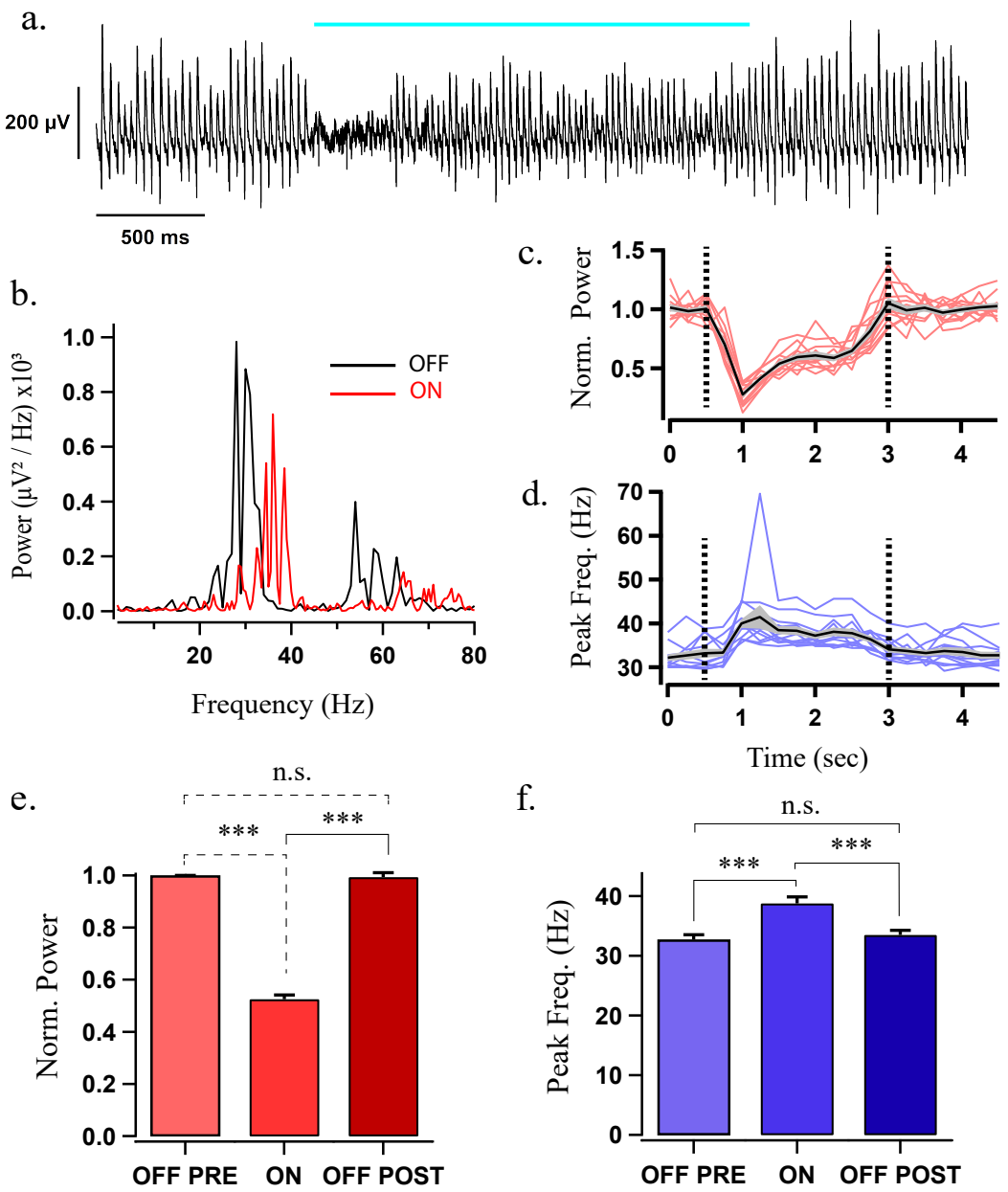


Figure 3.6: Sustained photo-activation of PV+INs decreases the power and increases the frequency of γ oscillations. a) Representative LFP recording from CA3 area illustrating network inhibition of cch-induced γ oscillations to constant blue light illumination (155 μW). b) Power spectrum of the recordings in a) showing that the power of the oscillation decreases whereas the frequency increases, ON = 2 second light stimulation period, OFF = 1 second baseline period preceding light stimulation. c) Power-area of the oscillation normalised to baseline and calculated in 0.5 second bins across experiments (n = 12). d) Peak frequency of the oscillation calculated in 0.5 second bins across experiments (n = 12); Time between dotted lines indicates the duration of LED illumination. e) Average change in power-area during (ON) and after light stimulation (OFF POST) normalised to baseline (OFF PRE); one sample t-tests for comparison of ON and OFF POST periods to baseline, paired t-test for between conditions comparison (ON - OFF POST). f) Average peak frequency; Repeated measures ANOVA followed by post-hoc paired t-test with correction for multiple comparisons. rmANOVA: $F(1.14, 12.50) = 44.14$, $p < 0.0001$. *$p < 0.05$, **$p < 0.01$, ***$p < 0.001$, $^{n.s.}p >= 0.05$. Dashed brackets represent one sample t-tests and solid brackets represent paired t-tests.

Next, we tested how the changes in power and frequency of γ oscillations between baseline and light on periods varied with increasing light strengths. We found progressive decrease in power-area (r = -0.61) and elevation of peak-frequency (r = 0.42) as light intensity increased (Fig. 3.8a,b). The peak frequency increase was found to be proportional (r = -0.50) to the change in power-area (Fig. 3.8e). Therefore as the light intensity increased, the γ oscillation decreased in power and increased in frequency. This was true until a certain threshold was reached and the oscillation collapsed. As can be seen in the power plot in Fig. 3.8b the change in peak frequency returns to zero towards higher light intensities.

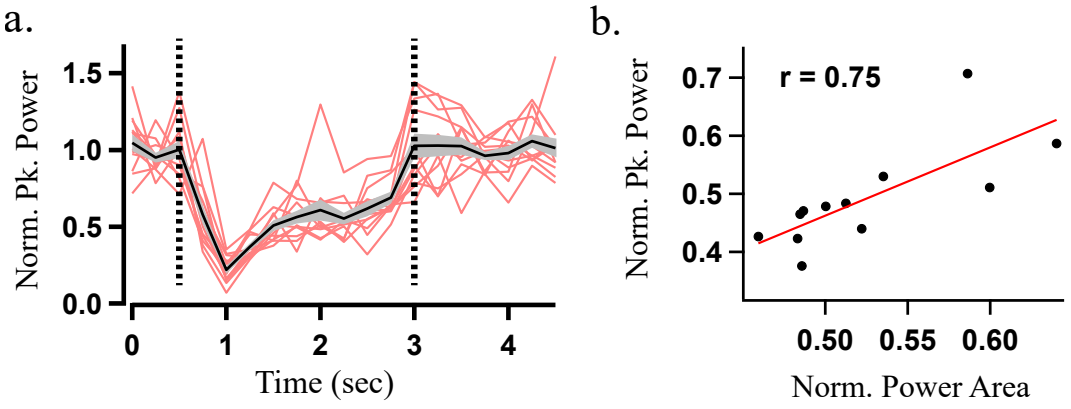


Figure 3.7: Peak power is directly proportional to power area. a) Peak power of the oscillation during light stimulation when normalised to baseline and calculated in 0.5 second bins across experiments (n = 12); Time between dotted lines indicates the duration of LED illumination. b) Change in peak power plotted against change in power-area between light stimulation period and baseline ; Pearson Correlation: r = 0.75, n = 12, p $<$ 0.005.

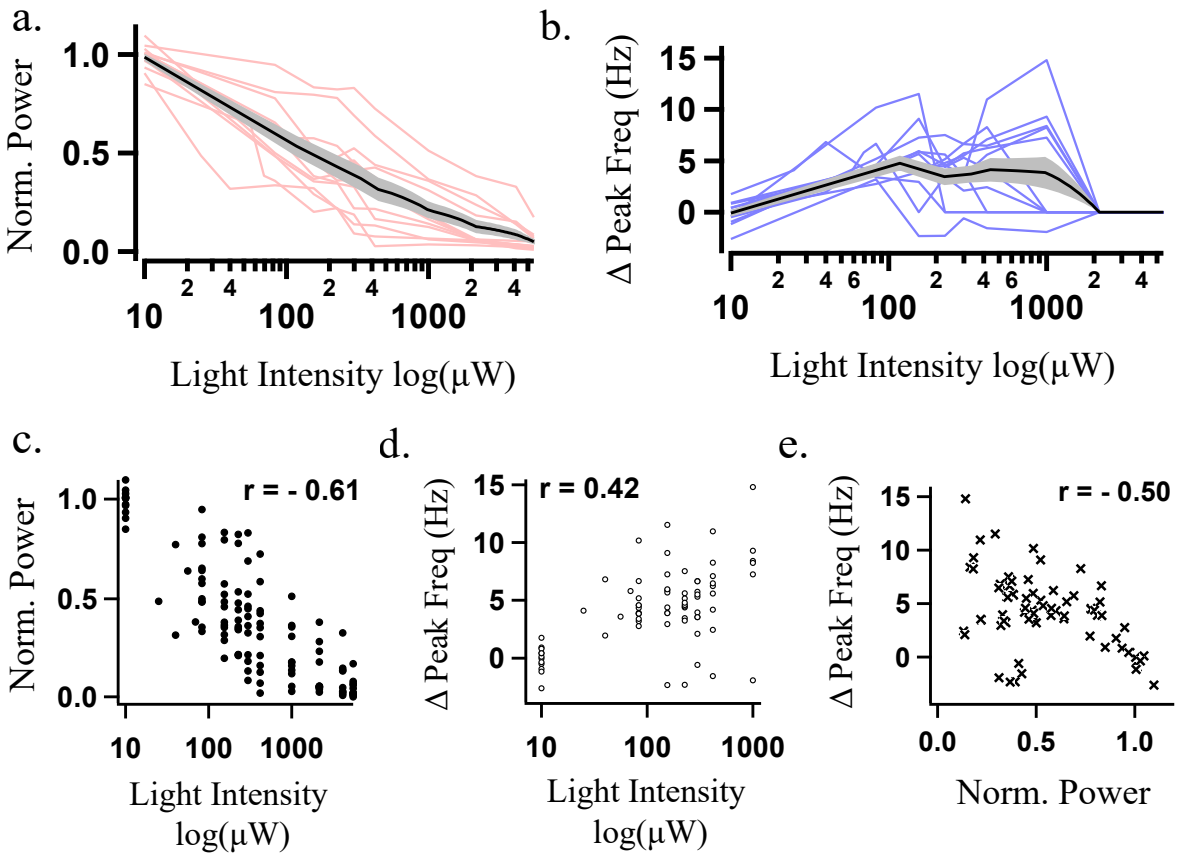


Figure 3.8: γ power decrease and peak frequency increase are proportional to light intensity. a) Power-area change between light stimulation period and baseline plotted against light intensity. Red lines represent single experiments (n = 12). The black line is the average response and the grey shaded area represents standard error of the mean (SEM). b) Frequency difference between light stimulation period and baseline plotted against light intensity. Blue lines represent single experiments (n = 12). The black line is the average response and the grey shaded area represent SEM. c) Power-area change between light stimulation period and baseline plotted against light intensity; Pearson correlation: r = -0.61, n = 121 , $p < 0.00001$. d) Frequency difference between light stimulation period and baseline plotted against light intensity; Pearson correlation: r = 0.42, n = 75, $p < 0.0002$. e) Power-area change plotted against peak frequency difference between light stimulation period and baseline; Pearson correlation: r = -0.50, n = 75, $p < 0.00001$.

In order to estimate the maximal effect of PV+ IN stimulation, we pooled experiments using strong light intensity (n = 14 at 5.5 mW, n = 9 at 2.2 mW). Although the light intensity-response curves were not assessed in all cases, the experiments were merged because they exhibited similar effects. Overall, strong light illumination caused a substantial decrease in the normalised power-area (0.09 $\pm$ 0.029, $p < 0.001$, one-sample t-test; Fig. 3.9). The normalised power-area recovered significantly in the period following light stimulation (0.74 $\pm$ 0.004, $p < 0.001$, paired t-test) but not back to baseline levels ($p < 0.001$, one-sample t-test; Fig. 3.9). Indeed, the oscillations were abolished during strong light intensity illumination in 18 of the 23 experiments (as assessed by low power-area and impaired rhythmicity in the auto-correlation. See methods section 2.8.1 for further details). It is possible that the strong decrease in cch-induced γ oscillations could emerge from impaired action potential generation in PV+INs. This could arise from strong photocurrents in PV+INs leading to depolarisation block. However, it is unlikely that depolarisation block of PV+INs produces the observed changes, because the effects are graded and monotonic between low and strong light intensities (Fig. 3.8a). In order to further verify this, we recorded the LFP without the presence of cch during strong PV+IN light illumination (2.2 mW). Strong PV+IN photo-activation did not increase the LFP responses as demonstrated by the non-significant change in the root mean square between light on and off conditions (Fig. 3.10). On the contrary, PV+IN photo-activation silenced the network when activity was present (Fig. 3.10a). Therefore, strong PV+IN photo-activation does not seem to induce hyper-excitability or epileptiform bursts in neither the presence nor absence of cch. These results cannot exclude effects of depolarisation block at high light intensities, but are consistent with progressive inhibition of the hippocampal network that leads to its eventual silencing.

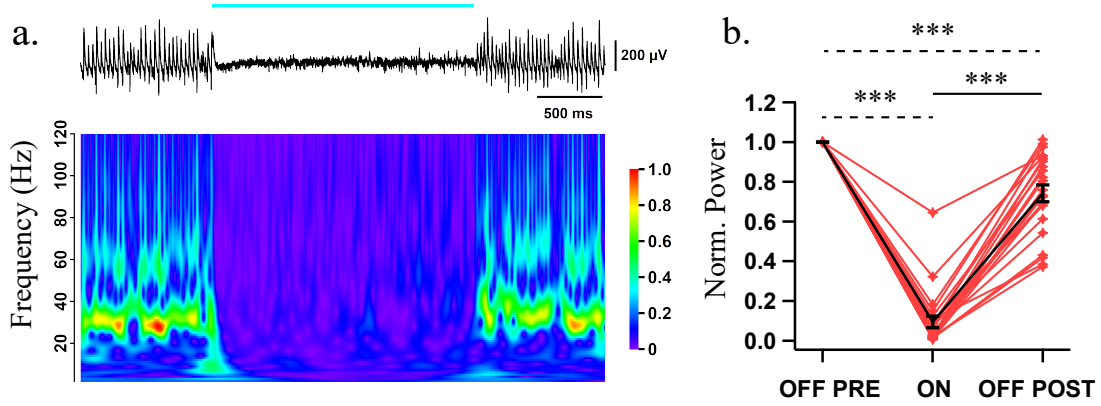


Figure 3.9: Strong photo-activation of PV+IN abolishes γ oscillations. a) Top: Representative LFP recording from CA3 area illustrating the inhibition of cch-induced γ oscillations to constant blue light illumination (5.5 mW). Bottom: Magnitude component of the wavelet transform normalised by its maximum value, brighter colours represent larger magnitude. b) Average change in power-area during (ON) and after light stimulation (OFF POST) normalised to baseline (OFF PRE). Red lines represent single experiments (n = 23). The black line is the average response and error bars represent SEM. One sample t-tests for comparison of ON and OFF POST periods to baseline, paired t-test for between conditions comparison (ON - OFF POST); ***p < 0.0001. Dashed brackets represent one sample t-tests and solid brackets represent paired t-tests.

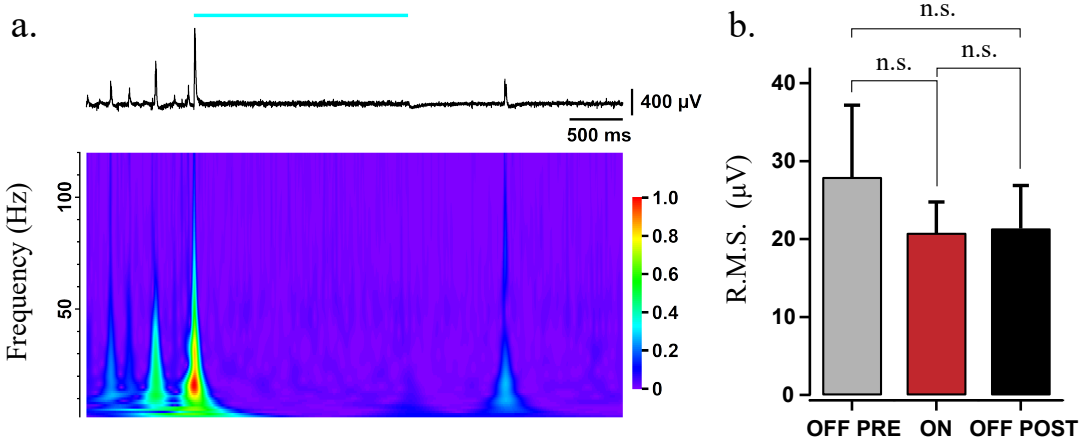


Figure 3.10: Strong photo-activation of PV+IN during spontaneous activity does not increase the local field potential. a) Top: Representative LFP recording from CA3 area illustrating the inhibition of spontaneous network activity (aCSF only) to constant blue light illumination (2.2 mW). Bottom: Magnitude component of the wavelet transform normalised by its maximum value, brighter colours represent larger magnitude. b) Average change in power-area normalised to baseline (n = 5). rmANOVA followed by post-hoc paired t-test for multiple comparisons. rmANOVA: $F(2, 8) = 1.073$, $p = 0.387$; $^{n.s.}p >= 0.05$.

3.6 THETA PHOTO-ACTIVATION OF PV+ INTERNEURONS DURING GAMMA OSCILLATIONS

γ oscillations that occur *in vivo* during exploration are usually observed nested in slower theta oscillations (8 - 12 Hz) (Bragin et al. 1995; Buzsáki 2002; Lisman et al. 2013). It is thus important to understand how this transient activation of PV+INs modulates ongoing γ oscillations. We therefore tested how theta drive to the PV+IN network would affect γ oscillation properties. Sinusoidal 8 Hz light stimulation (theta photo-activation) of PV+INs strongly modulated the amplitude of ongoing γ activity (Fig. 3.11a). Specifically, the instantaneous γ magnitude, assessed using the Hilbert transform, was negatively correlated with light intensity (Fig. 3.11 a) and was statistically significant across all experiments with an average Pearson coefficient of r = -0.51 $\pm$ 0.04 (Pearson correlation, n = 9501, Tcrit= 1.96, T> 23.2 in all experiments; Fig. 3.11c). These findings indicate that a transient increase in PV+IN activity causes a decrease in the power of the oscillation and vice versa. The peak frequency of the oscillation increased from 31.67 $\pm$ 0.620 Hz in the baseline period to 37.04 $\pm$ 1.312 Hz during theta photo-activation ($p < 0.01$, paired t-test; Fig. 3.11b). Like before, we quantified these experiments together with another batch of experiments at high light intensities and merged them because of similar effects (n = 12 at 5.5 mW, n = 7 at 2.2 mW). Strong theta photo-activation of PV+INs decreased the power of the oscillation robustly compared to the baseline period (0.20 $\pm$ 0.036, $p < 0.01$, one sample t-test; Fig. 3.11d, e and f). This resulted in the collapse of cch-γ oscillations in about half of the experiments (10 of 19). These experiments indicate that transient modulation of PV+IN activity at theta frequency can reliably modulate the power of cch-induced γ oscillations.

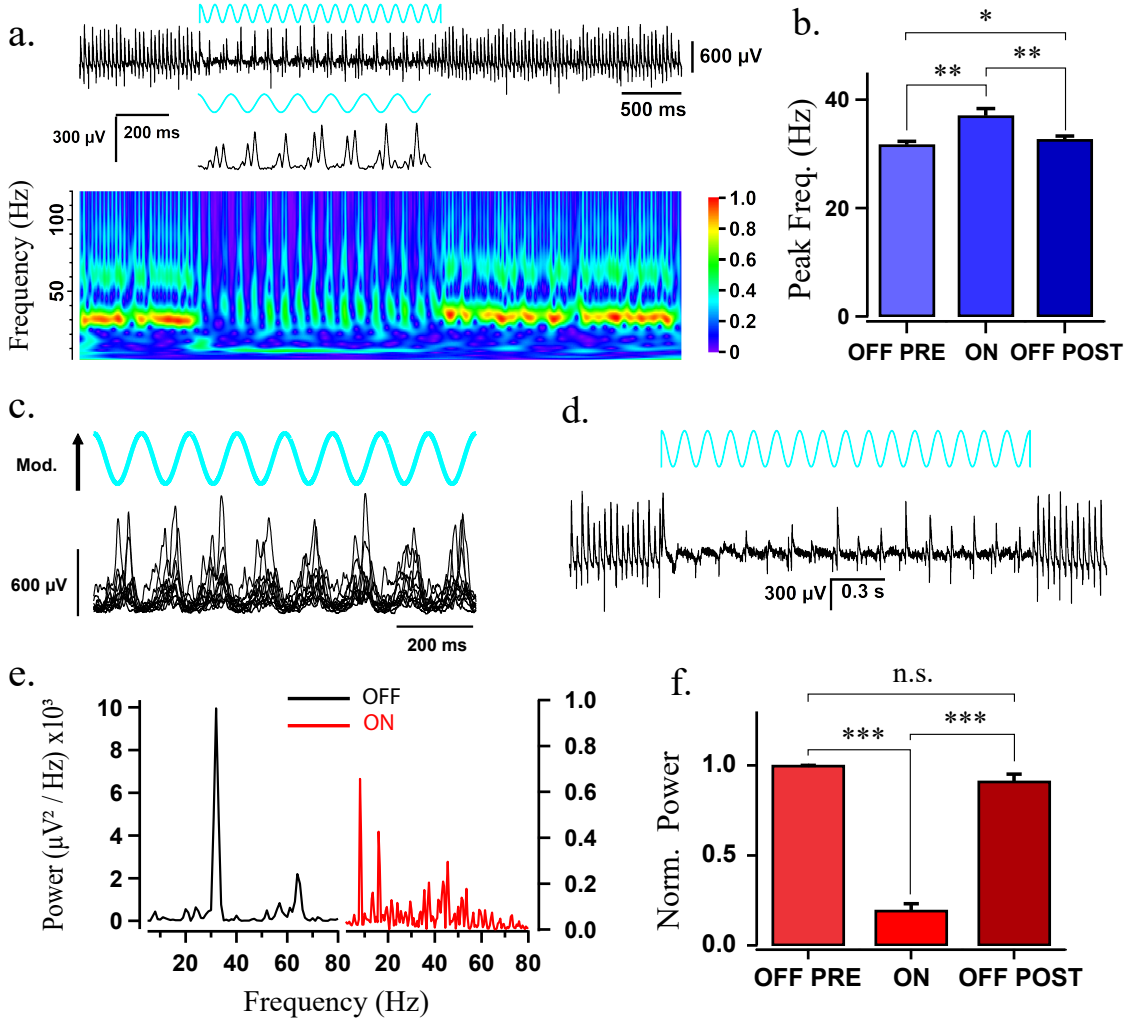


Figure 3.11: Theta photo-activation of PV+INs modulates γ oscillation amplitude. a) Top: Representative LFP recording from CA3 area illustrating the modulation of cch-induced γ oscillation envelope to 2 second sinusoidal blue light illumination (theta photo-activation) (1 mW). Middle: Instantaneous γ amplitude of the Hilbert transform of an enlarged section during theta photo-activation from a). Bottom: Magnitude component of the wavelet transform normalised by its maximum value, brighter colours represent larger magnitude. b) Average peak frequency before (OFF PRE), during (ON), and after (OFF POST) theta photo-activation (n = 12); rmANOVA followed by post-hoc paired t-test for multiple comparisons, rmANOVA, $F(1.09, 12.02) = 20.03$, $p < 0.0006$. c) Instantaneous γ amplitude of the Hilbert transform during theta photo-activation overlaid across experiments (n = 12). d) Representative LFP recording from CA3 area illustrating the inhibition of cch-induced γ oscillations by strong theta photo-stimulation (max 5.5 mW). e) Power spectrum of the recordings in d) showing that the power of the oscillation decreases greatly, ON = light stimulation period of 2 seconds, OFF = 1 second baseline period preceding light stimulation. f) Average change in power-area normalised to baseline (n = 19); one sample t-tests for comparison of ON and OFF POST periods to baseline, paired t-test for between conditions comparison (ON - OFF POST); *$p < 0.05$, **$p < 0.01$, ***$p < 0.001$, $^{n.s.}p >= 0.05$. Dashed brackets represent one sample t-tests and solid brackets represent paired t-tests.

3.7 MULTI-ELECTRODE ARRAY RECORDINGS DURING PV+ INTERNEURON PHOTO-ACTIVATION

In order to examine if PV+IN photo-activation silences the hippocampal network and to explore γ oscillation mechanisms in further detail we recorded unit activity during cch-induced γ oscillations. We used a 16 channel multi electrode array (MEA) to record unit-activity from CA3 hippocampal area (Fig. 3.12a). Spikes were detected as in Quian Quiroga 2009 and were clustered as in Fee et al. 1996 (Section 2.8.2). Following initial automatic clustering, clusters were manually merged but only if they had similar waveforms and responses to optogenetic stimulation. Clusters were then divided into fast-spiking (FS) if they had peak-to-trough (P2T) width less than 0.4 ms and into regular-spiking (RS) if had P2T width larger than 0.4 ms. If clusters had less than 1.4 % of their waveforms within 2 ms of their refractory period they were classified as single units (FS single and RS single) otherwise they were classified as multi-units (FS multi or RS multi). Using this classification a total of 9 FS single units, 19 RS single units, 15 FS multi-units and 42 RS multi-units were obtained from a total of 23 slices (n = total 27 sites). Sustained photo-activation of PV+INs (5.5 mW) decreased the spike counts in the majority of RS units and multi-units (RS single = 16/19, RS multi = 36/42; Fig. 3.12b). In addition, the majority of FS units and multi-units were also inhibited (FS single = 6/9, FS multi = 9/15; Fig. 3.12b). In order to ensure that these results did not depend on our classification criterion, we re-classified the clusters into FS if P2T width was smaller than 0.5 ms. Again, using this classification the majority of RS units were inhibited (RS single = 15/17, RS multi = 31/37; Fig. 3.12c). This indicates that RS unit activity decreases during PV+IN photo-activation and argues against network excitation via depolarisation block. In addition, the RS single/multi units fired on average at the trough of the γ cycle (1.02 Rad or 0.33 pi, NSOAValue > NSOA cirtical, Moore's version of Rayleigh's test, ; Fig. 3.12d). The FS single/multi units fired slightly

later in the cycle (1.70 or 0.54 pi, NSOAValue > NSOA cirtical, Moore's version of Rayleigh's test, ; Fig. 3.12d). This is consistent to previous studies which reported that fast-spiking interneurons fire with a monosynaptic delay after principal cells (Mann et al. 2005a). We also found 3 photo-tagged single units (+ 1 FS multi unit-P2T = 0.39 ms) that could follow light pulses at 40 Hz (P2T widths = 0.3, 0 0.39, 0.42 ms). These three units increased their firing in response to sustained light illumination and fired on the rising phase of the γ cycle. We present here one of those units (Fig. 3.13d).

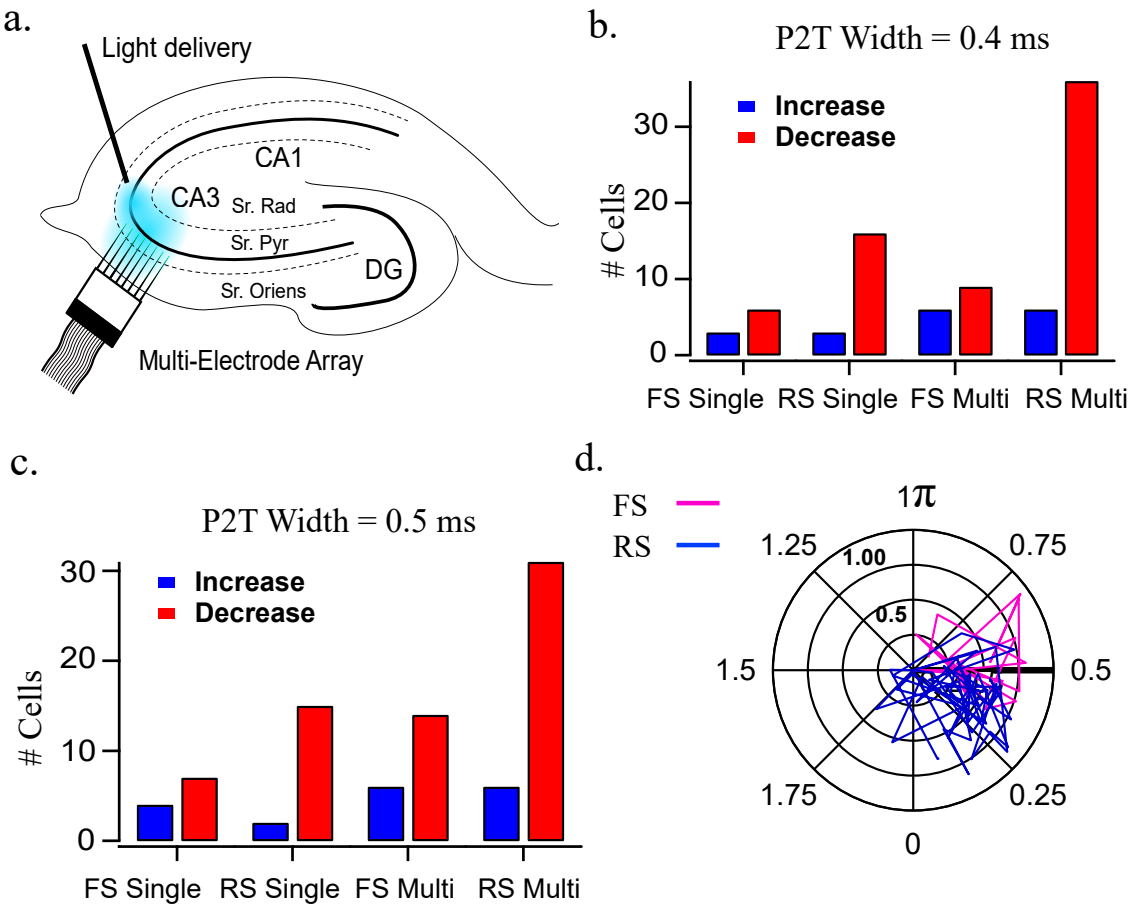


Figure 3.12: PV+IN photo-activation decreases unit activity during cch γ oscillations. a) Schematic diagram of the hippocampus illustrating MEA recordings during blue light illumination (5.5 mW) in CA3. b) Quantification of the number of clusters which change their firing in response to blue light illumination with cluster separation at 0.4 ms P2T width. c) Same as b) but the cluster separation threshold was set to 0.5 P2T width. d) Average firing phase of FS and RS clusters. CA3 = Cornu Ammonis 3, CA1 = Cornu Ammonis 1, DG = Dentate Gyrus, sr. Pyr. = stratum Pyramidale, sr. Rad. = stratum Radiatum, sr. Oriens = Stratum Oriens.

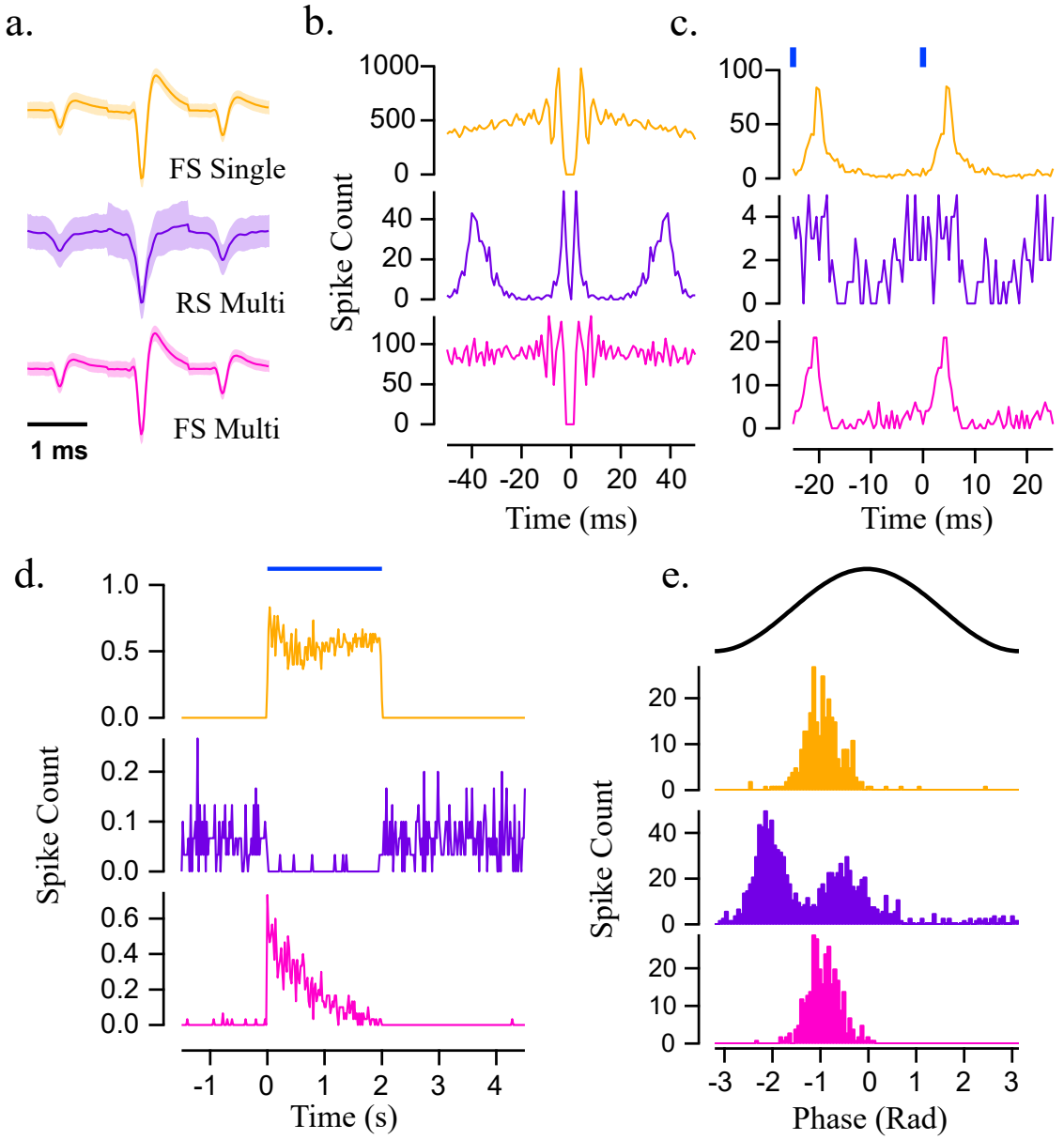


Figure 3.13: Example of PV+IN photo-activated unit (5.5 mW). a) Average waveforms of the detected clusters along three electrodes. Shaded regions represent standard deviation. b) Autocorrelation of the spike times of the clusters in a). c) Spike count of clusters in a) in responses to 1 ms pulses at 40 Hz (two pulses illustrated). d) Spike count of clusters in a to 2 second sustained light illumination. e) Phase occurrence (radians) of spikes from clusters in a) during cch-oscillations in the absence of light stimulation. Bimodal phase histogram of RS cluster could suggest that this recording includes pyramidal cells and RS interneurons.

3.8 PHOTO-INHIBITION OF PV+ INTERNEURONS DURING GAMMA OSCILLATIONS

Our photo-activation experiments demonstrated that PV+INs are sufficient for controlling γ network activity. In order to test if PV+IN activity is also necessary during cch-induced γ oscillations we expressed the inhibitory proton pump archaerhodopsin (Arch) in PV+INs (Chow et al. 2010). This was done in order to test how PV+IN photo-inhibition affects ongoing γ oscillation maintenance. We injected PV-cre mice with AAV carrying archaerhodopsin (Arch3-eYFP or ArchT-GFP). Expression of Arch in PV-cre mice was restricted to the pyramidal cell layer, in agreement to ChR2 injections (Fig. 3.14a).

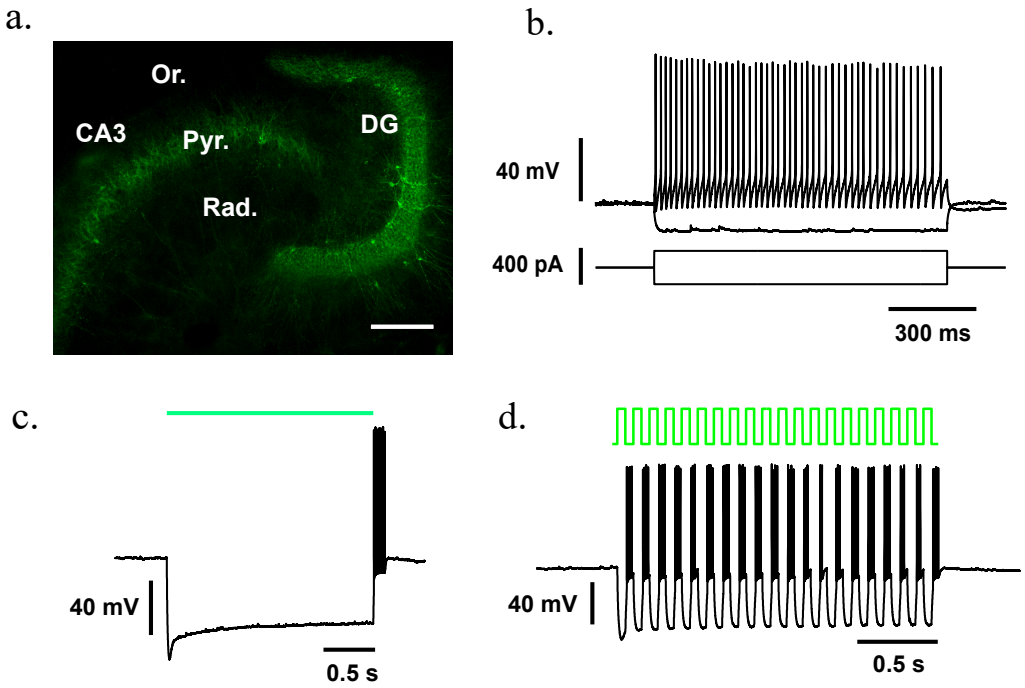


Figure 3.14: Functional expression of Arch in PV+INs. a) Confocal image of ventral hippocampus (350 μm slice) from PV-cre mice with eYFP-Arch3 expression. b) Current clamp recording in a PV+IN from CA3 area expressing ArchT-GFP in response to steps of depolarising and hyperpolarising current injections. c) Potent hyperpolarisation of a PV+IN during green light illumination (1.45 mW). d) Rebound spiking of a PV+IN during theta pulse illumination (10 Hz - 50 ms, 1.45 mW). CA3 = Cornu Ammonis 3, CA1 = Cornu Ammonis 1, DG = Dentate Gyrus, sr. Pyr. = stratum Pyramidale, sr. Rad. = stratum Radiatum, sr. Oriens = Stratum Oriens. Scale bars = 200 μm.

Intracellular recordings were performed from putative PV+INs cells (Fig. 3.14b) and a 2 second constant light illumination was applied. Sustained light illumination in opsin expressing cells caused a strong hyperpolarisation (Fig. 3.14c) with an average decrease of 29.9 ± 6.18 mV (n = 4 cells). Rhythmic light illumination was able to induce strong rebound spiking, making it unsuitable for reliable photo-inhibition of PV+INs (Fig. 3.14d). These results suggest that reliable photo-inhibition of PV+INs can be achieved by sustained green light illumination. Are PV+INs necessary for the maintenance of cch-γ oscillations? In order to address this question we recorded the LFP from hippocampal slices of PV-cre mice injected with Arch during cch-induced γ oscillations. Sustained photo-inhibition of PV+INs resulted in a small but significant reduction in the power-area in comparison to baseline period (0.83 ± 0.067, $p < 0.05$, one sample t-test; Fig. 3.15c). This was not accompanied by a significant change in the average peak frequency (OFF PRE = 30.83 ± 0.723 Hz, ON = 30.52 ± 1.26 Hz, $p >= 0.05$, paired t-tests; Fig. 3.15d). While the average changes in power and frequency were small, photo-inhibition of PV+INs often appeared to induce reversible effects, but these were not in the same direction across slices. However, in each case, the effects on power and frequency were not independent ($p < 0.005$, Pearson correlation, Fig. 3.16a). Specifically, in some experiments γ power was suppressed and the peak frequency was elevated (22 / 35 slices, Fig. 3.15ai and bi). Whereas, in other experiments the γ power increased and this was accompanied by a decrease in peak frequency (13 / 35 slices, Fig. 3.15aii and bii). This change along the frequency-amplitude axis is consistent with oscillations observed during *in vivo* recordings (Buzsáki et al. 2004). The direction of the effect could not be explained by the initial conditions, as the initial power of the oscillation during baseline period was not correlated with the change in power-area during PV+IN photo-inhibition (r = 0.19; Fig. 3.16b). In addition, the initial frequency of the oscillation during baseline was not correlated to either peak frequency difference or to the power-area change during PV+IN photo-inhibition (r = 0.17, r = 0.09, respectively; Fig. 3.16c, d).

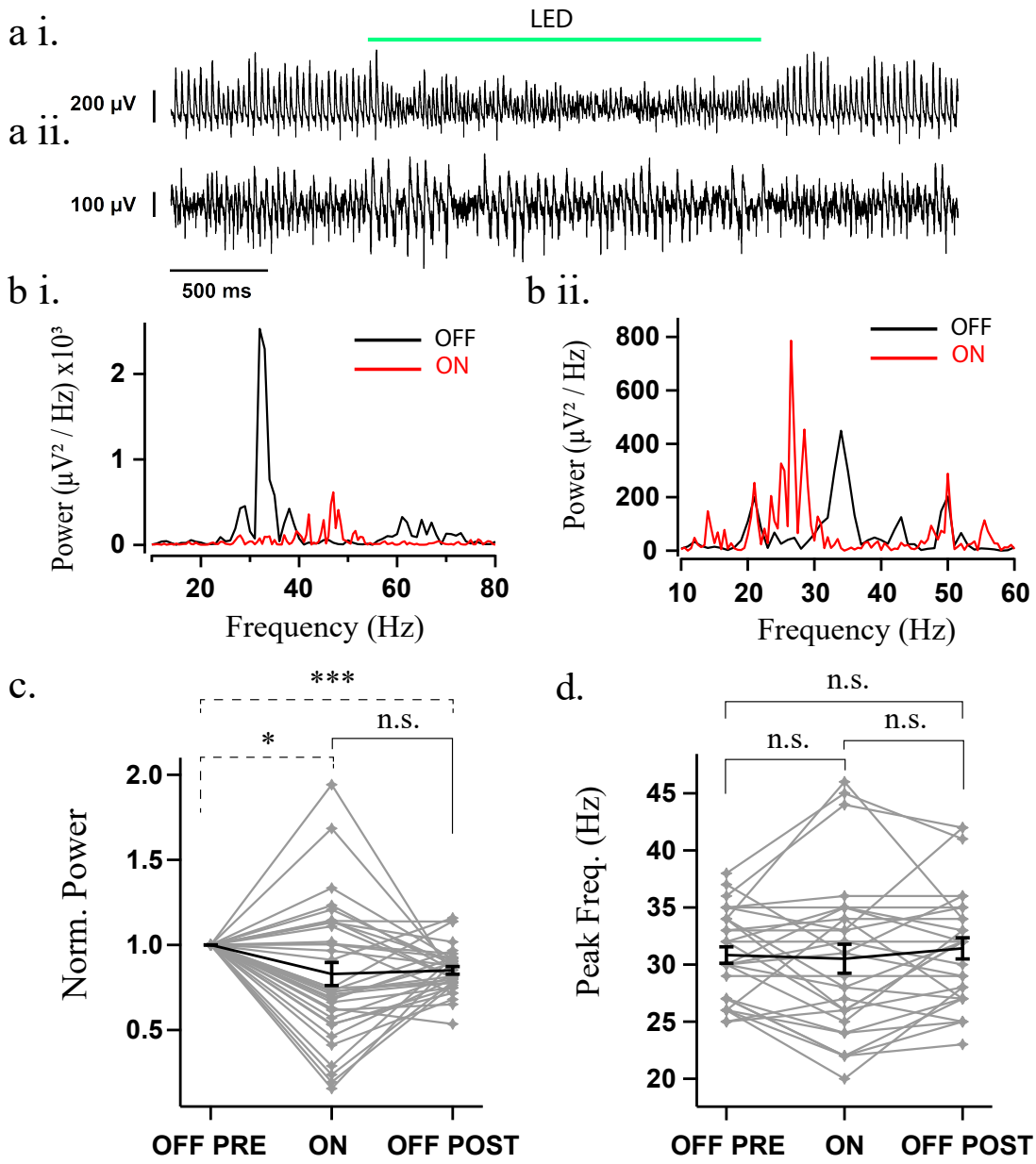


Figure 3.15: Sustained LED photo-inhibition of PV+INs produces inconsistent responses in γ oscillation power and frequency. a) Representative LFP recordings from CA3 area illustrating the two types of responses observed during sustained inhibition of PV+INs (2 second green light illumination - 4.25 mW). bi) Power spectrum of the LFP from ai) where γ power decreases and frequency increases. bii) Power spectrum of the LFP from ai) showing that the γ power increases and frequency decreases. c) Power-area during (ON) and after light stimulation (OFF POST) normalised to baseline (OFF PRE); one sample t-tests for comparison of ON and OFF POST periods to baseline, paired t-test between conditions comparison (ON - OFF POST), (n = 35). d) Average peak frequency; rmANOVA followed by post-hoc paired t-test for multiple comparisons, (n = 29). rmANOVA, $F(1.46, 40.74) = 0.69$, $p = 0.464$; *$p < 0.05$, **$p < 0.01$, ***$p < 0.001$, $^{n.s.}p >= 0.05$. Grey Lines represent single experiments, black line the population average, and error bars the SEM. Dashed brackets represent one sample t-tests and solid brackets represent paired t-tests.Yulin Tan contributed to data collection.

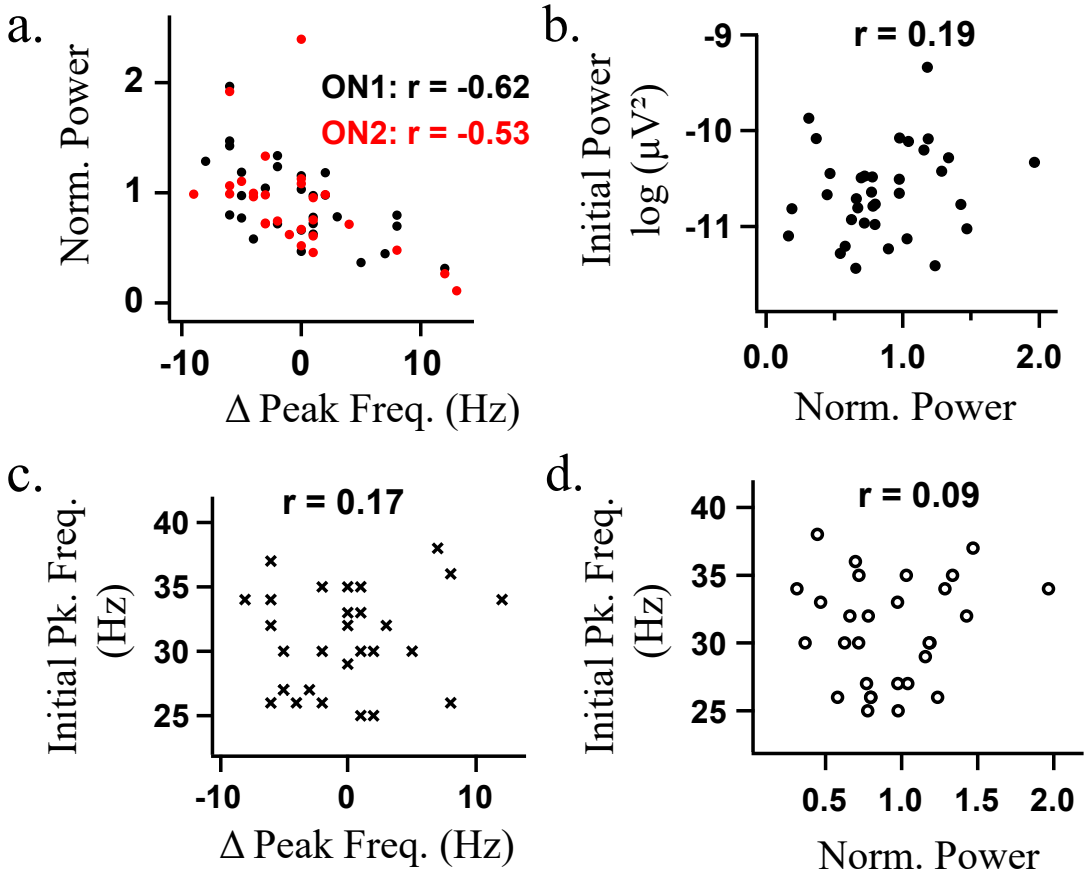


Figure 3.16: Sustained LED photo-inhibition of PV+INs elicits changes in power that are negatively correlated to differences in peak frequency (first half of stimulation: 1 - 2 seconds). a) power-area change against peak frequency difference during first and second halves of stimulation period (ON1: 0 - 1 seconds, ON2: 1 - 2 seconds) when compared to baseline period light-off period; Pearson correlation: ON1, r = -0.62, n = 29, p $<$ 0.0003 ; ON2, r = -0.53, n = 27, p $<$ 0.005. b) Logged initial power-area during baseline period plotted against power-area change during (ON1) and before light illumination; Pearson correlation, r = 0.19, n = 35, p = 0.28. c) Initial peak frequency during baseline period plotted against peak frequency difference during (ON1) and before light illumination; Pearson correlation, r = 0.17, n = 29, p = 0.37. d) Initial peak frequency during baseline period plotted against peak frequency difference during (ON1) and before light illumination; Pearson correlation, r = 0.04, n = 29, p = 0.82. Yulin Tan contributed to data collection.

It is possible that differential patterns of expression across slices could be responsible for driving the diversity of responses in these experiments. Interestingly, there was a small but consistent decrease of γ power-area (31 of 35 slices) in the period following light stimulation (0.851 $\pm$ 0.023, $p < 0.001$; Fig. 3.15c). In contrast, the peak frequency was not different during the the period following PV+IN photo-inhibition (31.41 $\pm$ 0.937 Hz, $p = 1.00$, paired t-test; Fig. 3.15d). It is important to mention that few of these experiments were performed with an amber led ($n = 9$). In addition, animals expressing either Arch3.0-eYFP or ArchT-GFP were used in these experiments ($n = 6$, $n = 29$, respectively). Importantly, the two types of responses were observed in a batch of animals with just ArchT expression and where the green led was used only ($n = 20$ slices). Collectively, these results suggest that LED photo-inhibition of PV+INs at light intensities of 2 - 5 mW did not produce consistent effects.

3.9 PHOTO-INHIBITION OF PV+ INTERNEURONS WITH LASER ILLUMINATION

There is a possibility that these inconsistent effects arising from PV+IN inhibition are caused by the inability of our system to break the strong recurrent feedback with pyramidal cells and silence PV+INs (Mann et al. 2005b; Oren et al. 2006). Particularly, photo-inhibition of PV+INs can dis-inhibit pyramidal cells and lead to increased excitatory drive on PV+INs, making it difficult to prevent their spiking. To circumvent this possibility, we used green laser illumination with greater light intensity that lasted for a longer duration with the prospect of increasing photo-inhibition and potentially silencing PV+IN terminals (El-Gaby et al. 2016). To achieve this, slices with PV+ cells expressing ArchT-GFP were illuminated with a green laser light for a duration of approximately 20 seconds. Inhibition of PV+INs with sustained laser illumination decreased the power of the oscillation reliably (Fig. 3.17a, b). Even though the power of the oscillation sometimes increased in the first

half of the stimulation (ON1) this was not statistically different on the population average when compared to baseline (ON1= 1.00 ± 0.088, p = 1.00, one sample t-test; Fig. 3.17d). Moreover, the power was significantly lower during the second half of the stimulation (ON2) (ON2 = 0.58 ± 0.085, $p < 0.01$, one sample t-test) and remained depressed in the 10 second period following light stimulation (OFF POST= 0.77 ± 0.071, $p < 0.05$, one sample t-test; Fig. 3.17d). The decrease in power during the light off period after stimulation could arise from successfully silencing of PV+IN terminals. On the other hand, the peak frequency of the oscillation did not change on average during light stimulation when compared to baseline (OFF PRE= 32.51 ± 0.727 Hz, ON1 = 30.30 ± 1.115 Hz, ON2 = 32.14 ± 1.229 Hz ;, OFF POST = 34.21 ± 0.0692 Hz, $p > 0.05$, paired t-tests; Fig. 3.17c,e). Lastly, we plotted the power change in the second half of the stimulation against different light intensities (Fig. 3.18a). We found that there was negative correlation between light intensity (approximate) and change in power-area (r = -0.49; Fig. 3.18b), meaning that as light increased the γ power progressively decreased. A weak and positive correlation of peak frequency difference to light intensity was also found (r = 0.24; Fig. 3.18c), meaning that the frequency of the oscillation increased as the light intensity became greater. However, this does not reflect an increase in frequency above baseline, but rather a stronger reduction in frequency at lower laser powers. Moreover, the peak frequency difference was not found correlated to power-area change (r = -0.19; Fig. 3.18d), and this breakdown in the frequency-amplitude relationship could be consistent with slightly different mechanisms of inhibition via activation of ArchT with LED and laser illumination. In support of this, the time-course of γ power reduction was much slower during the laser experiments consistent with that of terminal inhibition (El-Gaby et al. 2016). Overall, it appears that strong photo-inhibition of PV+INs by ArchT reliably impairs the power of γ oscillations, suggesting that PV+INs are necessary for proper functioning of the network generating γ oscillations.

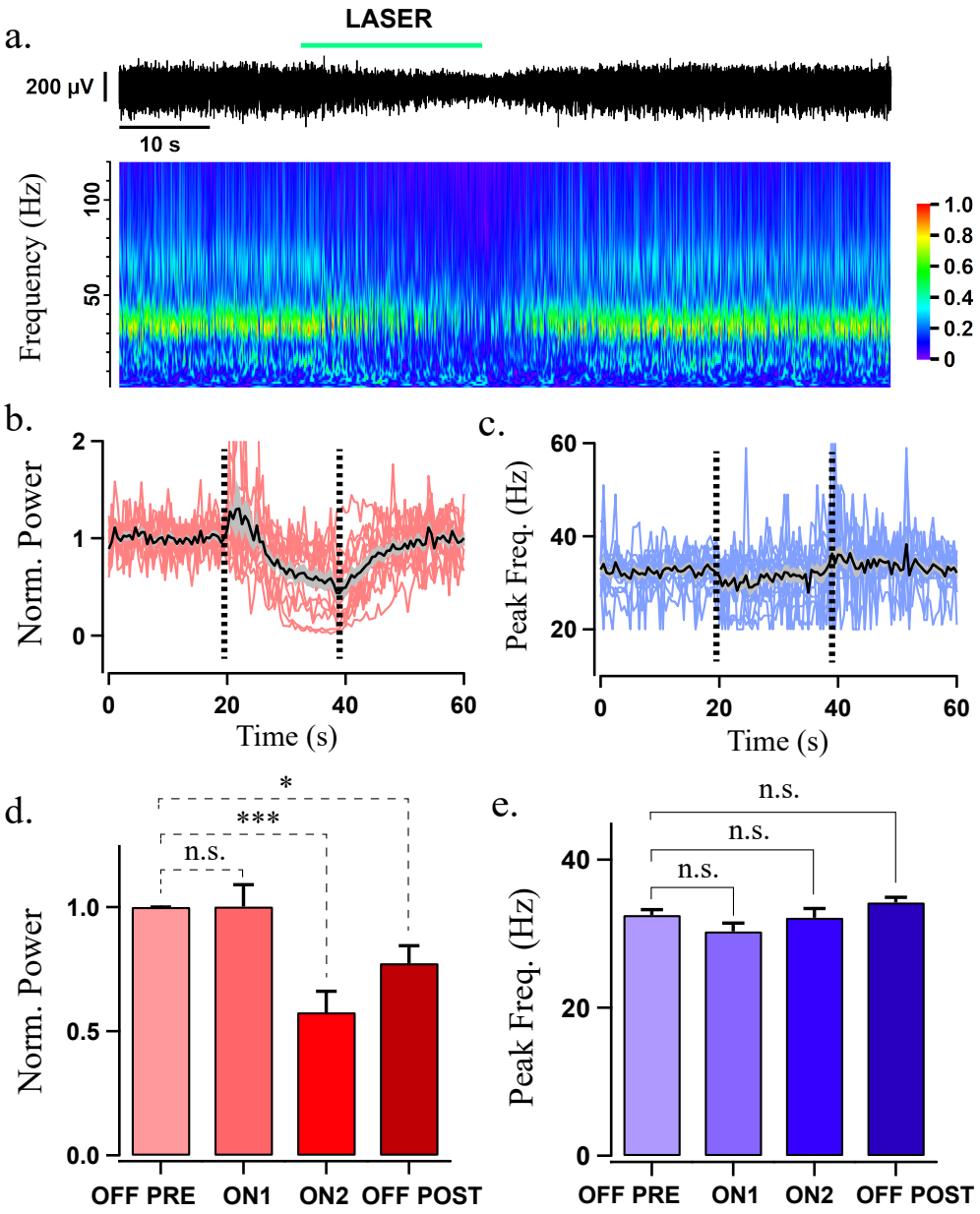


Figure 3.17: Sustained photo-inhibition of PV+INs using laser illumination suppresses γ power. a) Top: Representative LFP recording from CA3 area during inhibition of cch-induced γ oscillations by green laser illumination (approx. 18.6 mW). Bottom: Magnitude component of the wavelet transform normalised by its maximum value, brighter colours represent larger magnitude. b) Change in power-area normalised to baseline calculated in 1 second bins across experiments (n = 14). c) Peak frequency of the oscillation calculated in 1 second bins across experiments (n = 14). Time between dotted lines indicates the duration of laser illumination. d) Average power-area change normalised to baseline; one sample t-tests for comparison of ON1, ON2 and OFF POST periods to baseline. e) Average peak frequency; rmANOVA, $F(1.53, 19.83) = 7.13$, $p < 0.008$. Repeated measures ANOVA followed by post-hoc paired t-test for multiple comparisons; *$p < 0.05$, **$p < 0.01$, ***$p < 0.001$, $^{n.s.}p >= 0.05$. OFF PRE: 20 second Baseline, ON1: 0 - 10 seconds laser stimulation, ON2: 10 - 20 seconds laser stimulation, OFF POST: 10 second period following light stimulation. Dashed brackets represent one sample t-tests and solid brackets represent paired t-tests.

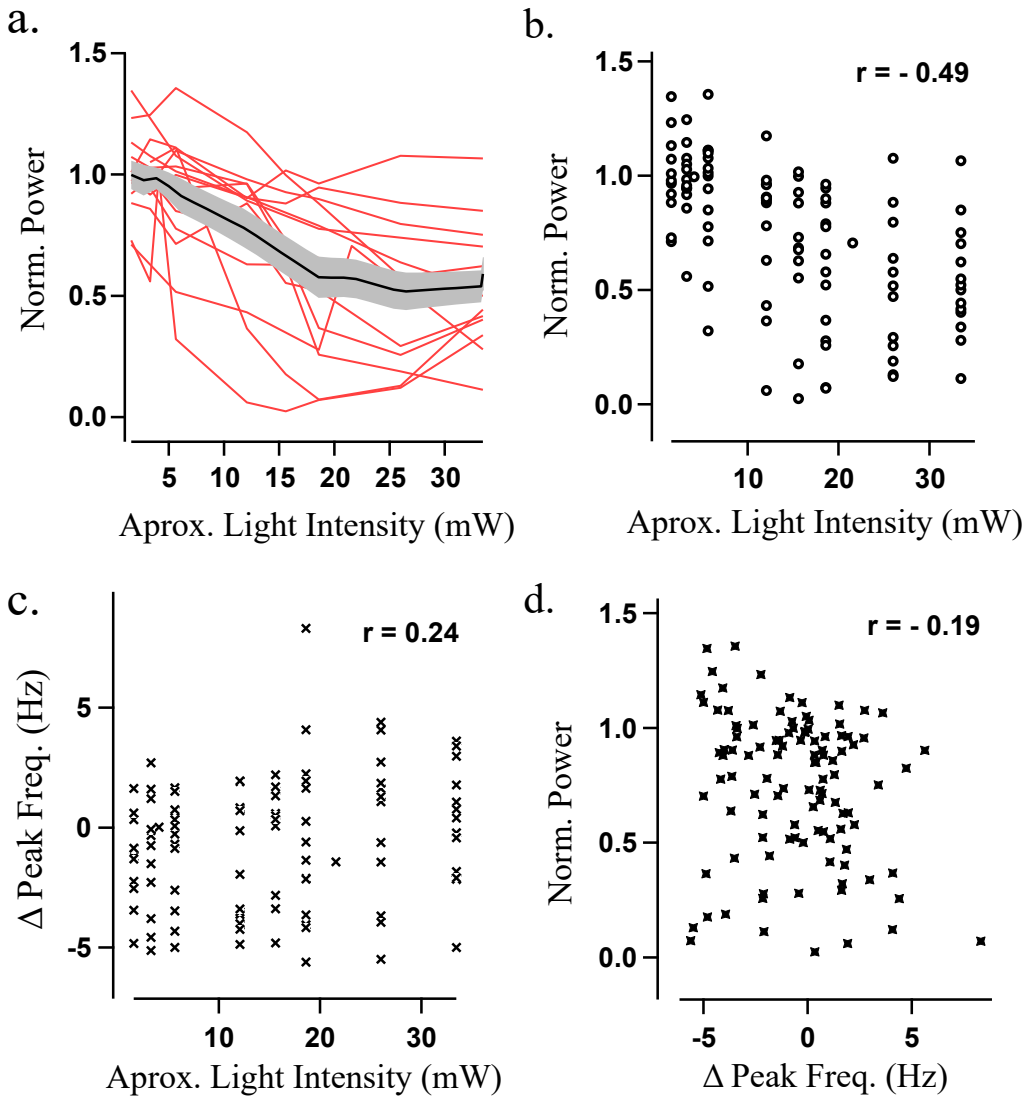


Figure 3.18: Laser power correlates negatively with γ oscillation power. a) Power-area change between the last half of laser stimulation to baseline against approximate light intensity. Red lines represent single experiments (n = 14). The black line is the average response and the grey shaded area represents SEM. b) power-area change between the last half of laser stimulation to baseline against approximate light intensity. Pearson correlation: r= -0.49, n = 107, $p < 0.0001$. c) Frequency difference between the last half of laser stimulation to baseline against approximate light intensity. Pearson correlation: r = 0.24, n = 107, $p < 0.012$. d) Power-area change against peak frequency difference between last half of laser stimulation period and baseline. Pearson correlation: r = -0.19, n = 107, p = 0.053.

3.10 SUPPLEMENTARY INFORMATION

In order to ensure that the effects of PV+IN inactivation to γ oscillation power were not caused by strong light intensity, we tested whether high laser power illumination (approx. 41 mW) can alter γ properties. We illuminated ventral hippocampal slices expressing tdTomato in PV+ cells with a constant green laser stimulus for approximately 1 minute. There was no significant change in frequency and power during laser illumination when compared to baseline period (Fig 3.19). Consequently, the effects we observed before cannot be replicated by laser stimulation in PV+INs that express only reporter fluorophore.

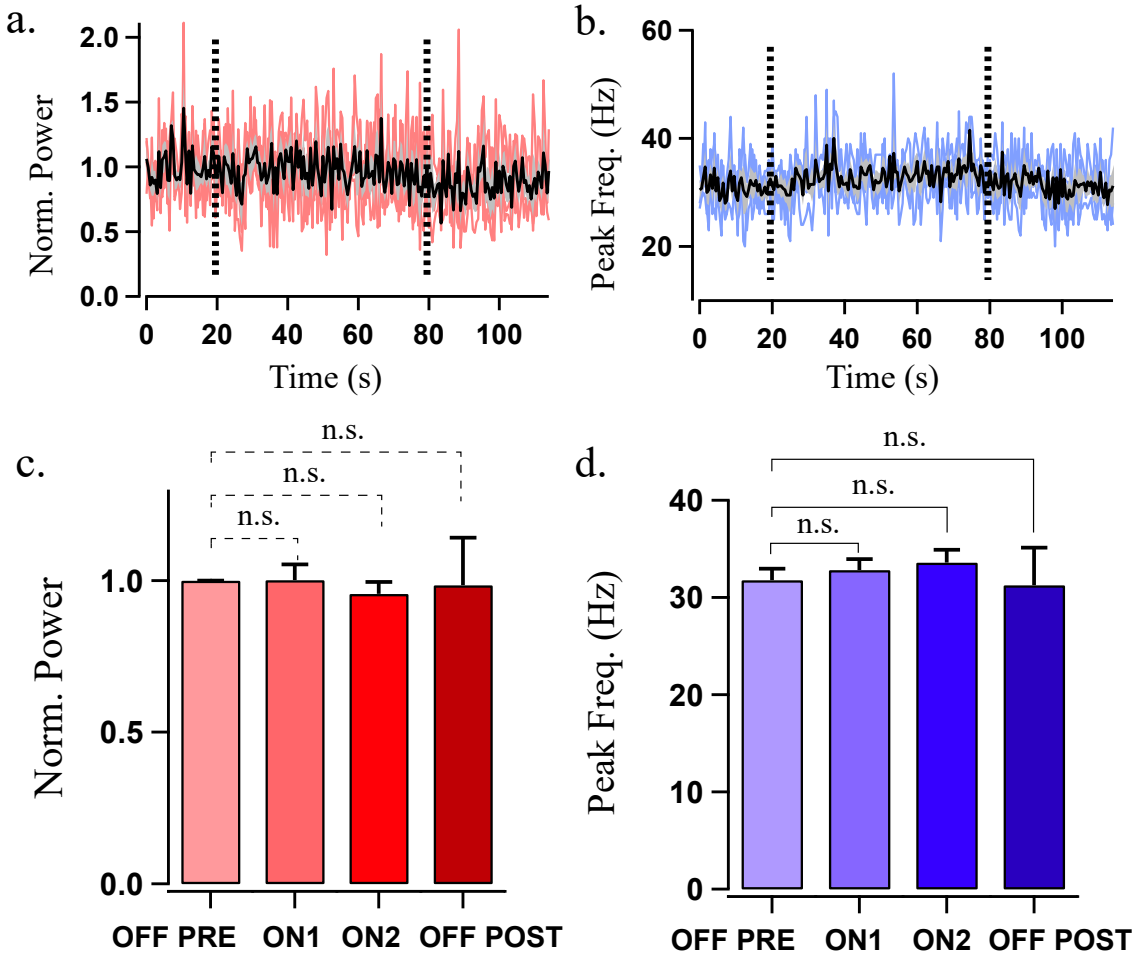


Figure 3.19: Laser illumination in PV+INs expressing tdTomato is not sufficient to alter γpower. a) Change in power-area normalised to baseline calculated in 1 second bins across experiments (n = 4). b) Peak frequency of the oscillation calculated in 1 second bins across experiments (n = 4). Time between dotted lines indicates the duration of laser illumination (duration of approx. 1 minute and a light intensity of approx. 41 mW). c) Average power-area change normalised to baseline; one sample t-tests for comparison of ON1, ON2 and OFF POST periods to baseline. d) Average peak frequency; rmANOVA, $F(3, 9) = 0.46$, $p = 0.716$. Repeated measures ANOVA followed by post-hoc paired t-test for multiple comparisons; *$p < 0.05$, **$p < 0.01$, ***$p < 0.001$, $^{n.s.}p >= 0.05$. OFF PRE: 20 second Baseline, ON1: 0 - 10 seconds laser stimulation, ON2: 10 - 20 seconds laser stimulation, OFF POST: 10 second period following light stimulation. Dashed brackets represent one sample t-tests and solid brackets represent paired t-tests.

3.11 DISCUSSION

The results presented here illustrate that PV+INs are powerful modulators of the hippocampal network and that their activity is required for cch-induced γ oscillations. Specifically, we demonstrated that 40 Hz photo-stimulation of PV+INs was capable of entraining ongoing cch-oscillations in the CA3 (even though the power of the oscillation often decreased) (Fig. 3.5). This reinforces previous findings suggesting that perisomatic inhibition is critical for the synchronisation of principal cells at fast time-scales, a requirement for the generation of γ oscillations across cortical circuits (Bartos et al. 2007; Buzsáki et al. 2012; Cardin et al. 2009; Mann et al. 2005b; Sohal et al. 2009). Furthermore, we found that tonic photo-activation of PV+INs decreased the power and increased the frequency of the cch-oscillations (Fig. 3.6). This suggests that activation of PV+INs can strongly modulate γ oscillation properties of the CA3 hippocampal network. Moreover, strong photo-activation of PV+INs abolished γ oscillations in most experiments and decreased unit activity demonstrating that strong perisomatic inhibition may be able to silence the hippocampal network (Fig. 3.9 and 3.12). The above experiments show that PV+INs are capable of modulating ongoing γ oscillations but not if they are also necessary for their generation. Thus, we directly tested this by photo-inhibiting PV+INs during ongoing cch-γ oscillations. Even though LED photo-inhibition of PV+INs produced inconsistent responses (Fig. 3.15), strong laser illumination resulted in robust decreases of γ power (Fig. 3.17) indicating that PV+IN activity is required for cch-induced γ oscillation maintenance in CA3.

3.11.1 MECHANISMS GOVERNING HIPPOCAMPAL NETWORK MODULATION DURING PV+ INTERNEURON PHOTO-ACTIVATION

3.11.1.1 CELLULAR DISINHIBITION THROUGH DEPOLARISATION BLOCK

As mentioned before, we found that progressive photo-activation of PV+INs decreased the power and increased the frequency of γ oscillations leading to an eventual collapse of the LFP. One consideration is that ChR2 activation in PV+INs could cause depolarisation block thereby silencing PV+INs and inducing the observed effects through disinhibition of pyramidal cells (or other interneurons). In support of this, interneurons have been shown to be especially prone to depolarisation block from ChR2 activation (Herman et al. 2014). However, we observed that the changes in power and frequency were graded and monotonic. Even if the depolarisation block of PV+INs produces graded responses at increasing light intensities it is unlikely that its effects would be monotonic. Instead, a biphasic response curve would be expected. This would occur since at low light intensities less cells would enter depolarisation block than become photo-activated whereas, at high light intensities the opposite would occur. Therefore, as the light intensity increases, the magnitude of the observed response would reverse producing a biphasic response curve. There is however a possibility that the light steps we used to photo-activate PV+INs were not small enough to sample the first portion of the curve and thus it is possible that we have sampled only the portion of the curve where depolarisation block prevails. However, this is not supported by our finding that PV+IN photo-activation decreases unit activity of RS cells (Fig. 3.12). RS cells are thought to mainly consist of principal/pyramidal cells (Csicsvari et al. 1999; McCormick et al. 1985; Mitchell et al. 2007; Vinck et al. 2013). Thus, it seems that strong PV+IN photo-activation decreases pyramidal cell activity. This would be inconsistent with depolarisation block of PV+INs as this would have disinhibited the pyramidal cell population and increased their activity (as in Herman et al. 2014). The activity of some FS cells also

decreased (Fig. 3.12). PV+ interneurons have been shown to be a major component of this group (Csicsvari et al. 1999; McCormick et al. 1985; Mitchell et al. 2007; Vinck et al. 2013). Thus, the data indicate that some of the PV+ cells could be entering depolarisation block. However, it has been shown that construct delivery using the same viral serotype does not infect all the PV cells in cortex (Sohal et al. 2009). In addition, FS cells also consist of other interneuron types like somatostatin interneurons (E. H. Buhl et al. 1996; Ma et al. 2006; Vinck et al. 2016), a finding that we also observed from our intracellular recordings. Lastly, strong photo-activation of PV+INs silenced the spontaneous network activity in the LFP (when present) arguing against disinhibition of the pyramidal cell population (Fig 3.10). All in all, our experiments point against but cannot fully exclude depolarisation block as the major determinant γ modulation during PV+IN photo-activation.

3.11.1.2 DIRECT PV+ INTERNEURON EXCITATION DURING PHOTO-STIMULATION

It has been demonstrated that cch-induced oscillations in CA3 support a PING mechanism of generation, where phasic synaptic excitation from pyramidal cells is critical for the synchronisation of the hippocampal network (Hajos 2004; Mann et al. 2005b; Oren et al. 2006). Specifically, phasic excitation of PV+INs and their feedback inhibition back to pyramidal cells is the mechanism that has been proposed to give rise to cch γ oscillations (Buzsáki et al. 2012; Hájos et al. 2009; Mann et al. 2007; Oren et al. 2006, 2010; Traub et al. 2000). If PV+IN activity is indeed elevated during photo-activation, then the duration required for PV+INs to reach the action-potential threshold on average will be reduced. This decreases the time taken for PV+INs to apply synaptic inhibition and shortens the γ cycle hence increasing the frequency of the oscillation. In addition, the pyramidal cells will receive on average more inhibition hence, producing less excitation leading to cycles of smaller amplitude. The oscillation likely collapses during strong PV+IN photo-activation because perisomatic inhibition from PV+INs silences the principal cells completely

(Li et al. 2017; Sachidhanandam et al. 2013).

On the other hand, the PV+IN network also has the anatomical and physiological properties required to generate interneuron network γ (ING) oscillations without the requirement of phasic excitation (Section 1.5.3.1). Our results could also be consistent with an ING mechanism where stronger activation of interneurons results in smaller and faster oscillations (Traub et al. 1996b; Whittington et al. 2011). However, tonic PV+IN photo-activation during spontaneous network activity is not sufficient to generate oscillations (Fig. 3.10). This probably results from the strong perisomatic inhibition that PV+INs exert on the pyramidal cell population and leads to their complete silencing. More tests are required where subtle elevation of PV+IN activity matches an increase in tonic excitation of the hippocampal network. Given that tonic excitation alone is not sufficient to generate oscillations.

3.11.2 MECHANISMS GOVERNING HIPPOCAMPAL NETWORK MODULATION DURING PV+ INTERNEURON PHOTO-INHIBITION

Weak photo-inhibition of PV+INs (LED $<$ 5mW) produced inconsistent responses in γ oscillation properties but strong laser illumination (approx. 18 mW) resulted in a reliable decrease in γ power (Fig. 3.15, 3.17). The difficulty of PV+IN photo-inhibition may arise from a combination of PV+IN circuit properties along with the difficulty of inhibiting synaptic release. Firstly, PV+INs receive fast and strong synaptic inputs from pyramidal cells during γ oscillations (Oren et al. 2006) which are difficult to suppress. Furthermore, PV+INs have strong reciprocal connections with pyramidal cells (Bartos et al. 2012; Hofer et al. 2011; Kohus et al. 2016; Oren et al. 2006; Packer et al. 2011). Thus, photo-inhibition of PV+INs will lead to up-regulation of pyramidal cell activity that in turn results to even stronger excitation back to PV+INs. Therefore, it seems difficult to prevent PV+INs from spiking during γ oscillations.

One alternative way to inhibit PV+IN function is by silencing their synaptic

terminals. However, to affect synaptic terminal release using optogenetics it seems that stronger light intensity is required than somatodendritic compartments (Jackman et al. 2014). Furthermore, to silence the presynaptic terminals it seems that longer stimulation times are required (El-Gaby et al. 2016). In support of this, it has been demonstrated that acute hyperpolarisation of synaptic terminals boosts action potential driven (evoked) release (given that action potential induction is not inhibited; Rama et al. 2015). Indeed, our laser illumination impaired oscillations reliably but required a longer timescale (around 10 sec) than arch photo-activation (in the order of milliseconds, Chow et al. 2010). However, it has also been shown that long term illumination of synaptic terminals expressing Arch can result in either increase in spontaneous release (Mahn et al. 2016) or decrease in evoked release (El-Gaby et al. 2016; Mahn et al. 2016). The altered neurotransmitter release in both experiments may have been caused from elevated pH and increased calcium (El-Gaby et al. 2016; Mahn et al. 2016). Moreover, it has been suggested that the differences in effects between spontaneous and synaptic release could be due to their differential dependence on calcium concentration (El-Gaby et al. 2016; Ramirez et al. 2011).

Our experiments indicate that evoked release was most likely affected during PV+IN photo-inhibition since the time taken for reliable γ inhibition (around 10 seconds) coincides only with robust changes in evoked release (El-Gaby et al. 2016; Mahn et al. 2016). In addition, during γ oscillations PV+INs fire action potentials at high rates (Gulyás et al. 2010; Hajos 2004) thus the synaptic inhibition received by pyramidal cells will likely be dominated by evoked release. Consequently, it seems that a decrease in γ power arises due to decreased GABA release from PV+INs. Furthermore, in the light – off period following laser stimulation, γ power did not recover immediately (Fig. 3.17). This reinforces the assumption that PV+IN terminals have been biochemically silenced and that the PV+IN - pyramidal feedback loop has been successfully impaired. In conclusion, we have shown for the first time that direct reduction in PV+IN activity impairs γ oscillations in the CA3. Taken

together with the photo-activation experiments our data show that PV+INs are powerful modulators of principal cell activity that can synchronise principal cells but are also necessary for cch γ generation. Moreover, PV+IN excitation and inhibition are likely to have similar effects, because they both interfere with PING mechanisms.

Chapter 4

The Role of Somatostatin - Expressing Interneurons in Hippocampal Gamma Oscillations

4.1 INTRODUCTION

In the previous chapter it was confirmed that parvalbumin (PV+) interneurons significantly contribute to the generation of carbachol-induced γ oscillations in CA3. However, PV+ interneurons represent about a third of the interneuron population in the brain (Hua Hu et al. 2014; Pfeffer et al. 2013), it is therefore possible that other interneuron populations are involved in the generation of γ-band oscillations. This could happen either from the direct involvement of another interneuron type to γ rhythmogenesis or indirectly affecting PV+ interneuron activity (Cardin 2016; Mann et al. 2005a). Indeed, dendrite-targeting somatostatin-expressing (SST+) interneurons have been recently implicated in high β / low γ frequency oscillatory activity generation in the primary visual cortex of awake mice (G. Chen et al. 2017; Veit et al. 2017). However, it is not yet known if the involvement of SST+ interneurons is specific to visually induced oscillations in V1 or if it is a general phenomenon that occurs across brain areas. In the current study, we examined whether SST+ interneurons are involved in the generation of oscillations induced *in vitro* by application of carbachol. We used optogenetic probes (as shown in Chapter 3 - PV+) to modulate the activity of SST+ interneurons. We first tested if rhythmic

photo-activation of SST+ interneurons could entrain carbachol-induced γ oscillations. We then proceeded by investigating how upregulation of SST+ interneuron activity could alter carbachol γ oscillations. Surprisingly, we found that strong photo-activation of somatostatin interneurons was sufficient to induce *de novo* high-frequency oscillations in the γ-band range even in the absence of carbachol. We therefore investigated the mechanisms of *de novo* high-frequency oscillations using intracellular, LFP and MEA recordings. Finally, we tested if SST+ interneuron activity is necessary for the maintenance of carbachol-induced γ oscillations. To achieve that, we selectively expressed the inhibitory light-activatable pump archaerhodopsin in SST+ interneurons and photo-inhibited them during carbachol-induced γ oscillations. These experiments indicate that SST+ interneuron activity is necessary for the generation of *in vitro* γ oscillations in CA3. In addition, they suggest that SST+ interneurons may be able to generate high-frequency γ oscillations in the hippocampus.

4.2 RHYTHMIC PHOTO-STIMULATION OF SST+ INTERNEURONS

Previously, we showed that perisomatic inhibition from PV+INs can entrain the hippocampal network at γ frequencies. This is in line with earlier findings which highlight the importance of this type of inhibition in network synchronisation during γ oscillations (Bartos et al. 2007; Mann et al. 2005a; Oren et al. 2006; Sohal et al. 2009). Here we first sought out to test if dendritic inhibition arising from SST+INs is also capable of synchronising the network at γ frequencies. In order to test if rhythmic activation of somatostatin - expressing interneurons (SST+INs) can affect the generation of γ oscillations in hippocampal area CA3, their activity had to be manipulated with temporal precision. To achieve that, we injected, AAV-ChR2 along with a fluorescent reporter (mCherry or eYFP) in SST-cre mice. Visualisation of the fluorescence signal from slices in these animals indicated that there was reliable expression of the viral construct. The fluorescent signal was widespread but mostly restricted to regions in CA3 where the dendrites of principal cells were present (Fig. 4.1). This is in agreement with SST+INs being mostly dendrite - targeting GABAergic neurons, even though they consist of a heterogeneous group of neurons (Lovett-Barron et al. 2012; Ma et al. 2006; Muller et al. 2014; Urban-Ciecko et al. 2016).

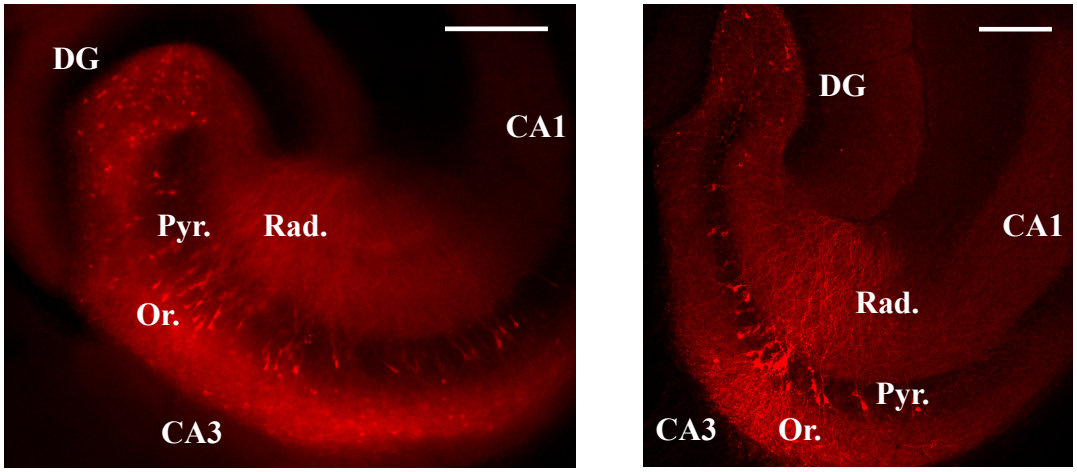


Figure 4.1: Expression of ChR2-mCherry in SST+INs. Left: Fluorescence and Right: Confocal image of ventral hippocampal slices (350 μm) from SST-cre mice with mCherry-ChR2 expression. The expression of mCherry is mainly restricted to the oriens, radiatum and lacunosum moleculare layer, as would be expected when visualising the projections of SST+ dendrite-targeting interneurons. CA3 = Cornu Ammonis 3, CA1 = Cornu Ammonis 1, DG = Dentate Gyrus, sr. Pyr. = stratum Pyramidale, sr. Rad. = stratum Radiatum, sr. Oriens = Stratum Oriens. Scale bars = 200 μm.

Following successful expression of ChR2 in SST-cre mice, we rhythmically photo-stimulated SST+INs at 40 Hz (with 1 ms pulses) during carbachol (cch)-induced γ oscillations. Rhythmic photo-stimulation of SST+INs reliably entrained ongoing γ oscillations to 40 Hz in 20 out of 22 experiments (1 entrained at 20 Hz and 1 not entrained; n = 17 at 5.5 mW, n = 5 at 2.2 mW; Fig. 4.2). These results indicate that transient activation of SST+ dendrite targeting interneurons is sufficient to synchronise the hippocampal network at γ frequencies. Unlike PV+IN activation, there was a strong negative deflection in the pulse-locked waveform (Fig. 4.2a, b). In order to study the SST+ induced waveform in isolation, we repeated the same experiment during spontaneous network activity in the absence of cch. Blue light pulses (1 ms width) at 40 Hz induced strong pulse-locked field responses (Fig. 4.3a, b).

As in the presence of cch, the negative deflection was more pronounced than the positive peak (Fig. 4.2b, d). Application of ionotropic glutamate receptor (iGluR: kynurenic acid or CNQX/AP5 or CNQX) blockers decreased the positive peak (71.1 $\pm$ 6.97 μV to 36.14 $\pm$ 7.19 μV) without affecting the negative deflection (243.8 $\pm$ 61.88 μV to 240.5 $\pm$ 60.23 μV; Fig. 4.2c, d). Furthermore, application of $GABA_A$ receptor ($GABA_AR$) blockers induced seizure activity contaminating the field responses, and thus did not allow further investigation (data not shown). These experiments suggest that there is a possible non-specific effect of ChR2 activation that generates synaptic excitation. Moreover, since the negative deflection is not blocked by iGluR blockers, it could represent dendritic inhibitory currents or synchronous spikes from surrounding cells. Given that pyramidal cells hyperpolarise in the presence of iGluR blockers, the GABAergic currents should have decreased. Furthermore, the negative deflections are too fast for SST+IN-induced synaptic currents (Rise time from stimulation onset = 2.89 $\pm$ 0.087 ms, Half-width of negative deflection = 1.47 $\pm$ 0.070 ms). These results suggest that the negative deflection arises from the synchronised firing of hippocampal cells. It is possible that the

synchronised firing comes from the spiking activity of SST+IN axons and does not preclude a role of SST+IN synchronisation via synaptic inhibition.

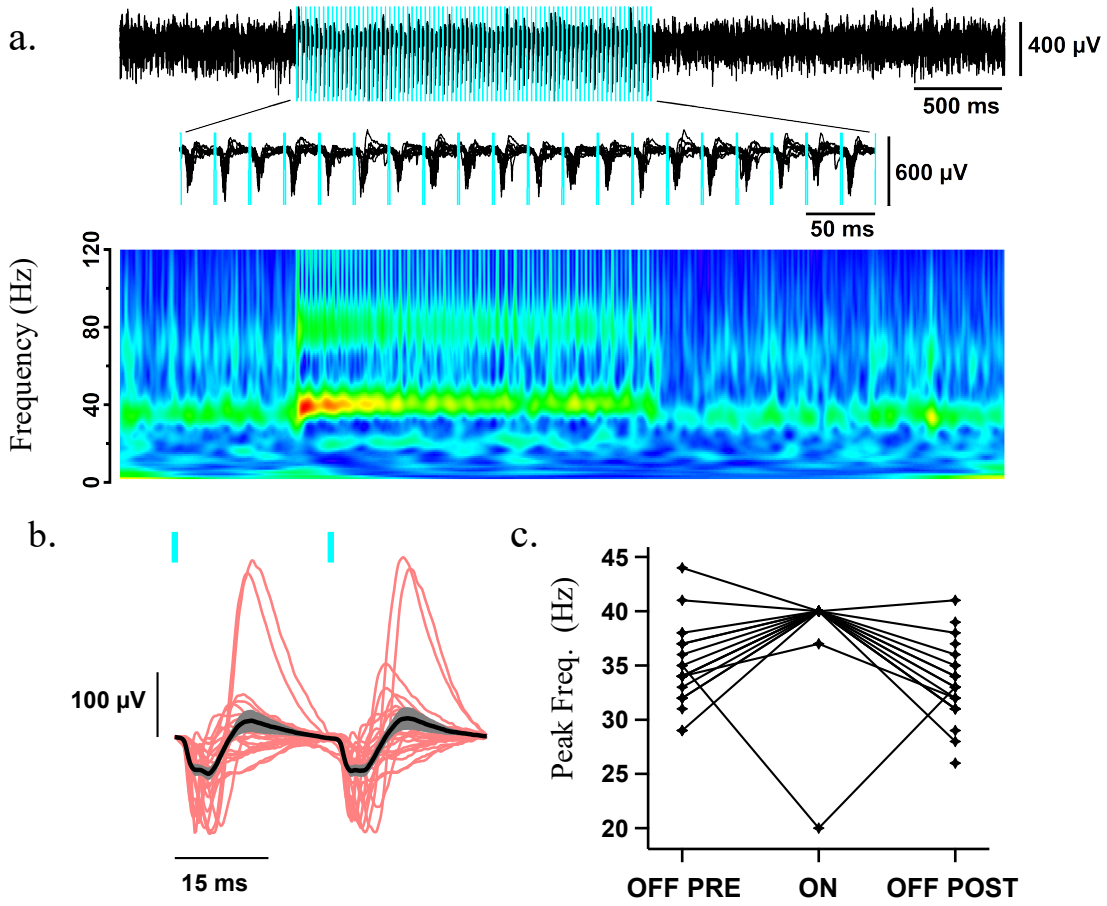


Figure 4.2: Rhythmic excitation of SST+INs entrains ongoing γ oscillation. a) Top: Representative LFP recording from CA3 area illustrating the entrainment of cch-induced γ oscillations to 40 Hz light pulses with width of 1 ms (2 second blue light illumination at 5.5 mW). Middle: Zoomed recordings from a) during pulse stimulation. Bottom: Magnitude component of the wavelet transform normalised by its maximum value. Brighter colours represent larger magnitude. b) Average waveform following two consecutive pulses at 40 Hz and 1 ms pulse width from each experiment (n = 22). Black line represents population average and grey shaded area the SEM. c) Peak frequency of oscillation before (OFF PRE), during (ON) and after (OFF POST) light stimulation (n = 22). Black lines represent single experiments.

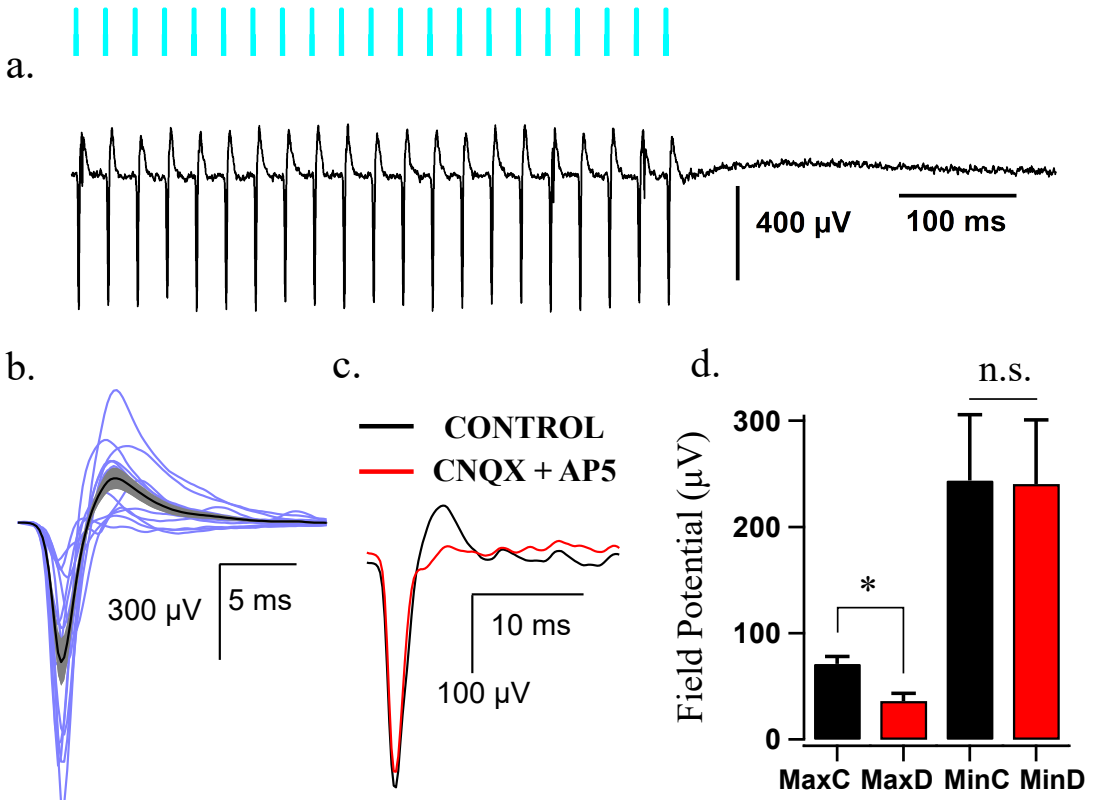


Figure 4.3: Possible non-specific effects of transient SST+IN activation. a) Top: Representative LFP recording from CA3 area illustrating field responses during 40 Hz light pulses with width of 1 ms (light power at 5.5 mW). b) Average waveforms obtained with 1 ms pulses at 40 Hz (n = 13). Black line represents population average and grey shaded area the SEM. c) Average waveform obtained with 1 ms pulse width at 40 Hz from one experiment before (black line) and after application of 20 μM CNQX and 40 μM AP5. In one experiment only 20 μM CNQX was applied but exhibited the same effect. d) The magnitude of negative and positive peaks before and after iGluR blocker application (n = 4). iGluR blockers used: 20 μM CNQX, 40 μM AP5, n = 3; 20 μM CNQX, n = 1. Positive peak before (MaxC) and after drug (MaxD) application. Negative peak before (MinC) and after drug (MinD) application. Paired t-tests (no correction applied); *p $<$ 0.05, **p $<$ 0.01, ***p $<$ 0.001, $^{n.s.}$p $>=$ 0.05.

4.3 SUSTAINED PHOTO-EXCITATION OF SST+ INTERNEURONS DURING GAMMA OSCILLATIONS

Our data indicate that inhibition from SST+INs may be able to synchronise the hippocampal network at γ frequencies. Thus, we tested if upregulation of SST+IN activity is sufficient to modulate the hippocampal network during cch-induced γ oscillations. The effects of sustained SST+IN photo-activation on γ oscillations were first quantified using the the half-maximal response, as described for on parvalbumin-interneuron (PV+IN) experiments (Section 3.5). This analysis showed that the power-area decreased significantly during light stimulation when compared to baseline (0.49 ± 0.029, $p < 0.001$, one sample t-test; Fig. 4.4a,c, e). There was no difference between baseline and the period following light illumination, which indicates successful recovery of the suppressed γ oscillations (1.03 ± 0.018;, $p = 0.14$, one sample t-test; Fig. 4.4c, e). Furthermore, the peak frequency increased from 34.08 ± 0.954 Hz during baseline period to 38.17 ± 1.400 Hz during light illumination ($p < 0.05$, paired t-test; Fig. 4.4b, d, f). No difference in peak frequency was found in the period following light illumination when compared to baseline (OFF POST = 34.28 $\pm$ 1.013 Hz, $p = 1.00$, paired t-test; Fig. 4.4d, f). These results demonstrate that upregulation of SST+IN activity decreases the power and increases the frequency of cch-induced hippocampal γ oscillations. The decrease in γ power may indicate that photo-activation of SST+INs inhibits the hippocampal network in the presence of cch. For experiments in which the light intensity was varied systematically, the changes in peak frequency and power-area were correlated with light intensity (Fig. 4.5). Particularly, as light intensity increased γ power decreased ($r = -0.41$; Fig. 4.5a, c) and frequency increased ($r = 0.74$; Fig. 4.5b, d). The change in power-area was negatively correlated ($r = -0.49$) with frequency difference between baseline and light ON conditions (Fig. 4.5e). Thus, decreases in power are accompanied by an elevation of peak frequency, in a similar way as in PV+IN experiments (Fig. 3.8).

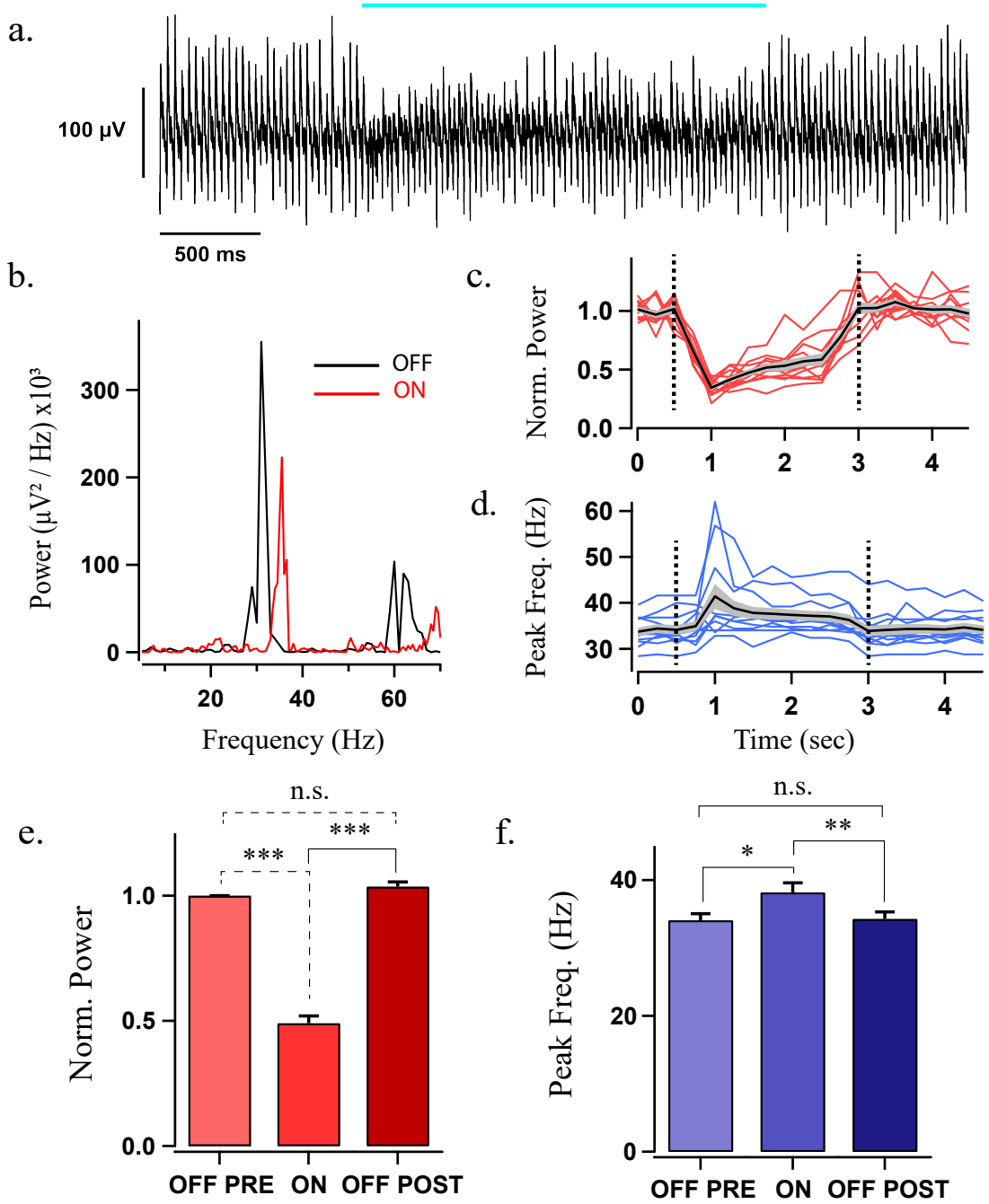


Figure 4.4: Sustained photo-activation of SST+INs decreases the power and increases the frequency of γ oscillations. a) Representative LFP recording of cch-induced γ oscillations to constant blue light illumination (155 μW). b) Power spectrum of the recordings in a); ON = light stimulation period, OFF = baseline period. c) Change in power-area of the oscillation normalised to baseline and calculated in 0.5 second bins across experiments (n = 12). d) Peak frequency of the oscillation and calculated in 0.5 second bins across experiments (n = 12). Time between dotted lines indicates the duration of LED illumination. e) Average change in power-area during (ON) and after light stimulation (OFF POST) normalised to baseline (OFF PRE). f) Average peak frequency; Repeated measures ANOVA (rmANOVA) was followed by post-hoc paired t-test for multiple comparisons. rmANOVA: $F(1.03, 11.33) = 14.78$, $p < 0.002$; *$p < 0.05$, **$p < 0.01$, ***$p < 0.001$, $^{n.s.}p >= 0.05$. Dashed brackets represent one sample t-tests and solid brackets represent paired t-tests.

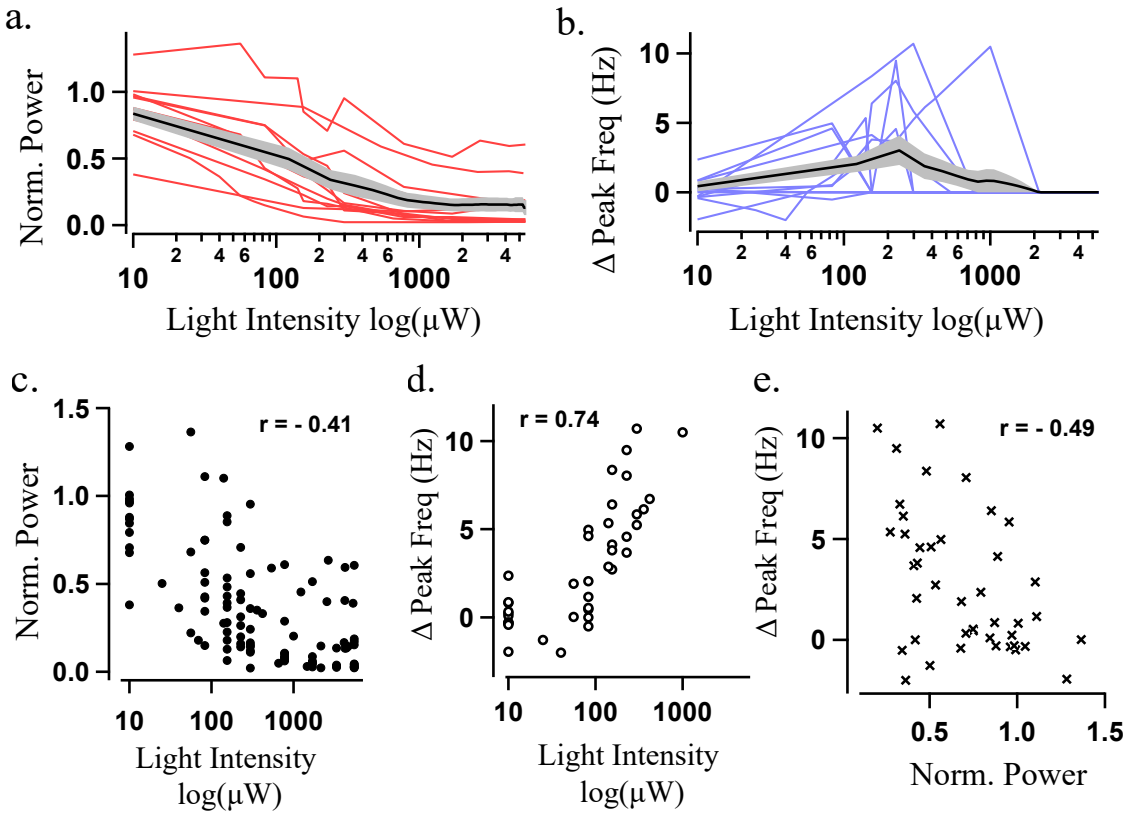


Figure 4.5: γ power decrease and peak frequency increase are correlated to light intensity. a) Power-area change between light stimulation period and baseline against light intensity. Red lines represent single experiments (n = 12). b) Peak frequency difference between light stimulation period and baseline against light intensity. Blue lines represent single experiments (n = 12). The black line is the average response and the grey shaded area represent SEM. c) Power-area change between light stimulation period and baseline plotted against light intensity. Pearson correlation: r = -0.41, n = 107, $p < 0.00001$. Frequency difference between light stimulation period and baseline against light intensity. Pearson correlation: r= 0.74, n = 42, $p < 0.00001$. power-area change against peak frequency difference between light stimulation period and baseline. Pearson correlation: r = -0.49, n = 42, $p < 0.0012$.

In addition, similar to PV+IN activation, the peak frequency appeared to increase until a certain threshold where the oscillation collapsed (for each experiment, Fig. 4.5b). Across all experiments, strong photo-activation of SST+INs (maximal intensity applied; n = 18 slices at 5.5 mW and n = 13 slices at 2.2 mW, merged) reduced γ power during light stimulation when compared to baseline period (0.38 $\pm$ 0.150, $p < 0.001$, one sample t-test; Fig. 4.6b). The γ power remained suppressed in the period following light stimulation (0.72 $\pm$ 0.051, $p < 0.001$, one-sample t-test; Fig. 4.6b), but changes in frequency were rapidly reversible ($p > 0.05$, one-sample t-test; Fig. 4.6c). More specifically, in a subset of experiments γ oscillations were fully abolished (n = 16/31 slices ; Fig. 4.6aii). On the contrary, in other experiments high-frequency oscillations emerged (n = 15/31 slices; 4.6ai). The frequency of the induced oscillations shifted on average from 34.1 $\pm$ 0.77 Hz during baseline to 53.2 $\pm$ 2.62 Hz during light activation ($p < 0.01$, paired t-test; Fig. 4.6c). It is therefore possible, that strong SST+IN photo-activation can reliably abolish endogenous CA3 hippocampal γ oscillations and give rise to distinct SST+IN oscillations. It is important to mention that experiments in which high-frequency oscillations were observed during light stimulation rarely occurred in the batch of animals that was used to derive light-intensity response curves.

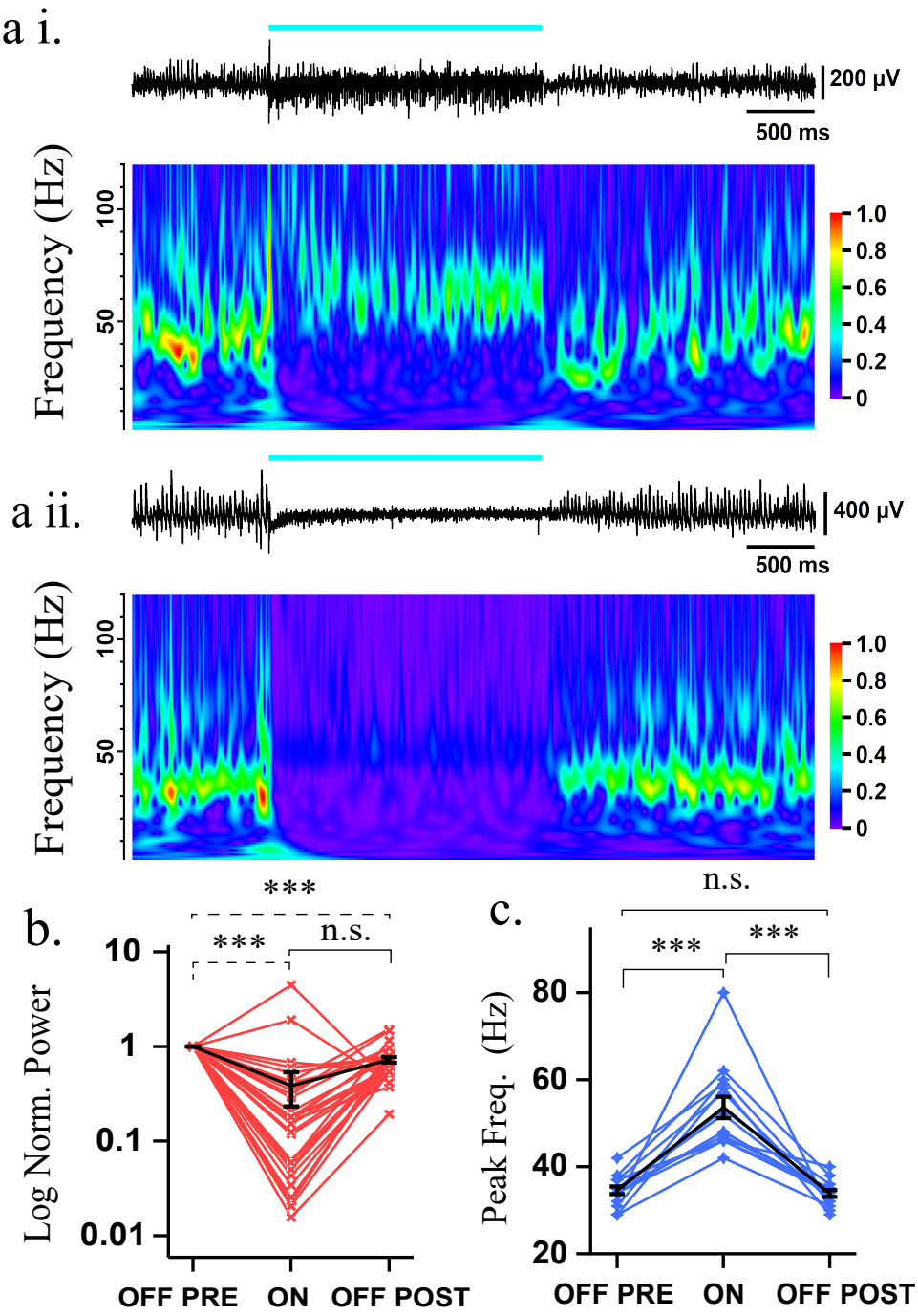


Figure 4.6: SST+IN strong photo-activation elicits variable responses. a) Top: Representative LFP recording from CA3 area illustrating i) induction of high-frequency γ and ii) the inhibition of cch-induced γ oscillations upon constant blue light illumination (5.5 mW). Bottom: Magnitude component of the wavelet transform normalised by its maximum value, brighter colours represent larger magnitude. b) Power-area change (log) during (ON) and after light stimulation (OFF POST) normalised to baseline (OFF PRE);. Red lines represent single experiments (n = 31). c) Peak frequency, blue lines represent single experiments where γ oscillations were not abolished (n = 15). rmANOVA followed by post-hoc paired t-test for multiple comparisons. rmANOVA, power-area, $F(1.08, 14.1) = 42.4$, $p < 0.00001$; *$p < 0.05$, **$p < 0.01$, ***$p < 0.001$, $^{n.s.}p >= 0.05$. The black line is the average response and error bars represent SEM. Dashed brackets represent one sample t-tests and solid brackets represent paired t-tests.

4.4 SST+ INTERNEURON PHOTO-ACTIVATION CAN GENERATE *DE NOVO* GAMMA OSCILLATIONS

In order to test if SST+IN photo-activation alone is sufficient to generate γ oscillations we repeated the same experiments without the presence of cch. Sustained photo-activation of SST+INs induced *de novo* oscillations in the γ-band range with peak frequency of 81.3 $\pm$ 2.57 Hz (13/16 slices; Fig. 4.7ai). Isolating the CA3 area from DG did not prevent the generation of *de novo* oscillations (n = 3 slices). Therefore, SST+IN photo-activation in CA3 is sufficient in generating high-frequency γ oscillations. Interestingly, in two experiments in which cch was applied subsequently, SST+ activation elicited strong oscillatory activity in spontaneous conditions but silenced cch-induced γ oscillations (n = 2 slices). Furthermore, 21 out of the 27 analysed slices in acsf generated γ oscillations. Whereas, 15 out of 31 analysed slices in cch generated γ oscillations. These experiments suggest that high cholinergic tone may have an inhibitory effect on *de novo* γ rhythmogenesis.

As mentioned before, γ oscillations in the hippocampus usually occur nested in slower θ oscillations during REM sleep and spatial exploration (Buzsáki 2002; Lisman et al. 2013). Sinusoidal light activation at 8 Hz (theta photo-activation) induced robust γ oscillations with higher peak frequency than the tonic activation 109.4 $\pm$ 2.97 Hz (14/17 slices, $p < 0.001$, paired t-test; Fig. 4.7aii, c). This is consistent with other manipulations indicating that transient light activation induces higher frequency oscillations than more sustained activation (Betterton et al. 2017; Butler et al. 2016). Therefore, it seems possible that tonic elevation of an interneuron population can generate γ oscillations via ING model in the CA3. However, it is also possible that direct or indirect synaptic excitation caused by ChR2 photo-activation is also responsible for the generation of *de novo* high-frequency oscillations.

One possibility for the generation of synaptic excitation is depolarisation block of SST+INs during light illumination. This would dis-inhibit pyramidal cells and

other interneurons and lead to a net excitation in the CA3 network that could be sufficient in generating γ oscillations. We therefore assessed how different light intensities could affect *de novo* high-frequency oscillation properties induced by theta photo-stimulation of SST+INs. This stimulation paradigm was chosen because it mimics the physiological θ drive and oscillations could be produced more robustly. Stimulation at increasing light intensities was strongly correlated to the power-area levels and frequency of the induced oscillation (Power Area: r = 0.67, Peak frequency: r = 0.78; Fig. 4.8c ,d). Specifically, as the light intensity became larger the power of the oscillations increased, together with the frequency (Fig. 4.8a, b). The power-area change was also proportional to peak frequency difference (Fig. 4.8e). Thus, the graded and monotonic increase in the power of *de novo* SST-induced oscillations between low and high light intensities argues against depolarisation block dependent effects. Moreover, the monotonic increase in peak frequency is in contrast to γ oscillations induced by photo-activation of principal cells in the hippocampus, where the frequency of the oscillations remains relatively constant (Betterton et al. 2017; Butler et al. 2016, 2018). Furthermore, the power of the SST-induced *de novo* oscillations increases along with frequency. This is in contrast to cch-induced oscillations where the power decreases when frequency increases during either SST+IN or PV+IN photo-activation. Collectively, these data support that an elevated drive to SST+INs can alter the frequency of SST-induced γ oscillations and potentially induce fast γ oscillations. This effect is also contrasting to the PV+IN photo-activation experiments. It should be emphasised that the power-spectrum in these SST experiments performed in aCSF was analysed in the range of 50 - 149 Hz. The analysed range was extended because SST+IN photo-activation sometimes induced oscillations beyond 100 Hz.

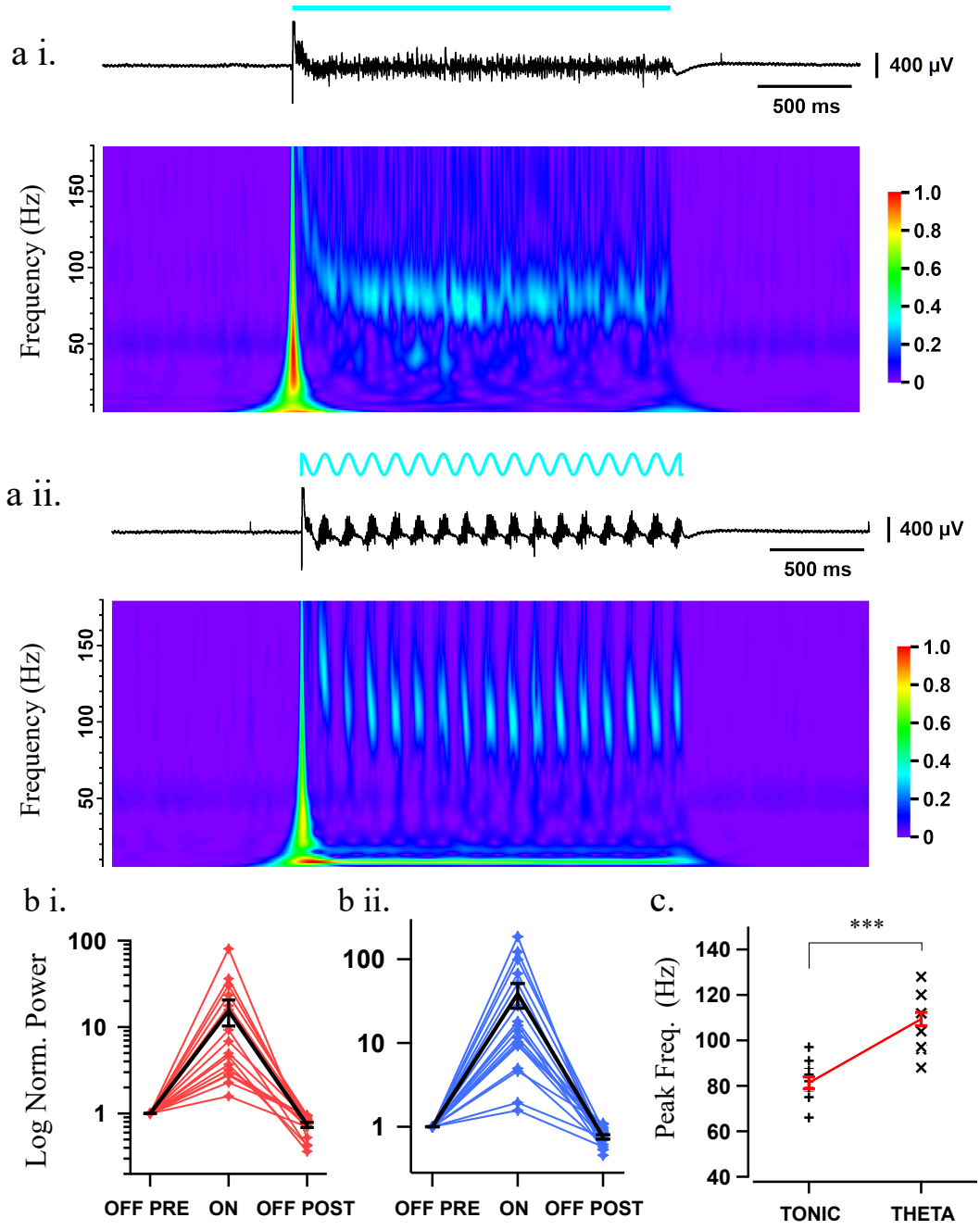


Figure 4.7: Photo-activation of SST+INs induces *de novo* γ oscillations. a) Top: Representative LFP recording from CA3 area illustrating induction of high-frequency γ oscillations by i) constant and ii) theta blue light illumination (10 mW). Bottom: Magnitude component of the wavelet transform normalised by its maximum value, brighter colours represent larger magnitude. b) Log power-area change compared to baseline during i) constant (n = 16) and ii) theta blue light illumination (n = 17). c) Peak frequency of the SST oscillations is higher when induced by theta stimulation when compared to tonic activation; two-sample t-test, ***p < 0.001.

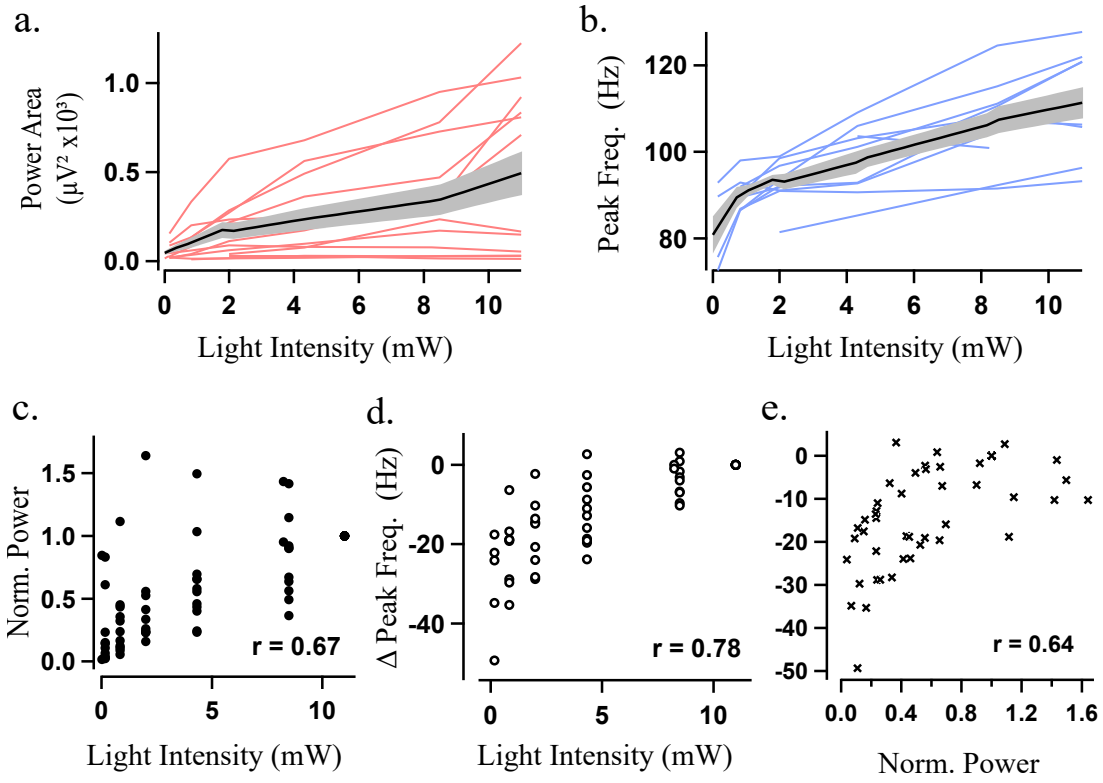


Figure 4.8: Effects of light power on γ oscillations induced by theta photo-activation of SST+INs. a) Power-area obtained during light stimulation period plotted against light intensity. Red lines represent single experiments. b) Peak frequency obtained during light stimulation period against light intensity. Coloured lines represent single experiments (n = 12). The black line is the average response and the grey shaded area represent SEM. c) Power-area change obtained at each stimulation level compared to lowest light level against light intensity. Pearson correlation: r = 0.67, n = 70, p < 0.00001. Peak frequency difference obtained at each intensity level compared to lowest light level stimulation against light intensity. Pearson correlation: r = 0.78, n = 55, p < 0.00001. Power-area change against peak frequency difference obtained at each intensity level compared to lowest light level stimulation. Pearson correlation: r = 0.64, n = 55, p < 0.00001.

4.5 MECHANISMS OF GENERATION OF SST-INDUCED *DE NOVO* GAMMA OSCILLATIONS

4.5.1 *DE NOVO* OSCILLATIONS DEPEND ON SYNAPTIC EXCITATION AND INHIBITION

We next examined the dependence of SST-induced γ oscillations to synaptic glutamatergic and GABAergic transmission. To test this, oscillations were induced by theta photo-activation of SST+INs and synaptic blockers were applied. Application of iGLuR blockers (kynurenic acid or CNQX/AP5 or CNQX) completely abolished *de novo* oscillations (Fig. 4.9ai, bi, ci). This indicates that excitation has an important contribution to the LFP production of these oscillations. We then applied $GABA_AR$ blockers (Bicuculline or Gabazine) during theta stimulation of SST+INs. Like before this caused seizure activity. However, in all experiments tested the oscillations were abolished before seizure induction (Fig. 4.9aii, bii, cii). These results suggest, that SST-induced *de novo* γ oscillations require both fast synaptic excitation and inhibition. However, with iGluR blockers present the *de novo* oscillations could still occur, but due to hyperpolarisation of the cells receiving the IPSCs, a detectable field could not be produced (Mann et al. 2005b). On the other hand, the generation of robust network activity from photo-activation of inhibitory cells is counter-intuitive. It is possible that network excitation could be generated by several mechanisms such as i) off-target expression of ChR2 in excitatory cell populations, ii) depolarisation through GABAergic transmission (EGABAR reversal), iii) ephaptic coupling between SST+IN and pyramidal axons and iv) from depolarisation block during ChR2 photo-activation in SST+INs. To discriminate between these possibilities, we measured cellular responses and inputs during photo-activation of SST+INs.

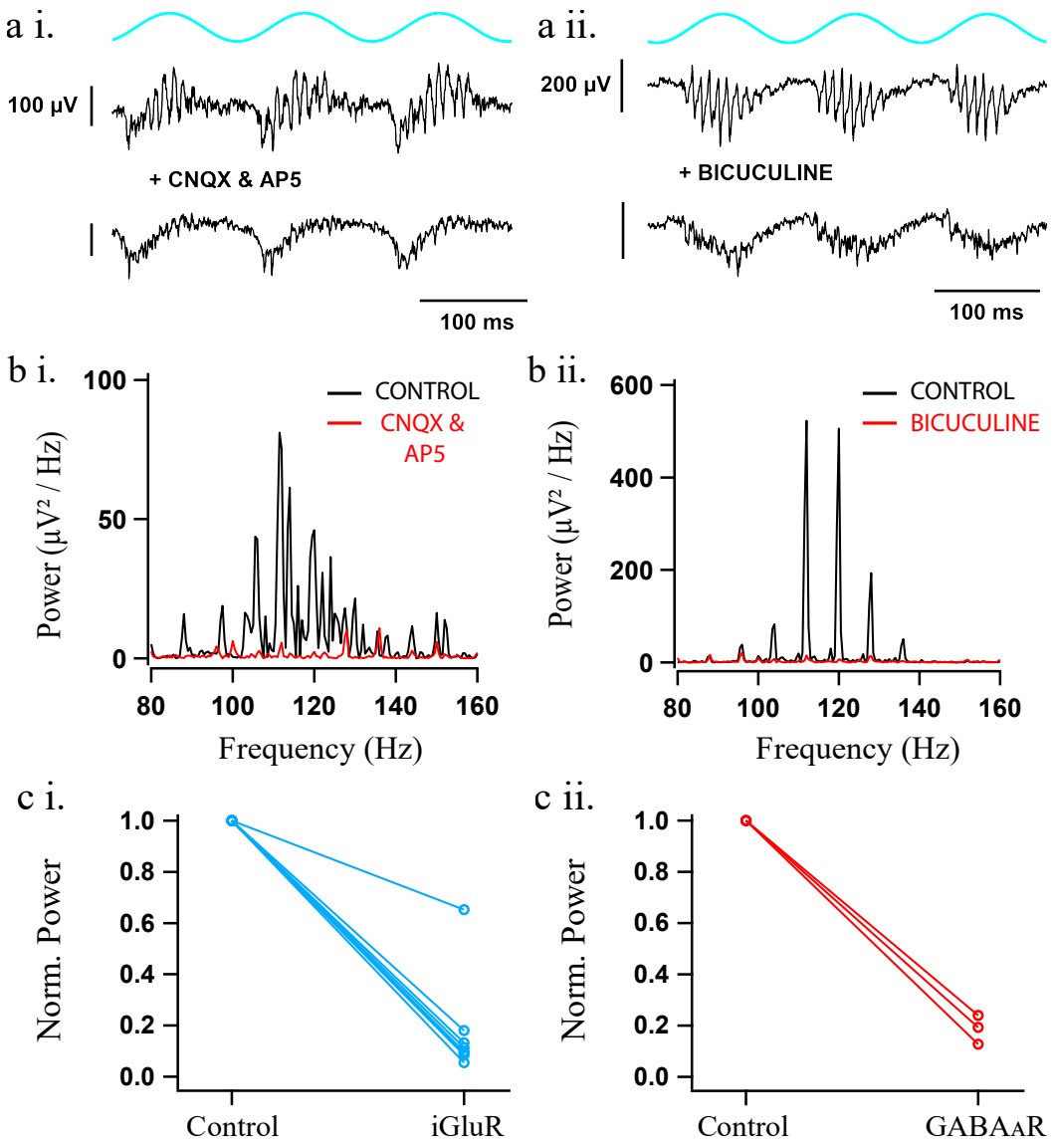


Figure 4.9: *De novo* high-frequency oscillations require fast synaptic excitation and inhibition. Activation of SST+INs by theta light stimulation (1 - 10 mW). a) Representative LFP recording in CA3 before (top) and after application of i) iGLUR and ii) $GABA_AR$ blockers. b) Power spectrum of the recordings in a). c) Power-area change before (control) and after application i) iGLUR and ii) $GABA_AR$ blockers. iGluR blockers used: 20 μM CNQX, 40 μM AP5, n = 3; 10 μM CNQX, 20 μM AP5, n = 1; 20 μM CNQX, n = 1; 3mM kynurenic, n = 3. $GABA_AR$ used: 20 μM Bicuculline, n = 2; 20 μM Gabazine, n = 1.

4.5.2 SINGLE CELL ACTIVITY DURING SST+ INTERNEURON PHOTO-ACTIVATION

In order to examine if SST+INs directly contribute to *de novo* oscillation generation, we tested whether SST+IN activity is phase-locked to the induced oscillations during light stimulation. Thus, we performed parallel whole-cell current clamp and LFP recordings during light illumination in a submerged set-up. However, the *de novo* oscillations could not be induced reliably during submerged recordings. Therefore, we could not correlate single cell activity to γ oscillation phase in this recording environment. Nevertheless, we proceeded with investigating the properties of opsin-expressing cells and the responses they elicit in non-expressing cells during SST+IN photo-activation. Opsin-expressing cells had diverse electrophysiological phenotypes in agreement to the heterogeneous nature of SST+INs with spikes half-widths ranging from 0.35 ms to 1.04 ms (n = 19 cells). Some of the cells also had the characteristic fast-spiking phenotype with spike amplitude adaptation (Hang Hu et al. 2011; Fig. 4.10a). The opsin-expressing cells reliably followed light at 40 Hz (1 ms pulse width; Fig. 4.10b). In addition, some of the opsin-expressing cells were filled with biocytin and visualised (n = 5 cells). All of the filled cells had axons terminating in regions where the dendrites of hippocampal principal cells were present and did not exhibit a characteristic pyramidal cell morphology (Fig. 4.10c). These results indicate that ChR2 is expressed in dendrite-targeting interneurons. However, the possibility of off-target expression still exists. Furthermore, more than 50% of the opsin-expressing cells entered depolarisation block during sustained light illumination. We therefore recorded from putative non-opsin expressing cells (as sometimes ChR2-expression was not visible at the cell body) and observed their responses during sustained light illumination (n = 43). Only responses that changed the membrane voltage equal to or more than 1 mV were included. Sustained light-illumination caused hyperpolarisation in most cells recorded (n = 27 cells, Fig. 4.11a, b).

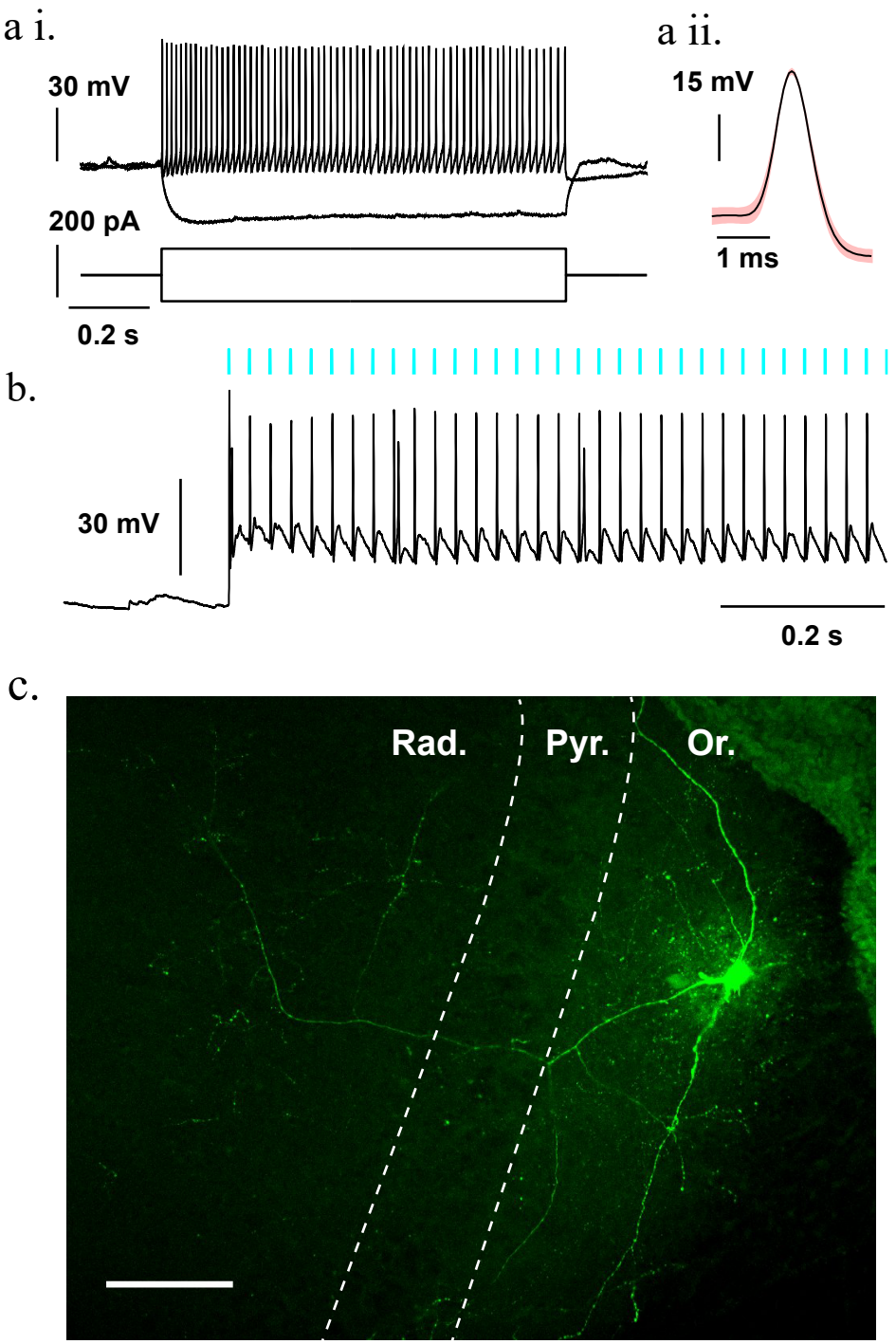


Figure 4.10: Current clamp recordings of an SST+IN. ai) Current clamp recording in a SST+IN in response to depolarising and hyperpolarising current injections. aii) Average action potential waveform of the SST+IN obtained from responses to depolarising current injection. Red shaded area represents standard deviation. b) High-frequency action potential firing of a SST+IN in response to rhythmic (40 Hz, 1 ms pulse width) blue light illumination (1.53 mW). c) Maximum intensity projection of the confocal image of the recorded cell filled with biocytin and visualised with Alexa Fluor 488. Sr. Pyr. = stratum Pyramidale, sr. Rad. = stratum Radiatum, sr. Oriens = Stratum Oriens. Scale bars = 100 μm.

Even in cells with small hyperpolarisation (-1.57 mV), spontaneous spiking was inhibited upon sustained light illumination (Fig. 4.11ci). There were some cells however that were also depolarised (n = 7, Fig. 4.11a, b). These cells were situated in stratum oriens (1 not confirmed). Furthermore, the cells that increased their spiking did not have a regular spiking phenotype, indicating that they could be inhibitory interneurons (n = 5, Fig. 4.11cii). One of these cells had low opsin-expression which was revealed as a tonic photo-current by application of iGluR blockers (data not shown). These experiments suggest that most cells are synaptically inhibited during SST+IN photo-activation. This is in contrast to the large proportion of cells that enter depolarisation block during sustained light illumination. This discrepancy between synaptic responses and cells entering depolarisation block probably occurs because only superficial cells are sampled with the patch clamp technique. Cells that are embedded deeper in the slice may be less susceptible to depolarisation block, and thus generate reliable synaptic inhibition during light illumination. It is also possible that SST+ terminals are directly photo-activated even if the SST+ cells enter depolarisation block. These experiments also suggest that a significant number of cells in the stratum oriens receives a net depolarisation that could arise partly from the depolarisation block of SST+INs observed.

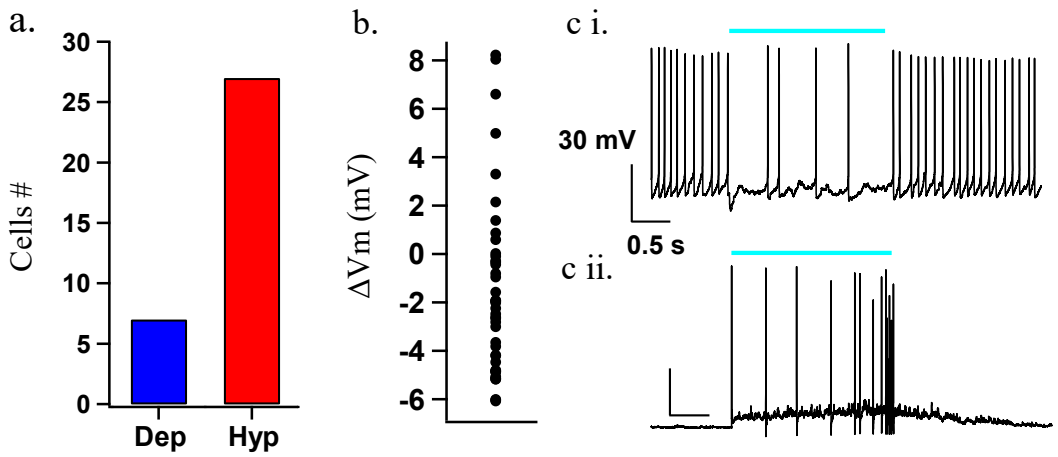


Figure 4.11: Cellular responses of non-opsin expressing cells to SST+IN photo-activation. a) Number of putative non-opsin expressing cells that had a change in membrane voltage during sustained SST+IN photo-activation (1.53 mW). Red bar = cells that hyperpolarised equal or more than 1 mV, Blue bar = cells that depolarised equal or more than 1 mV. b) Membrane voltage of non-opsin expressing cells during sustained SST+IN photo-activation (n = 43 cells). ci) Suppression of action potential firing in an oriens non-expressing cell during sustained SST+IN photo-activation. cii) Increased action potential firing during SST+IN photo-activation in a narrow fast-spiking and non-expressing cell in oriens during sustained SST+IN photo-activation.

In order to measure the synaptic inputs that pyramidal cells receive, we performed whole-cell voltage clamp recordings during sustained light illumination. We recorded the synaptic currents in putative pyramidal cells during SST+IN photo-activation. Recordings were performed in a total of 18 putative pyramidal cells. Six of the cells were visualised and had the typical pyramidal cell morphology (Fig. 4.12a). SST+ tonic photo-activation induced strong inhibitory currents with a mean of 152.3 ± 21.66 pA (Fig. 4.12bi, ci), but also induced weak excitatory currents with a mean of 35.7 ± 8.01 pA (Fig. 4.12bii, cii). IPSCs were blocked upon perfusion of the $GABA_AR$ antagonist bicuculline (n = 2; Fig. 4.12f). Furthermore, all of the cells received greater synaptic inhibition than excitation (Fig. 4.12e) and none of the cells seemed to have opsin related photo-currents. These experiments argue against non-specific expression of ChR2 in principal cells. Nevertheless, the sample size is small in order to allow assumptions at the population level. It is still possible that some of the cells expressing ChR2 in the pyramidal cell layer (with a pyramidal-like morphology) are excitatory principal cells (Fig. 4.1). Moreover, it has been demonstrated that strong repetitive stimulation can switch dendritic GABAergic transmission from an inhibitory to an excitatory nature (Marty et al. 2005). It is therefore possible that during SST+IN photo-activation, cells receive strong GABAergic input, that results in depolarisation and spike production. To test that possibility we performed whole-cell current clamp recordings using perforated patch. We used this method as it does not alter the intracellular contents of the target cell, and hence leaving GABAR reversal potential unclamped. Recordings were obtained from cells in the pyramidal cell layer during SST+IN photo-activation (Fig. 4.13a). Sustained light illumination hyperpolarised the membrane voltage of the recorded cells (n = 6 cells; Fig. 4.13b, c). This indicates that GABAergic input during SST+IN photo-activation is inhibitory in nature. One cell in stratum oriens with membrane voltage at -54.5 mV underwent a net depolarisation (1.4 mV), which changed to hyperpolarisation (-2.0 mV) after application of the iGluR blocker CNQX (10 μM), indicating that the depolarisation did not arise from GABAergic

transmission directly. Therefore, that cell was excluded from the analysis. These results show that dendritic GABAergic transmission here is inhibitory in nature.

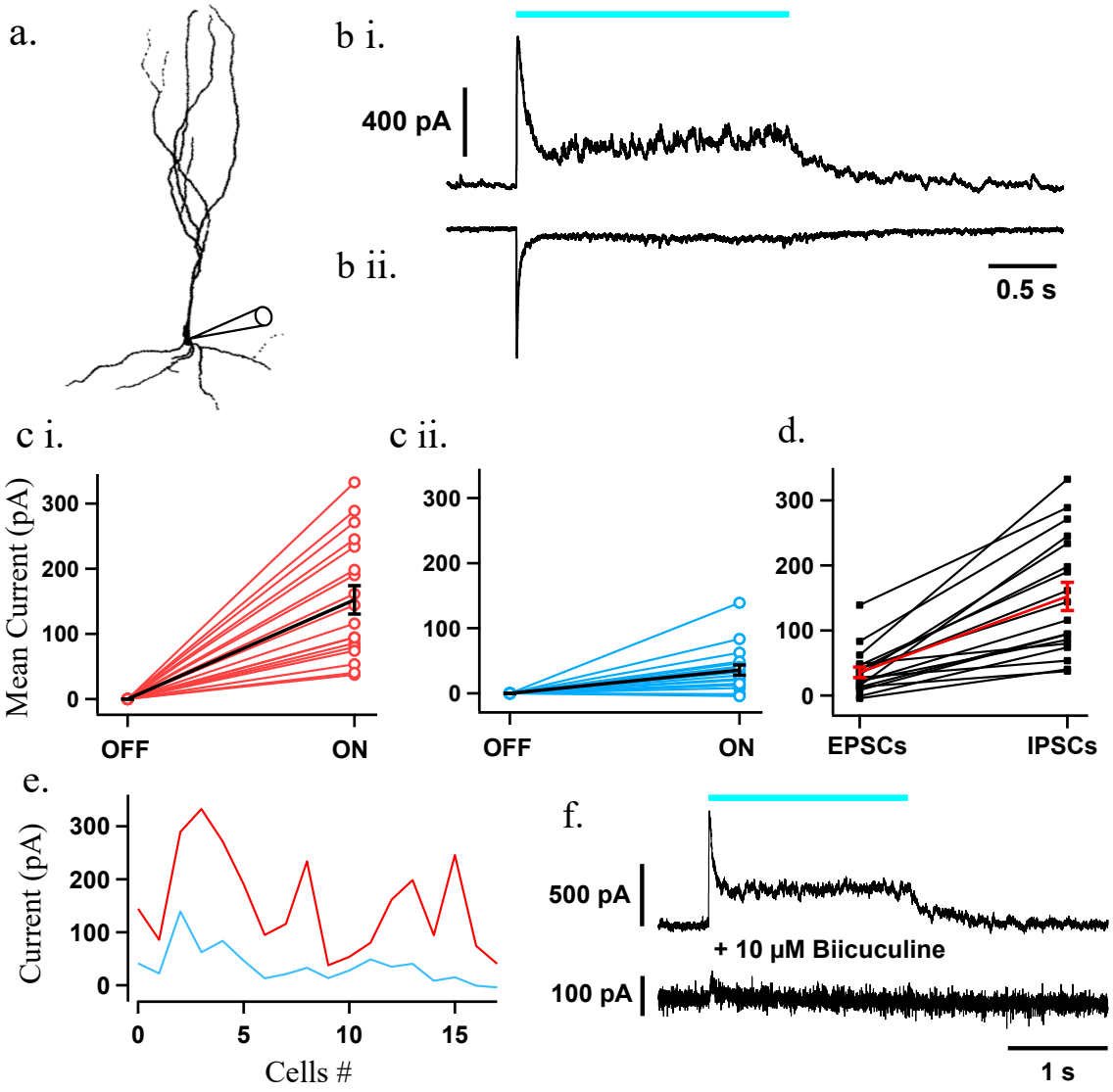


Figure 4.12: Inhibition prevails during SST+IN activation. Whole-cell recordings in voltage clamp mode from putative pyramidal cells. a) Reconstruction of a cell with typical pyramidal cell morphology in CA3 hippocampal area. b) Representative voltage clamp recording of the cell in a) held at i) 0 mV and ii) -70mV to isolate IPSCs and EPSCs respectively. c) Mean i) inhibitory and ii) excitatory currents before (OFF) (from at least 5 repetitions) and during SST+IN photo-activation (ON). Black line represents population average and error bars SEM. e) Comparison of EPSCs and IPSCs during SST+IN photo-activation across cells. Blue line EPSCs, Red line IPSCs. f) Application of 10 μM bicuculine blocks IPSCs during SST+IN photo-activation.

In agreement with this, cells that received IPSCs during SST+IN photo-activation did not produce action potentials during cell attached recordings (n = 3; data not shown). In addition, preliminary experiments (n = 2) showed that reduction in bicarbonate levels did not abolish *de novo* high-frequency oscillations, even though they reversibly abolished cch-induced γ oscillations. This may suggest that depolarising GABA is not essential for the induction of *de novo* high-frequency oscillations. Together, this evidence suggests that synaptic inhibition is predominant during SST+IN photo-activation in hippocampal area CA3. Furthermore, photo-activation of SST+INs induces a synaptic excitation component that could be essential in the induction SST-induced γ oscillations. The synaptic excitation could partly arise from dis-inhibition of pyramidal cells due to depolarisation block of some SST+INs during their photo-activation. More experiments are required in order to reveal how the synaptic excitation is generated.

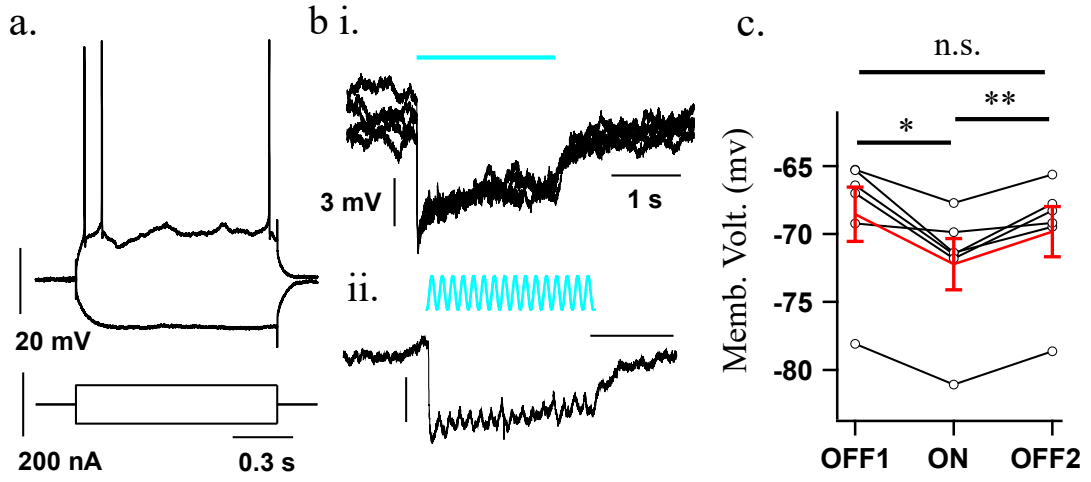


Figure 4.13: Dendritic GABAergic transmission is inhibitory. Whole-cell recordings in current clamp mode from cells in the stratum pyramidale using gramicidin perforated patch. a) Current clamp recording in a putative pyramidal cell in response to depolarising and hyperpolarising current injections (note that the bridge balance errors arises probably from high access resistance in perforated patch). b) Hyperpolarisation of the membrane voltage of the cell from a) during i) sustained and ii) theta blue light illumination (1.53 mW). c) Average membrane voltage (n = 6). rmANOVA, F(2, 10) = 16.54, p < 0.001. Paired t-tests, df= 5, OFF1-ON: Tvalue = 4.49, p < 0.019; OFF1-OFF2: Tvalue= 2.07, p = 0.28; OFF2-ON Post: Tvalue = 5.22, p < 0.010.

4.6 MULTI-ELECTRODE ARRAY RECORDINGS DURING *DE NOVO* OSCILLATIONS

The conditions in submerged and interface chambers cannot be identical, as photo-activation of SST+INs in submerged conditions did not robustly induce γ oscillations. To explore cellular activity during light-induced γ, we also used MEA recordings in the interface condition. Using MEA recordings in CA3 we identified 3 fast-spiking (FS) single units, 13 regular-spiking (RS) single units, 7 FS multi-units and 57 RS multi units from a total of 26 slices (n = total 31 sites). During light illumination in the absence of cch we found that most units increase their firing (FS single = 3/3, RS single = 3/13, FS multi = 6/7, RS multi = 56/57; Fig. 4.14a). This indicates that SST+IN sustained photo-activation increases network excitation during spontaneous conditions in CA3. We found that RS cells were phase-locked to the trough of the γ cycle (RS = 0.96 rad or 0.31 pi, NSOAValue > NSOACritical, Moore's version of Rayleigh's test; Fig. 4.14b). FS cells on average fired later than RS cells (FS = 1.27 rad or 0.40 pi, NSOAValue > NSOACritical, Moore's version of Rayleigh's test; 4.14b), but the sample sizes are too small for a reliable comparison. In addition, we identified 4 single units with variable P2T widths (0.23 ms to 0.64 ms) that were opto-tagged as they followed light pulses at 40 Hz faithfully. The putative SST+IN units were significantly phase-locked to the oscillation ($p < 0.001$, Rayleigh test) and increased their firing during sustained light illumination (1.22 rad or 0.39 pi, NSOAValue > NSOACritical, Moore's version of Rayleigh's test; Fig. 4.14c, d, e). This could indicate that SST+IN activity significantly contributes to the generation of *de novo* high-frequency oscillations. More recordings are required in order to confirm the involvement of SST+INs in high-frequency oscillations.

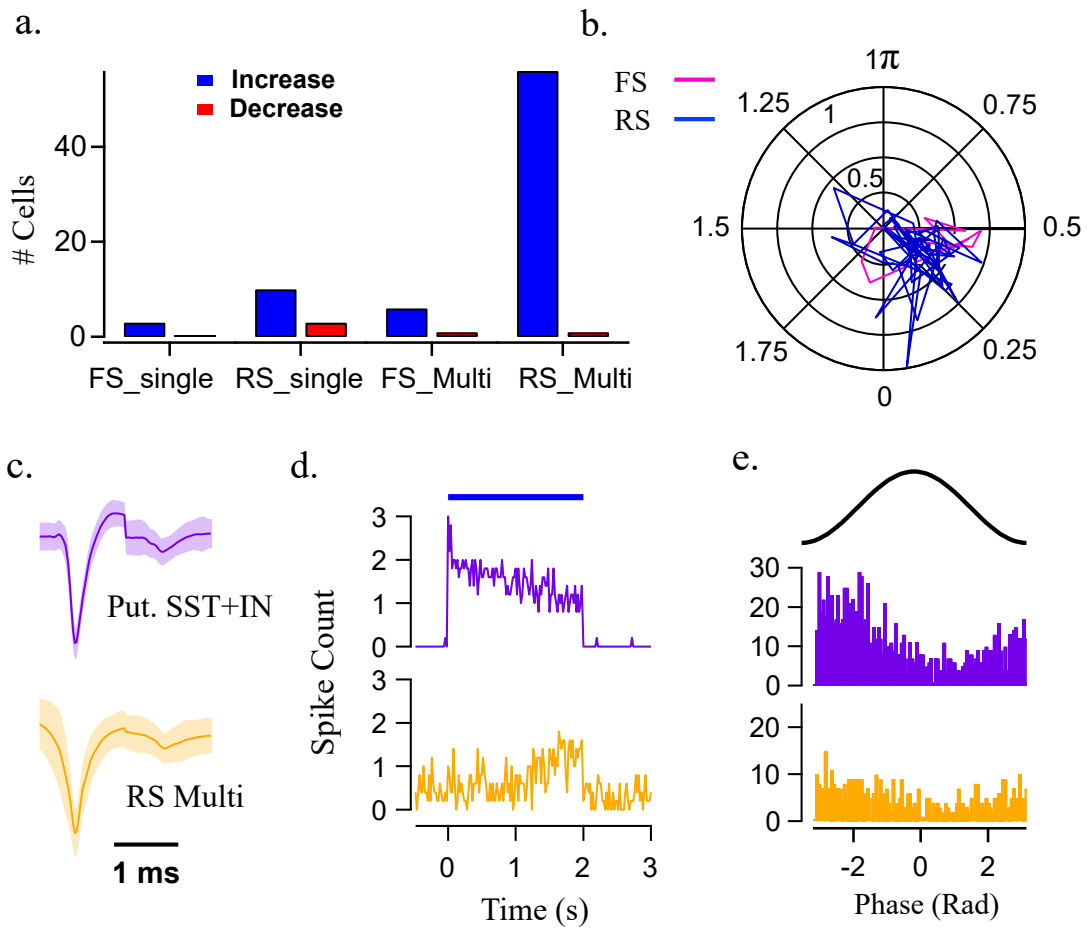


Figure 4.14: SST+IN photo-activation increases unit activity. a) Quantification of the number of clusters which change their firing in response to blue light illumination (10 mW) with cluster separation at 0.4 ms P2T width. b) Average firing phase of FS and RS clusters. c) Average waveforms of the detected clusters along two electrodes. Shaded regions represent standard deviation. d) Spike count of clusters in c) during 2 second sustained light illumination. e) Phase occurrence (radians) of spikes from clusters in c) during light stimulation period.

4.7 PHOTO-INHIBITION OF SST+ INTERNEURONS DURING GAMMA ACTIVITY

Our experiments show that photo-activation of SST+INs can control the hippocampal network activity during cch-induced γ oscillations. In addition, SST+IN photo-activation promotes the generation of *de novo* high-frequency oscillations. Therefore, we next examined if SST+IN activity is also necessary during cch-induced γ oscillations. To achieve that, we injected SST-cre mice with the viral vector AAV5 containing the inhibitory protein pump Arch (Arch3 or ArchT) along with a reporter protein (eYFP or GFP, respectively). This allowed robust expression of Arch in hippocampal slices. Expression of Arch was restricted to the strata oriens, radiatum and lacunosum moleculare (Fig. 4.15a). This is in agreement with expression of Arch in SST+ dendrite targeting interneurons. Whole-cell recordings were performed in four opsin positive cells with narrow action potential waveforms and spike amplitude adaptation (Fig. 4.15b). Sustained green light illumination induced strong hyperpolarisation in the opsin-expressing cells (Fig. 4.15c). Theta light stimulation induced phase-locked inhibition with rebound spiking activity (Fig. 4.15d). Therefore, there was functional expression of Arch in SST+INs that induced strong and reliable photo-inhibition. Furthermore, rhythmic photo-inhibition should be used with caution in these interneurons as it can induce rebound-spiking and confound interpretation of results.

In order to test the importance of SST+INs in γ maintenance, we applied two second sustained light illumination in slices with expression of Arch in SST+INs. SST+IN photo-inhibition consistently decreased the power during light stimulation when compared to baseline period (0.69 ± 0.055, $p < 0.001$, one sample t-test; Fig. 4.16a, b, d). The power of the oscillation did not recover fully in the 1 s period following light stimulation (0.75 ± 0.038, $p = 0.09$, paired t-test: ON-OFF POST; Fig. 4.16d). SST+IN photo-inhibition also reliably increased the peak frequency

of the oscillation from 37.97 ± 1.101 Hz to 43.4 ± 1.705 Hz ($p < 0.01$, paired t-test; Fig. 4.16a, b, e). Consequently, photo-inactivation of SST+INs decreases the power and increases the frequency of cch-induced oscillations. It is interesting to note that in the period following light stimulation, the power of the oscillation remains decreased but the frequency returns back to baseline on average (37.3 ± 0.925 Hz, $p = 0.263$, paired t-test: OFF PRE-OFF POST; Fig. 4.16d, e). Therefore, in contrast to PV+INs, SST+IN photo-inhibition consistently decreases the power with relatively low intensity light illumination (2 - 5 mW). The differences in effect size could arise because more opsin-expressing cells are present in SST+IN than PV+IN experiments. SST+INs could also have weaker reciprocal connectivity with pyramidal cells and thus are likely to receive less synaptic excitation from pyramidal cells following their photo-inhibition.

On the other hand, the change in power-area was not correlated with the peak frequency difference during the first half (ON1, $r = -0.31$), but was correlated to the second half of the light stimulation period (ON2, $r = -0.46$; Fig. 4.16c). Nevertheless, the modulation along the power-frequency coupling was weaker than PV+ experiments (ON1: $r = -0.62$ and ON2: $r = -0.53$). Specifically, SST+IN photo-inhibition resulted in an increased oscillation frequency in the majority of experiments (ON1 31/32 slices and ON2 = 33/35 slices). This difference in frequency is difficult to be explained by altered number of cells expressing as it is qualitatively different from PV+IN photo-inhibition (Fig. 3.15, 3.17).

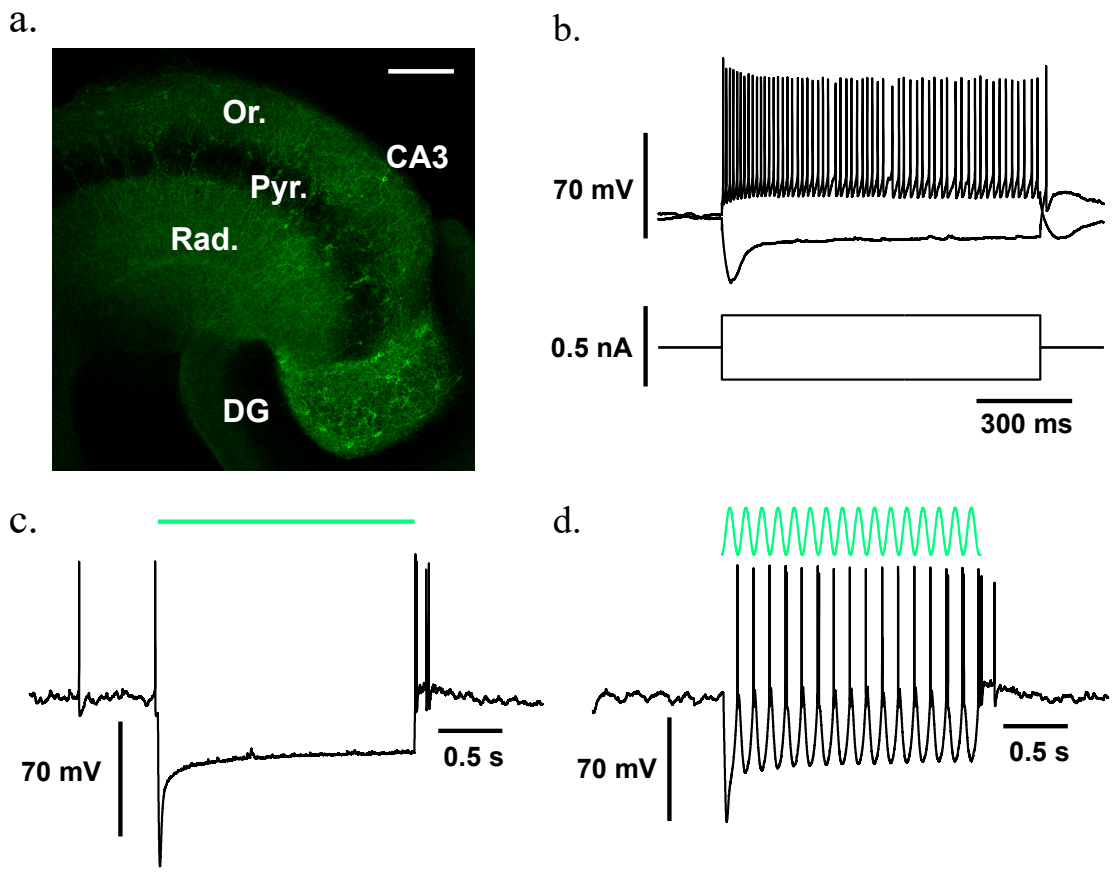


Figure 4.15: Functional expression of Arch in SST+INs. a) Confocal image of ventral hippocampus (350 μm slice) from PV-cre mice with eYFP-Arch3 expression. b) Current clamp recording in a SST+IN from CA3 area expressing ArchT-GFP in response to depolarising and hyperpolarising current injection. c) Hyperpolarisation of the SST+IN membrane voltage during sustained green light illumination (1.45 mW). d) Rebound spiking of a SST+IN during theta light illumination (1.45 mW). CA3 = Cornu Ammonis 3, DG = Dentate Gyrus, sr. Pyr. = stratum Pyramidale, sr. Rad. = stratum Radiatum, sr. Oriens = Stratum Oriens. Scale bars = 200 μm.

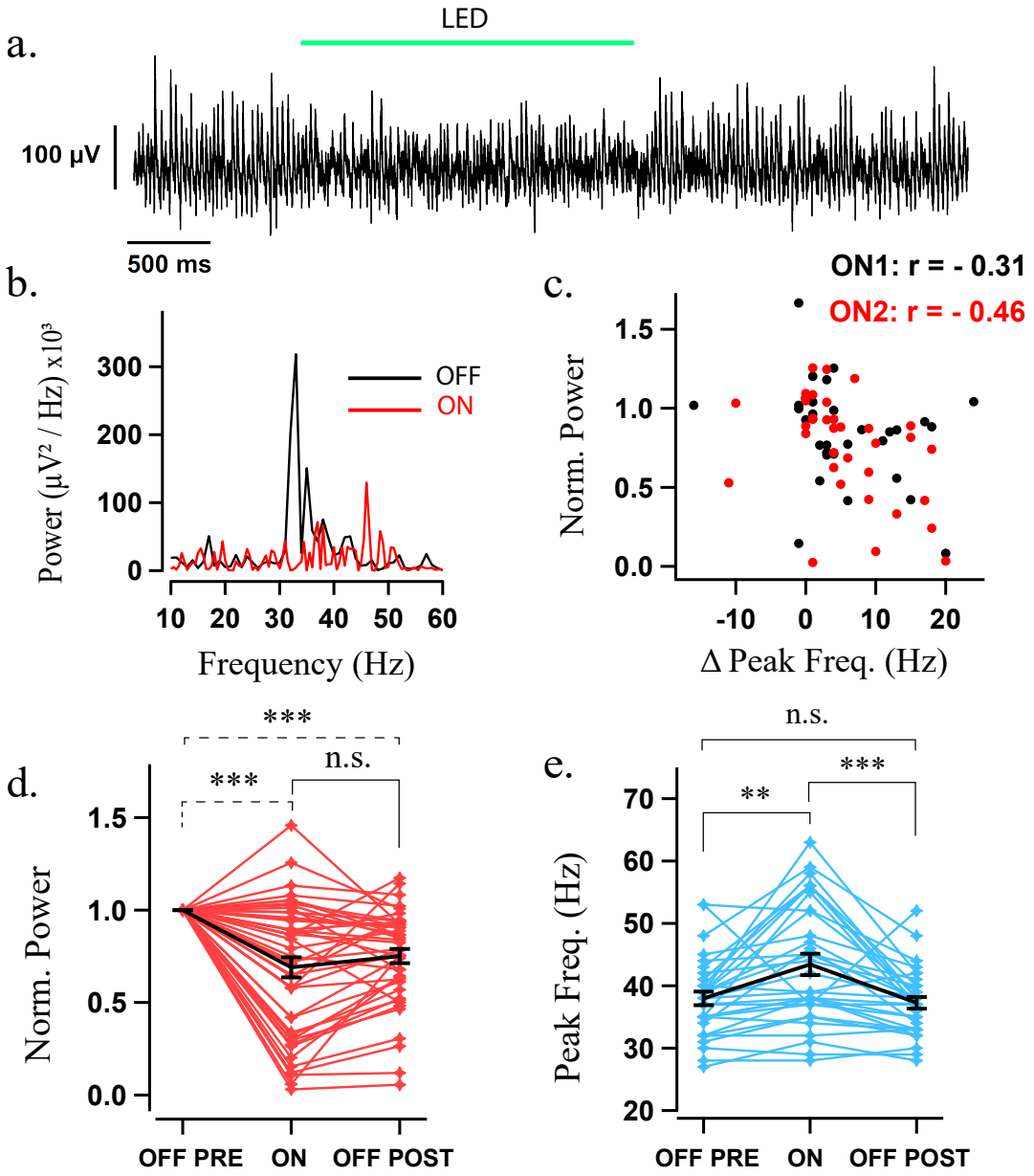


Figure 4.16: Sustained LED photo-inhibition of SST+INs consistently decreases the power and increases the frequency of cch-induced γ oscillations. a) Representative LFP recording from CA3 area illustrating responses to sustained green light illumination (4.25 mW). b) Power spectrum of the LFP from a). c) Power-area change against peak frequency difference during stimulation period (ON1: 0 - 1 seconds, ON2: 1 - 2 seconds) when compared to baseline period light-off period; Pearson correlation: ON1, r = -0.31 n = 32, p = 0.08 ; ON2, r= -0.46, n = 35, $p < 0.006$. d) Power-area during (ON) and after light stimulation (OFF POST) normalised to baseline (OFF PRE); one sample t-tests for comparison of ON and OFF POST periods to baseline, paired t-test for between conditions comparison (ON - OFF POST) (n = 44). e) Peak frequency for experiments in which oscillatory activity was not abloished (n = 32); rmANOVA followed by post-hoc paired t-test for multiple comparisons. ($F(1.12, 34.61) = 16.34$, $p < 0.0001$; *$p < 0.05$, **$p < 0.01$, ***$p < 0.001$, $^{n.s.}p >= 0.05$. Coloured lines represent single experiments. The black line is the average response and error bars represent SEM. Dashed brackets represent one sample t-tests and solid brackets represent paired t-tests. Yulin Tan contributed to data collection.

In order to test how greater SST+ photo-inhibition affected γ oscillations, green laser stimulation was employed. Laser illumination resulted in a strong inhibition of ongoing γ oscillations (Fig. 4.17a). Specifically, γ power was decreased to 0.70 $\pm$ 0.064 during the first-half of light illumination period and suppressed even further in the second half (ON2: 0.36 $\pm$ 0.090) when compared to baseline ($p < 0.001$, paired t-tests: OFF PRE-ON1, OFF PRE-ON2; Fig. 4.17b, d). γ power remained significantly suppressed in the following light off period when compared to baseline (0.51 $\pm$ 0.082,$p < 0.001$, paired t-test; Fig. 4.17b, d). The frequency of the oscillation was significantly elevated only in the first half of light stimulation period from 35.0 $\pm$ 0.921 Hz to 39.17 $\pm$ 1.354 ($p < 0.001$, paired t-test; Fig. 4.17c, e). This effect probably occured because the oscillations were often abolished in the second half of light stimulation period (Fig. 4.17a, b). Indeed, the peak-frequency was elevated for the whole duration of the light stimulation period in experiments where oscillations are not eliminated (Fig. 4.18a). Therefore, strong SST+IN photo-inhibition decreases the power and increases the frequency of cch-induced γ oscillations in CA3 hippocampal area. Furthermore, as the light intensity increased during stimulation period, power-area became smaller (r = -0.29; Fig. 4.18a,b). However, the peak frequency was not correlated to light intensity as it remained equally elevated from lower light intensities (r = 0.04; Fig. 4.18c). This could occur because increase in frequency was saturated from low light intensities, but more investigation is required. Similarly to PV+ laser experiments the time-course of γ power reduction was much slower during the laser experiments, consistent with terminal inhibition (El-Gaby et al. 2016). Together, these results indicate that SST+IN activity is necessary for proper maintenance of cch-induced γ oscillations in the CA3 area of the hippocampus. They also indicate that SST+IN activity could be important in the regulation of γ oscillation frequency in CA3.

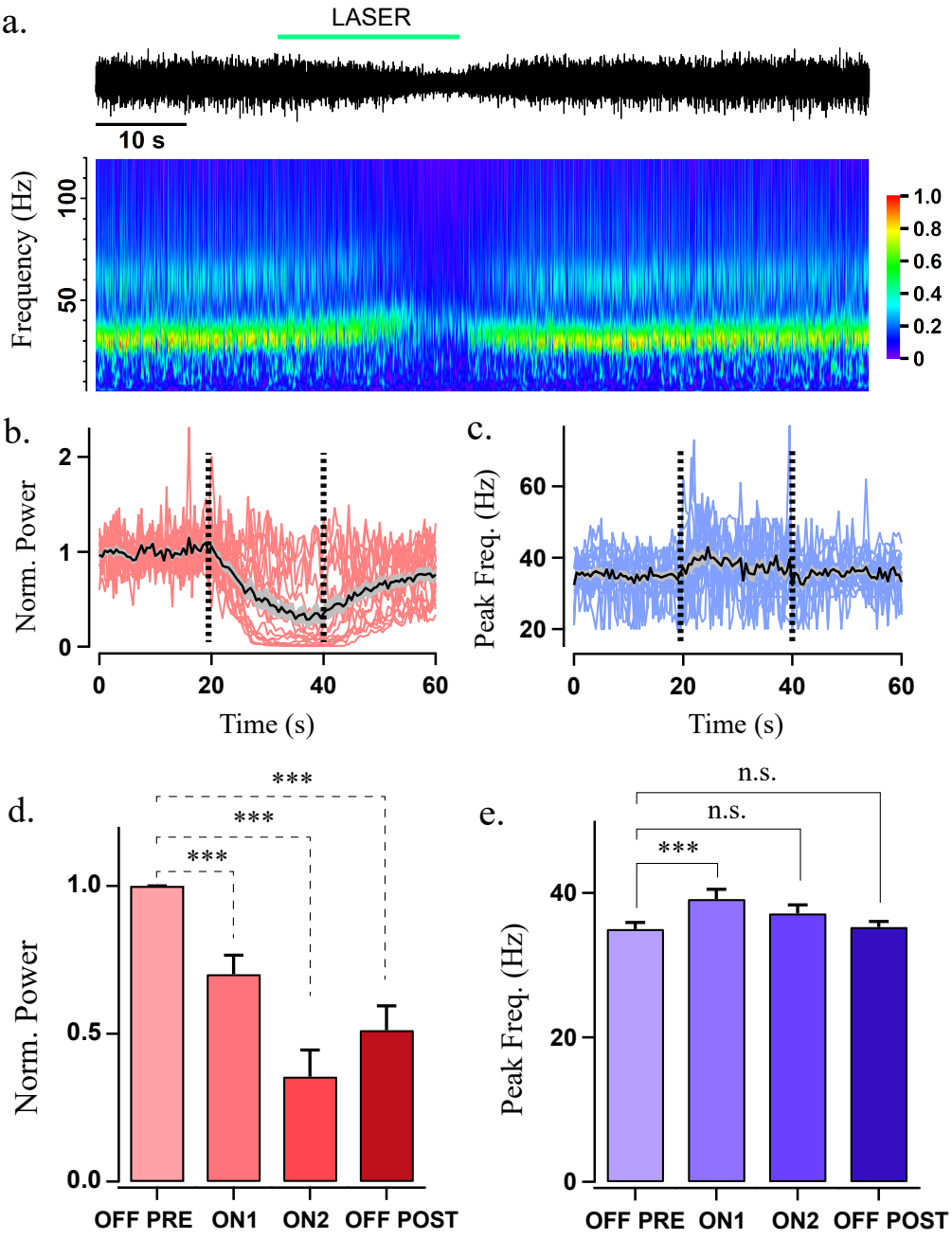


Figure 4.17: Sustained photo-inhibition of SST+INs using laser illumination suppresses γ power and increases frequency. a) Top: Representative LFP recording from CA3 area during inhibition of cch-induced γ oscillations by green laser illumination (approx. 18.6 mW). Bottom: Magnitude component of the wavelet transform normalised by its maximum value, brighter colours represent larger magnitude. b) Change in power-area normalised to baseline and calculated in 1 second bins across experiments (n = 17). c) Peak frequency of the oscillation and calculated in 1 second bins across experiments (n = 17). Time between dotted lines indicates the duration of laser illumination. d) Average power-area change normalised to baseline. e) Average peak frequency; rmANOVA, $F(1.93, 30.94) = 6.90$, $p < 0.008$. rmANOVA followed by post-hoc paired t-test for multiple comparisons; $^{*}p < 0.05$, $^{**}p < 0.01$, $^{***}p < 0.001$, $^{n.s.}p >= 0.05$. OFF PRE: 20 second Baseline, ON1: 0 - 10 seconds laser stimulation, ON2: 10 - 20 seconds laser stimulation, OFF POST: 10 second period following light stimulation. Dashed brackets represent one sample t-tests and solid brackets represent paired t-tests.

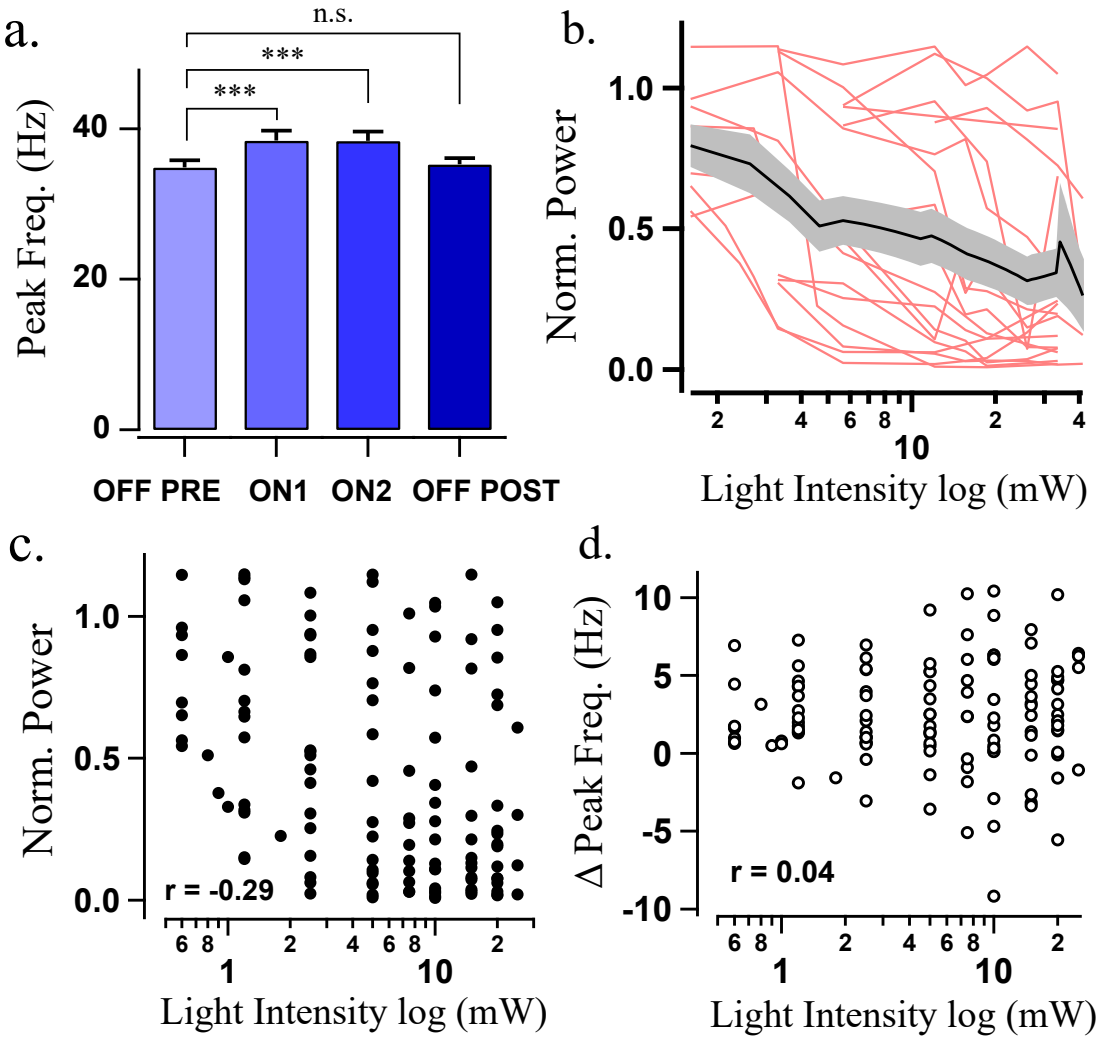


Figure 4.18: Light intensity correlates negatively with γ oscillation power but not frequency. a) Average peak frequency for half-maximal response of SST+IN photo-inhibition (light intensity for each experiment that changed power-area by half of the maximum response). rmANOVA, F(3, 48) = 19.27, p < 0.00001; rmANOVA followed by post-hoc paired t-test for multiple comparisons; b) Power-area change between the last half of laser stimulation to baseline against approximate light intensity. Red lines represent single experiments (n = 17). The black line is the average response and the grey shaded area represents SEM. c) Power-area change between the last half of laser stimulation to baseline against approximate light intensity. Pearson correlation: r = -0.29, n = 124, p < 0.0009. d) Frequency difference between the last half of laser stimulation to baseline against approximate light intensity. Pearson correlation: r= 0.04, n= 124, p = 0.66; *p < 0.05, **p < 0.01, ***p < 0.001, $^{n.s.}$p >= 0.05. OFF PRE: 20 second Baseline, ON1: 0 - 10 seconds laser stimulation, ON2: 10 - 20 seconds laser stimulation, OFF POST: 10 second period following light stimulation.

4.8 SUPPLEMENTARY INFORMATION

As mentioned before, intracellular recordings demonstrated that many SST+IN went into depolarisation during light illumination in submerged conditions. Even though, under the same conditions, non-expressing cells received strong synaptic inhibition. It is still possible that application of cch in combination with interface conditions results into more cells undergoing depolarisation block. Therefore, it is possible that SST-induced γ oscillations arise from inactivation of SST+ spiking that results in an indirect excitation of the hippocampal network. We thus, tested the effects of SST+IN photo-inhibition during spontaneous network activity. Photo-inhibition of SST+INs with green laser illumination failed to induce any oscillatory activity and decreased the overall power in γ-band range (n = 3 slices; Fig. 4.19). Moreover, photo-inhibition of the same slices reliably inhibited cch-induced γ oscillations (Fig. 4.19a). In conclusion, it seems that SST+IN inhibition is not sufficient to induce γ-band oscillatory activity in the hippocampal area CA3.

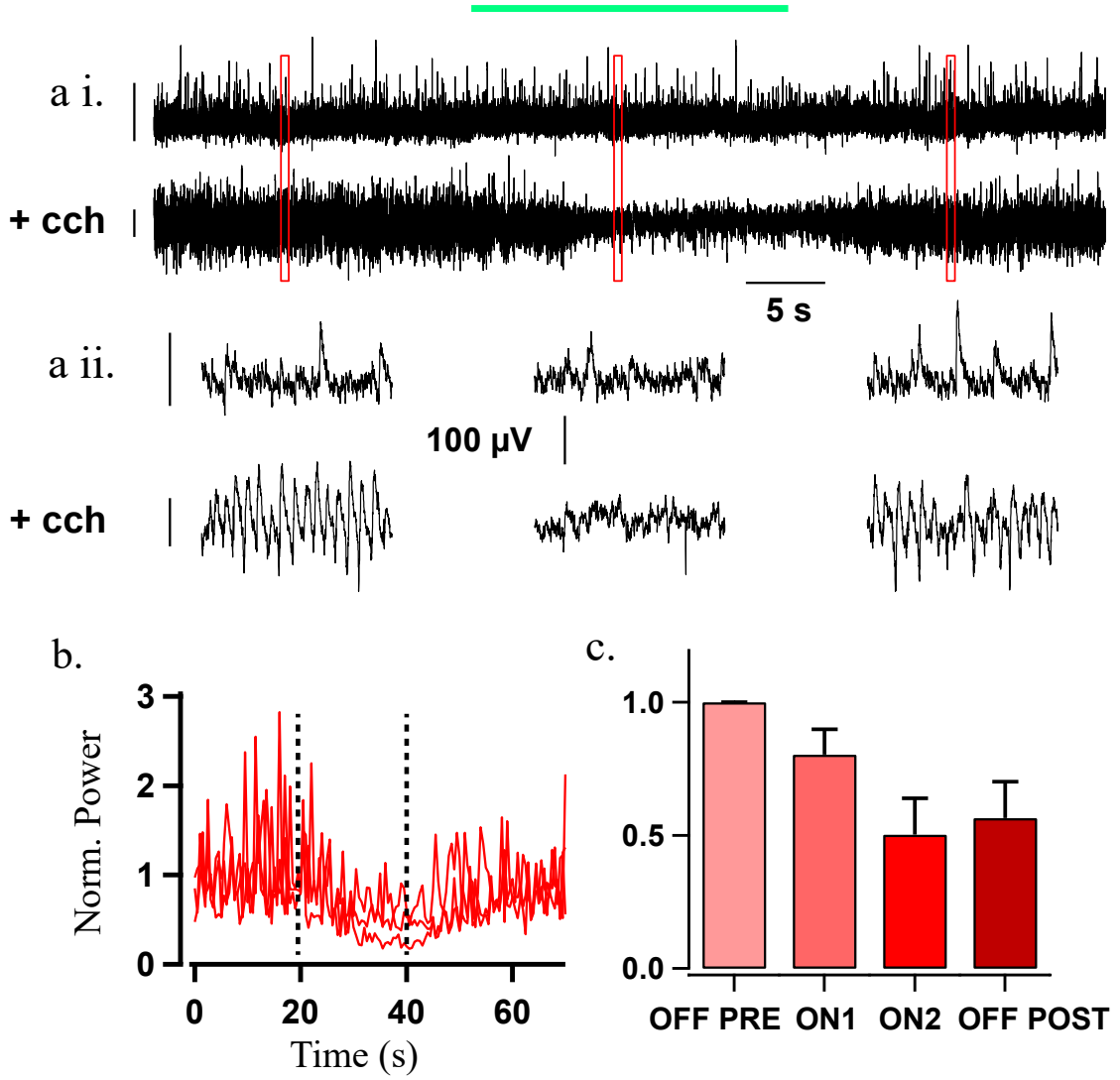


Figure 4.19: Sustained photo-inhibition of SST+INs is not sufficient to induce γ oscillations. ai) Representative LFP recording from the same slice top) with and bottom) without the presence of cch during inhibition of cch-induced γ-oscillations by green laser illumination (approx. 18.6 mW). b) Change in power-area normalised to baseline calculated in 1 second bins across experiments (n = 3); Red squares represent the sections of the magnified LFP in aii) from ai). c) Average power-area change normalised to baseline. MEAN ± SEM = OFF PRE: 1.00, ON1: 0.81 ± 0.095, ON2: 0.51 ± 0.137 OFF POST: 0.56 ± 0.136. OFF PRE: 0-20 s, ON1: 20-30 s, ON2: 30-40 s, OFF POST: 40-50 s.

4.9 DISCUSSION

In the current chapter, we examined how alterations in SST+IN activity affect γ oscillations in the CA3 area of the hippocampus. We found that 40 Hz rhythmic photo-stimulation of SST+INs could robustly entrain the ongoing oscillation indicating that dendritic inhibition may be sufficient in synchronising principal cells during fast oscillations (Fig. 4.2). Furthermore, tonic upregulation of SST+IN activity decreased the power and increased the peak-frequency of cch-induced oscillations, as in PV+ experiments (Fig. 4.4). This suggests that SST+INs can powerfully modulate the hippocampal network during γ activity. Surprisingly, we also observed that sustained SST+IN photo-activation sometimes induced high-frequency oscillations during cch-γ (Fig. 4.6ai). Furthermore, sustained SST+IN photo-activation alone (without cch application) was sufficient to induce *de novo* high-frequency oscillations (Fig. 4.7ai). Therefore, the SST+IN network may be able to produce high-frequency rhythmic inhibition that can entrain the hippocampal network. However, the interpretation of our results is complicated by the requirement of synaptic excitation for the emergence of the *de novo* high-frequency γ oscillations. We discuss below possible mechanisms for the generation of *de novo* oscillations along with possible sources of synaptic excitation. Furthermore, we tested if SST+IN activity is necessary during cch-oscillations. We found that sustained photo-inhibition of SST+INs robustly decreased the power and increased the frequency of cch γ oscillations (Fig. 4.16, 4.17). These results demonstrate for the first time that SST+IN activity is necessary for the production of γ oscillations in the CA3 area of the hippocampus.

4.9.1 MECHANISMS GOVERNING HIPPOCAMPAL NETWORK MODULATION DURING SST+ INTERNEURON PHOTO-ACTIVATION

As discussed earlier, tonic upregulation of SST+IN activity decreased the power and increased the frequency of cch γ oscillations. Moreover, increasing the light intensity caused the collapse of cch-induced oscillations in about 50% of the experiments

(Fig. 4.5 and 4.6aii). These findings are very similar to the PV+IN photo-activation experiments. As before, this could be potentially explained by a progressive reduction in the number of active pyramidal neurons, causing a decrease in oscillation amplitude and a shorter duration cycle resulting from a PING mechanism, until the oscillation collapses.

There seem to be two main possibilities with which SST+INs could influence the hippocampal network PING mechanisms. Firstly, SST+INs could modulate the pyramidal cell - parvalbumin interneuron oscillator (Pyr-PV). In this case, SST+INs would have to inhibit both pyramidal and PV+ cells. There are converging evidence indicating that dendrite-targeting SST+INs potently inhibit pyramidal cells in the hippocampus (Katona et al. 1999; Lovett-Barron et al. 2012, 2014; Miles et al. 1996; Muller et al. 2014. There are also some evidence suggesting that SST+INs innervate PV+INs (Katona et al. 1999). In addition, PV+IN dendrites extend across most hippocampal layers (including the layers where SST+INs axons project) so it is likely that they receive GABAergic input from SST+INs (Gulyás et al. 1999; Tukker et al. 2013). On the other hand, it seems that there are less evidence regarding how strong is the GABAergic input that PV+INs receive from SST+INs (Chamberland et al. 2012; Cobb et al. 1997; Lacaille et al. 1987; Muller et al. 2014; Pelkey et al. 2017). However, it is possible that SST+INs strongly inhibit PV+INs either synaptically as has been shown in the cortex (Pfeffer et al. 2013) or through extrasynaptic GABA receptors (Ferando et al. 2015; Mann et al. 2010). Nevertheless, our data are not consistent with this hypothesis as synaptic inhibition from SST+INs would hyperpolarise both pyramidal and PV+INs, resulting in longer duration cycles and lower oscillation frequency, a phenomenon that we did not observe in our experiments (Fig. 4.4).

Alternatively, it is possible that SST+INs could be part of a separate or intertwined oscillator. In this case, making SST+INs more active could speed up the network while also preventing the Pyr-PV loop from entering slower γ oscillations (Brunel et al. 2003; Hajos 2004). For that to be true at least some SST+INs must

have fast signalling and strong reciprocal connections with pyramidal cells (Brunel et al. 2003). Interestingly, bistratified interneurons which express SST share similarities with PV+INs (Muller et al. 2014). Bistratified interneurons can fire action potentials with high-frequency (E. H. Buhl et al. 1996) and it also seems that they can be recruited with high-frequency input (Pouille et al. 2004). Furthermore, bistratified cells both receive strong inputs from and apply strong inhibition to pyramidal cells (Ali et al. 1998; Maccaferri et al. 2000). Therefore, it is possible that these cells are readily recruited via ChR2 photo-activation in our experiments and powerfully modulate the hippocampal network through their reciprocal connections.

Our data are also consistent with an ING model where tonic-activation of interneurons increases the frequency and decreases the power of oscillations (Traub et al. 1996b; Whittington et al. 2011). Even though it has been reported that SST+INs avoid inhibiting each other in the cortex (Pfeffer et al. 2013), in the hippocampus olm and bistratified cells (both expressing SST+) have been reported to inhibit each other (Leão et al. 2012). Furthermore, olm and bistratified cells form electrical synapses with gap junctions which could assist in γ generation of an interneuron network (Bartos et al. 2007; Baude et al. 2007; Leão et al. 2012; Traub et al. 2001).

4.9.2 MECHANISMS OF *DE NOVO* OSCILLATION GENERATION

4.9.2.1 GENERATION OF NETWORK EXCITATION DURING SST+ INTERNEURON PHOTO-ACTIVATION

It is possible that network excitation is responsible for the *de novo* oscillation generation as iGluR blockers abolished the oscillations during light stimulation (Fig. 4.9). In addition, single and multi-unit activity were elevated during SST+IN photo-activation (Fig. 4.14). Therefore, synaptic excitation is both produced during SST+IN photo-activation and may also be required for the induction of de novo oscillations in the LFP. We did not expect network excitation to arise during stimulation of SST+INs as they consist of GABAergic interneurons which are supposed to inhibit hippocampal and other cortical circuits (Hang Hu et al. 2013; Leão et al.

2012; Lovett-Barron et al. 2012, 2014; Ma et al. 2006; Pfeffer et al. 2013; Royer et al. 2012; Somogyi et al. 2005; Taniguchi et al. 2011; Urban-Ciecko et al. 2016). Thus, one possible explanation for this discrepancy is that many SST+INs go into depolarisation block during ChR2 activation and hence the hippocampal network gets excited through principal cell disinhibition. Indeed, we found that more than 50% SST+INs went into depolarisation block during blue light illumination. However, even if depolarisation block of SST+INs is responsible for some of the synaptic excitation observed, it is unlikely that it is sufficient for the generation of de novo oscillations. Firstly, photo-inhibition of SST+INs during spontaneous network activity is not able to induce γ activity (Fig. 4.19). Additionally, field responses during SST+IN photo-activation are graded and monotonic between low and high light intensity-levels (Fig. 4.5). Thus, it seems that disinhibition of pyramidal cells from depolarisation block of SST+INs cannot explain our results.

Another possible source of synaptic excitation is direct photo-activation of pyramidal cells that could arise from either off-targeting of our cre-lox virus system or from SST expression in a subpopulation of pyramidal cells. In agreement with this, we observed a small population of cells with somata in the pyramidal cell layer expressing ChR2 (Fig. 4.1). This would also be in line with the population spikes we observed during pulse photo-stimulation that could be arising from pyramidal cell firing (Fig. 4.3; P. Andersen et al. 1971; Wierenga et al. 2003). In addition, we found that during GABAR blockage, SST+IN photo-activation in aCSF induces seizure activity. These evidence support the notion that glutamatergic (or other types of excitatory) transmission are present during SST+IN photo-activation. Importantly, it has been demonstrated that pyramidal cell photo-activation alone can generate γ oscillations in the CA3 (Akam et al. 2012; Betterton et al. 2017; Butler et al. 2018). Therefore, it is possible that a small population of pyramidal cells is what generates γ oscillations in our experiments and thus dendritic inhibition from SST+INs is only permissive.

It is important to note that in these experiments we used the SST-IRES-cre mouse line that has been shown to be highly specific to SST+ cells (Taniguchi et al. 2011). Some off-target expression has been reported using this mouse line in juvenile animals but that was restricted to fast-spiking PV+ interneurons and not to excitatory pyramidal cells (Hang Hu et al. 2013). It is not that surprising that SST-cre may also express in some PV cells in young mice as these two groups of neurons have similar developmental origins and arise from the same clonal lineage (Harwell et al. 2015; Pelkey et al. 2017; Xu et al. 2004). Indeed, O-LM and bistratified SST+ cells have been reported to also express PV (Ferraguti et al. 2004; Klausberger et al. 2003). These dendrite-targeting cells do not seem to express in our PV-cre mice as there is lack of fluorescence in the dendrite layers of the CA3 (Fig. 3.2). The lack of expression in these cells may be explained by the low activity of their PV promoter (Ferraguti et al. 2004; Klausberger et al. 2003). Furthermore, we are not aware of any reports indicating that somatostatin is coexpressed in excitatory/pyramidal cells and in agreement with this we did not find any direct depolarisation in putative principal cells during light application. However, we sampled a small number of cells and it is still possible that some off-targeting occurs or that SST expressing pyramidal cells are present in CA3.

Alternatively, cells expressing ChR2 in the pyramidal cell layer could also be bistratified cells which have been shown to express somatostatin and target principal cell dendrites (Lovett-Barron et al. 2012; Muller et al. 2014; Pelkey et al. 2017; Somogyi et al. 2005). In that case synaptic excitation could be generated due to ephaptic coupling. In support of this, it has been shown that application of physiological electric fields is sufficient to alter the spiking of cortical cells (Anastassiou et al. 2011; Fröhlich et al. 2010).

4.9.2.2 SYNAPTIC INHIBITION AS THE MAIN INGREDIENT

It is also possible that synaptic excitation during SST+IN photo-activation has only a permissive role in the generation of *de novo* γ oscillations whereas dendritic inhib-

ition has a more instructive role required to synchronise principal cell assemblies. The simplest explanation of these results would be the generation of oscillations through an ING model since tonic photo-activation of an interneuron subtype could be capable of generating oscillations (Traub et al. 1996b; Whittington et al. 1995, 2011).

To begin with, we observed that sustained SST+IN photo-activation silences the LFP during cch-γ oscillations suggesting that SST+IN photo-activation produces strong synaptic inhibition. Indeed, whole-cell voltage clamp recordings showed that all recorded cells received stronger synaptic inhibition than excitation during SST+IN photo-activation in submerged conditions (Fig. 4.12). However, synaptic inhibition/excitation ratio may change in the interface conditions allowing for oscillation induction via increased network activity. Nevertheless, it is still possible that SST+INs could contribute to the generation of the oscillation as we have found some units that were phase-locked and increased their activity during the *de novo* oscillations (Fig. 4.14). Moreover, the frequency of the *de novo* oscillation increased with light intensity (Fig. 4.8). This contrasts photo-activation of principal cells at different light intensities, where the frequency of the oscillations remains relatively constant (Betterton et al. 2017; Butler et al. 2016). Therefore, the oscillation mechanisms could be different between SST+IN and pyramidal cell-induced γ. Further experiments are required to demonstrate whether SST+INs are indeed phase-locked and thus directly contribute to the generation of the *de novo* oscillation. Together, these results suggest that SST+IN photo-activation induces high-frequency oscillations that could be produced by cooperative effects of SST+IN dendritic inhibition and synaptic excitation.

4.9.3 SST+ INTERNEURONS ARE NECESSARY FOR HIPPOCAMPAL GAMMA OSCILLATIONS

Importantly, we addressed whether SST+IN activity is important during cch-γ oscillations. Sustained photo-inhibition of SST+INs at low intensities (2 - 5 mW)

decreased the power-area of cch-oscillations (Fig. 4.16). Furthermore, the oscillation frequency increased in more than 90% of the experiments very consistently (Fig. 4.16). Laser illumination at stronger light intensities (approx. 18 mW) robustly suppressed power and increased the peak frequency of the oscillation (Fig. 4.17). These experiments indicate that SST+IN activity is necessary for the maintenance of cch-induced oscillations in CA3. Furthermore, the decrease in γ power during laser illumination was much longer (5 - 10 seconds) than the time taken for Arch activation (order of milliseconds) in agreement with the PV+ experiments (Fig. 4.17). As before, γ power remained suppressed in the light-off period following laser stimulation (Fig. 4.17). This indicates that strong and long-lasting photo-inhibition may have successfully silenced the SST+IN terminals (El-Gaby et al. 2016; See PV chapter for detailed discussion). Our findings also reinforce recent experiments illustrating a critical role of SST+INs in the generation of low-frequency γ oscillations (around 30 Hz) in the visual cortex of awake animals (G. Chen et al. 2017; Veit et al. 2017). Taken together, these data may indicate that SST+INs may be important for γ oscillations across cortical circuits.

4.9.3.1 MECHANISMS GOVERNING HIPPOCAMPAL NETWORK MODULATION DURING SST+ INTERNEURON PHOTO-INHIBITION

SST+IN photo-inhibition decreases the power and robustly increases the frequency of cch γ oscillations (Fig. 4.16, 4.17). This means that SST+INs could be active signalling components that directly contribute to the generation of CA3 γ oscillations. Thus, it is possible that synchronised IPSCs from SST+INs contribute to pyramidal cell synchronisation during γ oscillations. Consequently, inhibition of SST+INs would lower the synchronous IPSCs in pyramidal cells resulting in reduced γ oscillation power. Synaptic inhibition received by pyramidal cells would then decrease, allowing them to reach the spike threshold faster, and hence increasing oscillation frequency. However, it has been demonstrated that the majority of current generation during γ oscillations arises from perisomatic inhibition around the principal

cell layer (Mann et al. 2005b; Oren et al. 2010). Thus, the decrease in γ power could also come from dendrite-targeting cells that synapse close to the cell body (We discuss this further in section 6.4 of the general discussion). Moreover, the increase in γ frequency could also arise from dis-inhibition on PV+INs (see PV chapter for detailed discussion on mechanism). Further investigation is required to reveal the precise cellular contributions to γ oscillation generation. Particularly, the critical experiments will be unit recordings from a large number of pyramidal cells, PV+ and SST+INs during optogenetic modulation of SST+INs.

Chapter 5

Effect Of Gamma Rhythm and Synchrony On Cell Input-Output Properties

5.1 INTRODUCTION

GABAergic interneurons are critically involved in the generation of cortical gamma (γ) oscillations in agreement with out findings (Chapters 4 & 5; Intro section 1.5). The emergence of these oscillations leads to both rhythmic inhibition of local pyramidal cells, and subsequent rhythmic excitation of local recurrently-connected neurons and downstream targets (Buzsáki et al. 2012; Sohal 2016; Whittington et al. 2011). However, γ oscillations are not simply turned on or off and variations in γ power are observed across distinct cognitive functions and brain disorders (Basar-Eroglu et al. 2007; Fries et al. 2001; Montgomery et al. 2007; Schomburg et al. 2014; Uhlhaas et al. 2006, 2010). Indeed, we observed a large variability in γ power of cch-oscillations across experiments (Fig. 3.15a, 4.9a). Furthermore, there was a dynamic variation in γ power even within short time-scales as has been reported before (Fig. 3.1b; Oren et al. 2006). Such variations in γ power could arise from changes in network size (the number of active neurons), synchrony or rhythmicity. Synchrony can be defined as the temporal precision of firing within each γ cycle and rhythmicity as the periodicity at which synchronous neuronal ensembles fire during oscillatory activities. Dissociating the effects of these network parameters on neuronal signalling could

be of critical importance in understanding the consequences of γ power alterations.

The role of network oscillations on single neuron processing can be examined by varying the temporal pattern of simulated synaptic inputs (which could include rhythmicity and synchrony) and observing how this affects the spiking response to increasing excitatory drive (for example the number of presynaptic inputs). Sohal and colleagues used this approach to examine the significance of γ oscillations for the input-output functions of neocortical pyramidal neurons (Sohal et al. 2009). They measured pyramidal cell spiking response to 3 different patterns of simulated excitatory synaptic inputs which are i) asynchronous trains (randomly sampled from uniform distribution), ii) theta-frequency inputs (turned on for only half of each 125 ms cycle, with average frequency conserved) and iii) γ frequency inputs (turned on for only half of each 25 ms cycle, with average frequency conserved). They found that gain was selectively enhanced by 40 Hz frequency inputs, suggesting that (γ) oscillations could provide state-dependent modulation of information transfer between brain regions (Sohal et al. 2009). While this study has spurred renewed interest in the possible functions of γ oscillations, numerous issues remain to be addressed. In particular, it was not examined whether the change in input-output gain was specific to rhythmic and synchronous synaptic inputs, or whether it could also be induced by aperiodic (low rhythmicity) synchronous inputs at the same frequency. Furthermore, there was no evidence as to whether the gain enhancement was specific for rhythmic excitatory versus rhythmic inhibitory inputs, or how gain would vary with changes in (γ) power.

To address these issues, we first tested how periodic and aperiodic excitatory inputs (constant synchrony) can impact gain of pyramidal cells in the mouse somatosensory cortex (S1). In addition, to explore whether these effects were generic across different types of cortical pyramidal neurons, we examined if different levels of rhythmic excitatory input (synchronous) at 40 Hz can also affect pyramidal cell gain in CA1 area of the hippocampus. To investigate whether gain enhancement would also be mediated by inhibitory inputs, we examined how alterations in the

rhythmicity of inhibitory inputs (synchronous) at 40 Hz affects the input-output properties of pyramidal cells. We thus used dynamic clamp to deliver simulated inhibitory post-synaptic conductances at 40 Hz, whilst measuring the spike output of principal cells at different tonic excitation strengths (square pulse). In these experiments, we examined the effects of independently varying either the rhythmicity or synchrony of the 40 Hz train, which both affect γ power. Lowering the synchrony and rhythmicity of 40 Hz inputs has opposing effects on train variability. Given the importance of variability in instructing action potential timing (Mainen et al. 1995), we considered the possibility that it could explain some of the differences observed between the synchrony and rhythmicity experiments. We thus tested how trains with different γ power, but with similar variability, could affect the gain in putative pyramidal cells. Lastly, it has been shown that noisy membrane potential fluctuations (in contrast to constant excitatory input) are very effective in eliciting action potentials with high temporal fidelity (Mainen et al. 1995). We thus examined how the changes in γ train properties, altered in the above experiments, affected spike fidelity.

5.2 INPUT RESISTANCE AND STABILITY

Whole-cell recordings were acquired from CA1 and S1 brain areas using the perforated patch configuration to maximise cell stability. To quantify cell stability over time the membrane voltage (Vm) and the input resistance (Ri) were measured throughout the experiment (Section 2.5). In the 46 patched cells (n = 1, normal breakthrough/ not perforated) Ri and Vm were compared at the beginning and end of the experiment (Fig. 5.1a). There was a significant decrease on average Ri of 8.53 ± 3.08 MΩ (Fig. 5.1b) and Vm of 3.05 ± 0.48mV (Fig. 5.1c). Despite the population average showing that there is a relatively small directional change (about 5 %), Ri changes may have been masked during single experiments. In order to quantify the stability of each experiment, the Ri and Vm for each cell were calculated as a percentage change from the start of the experiment (Fig. 5.1d). The average percentage change in Ri and Vm were calculated to be 9.63 ± 1.02% and 5.15 ± 0.45%, respectively with only two cells exceeding 20% change in Ri (Fig. 5.1d). Furthermore, any changes in Ri and Vm should have minimal impact on the outcome of our findings due to the use of our experimental protocol which will be described in the next section (See also section 5.10).

5.3 EXPERIMENTAL PROTOCOL AND INPUT GENERATION

In order to study how alterations in the rhythmicity or synchrony of γ oscillations affect principal cell output, we sought to generate appropriate input stimuli. We first generated synchronous compound synaptic events, made up of 1000 individual synaptic inputs, that repeated rhythmically at 40 Hz and resulted in γ oscillation conductance trains (Fig.5.2a Top). A frequency of 40 Hz was chosen because excitatory inputs at this frequency were previously shown to cause a multiplicative gain enhancement of pyramidal cell output (Sohal et al. 2009).

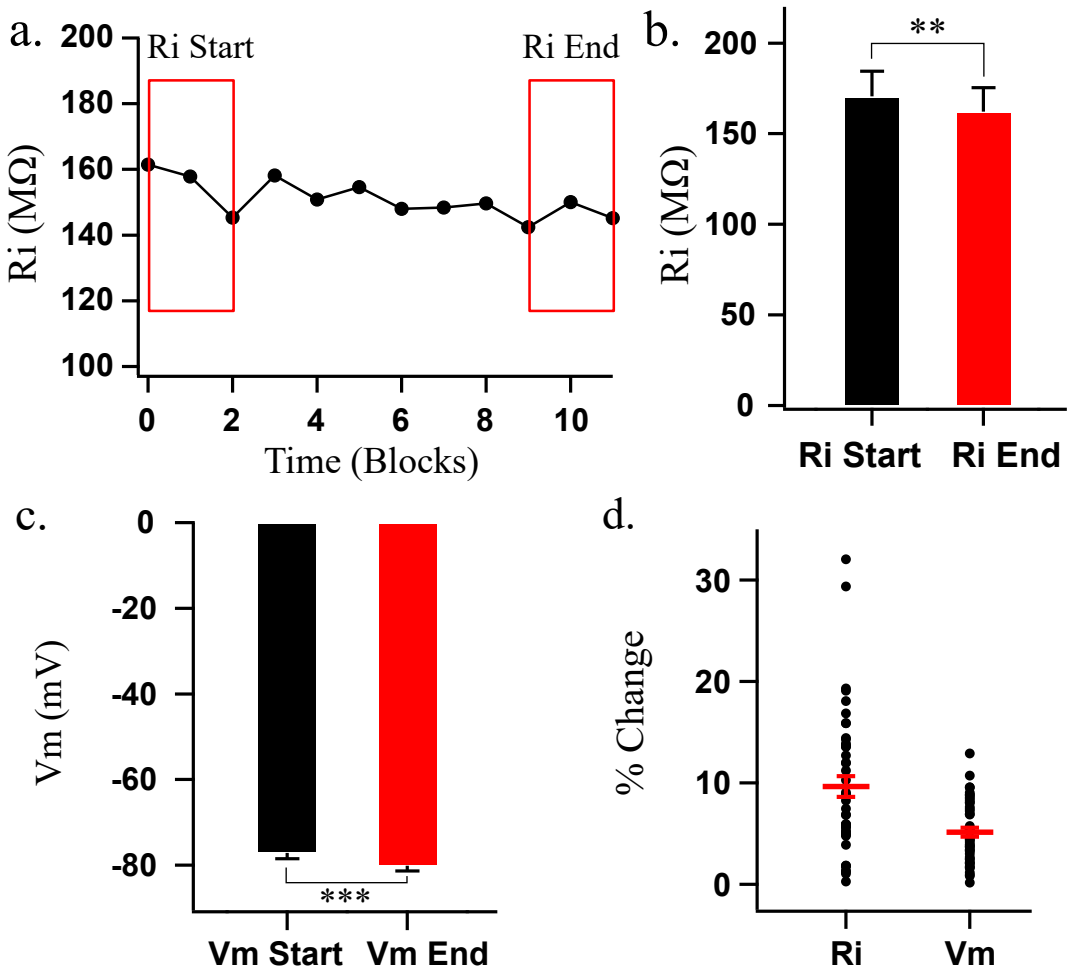


Figure 5.1: Input resistance and cell stability. Hyperpolarising pulses of 80 pA were applied at the start of each time block (1.5 - 2.5 minutes depending on number of repetitions) and input resistance (Ri) was calculated. a) Ri of one cell plotted against time in one experiment. The red squared indicate the times at which Ri and membrane voltage (Vm) where analysed. b) Average Ri between start and end of the experiment ($n = 46$, $p < 0.01$, paired t-test). c) Average Vm between start and end of the experiment ($n = 46$, $p < 0.001$, paired t-test). d) Percentage change of Ri and Vm between the start and end of each experiment. Red horizontal lines represent the population average change and error bars SEM.

We then proceeded with creating input conductance trains with different levels of rhythm or synchrony (Methods section 2.6). A reduction in rhythmicity (synchrony kept constant) was achieved by increasing the variability of synchronous-input periodicity, termed as coefficient of variation (CV) (Fig.5.2a Middle). A decrease in synchrony (cycle rhythmicity kept constant) was achieved by varying the time, termed as jitter, at which the individual synaptic inputs took place in each cycle (Fig.5.2a Bottom). A decrease in either synchrony (increasing jitter only) or rhythmicity (increasing CV only) resulted in a reduction in γ power (Fig.5.2b). A close inspection of the conductance trains revealed that lowering the rhythm or synchrony had opposing effects on the variance of their respective conductance trains (Fig.5.2c). Particularly, lowering the rhythm of the synaptic inputs increased the variability of the conductance train, while lowering the synchrony of the synaptic inputs decreased the variability of the conductance train (Fig.5.2a, c). Therefore, varying levels of synchrony and rhythmicity produce differential effects on γ oscillation synaptic conductance trains. For that reason, we also examined how trains with similar variability but different γ power could alter principal cell output.

To study the modulation of γ power on principal cell output, the 40 Hz stimuli were presented during increasing excitatory drive (tonic) and the membrane voltage of the cell was recorded. For each level of excitation the selected stimuli were presented along with an additional flat square pulse, which was used as a control (or normalisation reference). The control stimulus was used in order to quantify the effects on gain induced by the stimuli of interest. In addition, the stimuli were presented at least 5 times and shuffled for each excitation strength (Fig. 5.3). This was done to ensure that long-term changes in Ri or any other parameter equally affected all tested conditions. For clarity the quantification of our main findings (Excluding excitation-rhythm experiments in S1) is summarised in tables 5.1 and 5.2.

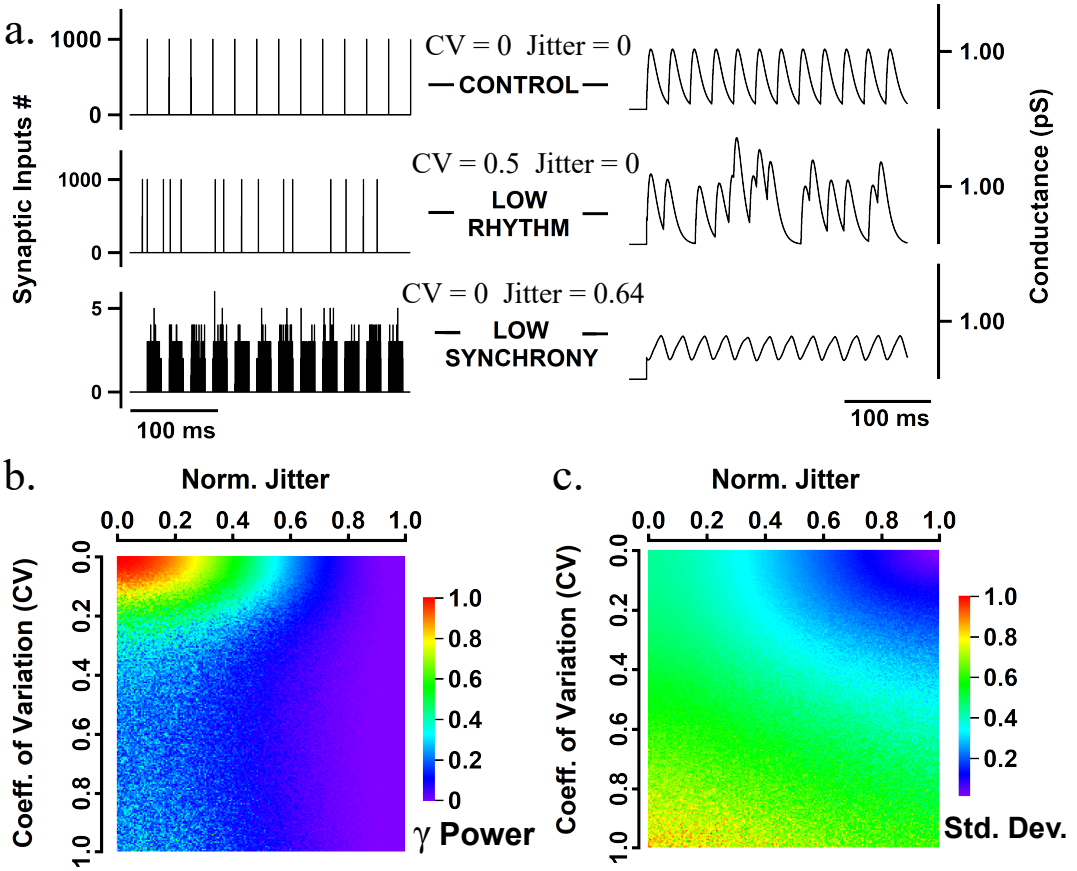


Figure 5.2: Generation of γ oscillation inputs. a) Simulated synaptic inputs and conductance stimuli; The conductance trains were generated by simulating 1000 post synaptic inputs occurring simultaneously 40 times per second (Top). The same inputs were created with reduced rhythm (middle, CV = 0.5) and synchrony (bottom, jitter = 0.64). b) Normalised γ power and c) standard deviation of synaptic conductance trains across a range of coefficient of variation (rhythmicity) and jitter (synchrony) values.

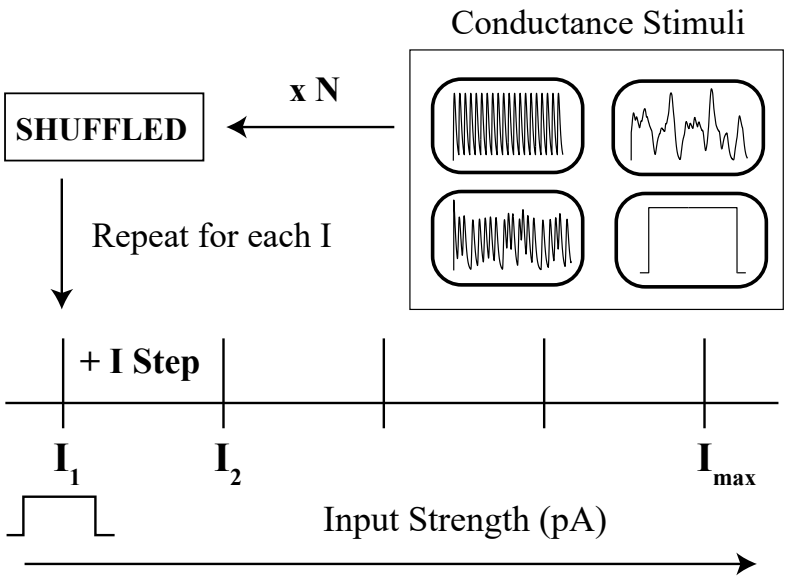


Figure 5.3: Experimental Protocol. The action potentials of each cell were recorded for increasing excitatory drives (square flat excitation). The current was increased with a fixed current step (Istep) from I1 to Imax. Each conductance stimulus was presented at least 5 times (n = 5) for each stimulation strength. The number of repetitions was fixed in each experiment. In the case of excitation, where current clamp was used, conductance stimuli were replaced with excitatory currents. The base rhythmic excitation stimulus had a peak of 1 pA. The other base excitation stimuli were created to have matching charge over the 2 second stimulation period. In addition, all conductance stimuli used for one experiment were quantified to have equal conductance sums over the stimulation period (2 seconds).

5.4 EFFECTS OF EXCITATORY GAMMA RHYTHM ON PRINCIPAL CELL GAIN IN S1

The purpose of the first experiment was twofold. Firstly, we wanted to observe the gain in principal cell output induced by 40 Hz rhythmic excitatory input as demonstrated before (Sohal et al. 2009). Secondly, we wanted to test if the same gain can be attained with 40 Hz arrhythmic synchronous excitatory input. To investigate this we patched putative pyramidal cells in layer 2/3 of primary somatosensory cortex (S1) and applied these two stimuli as excitatory trains using the current clamp (Fig. 5.4a). We thus injected the inputs as synaptic currents instead of synaptic conductances (Fig. 5.4a). In addition, we applied a flat square pulse as a control comparison for gain assessment (Fig. 5.4a). The current clamp configuration was used as the majority of excitatory glutamatergic synapses are present on dendritic spines. Thus, their activation would largely be experienced as conducted current inputs at the level of the patch-clamp recordings site at the cell somata. In all experiments the firing rate versus input (f-i) relationship was plotted for each condition, and multiplicative (or divisive) changes in gain were quantified by calculating the linear slope of the f-i plot (Fig. 5.4b). Multiplicative or divisive gain were observed as an increase or decrease of the linear slope, respectively. The differences between the three conditions were assessed with a repeated measures ANOVA (rmANOVA) and followed by post-hoc paired t-tests with correction for multiple comparisons (bonferroni correction).

Rhythmic excitation at 40 Hz (High (rhythm): CV = 0) increased the slope of the f-i plot when compared to the control (Flat) condition (High: 0.104 ± 0.015, Flat: 0.064 ± 0.013, $p < 0.01$, paired t-test; Fig. 5.4b, c). Interestingly, the arrhythmic stimulus (Low: CV = 0.30) also increased the slope when compared to the flat stimulus (Low: 0.095 ± 0.015, $p < 0.01$, paired t-test; Fig. 5.4b, c). There was also a small but significant decrease of the slope in arrhythmic when compared to rhythmic

stimuli ($p < 0.05$, paired t-test; Fig. 5.4b, c). These results demonstrate that both rhythmic and arrhythmic input at 40 Hz can lead to multiplicative enhancement of gain in S1 principal cells. However, rhythmic 40 Hz excitatory currents may be more effective at enhancing gain relative to aperiodic inputs.

To further explore possible additive (or subtractive) changes in gain of principal cells, the rheobase was quantified as the minimum excitation required for the cell to elicit three action potentials over the course of single trial (Fig. 5.4b). Additive or subtractive gain were observed as a decrease or increase in rheobase, respectively. The rheobase was not found significantly different between rhythmic, arrhythmic and control stimuli, suggesting that there was no additive change in gain. (Flat: 0.11 ± 0.033, Low: 0.08 ± 0.016, High: 0.12 ± 0.033, $p = 0.16$, rmANOVA; Fig. 5.4d). The maximum spike rate was increased by both rhythmic and arrhythmic stimuli when compared to flat stimulus (High: 0.989 ± 0.011, Low: 0.952 ± 0.016, Flat: 0.626 ± 0.045;, Flat-High: $p < 0.01$, Flat-Low, $p < 0.001$, paired t-tests; Fig. 5.4e), while the rhythmic and arrhythmic stimuli elicited similar maximum spike rates ($p = 0.64$, paired t-test; Fig. 5.4e). The increases in maximum spike rates for high-rhythm and low-rhythm trains compared to the flat stimulus, with no clear changes in the rheobase, are consistent with multiplicative increases in gain. It should be noted that for statistical comparisons, the slope and maximum spike rate for each condition were normalised by the maximum spike rate obtained in each experiment, and the rheobase was expressed as a fraction of the input yielding the max spike rate in each experiment.

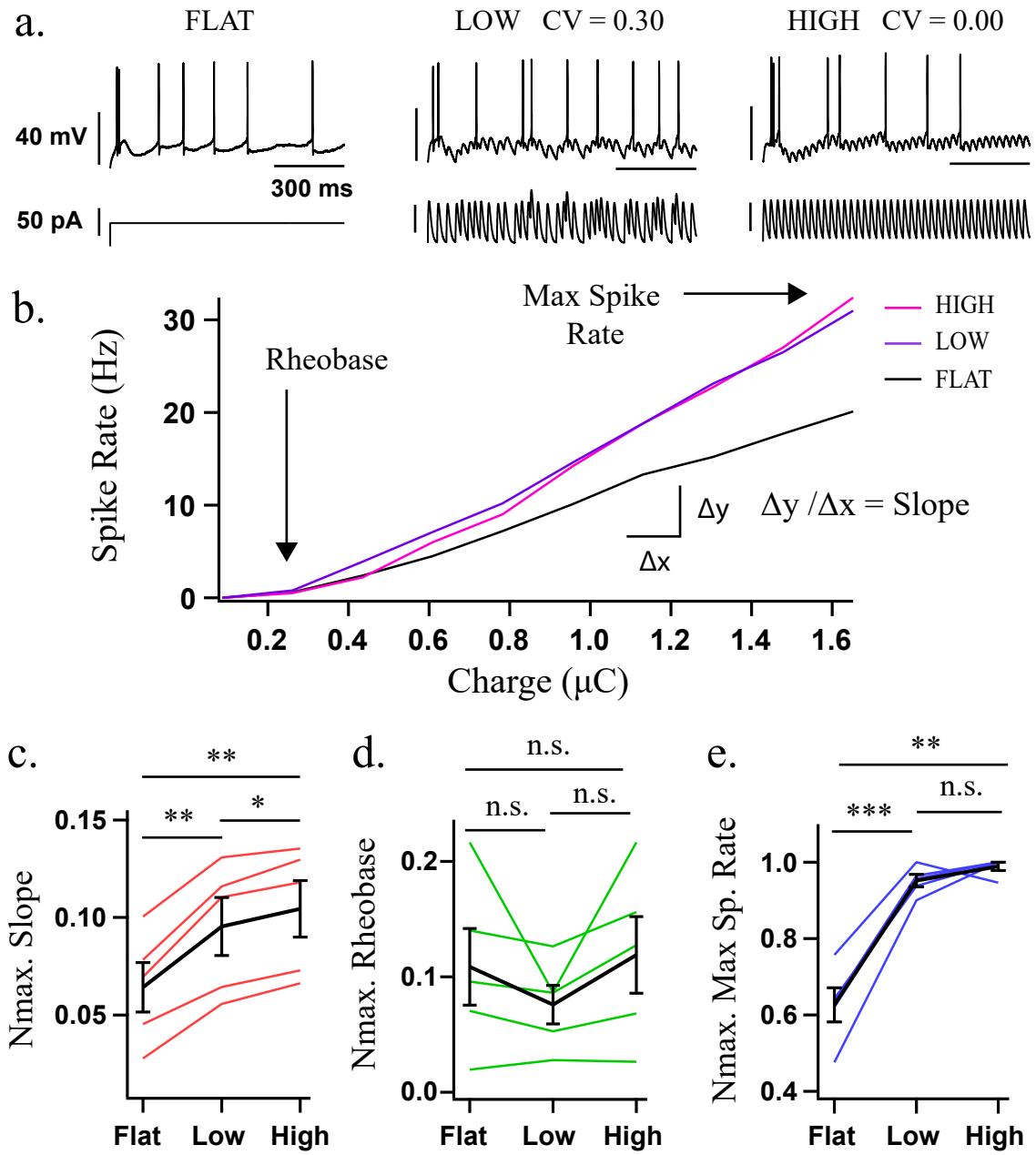


Figure 5.4: Rhythmic and arrhythmic 40 Hz excitation produce multiplicative enhancement of gain in cortical area S1. Current clamp experiments were performed in pyramidal cells of the S1 area (layer 2/3, n = 5). Paired t-tests were performed with bonferroni correction if rmANOVA was found significant. a) Top: Representative recordings when a putative pyramidal cell was injected with with rhythmic (High), arrhythmic (Low) and square-step (Flat) current inputs (Bottom) at 0.61 μC. b) Frequency - Input (f-i) plot derived from the pyramidal cell in a). c) Frequency - input slope for each condition normalised by the maximum spike rate in each experiment (Nmax. Slope); rmANOVA, $F(2, 8) = 73.99$, $p < 0.0001$. d) Rheobase for each condition, expressed as a fraction of the input yielding the maximum spike rate in each experiment (Nmax. Rheobase); rmANOVA: $F(2, 8) = 2.31$, $p = 0.16$. e) Maximum spike rate for each condition normalised by the maximum spike rate in each experiment (Nmax. MAx Sp. Rate); rmANOVA: $F(1.047, 4.190) = 55.22$, $p < 0.001$. Black lines represent the population average and bars the +/− SEM. rmANOVA followed by post-hoc paired t-test for multiple comparisons. *$p < 0.05$, **$p < 0.01$, ***$p < 0.001$, $^{n.s.}p >= 0.05$.

5.5 EFFECTS OF EXCITATORY GAMMA RHYTHM ON PRINCIPAL CELL GAIN IN CA1

Next we wanted to test how γ frequency inputs with varying levels of rhythmicity affect the output of principal cells in hippocampal area CA1. This was done to ensure that our findings were not restricted only to the function of layer 2/3 pyramidal cells of the S1 cortex. To achieve this we employed current clamp and injected excitatory currents at 40 Hz with three levels of rhythmicity in putative CA1 principal cells (High: CV = 0, Mid: CV = 0.2, Low: CV = 0.5; Fig. 5.5a). As before, an additional flat-square step was also applied as a control. All the parameters obtained from the 40 Hz stimuli were normalised with the equivalent parameters resulting from flat excitation. This was done in order to compare the effects between the 40 Hz trains. Decreasing the rhythmicity of excitatory 40 Hz stimuli resulted in a small reduction of the f-i plot slope (High: 1.46 ± 0.044, Mid: 1.42 ± 0.048, Low: 1.29 ± 0.034; Fig. 5.5c). This was found to be significant between High-Low (CV: 0 to 0.5) rhythm trains and between Mid-Low (CV: 0.2 to 0.5) rhythm trains, but not between High-Mid (CV: 0 to 0.2) rhythm trains (High-Low, $p < 0.01$, paired t-test, Mid-Low, $p < 0.05$, paired t-test, High-Mid, $p = 0.15$, paired t-test; Fig. 5.5c). Therefore, it seems that a strong reduction in the rhythm of 40 Hz current inputs produces divisive decreases in the gain of CA1 principal cells. Furthermore, the rheobase decreased when the rhythm of the 40 Hz trains was reduced (High: 0.99 ± 0.021, Mid: 0.93 ± 0.037, Low: 0.68 ± 0.027, High-Low: p< 0.001, Mid-Low: p; 0.001, paired t-tests; Fig. 5.5d). This means pyramidal cells in CA1 start spiking with less excitation in low rhythmic trains when compared to high rhythmic trains, hence there is a additive increase in gain. It should be noted that there was no statistical difference between trains with high and mid rhythmicity ($p = 0.08$, paired t-test). Lastly, the maximum spike rate was slightly reduced only when the rhythmicity was decreased between mid to low pairs (High: 1.565 ± 0.039, Mid: 1.572 ± 0.041,

Low: 1.482 ± 0.036, Mid-Low: $p < 0.05$, High-Low: $p = 0.096$, High-Mid: $p = 1.00$, paired t-tests; Fig. 5.5e). The modest effects of reduced rhythmicity on maximum spike rate probably arise due to the opposing additive and divisive effects of disrupting rhythmicity. Specifically, lowering rhythmicity divisively reduced the gain, but additively increased the gain, resulting in similar range of spike rates for the range of inputs tested. In addition, reducing rhythmicity from high to mid levels (CV from 0 to 0.2) did not have multiplicative or additive effects on gain. This suggests that changes in rhythmicity of this magnitude in 40 Hz excitatory trains are not sufficient to alter the gain of CA1 pyramidal cells. All three trains increased the slope when compared to flat control (Flat-Low: $p< 0.01$, Flat-Mid: $p< 0.01$,Flat-High: $p< 0.001$; Fig. 5.5e). This reinforces the previous findings in S1, illustrating that arrhythmic excitatory input at 40 Hz produce a multiplicative enhancement of gain, but to a lesser extend than their rhythmic counterpart. As these effects were not qualitatively different between CA1 and S1 areas, in the following experiments the results were merged from both of these areas. It should be noted that the difference in rheobase and maximum spike rates were absent in S1. This is probably because the rhythmicity was not disrupted as much as in CA1 (S1 Low-CV = 0.3, CA1 Low-CV = 0.5). Indeed, in other CA1 and S1 experiments where identical trains were used, the rheobase and maximum spike rate changes were similar.

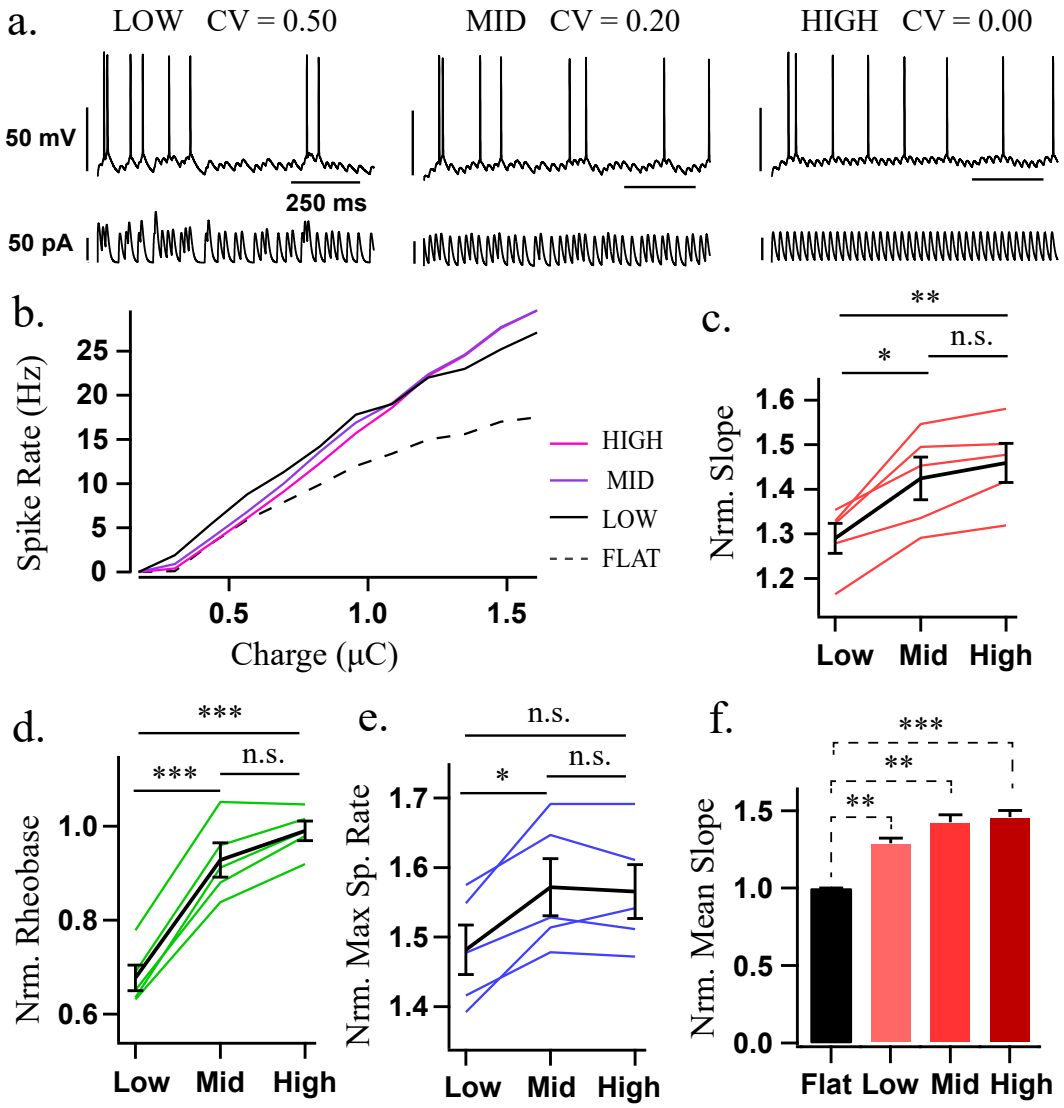


Figure 5.5: Reducing rhythmicity at 40 Hz decreases gain divisively in hippocampal area CA1. Current clamp experiments were performed in pyramidal cells of the CA1 hippocampus area (n = 5). a) Top: Representative recordings when a putative pyramidal cell was injected with Bottom) currents of different rhythm levels at 0.57 μC. b) F-i plot derived from the pyramidal cell in a). c) F-i slope for three trains of varying rhythmicity (High: CV = 0, Mid: CV = 0.2, Low: CV = 0.5;) normalised by the flat stimulus (Nrm. Slope); rmANOVA: $F(2, 8) = 33.22$, $p < 0.0001$. d) Rheobase for three trains of varying rhythmicity normalised by flat stimulus (Nrm. Rheobase); rmANOVA: ($F(2, 8) = 217.78$, $p < 0.0001$). e) Maximum spike rate for three trains of varying rhythmicity normalised by flat stimulus (Nrm. Max Sp. Rate); rmANOVA: ($F(2, 8) = 13.72$, $p < 0.003$). Black lines represent the population average and bars the +/− SEM. rmANOVA followed by post-hoc paired t-test for multiple comparisons. f) Mean slope for three trains of varying rhythmicity normalised by flat stimulus (Nrm. Mean Slope). The three conditions were compared with flat stimulus (value of 1) using one-sample t-tests. *$p < 0.05$, **$p < 0.01$, ***$p < 0.001$, $^{n.s.}p >= 0.05$. Dashed brackets represent one sample t-tests and solid brackets represent paired t-tests.

5.6 EFFECTS OF INHIBITORY GAMMA RHYTHM ON PRINCIPAL CELL GAIN

As mentioned before, GABAergic inhibition is critical for synchronisation of pyramidal/principal cells during γ oscillations. Therefore, we wanted to investigate i) if inhibitory rhythmic input at 40 Hz also affects the gain of principal cell output and ii) how changes in rhythmicity could alter that. Accordingly, we generated 40 Hz inhibitory post-synaptic conductance (IPSG) trains with different levels of rhythmicity (Fig. 5.2) and injected them in putative pyramidal cells using dynamic clamp (Fig. 5.6). The purpose of this was to mimic the perisomatic inhibitory inputs pyramidal cells receive during γ oscillations (Mann et al. 2005b; Oren et al. 2006). Therefore, three IPSG trains were applied, with varied levels of rhythmicity that matched the excitatory trains from the previous experiments, along with the flat control (High: CV = 0, Mid: CV = 0.2, Low: CV = 0.5; Fig. 5.7a). In agreement with the excitation experiments, the slope of the f-i plots was reduced as rhythmicity decreased (High: 1.28 $\pm$ 0.094, Mid: 1.15 $\pm$ 0.081, Low: 1.03 $\pm$ 0.072; High-Low: $p < 0.05$, Mid-Low: $p < 0.01$, paired t-test; Fig. 5.7b and c).

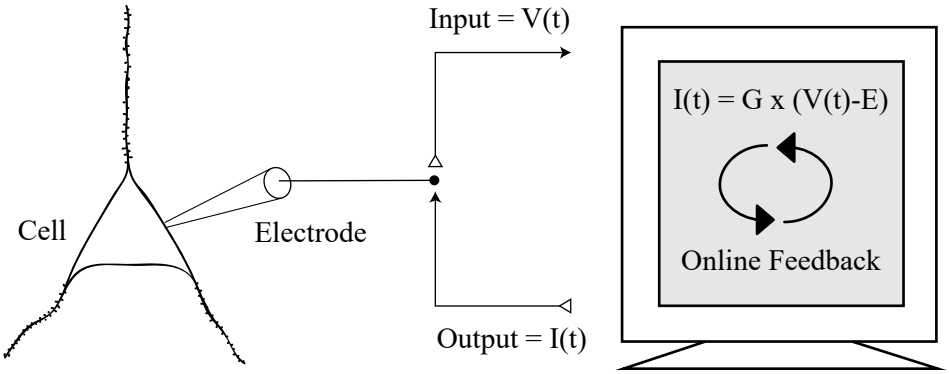


Figure 5.6: Schematic illustration of the dynamic clamp configuration. Dynamic clamp simulates synaptic currents when provided with a synaptic conductance input and a reversal potential value for the simulated receptor. It achieves this by taking advantage of a fast real-time feedback loop that consists of reading the membrane voltage and injecting the appropriate current output for a given conductance value at any given time.

This was not found to be statistically different between the high and mid rhythm pairs, as in excitation trains ($p = 0.75$, paired t-test). Therefore, it seems that reducing the rhythmicity of 40 Hz inputs decreases divisively the gain of principal cell output. In addition, as rhythmicity decreased the rheobase current was strongly reduced, hence increasing gain additively (High: 0.63 ± 0.047, Mid: 0.43 ± 0.082, Low: 0.27 ± 0.085; High-Low: $p < 0.001$, Mid-Low: $p < 0.001$, High-Mid: $p < 0.01$, paired t-test; Fig. 5.7d). Thus, less excitatory input is required to elicit spiking in pyramidal cells during 40 Hz inhibitory inputs of lower rhythmicity (Fig. 5.7b). Furthermore, the maximum spike rates were very similar between conditions and were not statistically different (Low: 1.396 ± 0.057, Mid: 1.431 ± 0.069, High: 1.465 ± 0.085; $p = 0.11$, rmANOVA; Fig. 5.7e). Given that the maximum spike rates did not change when the rhythm decreased, the additive increase in gain must have been balanced by the divisive decrease in gain, as previously shown.

Interestingly, the mean slope was higher only during rhythmic IPSG trains when compared to the flat control (Flat-High: $p < 0.05$, Flat-Mid: $p = 0.31$, Flat-Low $p = 1.00$, one sample t-tests; Fig. 5.7f). These experiments suggest that inhibitory rhythmic but not arrhythmic inputs at 40 Hz can multiplicatively increase the gain of principal cell outputs. On the other hand, both rhythmic and arrhythmic inputs strongly reduce rheobase, and lead to increased maximum spike rates in the range tested when compared to the flat stimulus ($p < 0.01$, one-sample t-tests). Therefore, reductions in rhythmicity of 40 Hz inhibitory inputs produce similar trends to excitation experiments. However, the overall slope of inhibitory rhythmic 40 Hz trains increases less than excitatory 40 Hz trains when compared to flat controls (inhibitory High train at 1.28 vs excitatory High train at 1.46). This could indicate that in our experiments excitatory currents are more effective than inhibitory ones in producing enhancement of multiplicative gain in principal cells.

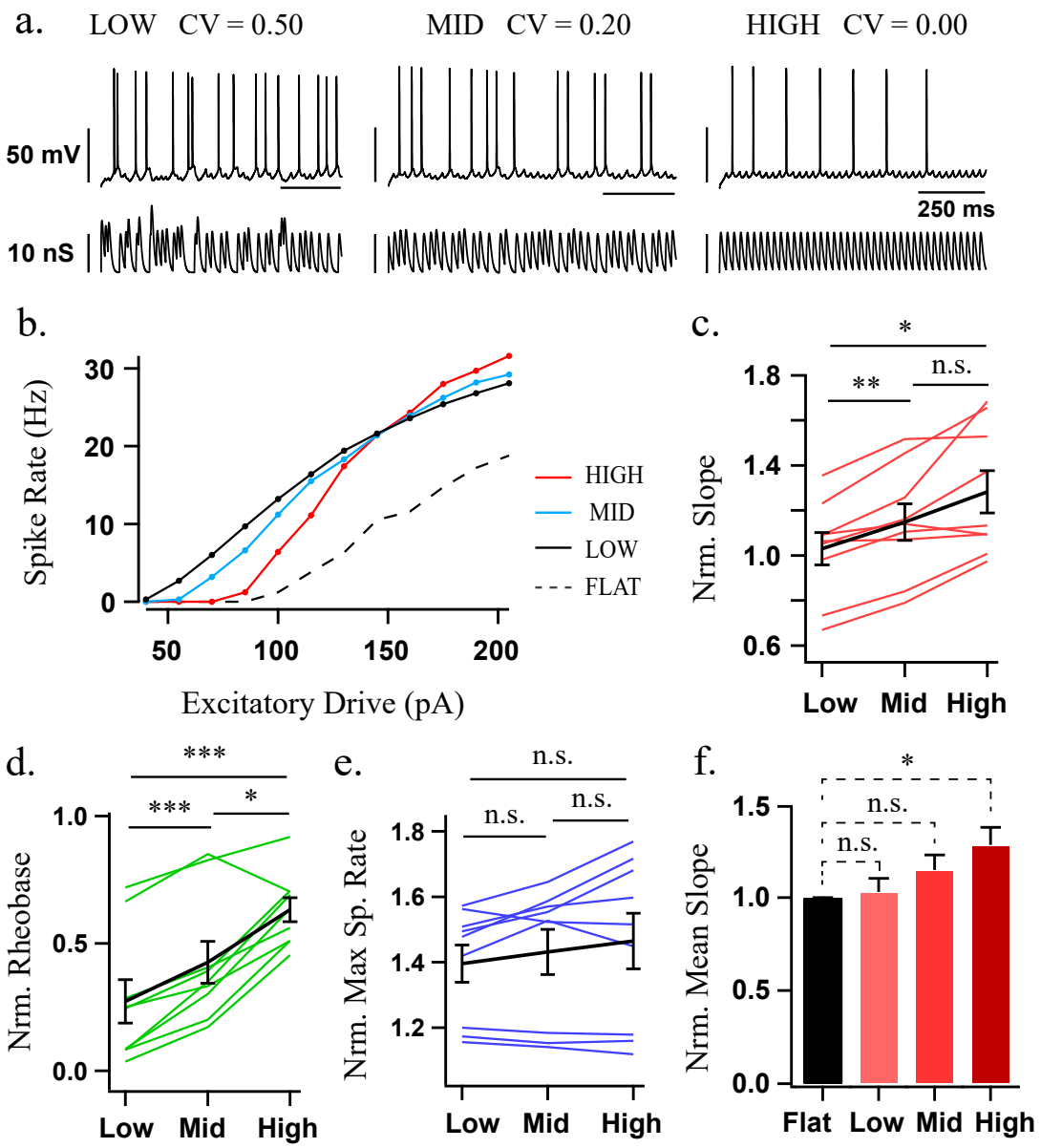


Figure 5.7: Impaired inhibitory rhythmicity produces divisive decreases and additive increases in gain. IPSG trains with different rhythmicity were applied using dynamic clamp to putative pyramidal cells in to measure the gain of their output (n = 9). a) Representative recordings Top) from a putative pyramidal cell in CA1 when presented with Bottom) 40 Hz IPSG trains with different rhythm and simultaneous tonic excitation of 100 pA. b) F-i plot derived by increasing positive current levels whilst injecting the conductance trains from a. c) F-i slope for three trains of varying rhythmicity (High: CV = 0, Mid: CV = 0.2, Low: CV = 0.5;) normalised by the flat stimulus (Nrm. Slope); rmANOVA: $F(1.11, 8.92) = 14.13$, $p < 0.004$. d) Rheobase current for three trains of varying rhythmicity normalised by flat stimulus (Nrm. Rheobase); rmANOVA: $F(1.16, 9.26) = 28.52$, $p < 0.0003$. e) Maximum spike rate for three trains of varying rhythmicity normalised by flat stimulus (Nrm. Max Sp. Rate); rmANOVA: $F(1.27, 10.13) = 2.97$, $p = 0.11$. Black lines represent the population average and bars the +/− SEM. rmANOVA followed by post-hoc paired t-test for multiple comparisons. f) Mean slope for three trains of varying rhythmicity normalised by flat stimulus (Nrm. Mean Slope). The three conditions were compared with flat stimulus (value of 1) using one-sample t-tests. *$p < 0.05$, **$p < 0.01$, ***$p < 0.001$, $^{n.s.}p >= 0.05$. Dashed brackets represent one sample t-tests and solid brackets represent paired t-tests.

5.7 EFFECTS OF SYNCHRONY ON PRINCIPAL CELL GAIN

γ power alterations can also arise from reduced synchronisation of pyramidal cells. We thus wanted to test how alterations in synchrony affected pyramidal cell output. Consequently, we generated 40 Hz trains with different levels of synchrony with γ power matching the three rhythm trains from the previous experiment (High: Jitter = 0, Mid: Jitter = 0.45, Low: Jitter = 0.66; Fig. 5.8a). The three synchronous trains were applied to putative pyramidal cells using dynamic clamp along with the flat control and the f-i plots for each cell were obtained as before (Fig. 5.8b). As the synchrony of the trains decreased the slope of f-i plots was also reduced (High: 1.22 $\pm$ 0.086, Mid: 1.14 $\pm$ 0.058, Low: 1.07 $\pm$ 0.041; High-Low: $p < 0.05$, Mid-Low: $p < 0.05$, paired t-tests: Fig. 5.8b, c). The difference in mid-high synchrony trains was not found to be statistically significant (High-Mid: $p = 0.11$, paired t-test). Thus, decreasing the synchrony of rhythmic inhibitory trains at 40 Hz produces divisive decreases in gain of putative principal cell output. In addition, reducing synchrony increased the rheobase current and thus subtractively reduced gain (High: 0.67 $\pm$ 0.066, Mid: 0.78 $\pm$ 0.039, Low: 0.86 $\pm$ 0.022; High-Low: $p < 0.05$, Mid-Low: $p < 0.01$; Fig. 5.8d). This was not found statistically different between the mid-high synchrony trains (High-Mid: $p = 0.13$, paired t-test). This is in contrast to lower rhythmicity that additively increases gain. Thus, a larger excitatory input is required to elicit spiking in pyramidal cells during 40 Hz inhibitory inputs of lower synchrony (Fig. 5.8b). Furthermore, the maximum spike rate decreased when synchrony was lowered (High: 1.37 $\pm$ 0.098, Mid: 1.22 $\pm$ 0.072, Low: 1.11 $\pm$ 0.036; High-Low: $p < 0.05$, Mid-High: $p < 0.01$; Fig. 5.8e). This was not found statistically different between the low-mid synchrony trains (High-Mid: $p = 0.13$, paired t-test).

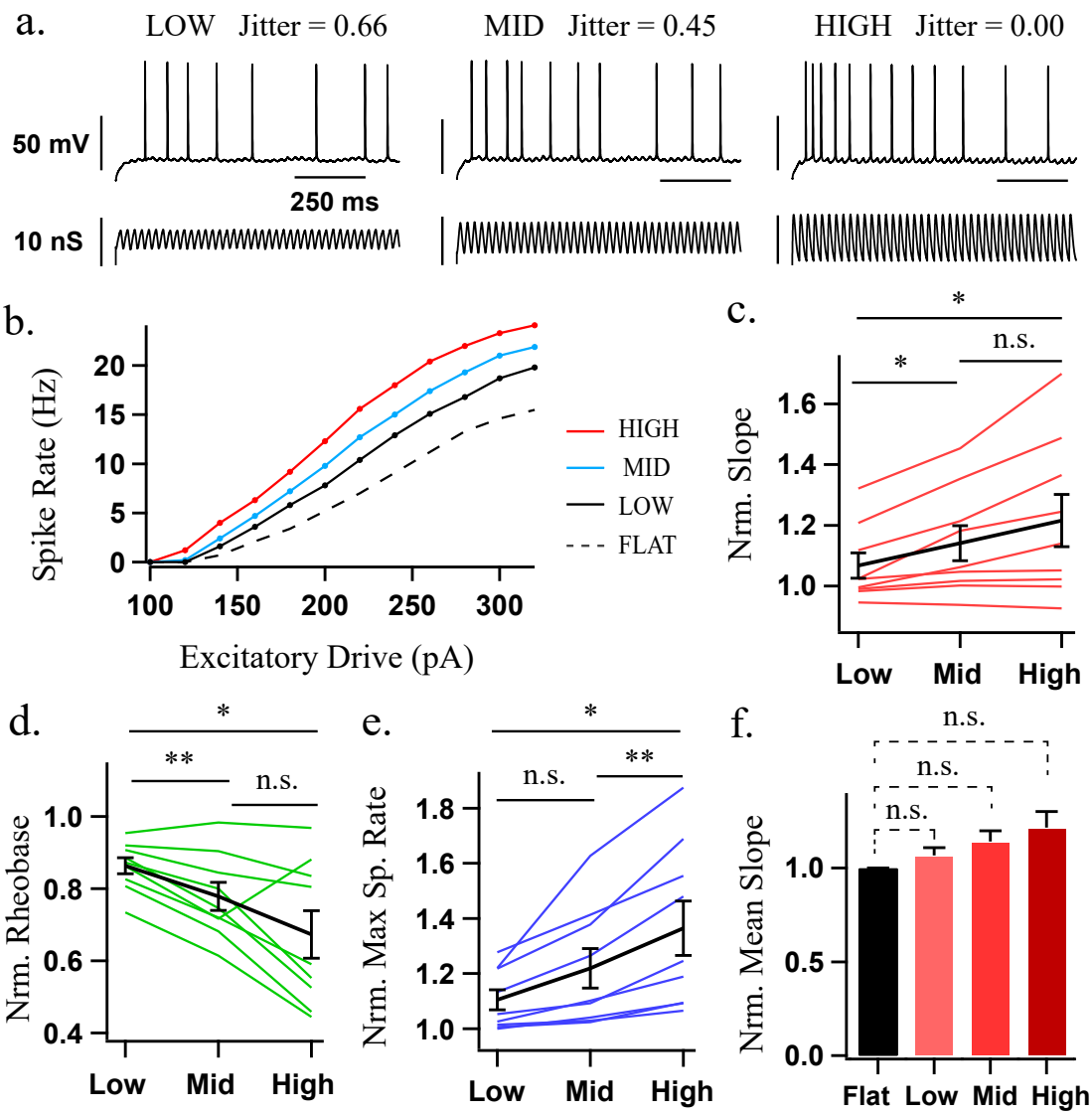


Figure 5.8: Impaired synchrony produces divisive and subtractive decreases in gain. IPSG trains with different synchrony were applied using dynamic clamp to putative pyramidal cells in order to measure the gain of their output (n = 9). a) Representative recordings (Top) from a putative pyramidal cell in CA1 when presented with 40 Hz γ-conductance trains with different synchrony (Bottom) and simultaneous tonic excitation of 180 pA. b) F-i plot derived by increasing positive current levels whilst injecting the conductance trains with different rhythm from a). c) F-i slope for three trains of varying synchrony (High: Jitter = 0, Mid: Jitter = 0.45, Low: Jitter = 0.66) normalised by the flat stimulus (Nrm. Slope); rmANOVA: slope ($F(1.08, 8.66) = 9.33$, $p < 0.013$. d) Rheobase current for three trains of varying synchrony normalised by flat stimulus (Nrm. Rheobase); rmANOVA: rmANOVA: ($F(1.23, 9.83) = 11.03$, $p < 0.006$. e) Maximum spike rate for three trains of varying synchrony normalised by flat stimulus (Nrm. Max Sp.Rate); rmANOVA: ($F(1.11, 8.90) = 14.19$, $p < 0.004$. Black lines represent the population average and bars the +/− SEM. rmANOVA followed by post-hoc paired t-test for multiple comparisons. f) Mean slope for three trains of varying synchrony normalised by flat stimulus (Nrm. Mean Slope). The three conditions were compared with flat stimulus (value of 1) using one-sample t-tests. *$p < 0.05$, **$p < 0.01$, ***$p < 0.001$, $^{n.s.}p >= 0.05$. Dashed brackets represent one sample t-tests and solid brackets represent paired t-tests.

Therefore, it seems that lowering the synchrony of rhythmic inhibitory trains at 40 Hz produces divisive and subtractive decreases in gain. We compared the difference between High and Low trains with altered rhythmicity and altered synchrony. We found that lowering rhythmicity (High − Low, CV: 0 to 0.5) reduced slope by 0.61 ± 0.17, whereas lowering synchrony (High − Low, Jitter: 0 to 0.66) reduced the slope by 0.31 ± 0.11. However, this difference was not found to be significant ($p = 0.17$, two sample t-test). More experiments need to be performed where trains with low synchrony and trains with low rhythmicity are directly compared in the same cell. Collectively, these experiments suggest that reducing γ power, by reducing either the synchrony or rhythmicity of inhibition, produces divisive decreases in gain.

However, the gain modulation for inhibitory inputs appears less robust than for excitatory inputs when compared to flat controls. Particularly, only the high rhythmicity condition has significant change in slope relative to flat condition, while high synchrony condition is not significant (despite being exactly the same stimulus). Indeed, the slope difference between high-stimulus excitatory trains and flat stimulus is higher than the slope difference between high-stimulus inhibitory trains and flat stimulus (Excitation: High − Flat = 0.98 ± 0.15 ($n = 10$), Inhibition: High − Flat = 0.59 ± 0.09 ($n = 35$); $p < 0.05$, two sample t-test). These findings suggest that 40 Hz excitatory inputs in our experiments produce a larger multiplicative gain enhancement than 40 Hz inhibitory trains. More experiments with 40 Hz excitation trains are required to equalise the sample sizes and consolidate this effect.

5.8 GAMMA POWER, VARIABILITY AND GAIN

While reducing rhythmicity and synchrony both reduce γ power, they have large and opposite effects on stimulus variability. As stimulus variability affects gain, this complicates the interpretation of these experiments manipulating the oscillatory properties of the input. However, it is not possible to conserve variability while

independently manipulating rhythmicity or synchrony. In order to test the importance of γ power directly, we created three trains with different γ power, but kept variability constant across the whole stimulus. This was done by balancing reduced rhythmicity with reduced synchrony (High: CV = 0, Jitter = 0, Mid: CV = 0.3, Jitter = 0.24, Low: CV = 0.67, Jitter = 0.94). We used dynamic clamp to inject three trains with these properties to putative pyramidal cells along with a flat control stimulus (Fig. 5.9a). The f-i slope robustly increased when the power of γ oscillation input became greater (Low: 1.06 $\pm$ 0.099, Mid: 1.27 $\pm$ 0.119, High: 1.53 $\pm$ 0.158; High-Low: $p < 0.001$, Mid-Low: $p < 0.01$, High-Mid: $p < 0.001$; Fig. 5.9b, c). This indicates that rhythmic inhibition at γ frequency is sufficient to multiplicatively increase the gain of principal cell output independent of overall stimulus variability. In addition, as the γ power increased, the rheobase current was elevated leading to subtractive decreases in gain (Low: 0.34 $\pm$ 0.054, Mid: 0.51 $\pm$ 0.077, High: 0.75 $\pm$ 0.086; $p < 0.001$, paired t-test; Fig. 5.9d). This means that more excitation is required to elicit action potentials in pyramidal cells receiving stronger γ inputs. Moreover, the maximum spike rate increased with γ power (Low: 1.277 $\pm$ 0.098, Mid: 1.513 $\pm$ 0.138, High: 1.634 $\pm$ 0.152; High-Low: $p < 0.01$, Mid-Low: $p < 0.001$, High-Mid: $p < 0.05$; Fig. 5.9e). This indicates that as γ power increased, the multiplicative rise in gain overcame the subtractive decrease in gain within the f-i range investigated. Furthermore, the high γ-power train was significantly different from the flat inhibition train ($p < 0.05$, one sample t-test: Fig. 5.9f). This reinforces previous findings indicating that γ inhibitory input at 40 Hz (CV = 0, Jitter = 0) is sufficient to cause multiplicative gain enhancement in principal cells. Indeed when the high γ train slope was compared with the flat slope across all inhibition experiments, it was found to be significantly increased (Flat = 1, High = 1.37 $\pm$ 0.072, $p < 0.0001$, one-sample t-test). In conclusion, 40 Hz inhibitory rhythmic and synchronous γ input can cause multiplicative enhancement of gain in principal cell output.

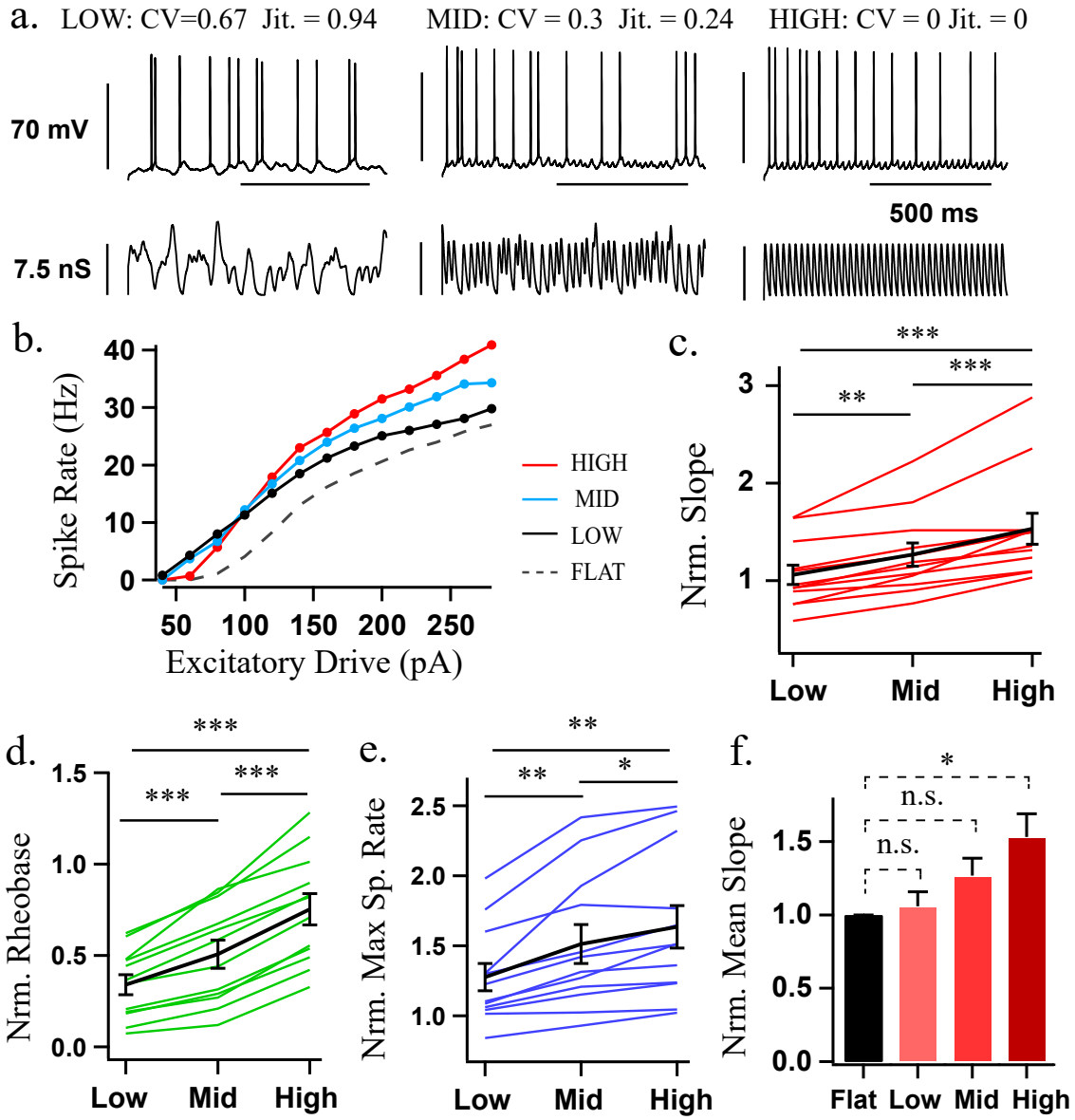


Figure 5.9: Increasing γ oscillation power, while conserving variability, produces multiplicative increases in gain. Dynamic clamp experiments were performed in putative pyramidal cells (n = 12). a) Representative recordings (Top) from a putative pyramidal cell in CA1 when presented with different IPSG trains (Bottom) and simultaneous tonic excitation of 100pA. b) F-i plot derived by increasing positive current levels whilst injecting the conductance trains from a-bottom in a CA1 pyramidal cell. c) F-i slope for three trains of varying γ power but similar variability (High: CV = 0, Jitter = 0, Mid: CV = 0.3, Jitter = 0.24, Low: CV = 0.67, Jitter = 0.94) normalised by the flat stimulus (Nrm. Slope); rmANOVA: slope ($F(1.08, 8.66) = 9.33$, $p < 0.013$. d) Rheobase current for three trains of varying synchrony normalised by flat stimulus (Nrm. Rheobase); rmANOVA: ($F(2, 22) = 105.24$, $p < 0.0001$. e) Maximum spike rate for three trains of varying synchrony normalised by flat stimulus (Nrm. Max Sp. Rate); rmANOVA: ($F(1.12, 12.32) = 19.40$, $p < 0.001$. Black lines represent the population average and bars the +/− SEM. rmANOVA followed by post-hoc paired t-test for multiple comparisons. f) Mean slope for three trains of varying synchrony normalised by flat stimulus (Nrm. Mean Slope). The three conditions were compared with flat stimulus (value of 1) using one-sample t-tests. *$p < 0.05$, **$p < 0.01$, ***$p < 0.001$, $^{n.s.}p >= 0.05$. Dashed brackets represent one sample t-tests and solid brackets represent paired t-tests.

5.9 GAMMA OSCILLATIONS, VARIABILITY AND SPIKE FIDELITY

It has been shown that noisy membrane potential fluctuations are very effective in eliciting action potentials with high temporal fidelity (Mainen et al. 1995). We thus examined how changes in the aforementioned γ inputs can also affect the control of spike firing in pyramidal cells. Since each stimulus was presented multiple times (Section 5.3), we were able to measure spike time fidelity by calculating the cross-correlation index. The cross-correlation index was obtained by averaging the cross-correlations between each repetition and then obtaining the peak value at 0 of the resulting cross correlation (Fig. 5.10a). We first studied how the mean correlation index (MCI), that is the cross-correlation index averaged across all excitation steps (average of each line in figure 5.10b), varied for rhythmic, arrhythmic and flat excitation stimuli in S1 (Section 5.4). The MCI was significantly different between the three conditions ($p < 0.0001$, rmANOVA). As expected, both rhythmic and arrhythmic stimuli had higher MCI than the flat stimulus (Flat: 0.073 ± 0.01, High: 0.25 ± 0.02, Low: 0.55 ± 0.07; Fig. 5.10c). In addition, the MCI of the arrhythmic stimulus was higher than the rhythmic stimulus ($p < 0.05$, paired t-test; Fig. 5.10c). The arrhythmic stimulus had higher variability than its rhythmic counterpart and they both had higher variability than the flat stimulus (Fig. 5.4a). These results might indicate that as the train variability increases (over a 2 second period) the spike fidelity of S1 principal cells becomes larger. This is in contrast to multiplicative gain enhancement which was dependent on γ power rather than train variability (Fig. 5.4 and 5.5). It should be noted that MCI in this set of experiments was normalised by the maximum spike rate obtained in each experiment.

Next we compared how 40 Hz excitatory trains with different rhythms (High: CV = 0, Mid: CV = 0.2, Low: CV = 0.5; Fig. 5.5) in CA1 affects spike reliability. In order to compare the three trains with different rhythms between them we normalised their MCI values by the MCI value of the flat control (Flat = 1). The MCI

value increased as the rhythm of the 40 Hz excitatory trains was decreased (High: 4.69 ± 0.25, Mid: 7.55 ± 0.60, Low: 11.45 ± 0.78; $p < 0.01$, paired t-tests; Fig. 5.11a). These results are in agreement to the experiments in S1 and indicate that as the rhythm of 40 Hz excitatory trains decreases the spike fidelity increases. We then examined how 40 Hz inhibitory inputs with different rhythms (High: CV = 0, Mid: CV = 0.2, Low: CV = 0.5; Fig. 5.7a) affect pyramidal cell spike reliability. When the rhythmicity of the inhibitory trains was reduced from High to Low or from High to Mid the MCI value was increased like before (High: 5.60 ± 0.74, Mid: 10.48 ± 1.60, Low: 10.78 ± 1.35; High-Low: $p < 0.001$, High-Mid: $p < 0.01$; Fig. 5.11c). This indicates that both excitatory and inhibitory arrhythmic 40 Hz trains increase spike fidelity more than rhythmic 40 Hz trains. Furthermore, the Mid and Low inhibitory rhythm trains had very similar MCI values and were not significantly different ($p = 0.44$, paired t-test, Fig. 5.11c). These findings are in contrast to excitatory trains where the Mid and Low 40 Hz trains had identical rhythms as their respective inhibitory trains, but had a big difference in their MCI values. Furthermore, the Mid and Low inhibitory rhythm trains had difference in their effects on gain (Fig. 5.7). This could indicate that inhibitory train variability (over a 2 second period) can not explain fully the changes in spike fidelity. Furthermore, we compared how changes in synchrony of inhibitory 40 Hz trains (High: Jitter = 0, Mid: Jitter = 0.45, Low: Jitter = 0.66; Fig. 5.8a) affect spike reliability. The higher the synchrony of the 40 Hz trains the greater the MCI (Low: 3.47 ± 0.57, Mid: 4.57 ± 0.71, High: 5.09 ± 0.84;, High-Low: $p < 0.05$, Mid-Low: $p < 0.05$, paired t-tests; Fig. 5.11c). The Mid-High difference was not found statistically significant (High-Mid: $p = 0.38$, paired t-test). These experiments suggest that decreasing inhibitory train variability caused by a decrease in synchrony leads to less reliable spike timing. Lastly, we compared the MCI values obtained by inhibitory stimuli with different γ power and same variability (High: CV = 0, Jitter = 0, Mid: CV = 0.3, Jitter = 0.24, Low: CV = 0.67, Jitter = 0.94; Fig. 5.9a). Mid γ and Low γ trains had very similar MCI values as expected (10.06 ± 1.17 and 10.07 ± 1.21, respectively; $p =$

1.00, paired t-test; Fig. 5.11d). Contrary, the high γ train had a significantly smaller MCI of 5.70 $\pm$ 0.47 ($p < 0.001$, paired t-tests: Fig. 5.11d). Overall these results suggest that γ power does not correlate with MCI values. Instead the variability of the input trains can predict better the spike fidelity of pyramidal cells. However, variability over the two second period can not account fully for spike fidelity as i) trains with different variability can result in similar MCI (Mid-Low, Fig. 5.11b) and ii) trains with similar variability can result in different MCI values (High-Mid, Fig. 5.11b). Future experiments including the assessment of other parameters like variability of the train over shorter time periods will be required to delineate this effect.

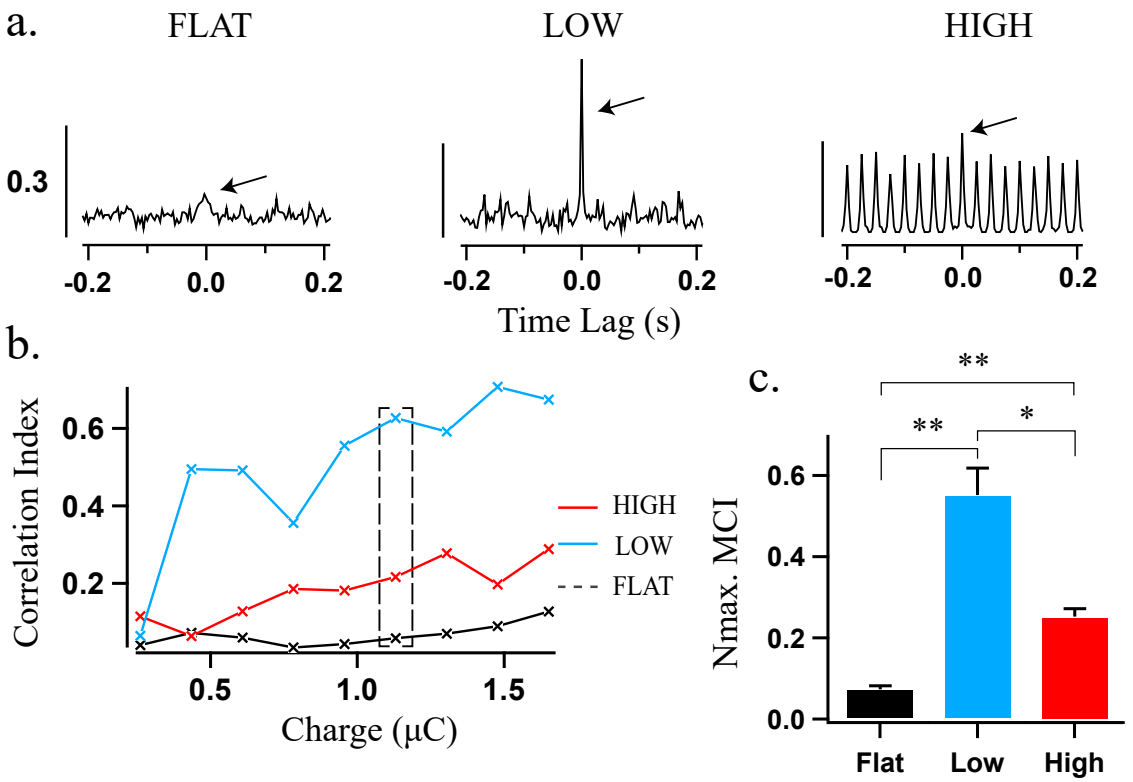


Figure 5.10: Arrhythmic excitatory input at 40 Hz increases spike fidelity in S1. a) Average cross correlation obtained for rhythmic (High - CV = 0), arrhythmic (low - CV = 0.3) and square (flat) stimuli at 1.13 μC (Fig.5.4a). The y-axis represents the correlation strength and the x-axis the Time lag. The correlation index was obtained by taking the correlation value at 0 time lag (black arrow). b) Correlation index plotted across increasing excitatory strength. The dashed highlighted region shows the stimulation strength at which the average cross correlations in a) come from. c) Mean correlation index (MCI) averaged across all excitation levels for the three conditions normalised by the maximum spike rate (Nmax. MCI, n = 5); rmANOVA: ($F(2, 8) = 33.28$, $p < 0.0001$. rmANOVA followed by post-hoc paired t-test for multiple comparisons. *$p < 0.05$, **$p < 0.01$, ***$p < 0.001$, $^{n.s.}p >= 0.05$.

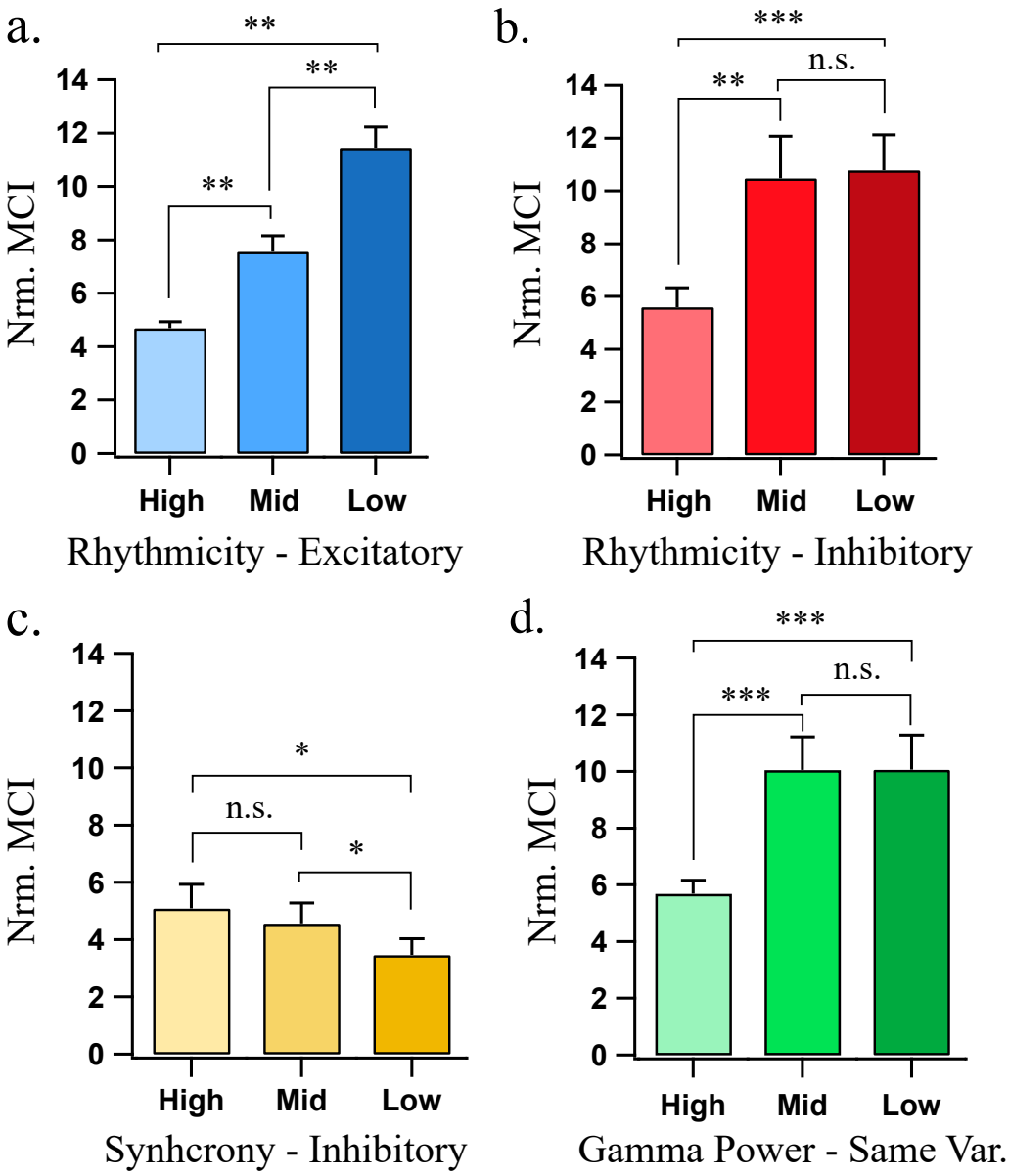


Figure 5.11: Spike time fidelity and γ oscillation properties. All plots indicate the mean correlation index (MCI) derived from the full range of excitatory drive. The MCI of the trains of interest was normalised by the MCI value of the flat control (Nrm. MCI). a) Excitatory stimuli with different levels of rhythmicity (High: CV = 0, Mid: CV = 0.2, Low: CV = 0.5; n = 5). b) Inhibitory stimuli with different levels of rhythmicity (High: CV = 0, Mid: CV = 0.2, Low: CV = 0.5: n = 9). c) Inhibitory stimuli with different levels of synchrony (High: Jitter = 0, Mid: Jitter = 0.45, Low: Jitter = 0.66; n = 9). d) Inhibitory stimuli with different levels of γ power and similar variability (High: CV = 0, Jitter = 0, Mid: CV = 0.3, Jitter = 0.24, Low: CV = 0.67, Jitter = 0.94; n = 12). rmANOVA followed by post-hoc paired t-test for multiple comparisons. *p $<$ 0.05, **p $<$ 0.01, ***p $<$ 0.001, $^{n.s.}$p $>=$ 0.05.

5.10 SUPPLEMENTARY INFORMATION

Multiplicative gain enhancement induced by application of inhibitory 40 Hz γ trains (CV = 0, Jitter = 0) was variable between the dynamic clamp experiments. It is possible that these changes could arise from altered inhibition levels applied during dynamic clamp recordings. We therefore compared the oscillation amplitude induced by the 40 Hz inhibitory trains (CV = 0, Jitter = 0) on putative pyramidal cell membrane voltage at rheobase current. We found that there was no significant correlation between normalised slope (High/Flat) with γ power (r = - 0.10, Pearson correlation; Fig. 5.12a). Furthermore, the flat conductance relative to the 40 Hz trains was reduced in some experiments since with similar conductance values the pyramidal cells needed much more current to start firing with flat inputs. This was done to allow us to obtain the whole spike rate to input (f-i) plot for flat conductance and reliably measure the multiplicative slope. We therefore correlated the relative flat conductance to normalised slope. We found no correlation between multiplicative gain and flat conductance (r = 0.02, Pearson correlation; Fig. 5.12b). Next we compared the normalised slope with changes in input resistance and membrane voltage of putative pyramidal cells between the start and end of experiments. We found that there was no correlation with input resistance (Ri) change but there was a positive correlation with membrane voltage (Vm) change (Ri: r = 0.29, Vm: r = 0.41,Fig. 5.12c, d). It therefore seems that on average for bigger changes in membrane voltage the normalised slope and multiplicative increased. However, cells with different voltage changes can have similar slopes and cells with equal voltage changes can have very different slopes. Furthermore, there was no correlation between changes in Vm and Ri with the difference of slopes between High-Low trains ($p > 0.3$, Pearson correlation). Therefore, even though Vm changes could affect multiplicative gain, they cannot explain the variability in responses.

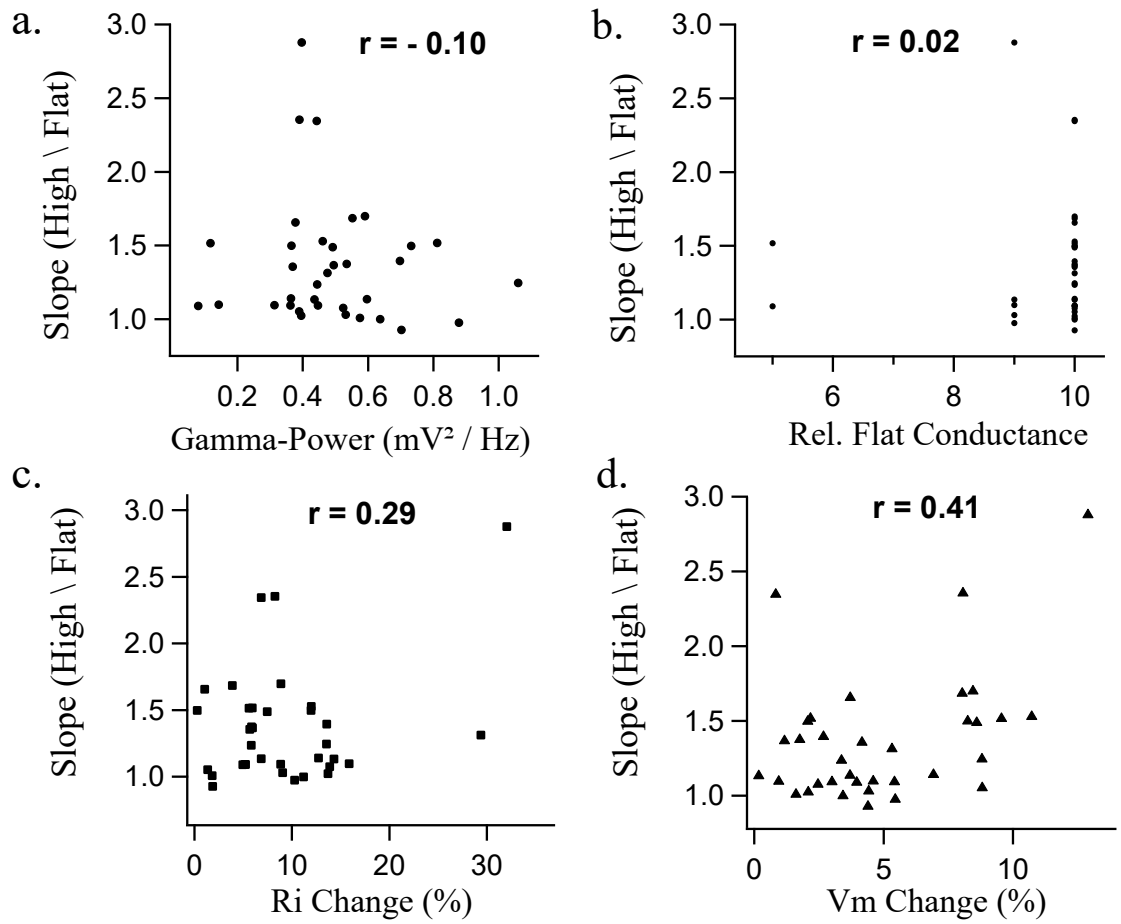


Figure 5.12: Slope correlation with input parameters. Format: Y-axis plotted against X-axis. a) Normalised slope (High/Flat) plotted against γ power of putative pyramidal cell membrane voltage at rheobase current; Pearson correlation, r = -0.10, n = 35, p = 0.57. b) Normalised slope (High/Flat) plotted against γ relative flat conductance; Pearson correlation, r = 0.02, n = 35, p = 0.90. c) Normalised slope (High/Flat) plotted against input resistance change between start and end of experiment; Pearson correlation, r = 0.29, n = 35, p = 0.09. Normalised slope (High/Flat) plotted against membrane voltage change between start and end of experiment; Pearson correlation, r = 0.41, n = 35, p = 0.012.

Table 5.1: Normalised F-I Slope (Mean ± SEM)

Input	Flat	Low	Mid	High
Excitatory - Rhythmic (CA1)	1	1.29 ± 0.034	1.42 ± 0.048	1.46 ± 0.044
Inhibitory - Rhythmic	1	1.03 ± 0.072	1.15 ± 0.081	1.28 ± 0.094
Inhibitory - Synchronous	1	1.07 ± 0.041	1.14 ± 0.058	1.22 ± 0.086
Gamma - Same variability	1	1.06 ± 0.099	1.27 ± 0.119	1.53 ± 0.158

Table 5.2: Normalised Rheobase (Mean ± SEM)

Input	Flat	Low	Mid	High
Excitatory - Rhythmic (CA1)	1	0.68 ± 0.027	0.93 ± 0.037	0.99 ± 0.021
Inhibitory - Rhythmic	1	0.27 ± 0.085	0.43 ± 0.082	0.63 ± 0.047
Inhibitory - Synchronous	1	0.86 ± 0.022	0.78 ± 0.039	0.67 ± 0.066
Gamma - Same variability	1	0.34 ± 0.054	0.51 ± 0.077	0.75 ± 0.086

5.11 DISCUSSION

In these experiments we have tested how changes in the rhythm or synchrony of 40 Hz trains affected the output of principal/pyramidal cells. In support of previous findings, we found that 40 Hz periodic excitatory input causes a multiplicative increase in the gain of principal cells when compared to flat control (Sohal et al. 2009; Fig. 5.4, 5.5). In addition, we extended these findings by showing that aperiodic 40 Hz excitatory input can also produce multiplicative increase in gain of principal cells but to a lesser extent than its periodic counterpart (Fig. 5.4, 5.5). Particularly, reducing the rhythmicity of the excitatory 40 Hz input produced divisive decreases and additive increases in gain (additive increases in CA1 only; Fig. 5.4, 5.5). Importantly, we found that 40 Hz periodic inhibitory input also leads to a multiplicative increase in the gain of principal cells (Fig. 5.7, 5.9). Any reductions in either the rhythm or synchrony of the 40 Hz inhibitory input caused divisive decreases in gain of principal cells (Fig. 5.7, 5.8). However, reductions in the rhythm or synchrony of 40 Hz inhibitory trains caused opposite effects on additive gain and variance of the input trains (Fig. 5.7, 5.8). Particularly, reducing rhythmicity increased train variability and pyramidal cell additive gain (Fig. 5.7). On the other hand, reducing synchrony, decreased train variability and produced a subtractive gain of pyramidal cell output (Fig. 5.8). For this reason, we tested how trains with similar γ power but different variability could affect principal cell output. We found that trains with similar variability had different effects on gain that were dependent on γ power. Specifically, increasing γ power produced multiplicative increases and subtractive decreases in gain. Therefore, it seems that any perturbation of the γ rhythm leads to divisive reductions in gain. Lastly, we also examined how changes in the rhythm or synchrony of 40 Hz trains affect temporal spike fidelity of principal cell output. Our findings suggest that temporal spike fidelity does not depend on γ power but mostly on overall train variability (Fig. 5.11).

5.11.1 GAMMA OSCILLATIONS PRODUCE MULTIPLICATIVE INCREASES IN PRINCIPAL CELL GAIN

In our experiments any deviation from γ (rhythmic and synchronous) input at 40 Hz caused divisive changes in the gain of principal cells. Thus, γ input is very effective in eliciting action potentials and increasing the input-output slope of principal cells in support of previous findings (Sohal et al. 2009). The effectiveness of γ input in eliciting action potentials can be explained by examining the sodium channel dynamics. Particularly, sustained activation or slow depolarisation decreases sodium conductance, and hence more input is required to make the cell spike as more sodium channels inactivate (Bean 2007; Hodgkin et al. 1952; Noble et al. 1966). In support of this, faster rates of membrane depolarisation have been shown to decrease action potential threshold and increase gain (Azouz et al. 2000, 2003; Henze et al. 2001). Therefore, the increased rate of membrane depolarisations arising by the high γ train (synchronous and rhythmic) in comparison to the flat control causes spikes to be elicited more effectively. Indeed, the max-spike rates are higher in the high γ train than the flat control (Table 5.1). Similarly, the high γ train (synchronous and rhythmic) produces a higher amount of fast membrane depolarisations in pyramidal cells than the asynchronous/arrhythmic train (Fig. 5.9). Thus, the high γ train increases the input-output slope because it more effectively recruits the activated sodium channels when compared to flat control and asynchronous/arhythmic trains.

Furthermore, lowering the synchrony of the high γ train causes the amplitude of membrane fluctuations to decrease and hence decreases spike induction efficiency (Fig. 5.8). However, the decrease in slope observed by lowering rhythmicity is probably not caused by a reduction in fast membrane depolarisations. It seems that lower rhythmic trains can elicit spikes with a similar efficiency as their rhythmic counterparts. In support of this, the max spike rate is not different between high and low rhythmic trains (Fig. 5.4, 5.5 & 5.7). The slope reduction arises probably due to the decreased rheobase current caused by low rhythmicity trains (Fig. 5.5,

5.7). This happens because the f-i curve begins increasing at earlier input strengths in low rhythmic than high rhythmic trains but saturates at similar levels (Fig. 5.5, 5.7). This causes the f-i slope to decrease in low rhythmic trains, resulting in a reduced multiplicative gain enhancement. Thus, changes in additive gain could be responsible for the decreased f-i slope observed during lower rhythmic trains.

On the other hand, the changes in additive/subtractive gain seem to correlate better to the overall train regularity and variability than γ power (Table 5.2). This occurs because more variable trains contain periods with more excitation (or less inhibition for inhibitory trains) than the less variable trains and can thus make pyramidal cells start spiking at lower input strengths.

5.11.2 RHYTHMIC EXCITATION VS. RHYTHMIC INHIBITION

Lowering rhythmicity in either excitatory or inhibitory trains had similar effects on the slope and rheobase of principal cells (Fig. 5.4f, 5.5f & 5.7f). However, only excitatory arrhythmic stimuli caused a significant multiplicative gain enhancement when compared to the flat control (Fig. 5.4f, 5.5f & 5.7f). This could suggest that excitatory currents are more effective in inducing multiplicative gain enhancements in principal cells. Thus, gain enhancement could be boosted during information transfer between different brain regions as long-range connections are mostly excitatory in nature (McGuire et al. 1991; Megias et al. 2001; Stepanyants et al. 2009). However, the differences observed between excitation and inhibition can be attributed to the different experimental manipulations used. Specifically, the excitatory trains were injected using current clamp and therefore the amplitude of the γ input progressively increased along with the input strength. On the other hand, the amplitude of γ fluctuations in inhibitory experiments was kept relatively constant using dynamic clamp (See methods section 2.6). Therefore, larger γ amplitude results in larger membrane deviations that initiate action potentials more effectively in excitation experiments.

5.11.3 VARIABILITY IN GAIN ENHANCEMENT OF INHIBITORY GAMMA TRAINS

It is also important to note that the high γ train in the synchrony experiments did not increase the slope significantly in comparison to flat controls (Fig. 5.8). These results indicate the variability in gain enhancement observed in our experiments (Fig. 5.12). This is because the same high γ train was sufficient to increase the slope in the rhythm experiments when compared to the flat control (Fig. 5.7). The variability in slope changes between experiments could arise due to variable levels of persistent sodium channels across different pyramidal cells (French et al. 1990). These sodium channels do not inactivate easily by persistent depolarisation (French et al. 1990). Therefore, they increase the effectiveness of slow depolarisations in initiating action potentials in cells containing higher levels of this channel. Consequently, a cell containing a high amount of persistent sodium channels would have a smaller slope difference between a high γ train and the flat control.

5.11.4 GAMMA POWER, VARIABILITY AND SPIKE FIDELITY

It has been demonstrated that noisy membrane potential fluctuations, in contrast to constant excitatory input, are very effective in eliciting action potentials with high temporal fidelity (Mainen et al. 1995). An input train with noisy fluctuations elicits more rapid changes in membrane potential than a constant excitatory input (flat control). Therefore, increased spike fidelity may also arise from the more efficient recruitment of sodium channels in these experiments. Our experiments suggest that larger train variability increases temporal fidelity (Fig. 5.11). Larger train variability induces bigger and faster membrane depolarisations thereby increasing the effectiveness of spike initiation and its temporal control. As a result, trains with low rhythmicity (low γ power and higher variability) have reduced multiplicative gain but enhanced temporal fidelity when compared to high rhythmicity trains (high γ power and lower variability) (Fig. 5.5, 5.7 & 5.11). However, train variability cannot

explain fully the observed responses, as trains with similar variability produced different levels of spike fidelity (Fig. 5.11). In particular, the high γ train induced lower spike fidelity levels than low γ trains with similar variability even though it induced greater multiplicative gain (Fig. 5.9, 5.11d). This supports previous experiments showing that γ oscillations (40 Hz) induce higher multiplicative gain but similar response variability to slower theta oscillations (8 Hz) (Sohal et al. 2009). Therefore, strong γ (rhythmic and synchronous) 40 Hz inputs may be able to enhance neuronal signal gain at the cost of temporal control.

Chapter 6

General Discussion

Network state is reflected in the patterns of oscillatory activity and communication between networks appears to be reflected in coherence (Bosman et al. 2012; Buzsáki et al. 2004, 2015; Fries 2005; Fries et al. 2001; Gray et al. 1989; Harris et al. 2003; Montgomery et al. 2007; Spellman et al. 2015; Uhlhaas et al. 2006). Studying these network oscillations thus provides a unique opportunity to study the dynamic signalling within and between networks, and how this relates to cognitive function. However, the current classification of network oscillations seems inadequate to capture the dynamics of neuronal network signalling (Cole et al. 2017; Womelsdorf et al. 2014). It is thus critical to first understand how a particular circuit gives rise to a specific network activity and how that activity in turn impacts the processing of participating neurons (Womelsdorf et al. 2014). Here, we examined the mechanisms of γ oscillation generation using optogenetic tools to dissect the hippocampal circuitry. Additionally, we explored how the input experienced by principal cells during γ oscillations affects their function.

Specifically, we explored the mechanistic role of PV+ and SST+ interneurons in carbachol (cch) induced γ oscillations in the CA3 hippocampal subfield. We found that rhythmic photo-activation of both neurons was sufficient to entrain ongoing γ oscillations (Fig. 3.5, 4.2). In addition, tonic photo-activation of PV+ or SST+ interneurons decreased the power and increased the frequency of γ oscillations (Fig. 6.1a, b). Progressive increase of PV+ or SST+ photo-activation potentiated

this effect until hippocampal network was completely silenced, thus abolishing γ oscillations. Surprisingly, in some experiments SST+ interneuron photo-activation induced high-frequency γ oscillations. Furthermore, the sustained photo-activation of SST+ interneurons was sufficient to generate *de novo* high-frequency γ oscillations without the presence of cch. Our experiments reveal that the *de novo* γ oscillations may have different properties than cch-induced oscillations (Fig. 6.1c) but also depend on synaptic excitation. We also found that photo-inhibition of PV+ interneurons decreased the cch-induced γ oscillation power (Fig. 6.1a, b left). Additionally, photo-inhibition of SST+ interneurons decreased cch-oscillation power and increased its frequency (Fig. 6.1a, b right). These experiments demonstrate that PV+ and SST+ activity is necessary for the maintenance of cch-induced γ oscillations. In addition, they demonstrate that SST+ interneurons may be critical for controlling γ oscillation frequency.

These data suggest that several different interneuronal subtypes may be necessary to generate and/or maintain oscillations across the γ range. However, they are also consistent with the idea that rhythmic perisomatic inhibition is a critical feature of low-frequency γ oscillations in the hippocampus. In order to further understand the function of rhythmic perisomatic inhibition we examined the effects of disturbing rhythmicity and/or synchrony on pyramidal cell spiking. This demonstrated that disruption of γ input in any way reduced the slope of pyramidal cell input-output suggesting that γ oscillations are ideally suited for enhancing multiplicative gain in cortical circuits. Furthermore, trains with high variability but not high γ power were better at controlling spike timing. This could indicate that γ oscillation input may enhance multiplicative gain at the expense of temporal control.

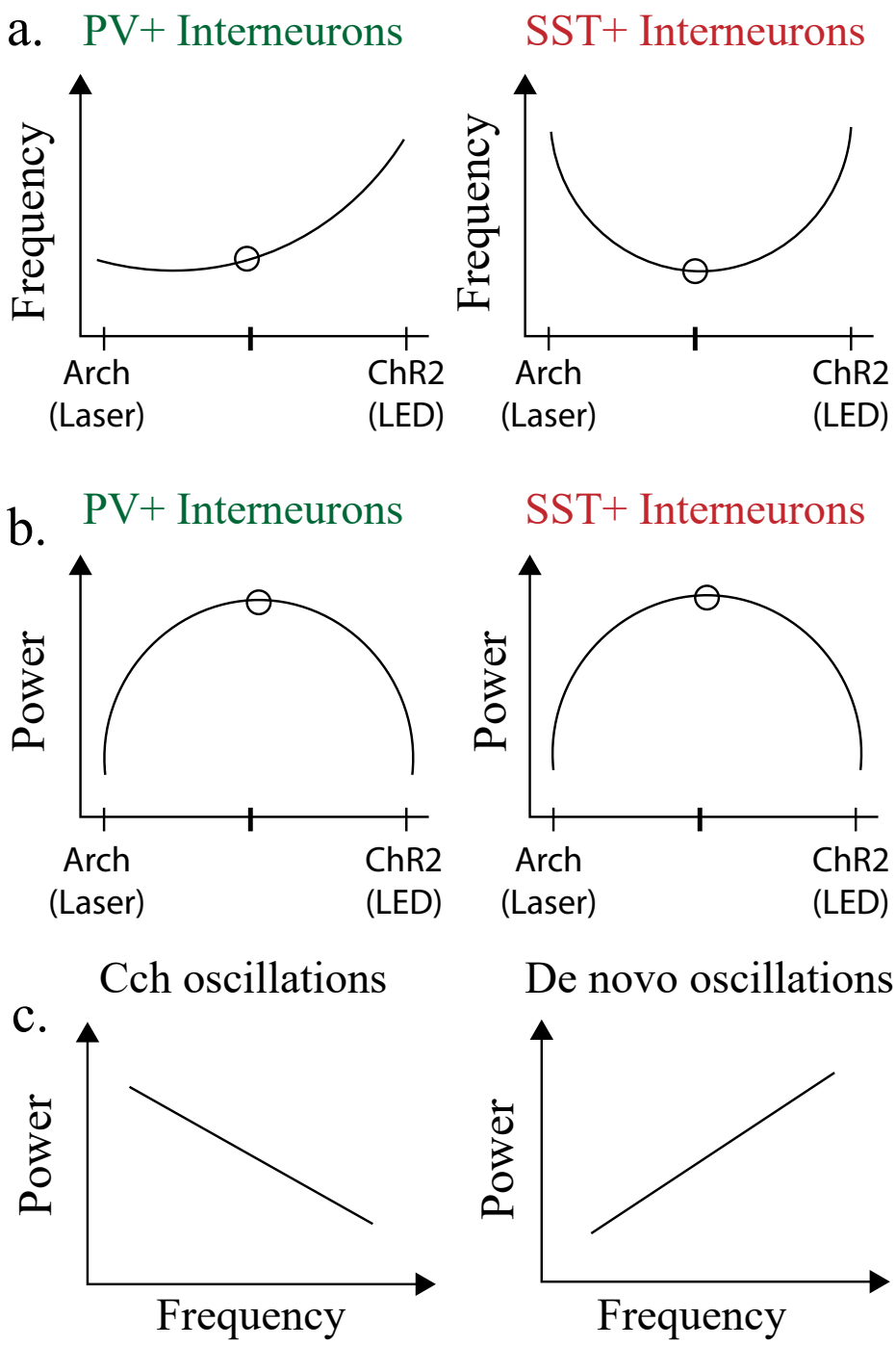


Figure 6.1: Role of PV+ and SST+ interneurons in hippocampal γ oscillations. Schematic diagram illustrating the a) frequency and b) power of cch-oscillations in response to PV+ or SST+ interneuron optogenetic modulation. c) Power-Frequency relationship of cch- and *de novo* oscillations.

6.1 INVESTIGATING GAMMA OSCILLATIONS IN ACUTE SLICES

In this study, we chose to examine γ oscillations in the CA3 subfield of *ex vivo* acute hippocampal slices. Acute slices cannot capture the dynamics of endogenous activity in the intact brain of behaving animals. Therefore, our findings will need to be extended and validated in awake animals, preferably during particular behaviours or cognitive tasks. On the other hand, acute slices are able to maintain the local brain circuitry and neuronal viability for many hours (Collingridge 1995; Mcilwain et al. 1951; C. Yamamoto et al. 1966). Furthermore, *ex vivo* slices allow greater control than *in vivo* recordings over several parameters including pharmacology, recording stability, recording position, ionic composition. They are also particularly useful for dissecting local brain circuits since the brain area under study can be isolated and interrogated in detail. For example, in acute slices, volume conduction of field potentials is restricted only to the brain areas contained within the slice under investigation. However, in live animals, volume conduction needs to be eliminated using current source density and/or independent component analyses that requires recordings with regularly spaced probes (Fernández-Ruiz et al. 2013; Lasztóczi et al. 2016; Nicholson et al. 1975; Schomburg et al. 2014). Indeed, many important properties of γ mechanisms were demonstrated using acute slice preparations (Bartos et al. 2007; Fisahn et al. 1998; Gloveli et al. 2005; Hajos 2004; Mann et al. 2005b; Whittington et al. 1995). These studies were also complemented and extended by computational and *in vivo* experiments (Börgers et al. 2005; Bragin et al. 1995; Brunel et al. 2003; Buzsáki et al. 2012; Csicsvari et al. 2003; Lasztóczi et al. 2016; Schomburg et al. 2014; Traub et al. 1996a, 2000, 2001; Wang et al. 1996; Whittington et al. 2011; Wilson et al. 1972).

Importantly, cch application is believed to model closely many aspects of the *in vivo* oscillations in CA3 (Hájos et al. 2009). Firstly, the hippocampus receives direct cholinergic projections from medial septum that are important for hippo-

campal dependent functions like working memory and spatial navigation (Chrobak et al. 1989; Mamad et al. 2015; Rawlins et al. 1979; Shute et al. 1963; Winson 1978). Additionally, cholinergic tone increases in the hippocampus during periods or behavioural tasks where γ activity is high (Bragin et al. 1995; Kametani et al. 1990; Marrosu et al. 1995; Montgomery et al. 2007; Teles-Grilo Ruivo et al. 2017). Moreover, blockage of muscarinic receptors *in vivo* impairs low-frequency γ oscillations in the cortex (Howe et al. 2017). Importantly, fast-spiking interneurons are coupled with greater strength to the oscillation and fire later than pyramidal cells supporting PING mechanisms (Csicsvari et al. 2003; Hajos 2004; Mann et al. 2005b; Senior et al. 2008). Therefore, our experiments may not capture the detailed dynamics of neuronal signalling that take place *in vivo*, but will likely reflect the basic characteristics/properties of the circuit engaged in γ oscillations.

6.2 CELL SPECIFICITY AND TARGETING EFFICIENCY

To control the activity of different classes of inhibitory interneurons with temporal precision we expressed optogenetic probes in the cells of interest (Chow et al. 2010; Nagel et al. 2003). To achieve that, an AAV-5 virus was used to deliver the optogenetic construct in PV-cre or SST-cre mice (Cardin et al. 2009; Sohal et al. 2009). Viral expression in both mouse lines was successfully expressed in the cells of interest as the fluorescence expression was restricted to the layers reflecting the projections of either PV+ (perisomatic) or SST+ (dendritic) interneurons (Fig. 3.2, 4.1). This was also confirmed with intracellular recordings and single-cell visualisation of the expressing cells (Fig. 3.3, 4.10). In agreement to this it has been shown, using the same virus vector and PV mouse line, that more than 90% of the cells transduced are PV positive in the cortex (Sohal et al. 2009). Furthermore, in the SST-cre mice more than 90% cells of the cre+ cells are SST positive (Taniguchi et al. 2011). Together, these observations indicate that we were selectively targeting the neurons of interest. As discussed before, SST+ cell photo-activation also induced synaptic

excitation but that could have been due to the optogenetic stimulation (or SST+ excitatory cells) rather than mistargeting of the mouse line we used (See SST chapter for detailed discussion).

In addition, we have not quantified directly the efficiency of viral infection (i.e. what proportion of the PV+/SST+ population we were targeting). One concern is that the observed differences in PV and SST experiments could arise due to the differential levels of expression. Here we used only slices where expression covered the CA3 layer and where observable light-induced effects were seen in the LFP. In addition, previous experiments showed that high levels of expression could be achieved similarly in both PV- and SST-cre mouse lines (G. Chen et al. 2017; D. Kim et al. 2016; Lovett-Barron et al. 2012; Miao et al. 2017; Royer et al. 2012). Importantly, some of our main conclusions do not depend on relative numbers of expression. For example, strong photo-inhibition of both PV+ and SST+ interneurons impaired γ oscillation power (Fig. 3.17, 4.17). In addition, SST+ interneuron photo-inhibition increased oscillation frequency whereas it had no consistent effect in PV experiments even though γ power was affected (Fig. 3.17, 4.17). On the other hand, different levels of viral expression may bias some of the comparisons made between PV+ and SST+ interneurons. For instance, LED photo-inhibition of PV+ interneurons produces inconsistent effects, while it robustly decreases the oscillation power in SST experiments (Fig. 3.15, 4.16). We hypothesised that the difficulty in inhibiting PV+ interneurons could be attributed to the strong feedback connections between them and pyramidal cells, and this feedback could be absent from SST+ cells (See PV/SST chapter for detailed discussion). However, this may be also explained by a smaller number of PV+ than SST+ interneurons expressing Arch. Future experiments that consider the relative numbers of infected cells should be conducted to validate this effect. Furthermore, these experiments should be cross-validated using other mouse lines specific for PV and SST cells as transgenic knock-in mice can introduce undesired side-effects (Huang et al. 2013; Viollet et al. 2017).

6.3 RHYTHMIC INHIBITORY GAMMA OSCILLATION INPUTS IN PYRAMIDAL CELLS

A central goal of the gain experiments was to investigate how reductions in the rhythm of 40 Hz trains affected the output of pyramidal cells. It is unlikely that such a highly rhythmic γ oscillation input, as used in our experiments, exists under physiological conditions. The changes in rhythmicity were also exaggerated in order to maximise, and thus differentiate better, the effects produced from different stimuli. Experiments that investigate changes in rhythmicity that occur from natural variability, rhythm disorders or from drug application should be carried out to understand the realistic effects of such changes in the brain. Furthermore, these results could be also validated with optogenetic studies, in which endogenous perisomatic inhibition is delivered by photo-stimulation of PV+ interneurons.

6.4 MECHANISMS OF GAMMA OSCILLATION GENERATION IN HIPPOCAMPAL AREA CA3

As mentioned previously, γ oscillations induced by cch-application in hippocampal area CA3 are believed to be generated via PING mechanisms (Fisahn et al. 1998; Hajos 2004; Mann et al. 2005b; Oren et al. 2006). This is in agreement with γ oscillations in awake animals (Bragin et al. 1995; Csicsvari et al. 2003; Fuchs et al. 2007; Intro section 1.5.1). In this model, a group of pyramidal cells reaches threshold and synaptically excites inhibitory interneurons, which in turn synchronously silence the local hippocampal network (Börgers et al. 2005; Brunel et al. 2003; Mann et al. 2005a; Traub et al. 2000). When this inhibition decays, the next group of pyramidal cells that was close to threshold fires and the process repeats cyclically (Börgers et al. 2005; Brunel et al. 2003; Mann et al. 2005a; Traub et al. 2000). Importantly, PV+ basket cells are thought to be the inhibitory neurons involved in this process (Bartos

et al. 2007; Buzsáki et al. 2012; Mann et al. 2005b; Whittington et al. 2011;). This is because they exhibit pacemaker properties and apply strong perisomatic inhibition that is capable of syncrhonising pyramidal cells at high frequencies (Bartos et al. 2007; Cardin et al. 2009; Sohal et al. 2009; Intro section 1.5.3.1). In addition, they have powerful reciprocal connections with pyramidal cells and are strongly phase-coupled to cch-induced γ oscillations (Hajos 2004; Mann et al. 2005b; Oren et al. 2006). Last but not least, the currents they produce are the major contributing factor to cch-γ oscillation generation (Mann et al. 2005b; Oren et al. 2010).

Our data are also consistent with PV+ interneurons being critical for γ oscillation generation. Firstly, photo-stimulation of PV+ interneurons at 40 Hz was sufficient to synchronise the hippocampal network (Fig. 3.5). Importantly, photo-inhibition of PV+ interneurons impaired γ oscillation generation in CA3 indicating that their activity is required for γ oscillation generation (Fig. 3.17). Additionally, we observed that PV+ interneuron tonic photo-activation decreased the power and increased the frequency of γ oscillations (Fig. 3.6). It is possible that this effect was caused due to upregulation of PV+ interneuron activity that decreased the time required for them to apply inhibition on pyramidal cells and thus reduced the γ cycle duration. The power/amplitude of the oscillation likely decreased due to the enhanced inhibitory drive on pyramidal cells (See PV chapter for detailed discussion).

However, the increase in frequency with photo-activation of PV+ interneurons may also be generated via ING mechanisms. Indeed, PV+ interneurons show strong reciprocal coupling, and have ideal properties for generation of ING oscillations (Intro section 1.5.3.1). Interestingly, it has been shown that higher γ oscillation frequencies decrease the delay between pyramidal cell and interneuron firing indicating possible shifts to ING mechanisms (Mann et al. 2010). This agrees with computational studies which indicate that purely interneuronal γ (ING) can attain higher frequencies than PING mechanisms (Brunel et al. 2003). Future experiments should address whether the delay between pyramidal cell and PV+ interneuron spiking also decreases during PV+ interneuron tonic photo-activation. Together, our data with

the existing literature provide substantial evidence indicating that PV+ interneurons are necessary components for γ oscillation generation in the CA3 hippocampal area which can powerfully regulate the hippocampal network activity.

Interestingly, it was recently demonstrated that photo-activation of dendrite-targeting SST+ interneurons can reliably synchronise pyramidal cells at low γ frequencies in V1 cortical slices (Veit et al. 2017). This is supported by our experiments where rhythmic photo-activation of SST+ interneurons was capable of entraining ongoing γ oscillations by synchronising the hippocampal network (Fig. 4.2). Importantly, SST+ interneuron activity was required for the generation of low-frequency γ oscillations (around 30 Hz) in the primary visual cortex (V1) of awake mice (G. Chen et al. 2017; Veit et al. 2017). Our experiments also indicate that SST+ interneuron activity is essential for γ oscillation generation in the hippocampal area CA3, as their photo-inhibition strongly impaired γ oscillations (Fig. 4.17, 4.17). Therefore, the participation of SST+ interneurons may be required for γ oscillation generation across cortical circuits. We additionally found that photo-inhibition of SST+ interneuron activity consistently increased oscillation frequency (Fig. 4.17, 4.17) suggesting that dendritic inhibition may be a powerful regulator of γ oscillation frequency in the hippocampus.

Furthermore, we found that SST+ interneuron photo-activation also decreased the power and increased the frequency of γ oscillations. Thus, both photo-excitation and photo-inhibition of SST+ interneurons increased the frequency and decreased the power of γ oscillations. This effect could be explained if a sub-type of SST+ interneurons that has similar properties to PV+ cells is not active during cch-induced oscillations and is only recruited during photo-activation experiments. Indeed, bistratified cells which have similar properties to PV+ interneurons (Ali et al. 1998; E. H. Buhl et al. 1996; Maccaferri et al. 2000; Pouille et al. 2004) have been reported to exhibit decreased GABA release in the presence of cch (Gulyás et al. 2010). It is imaginable that these cells are recruited only by ChR2-activation and hence induce analogous changes to γ oscillation properties as PV+ interneurons during tonic

photo-activation (See SST chapter for further discussion). Furthermore, the observed effects induced by SST+ photo-inhibition will not be mediated through these cells as they are not active (low synaptic release) during cch γ oscillations. Thus, SST+ photo-inhibition may only affect other SST+ interneurons with weak feedback connections to pyramidal cells. This would in turn dis-inhibit PV+ interneurons and pyramidal cells, hence decreasing cycle duration and increasing oscillation frequency. The power of the oscillations may decrease as IPSCs from SST+ cells directly contributing to pyramidal cell synchronisation become smaller. Therefore, the differential engagement of bistratified neurons could explain the similar effects observed during SST+ interneuron photo-activation and photo-inhibition. However, the effects observed here may not apply to other manipulations or endogenous conditions. Particularly, bistratified interneurons participate in almost every cycle of kainate induced γ oscillations (Gloveli et al. 2005). Additionally, they are strongly phase-coupled to γ oscillations of anesthetized rats (Tukker et al. 2007). Therefore, photo-inhibition of SST+ interneurons in kainate γ / anaesthetised conditions may produce similar results as PV+ interneuron photo-inhibition. Ultimately, optogenetic modulation of SST+ interneurons should be extended in the endogenous circuits of awake animals in order to delineate SST+ interneuron contribution in the hippocampus.

It was also demonstrated that PV+ interneurons do not directly contribute to the generation of low-frequency γ oscillations in V1 (G. Chen et al. 2017; Veit et al. 2017). However, our data indicate that both SST+ and PV+ interneurons are important for low-frequency cch-γ oscillations such as those occurring *in vivo* in CA3 (Bragin et al. 1995; Fisahn et al. 1998; Lasztóczi et al. 2016). Even though, our experimental results could vary due to the different manipulations employed (*in vivo* vs *ex vivo*), it is unlikely that PV+ interneurons are not important for low-frequency γ oscillations in CA3 given the substantial existing evidence (Intro section 1.5.3.1). The discrepancy between our results could instead arise due to the differences between brain areas V1 and CA3. Nevertheless, photo-inhibition of

PV+ interneurons using long-lasting laser illumination should be repeated in the CA3 of awake animals to directly confirm this. Furthermore, a large area of the hippocampus should be photo-inhibited otherwise volume conduction may mask the induced effects (See Royer et al. 2012).

Surprisingly, we also found that tonic photo-activation of SST+ interneurons can induce novel *de novo* oscillations with frequencies centred around 80 - 100 Hz (Fig. 4.7). Thus, our findings support previous experiments which demonstrated that the CA3 area can generate fast γ oscillations under certain conditions (Betterton et al. 2017; Mann et al. 2010). Furthermore, the generation of the *de novo* oscillations may depend on both dendritic inhibition and synaptic excitation (see SST chapter for detailed discussion). However, if synaptic excitation is permissive, activation of SST+ interneurons alone could be sufficient to induce high-frequency oscillations in the CA3. On the other hand, dendritic inhibition from SST+ interneurons at 100 Hz would be experienced as a tonic inhibitory current at the action initial segment which could not influence spike timing (Vaidya et al. 2013). Therefore, these oscillations would require SST+ interneurons that synapse close to the soma (ie. proximal dendrites) where attenuation of high-frequency currents will be reduced. Furthermore, these neurons would also need to have fast kinetics and the capability of applying fast and reliable inhibition at high-frequencies. As mentioned earlier, bistratified interneurons may be able to fulfil this role as they have similarities to fast spiking PV+ interneurons and also form a small portion of synapses close to the soma (Muller et al. 2014; Somogyi et al. 2005). Parallel intracellular recordings of bistratified cells will need to be correlated with extracellular *de novo* oscillations to reveal if these cells contribute to oscillation generation.

6.5 GAMMA OSCILLATIONS INDUCE MULTIPLICATIVE GAIN ENHANCEMENT IN PRINCIPAL CELLS

Our experiments, together with the existing literature, provide strong evidence that rhythmic and synchronous perisomatic inhibition arising from PV+ interneurons is critical for γ oscillation generation (Bartos et al. 2007; Buzsáki 2002; Cardin 2016; G. Chen et al. 2017; Mann et al. 2005b; Whittington et al. 2011). Our findings further demonstrate that somatic γ input at 40 Hz, mimicking PV+ interneuron perisomatic inhibition during γ oscillations, is very effective in inducing multiplicative gain increases of principal cell output. Therefore, the presence of γ oscillations during certain behaviours is sufficient to enhance the gain of participating cells in the local network. In particular, γ oscillations cause the input - output slope of pyramidal cells to become steeper, hence increasing their sensitivity to incoming inputs and amplifying their output signal (Silver 2010). This increased sensitivity is utilised in a plethora of cognitive processes in the brain such as attention and stimulus detection (R. A. Andersen et al. 1983; Fries et al. 2001; McAdams et al. 1999; Salinas et al. 2000). Thus, the evidence here demonstrates that γ oscillations could contribute to neuronal computations in the brain. However, it still has to be determined whether γ oscillations contribute to information transmission between different brain areas (Bastos et al. 2015; Ray et al. 2010; Intro section 1.4.2). Furthermore, we found that temporal control of action potential initiation was not correlated to γ power but to train variability and regularity. This suggests that γ oscillations would better support information transfer via a rate coding rather than temporal coding regime (Adrian et al. 1926; Dan et al. 2004; Ferster et al. 1995; Markram et al. 1997; Riehle et al. 1997; Zhang et al. 1998).

We did not study the effects of rhythmic dendritic inhibitory conductances on gain control. However, there are several lines of evidence suggesting that rhythmic and synchronous dendritic inhibition may also be important for γ oscillation gen-

eration, including the data presented in this thesis (G. Chen et al. 2017; Gloveli et al. 2005; Veit et al. 2017). Interestingly, it has been also shown that dendritic inhibition is more effective than perisomatic inhibition in regulating the input - output transformation of pyramidal cells (Lovett-Barron et al. 2012). It would thus be interesting to examine whether rhythmic dendritic inhibition at 40 Hz enhances multiplicative gain to a bigger extent than rhythmic perisomatic inhibition at the same frequency. To investigate this, experiments should be conducted where excitatory input to pyramidal cells is provided via its canonical way (either via dendritic dynamic clamp or dendrite glutamate uncaging) and not through the soma.

In conclusion, our findings indicate that perisomatic inhibition arising from PV+ interneurons and dendritic inhibition arising from SST+ interneurons are important for γ oscillation generation in the hippocampus. Furthermore, the rhythmic and synchronous input they generate during γ oscillations may be ideally suited for enhancing the multiplicative gain of pyramidal cells.

Bibliography

Adesnik, Hillel et al. (2010). 'Lateral competition for cortical space by layer-specific horizontal circuits'. In: *Nature* 464.7292, pp. 1155–1160. DOI: 10.1038/nature08935.

Adrian, E D (1942). 'Olfactory reactions in the brain of the hedgehog.' In: *The Journal of physiology* 100.4, pp. 459–73.

Adrian, E D et al. (1926). 'The impulses produced by sensory nerve endings: Part 3. Impulses set up by Touch and Pressure.' In: *The Journal of physiology* 61.4, pp. 465–83.

Adrian, E D et al. (1934). 'The interpretation of potential waves in the cortex.' In: *The Journal of physiology* 81.4, pp. 440–71.

Ahmed, Omar J et al. (2013). 'Finding synchrony in the desynchronized EEG: the history and interpretation of gamma rhythms.' In: *Frontiers in integrative neuroscience* 7, p. 58. DOI: 10.3389/fnint.2013.00058.

Akam, Thomas et al. (2010). 'Oscillations and Filtering Networks Support Flexible Routing of Information'. In: *Neuron* 67.2, pp. 308–320. DOI: 10.1016/j.neuron.2010.06.019.

Akam, Thomas et al. (2012). 'Oscillatory dynamics in the hippocampus support dentate gyrus–CA3 coupling'. In: *Nature Neuroscience* 15.5, pp. 763–768. DOI: 10.1038/nn.3081.

Ali, A B et al. (1998). 'CA1 pyramidal to basket and bistratified cell EPSPs: dual intracellular recordings in rat hippocampal slices.' In: *The Journal of physiology* 507 (Pt 1.Pt 1, pp. 201–17. DOI: 10.1111/J.1469-7793.1998.201BU.X.

Almeida, Licurgo de et al. (2009). 'A second function of gamma frequency oscillations: an E-max winner-take-all mechanism selects which cells fire.' In: *The Journal of neuroscience : the official journal of the Society for Neuroscience* 29.23, pp. 7497–503. DOI: 10.1523/JNEUROSCI.6044-08.2009.

Anastassiou, Costas A et al. (2011). 'Ephaptic coupling of cortical neurons'. In: *Nature Neuroscience* 14.2, pp. 217–223. DOI: 10.1038/nn.2727.

Andersen, P. et al. (1971). 'Unit analysis of hippocampal population spikes'. In: *Experimental Brain Research* 13.2, pp. 208–221. DOI: 10.1007/BF00234086.

Andersen, P. et al. (1978). 'Functional characteristics of unmyelinated fibres in the hippocampal cortex'. In: *Brain Research* 144.1, pp. 11–18. DOI: 10.1016/0006-8993(78)90431-6.

Andersen, R A et al. (1983). 'The influence of the angle of gaze upon the excitability of the light-sensitive neurons of the posterior parietal cortex.' In: *The Journal of neuroscience : the official journal of the Society for Neuroscience* 3.3, pp. 532–48. DOI: 10.1523/JNEUROSCI.03-03-00532.1983.

Atallah, Bassam V. et al. (2009). 'Instantaneous Modulation of Gamma Oscillation Frequency by Balancing Excitation with Inhibition'. In: *Neuron* 62.4, pp. 566–577. DOI: 10.1016/J.NEURON.2009.04.027.

Atkinson, R.C. et al. (1968). 'Human Memory: A Proposed System and its Control Processes'. In: *Psychology of Learning and Motivation* 2, pp. 89–195. DOI: 10.1016/S0079-7421(08)60422-3.

Awh, Edward et al. (2012). 'Top-down versus bottom-up attentional control: a failed theoretical dichotomy.' In: *Trends in cognitive sciences* 16.8, pp. 437–43. DOI: 10.1016/j.tics.2012.06.010.

Azouz, R. et al. (2000). 'Dynamic spike threshold reveals a mechanism for synaptic coincidence detection in cortical neurons in vivo.' In: *Proceedings of the National Academy of Sciences of the United States of America* 97.14, pp. 8110–5. DOI: 10.1073/pnas.130200797.

— (2003). 'Adaptive coincidence detection and dynamic gain control in visual cortical neurons in vivo.' In: *Neuron* 37.3, pp. 513–523. DOI: 10.1016/S0896-6273(02)01186-8.

Baddeley, A (1992). 'Working memory.' In: *Science (New York, N.Y.)* 255.5044, pp. 556–9. DOI: 10.1126/SCIENCE.1736359.

Bartos, Marlene et al. (2002). 'Fast synaptic inhibition promotes synchronized gamma oscillations in hippocampal interneuron networks.' In: *Proceedings of the National Academy of Sciences of the United States of America* 99.20, pp. 13222–7. DOI: 10.1073/pnas.192233099.

Bartos, Marlene et al. (2007). 'Synaptic mechanisms of synchronized gamma oscillations in inhibitory interneuron networks.' In: *Nature reviews. Neuroscience* 8.1, pp. 45–56. DOI: 10.1038/nrn2044.

Bartos, Marlene et al. (2012). 'Functional characteristics of parvalbumin- and cholecystokinin-expressing basket cells'. In: *The Journal of Physiology* 590.4, pp. 669–681. DOI: 10.1113/jphysiol.2011.226175.

Basar-Eroglu, Canan et al. (2007). 'Working memory related gamma oscillations in schizophrenia patients'. In: *International Journal of Psychophysiology* 64.1, pp. 39–45. DOI: 10.1016/j.ijpsycho.2006.07.007.

Bastos, Andre M et al. (2015). 'Communication through coherence with inter-areal delays'. In: *Current Opinion in Neurobiology* 31, pp. 173–180. DOI: 10.1016/J.CONB.2014.11.001.

Baude, A. et al. (2007). 'Immunoreactivity for the GABAA Receptor 1 Subunit, Somatostatin and Connexin36 Distinguishes Axoaxonic, Basket, and Bistratified Interneurons of the Rat Hippocampus'. In: *Cerebral Cortex* 17.9, pp. 2094–2107. DOI: 10.1093/cercor/bhl117.

Bazelot, Michaël et al. (2010). 'Unitary inhibitory field potentials in the CA3 region of rat hippocampus'. In: *The Journal of Physiology* 588.12, pp. 2077–2090. DOI: 10.1113/jphysiol.2009.185918.

Bean, Bruce P. (2007). 'The action potential in mammalian central neurons'. In: *Nature Reviews Neuroscience* 8.6, pp. 451–465. DOI: 10.1038/nrn2148.

Berger, Hans (1929). 'Über das elektrenkephalogramm des menschen'. In: *Archiv für psychiatrie und nervenkrankheiten* 87.1, pp. 527–570.

Betterton, Ruth T. et al. (2017). 'Acetylcholine modulates gamma frequency oscillations in the hippocampus by activation of muscarinic M1 receptors'. In: *European*

Journal of Neuroscience 45.12. Ed. by Panayiota Poirazi, pp. 1570–1585. DOI: 10.1111/ejn.13582.

Bibbig, Andrea et al. (2002). 'Long-Range Synchronization of γ and β Oscillations and the Plasticity of Excitatory and Inhibitory Synapses: A Network Model'. In: *Journal of Neurophysiology* 88.4, pp. 1634–1654. DOI: 10.1152/jn.2002.88.4.1634.

Börgers, Christoph et al. (2005). 'Background gamma rhythmicity and attention in cortical local circuits: a computational study.' In: *Proceedings of the National Academy of Sciences of the United States of America* 102.19, pp. 7002–7. DOI: 10.1073/pnas.0502366102.

Börgers, Christoph et al. (2008). 'Gamma Oscillations and Stimulus Selection'. In: *Neural Computation* 20.2, pp. 383–414. DOI: 10.1162/neco.2007.07-06-289.

Bosman, Conrado a et al. (2012). 'Attentional stimulus selection through selective synchronization between monkey visual areas.' In: *Neuron* 75.5, pp. 875–88. DOI: 10.1016/j.neuron.2012.06.037.

Bragin, A et al. (1995). 'Gamma (40-100 Hz) oscillation in the hippocampus of the behaving rat.' In: *The Journal of neuroscience : the official journal of the Society for Neuroscience* 15.1 Pt 1, pp. 47–60.

Brunel, Nicolas et al. (2003). 'What Determines the Frequency of Fast Network Oscillations With Irregular Neural Discharges? I. Synaptic Dynamics and Excitation-Inhibition Balance'. In: *Journal of Neurophysiology* 90.1, pp. 415–430. DOI: 10.1152/jn.01095.2002.

Brunet, N. et al. (2015). 'Visual Cortical Gamma-Band Activity During Free Viewing of Natural Images'. In: *Cerebral Cortex* 25.4, pp. 918–926. DOI: 10.1093/cercor/bht280.

Buffalo, Elizabeth A et al. (2011). 'Laminar differences in gamma and alpha coherence in the ventral stream.' In: *Proceedings of the National Academy of Sciences of the United States of America* 108.27, pp. 11262–7. DOI: 10.1073/pnas.1011284108.

Buhl, Derek L. et al. (2003). 'Selective Impairment of Hippocampal Gamma Oscillations in Connexin-36 Knock-Out Mouse In Vivo'. In: *Journal of Neuroscience* 23.3, pp. 1013–1018.

Buhl, Eberhard H. et al. (1996). 'Physiological properties of anatomically identified basket and bistratified cells in the CA1 area of the rat hippocampus in vitro'. In: *Hippocampus* 6.3, pp. 294–305. DOI: 10.1002/(SICI)1098-1063(1996)6:3<294::AID-HIPO7>3.0.CO;2-N.

Buhl, Eberhard H. et al. (1998). 'Cholinergic activation and tonic excitation induce persistent gamma oscillations in mouse somatosensory cortex in vitro'. In: *The Journal of Physiology* 513.1, pp. 117–126. DOI: 10.1111/j.1469-7793.1998.117by.x.

Burns, Samuel P et al. (2011). 'Is gamma-band activity in the local field potential of V1 cortex a "clock" or filtered noise?' In: *The Journal of neuroscience : the official journal of the Society for Neuroscience* 31.26, pp. 9658–64. DOI: 10.1523/JNEUROSCI.0660-11.2011.

Butler, J. L. et al. (2016). 'Intrinsic Cornu Ammonis Area 1 Theta-Nested Gamma Oscillations Induced by Optogenetic Theta Frequency Stimulation.' In: *The Journal*

of neuroscience : the official journal of the Society for Neuroscience 36.15, pp. 4155–69. DOI: 10.1523/JNEUROSCI.3150-15.2016.

Butler, J. L. et al. (2018). 'Comparison of three gamma oscillations in the mouse entorhinal-hippocampal system'. In: *European Journal of Neuroscience*. DOI: 10.1111/ejn.13831.

Buzsaki, Gyorgy (2006). *Rhythms of the Brain*. Oxford University Press.

Buzsáki, György (2002). 'Theta Oscillations in the Hippocampus'. In: *Neuron* 33.3, pp. 325–340. DOI: 10.1016/S0896-6273(02)00586-X.

Buzsáki, György et al. (2004). 'Neuronal oscillations in cortical networks.' In: *Science (New York, N.Y.)* 304.5679, pp. 1926–9. DOI: 10.1126/science.1099745.

Buzsáki, György et al. (2012). 'Mechanisms of Gamma Oscillations'. In: *Annual Review of Neuroscience* 35.1, pp. 203–225. DOI: 10.1146/annurev-neuro-062111-150444. arXiv: NIHMS150003.

Buzsáki, György et al. (2015). 'What does gamma coherence tell us about inter-regional neural communication?' In: *Nature Neuroscience* 18.4, pp. 484–489. DOI: 10.1038/nn.3952.

Cardin, J. A. (2016). 'Snapshots of the Brain in Action: Local Circuit Operations through the Lens of γ Oscillations'. In: *Journal of Neuroscience* 36.41, pp. 10496–10504. DOI: 10.1523/JNEUROSCI.1021-16.2016.

Cardin, J. A. et al. (2009). 'Driving fast-spiking cells induces gamma rhythm and controls sensory responses'. In: *Nature* 459.7247, pp. 663–667. DOI: 10.1038/nature08002.

Caton, Richard (1875). 'Electrical Currents of the Brain.' In: *The Journal of Nervous and Mental Disease* 2.4, p. 610.

Chalk, Matthew et al. (2010). 'Attention Reduces Stimulus-Driven Gamma Frequency Oscillations and Spike Field Coherence in V1'. In: *Neuron* 66.1, pp. 114–125. DOI: 10.1016/J.NEURON.2010.03.013.

Chamberland, Simon et al. (2012). 'Inhibitory control of hippocampal inhibitory neurons'. In: *Frontiers in Neuroscience* 6, p. 165. DOI: 10.3389/fnins.2012.00165.

Chen, Guang et al. (2017). 'Distinct Inhibitory Circuits Orchestrate Cortical beta and gamma Band Oscillations'. In: *Neuron* 96.6, 1403–1418.e6. DOI: 10.1016/j.neuron.2017.11.033.

Chen, Naiyan et al. (2015). 'An acetylcholine-activated microcircuit drives temporal dynamics of cortical activity'. In: *Nature Neuroscience* 18.6, pp. 892–902. DOI: 10.1038/nn.4002.

Cho, Kathleen K.A. et al. (2015). 'Gamma Rhythms Link Prefrontal Interneuron Dysfunction with Cognitive Inflexibility in Dlx5/6+/- Mice'. In: *Neuron* 85.6, pp. 1332–1343. DOI: 10.1016/J.NEURON.2015.02.019.

Cho, R Y et al. (2006). 'Impairments in frontal cortical gamma synchrony and cognitive control in schizophrenia.' In: *Proceedings of the National Academy of Sciences of the United States of America* 103.52, pp. 19878–83. DOI: 10.1073/pnas.0609440103.

Chow, Brian Y. et al. (2010). 'High-performance genetically targetable optical neural silencing by light-driven proton pumps'. In: *Nature* 463.7277, pp. 98–102. DOI: 10.1038/nature08652.

Chrobak, James J. et al. (1989). 'Intraseptal administration of muscimol produces dose-dependent memory impairments in the rat'. In: *Behavioral and Neural Biology* 52.3, pp. 357–369. DOI: 10.1016/S0163-1047(89)90472-X.

Cobb, S R et al. (1995). 'Synchronization of neuronal activity in hippocampus by individual GABAergic interneurons'. In: *Nature* 378.6552, pp. 75–8. DOI: 10.1038/378075a0.

Cobb, S R et al. (1997). 'Synaptic effects of identified interneurons innervating both interneurons and pyramidal cells in the rat hippocampus'. In: *Neuroscience* 79.3, pp. 629–648. DOI: 10.1016/S0306-4522(97)00055-9.

Cole, Scott R. et al. (2017). 'Brain Oscillations and the Importance of Waveform Shape'. In: *Trends in Cognitive Sciences* 21.2, pp. 137–149. DOI: 10.1016/J.TICS.2016.12.008.

Colgin, Laura Lee et al. (2009). 'Frequency of gamma oscillations routes flow of information in the hippocampus'. In: *Nature* 462.7271, pp. 353–357. DOI: 10.1038/nature08573.

Collingridge, Graham L. (1995). 'The brain slice preparation: a tribute to the pioneer Henry McIlwain'. In: *Journal of Neuroscience Methods* 59.1, pp. 5–9. DOI: 10.1016/0165-0270(94)00187-L.

Craig, Michael T et al. (2015). 'Fast gamma oscillations are generated intrinsically in CA1 without the involvement of fast-spiking basket cells.' In: *The Journal of neuroscience : the official journal of the Society for Neuroscience* 35.8, pp. 3616–24. DOI: 10.1523/JNEUROSCI.4166-14.2015.

Csicsvari, J et al. (1999). 'Oscillatory coupling of hippocampal pyramidal cells and interneurons in the behaving Rat.' In: *The Journal of neuroscience : the official journal of the Society for Neuroscience* 19.1, pp. 274–87. DOI: 10.1523/JNEUROSCI.19-01-00274.1999.

Csicsvari, J et al. (2003). 'Mechanisms of gamma oscillations in the hippocampus of the behaving rat'. In: *Neuron* 37.2, pp. 311–322. DOI: 10.1016/S0896-6273(02)01169-8.

Cunningham, Mark O et al. (2003). 'Gamma oscillations induced by kainate receptor activation in the entorhinal cortex in vitro.' In: *The Journal of neuroscience : the official journal of the Society for Neuroscience* 23.30, pp. 9761–9.

Dan, Yang et al. (2004). 'Spike Timing-Dependent Plasticity of Neural Circuits'. In: *Neuron* 44.1, pp. 23–30. DOI: 10.1016/J.NEURON.2004.09.007.

Dong, Yi et al. (2008). 'Synchrony and the binding problem in macaque visual cortex'. In: *Journal of Vision* 8.7, p. 30. DOI: 10.1167/8.7.30.

Fee, Michale S. et al. (1996). 'Automatic sorting of multiple unit neuronal signals in the presence of anisotropic and non-Gaussian variability'. In: *Journal of Neuroscience Methods* 69.2, pp. 175–188. DOI: 10.1016/S0165-0270(96)00050-7.

Fell, J et al. (2001). 'Human memory formation is accompanied by rhinal-hippocampal coupling and decoupling.' In: *Nature neuroscience* 4.12, pp. 1259–1264. DOI: 10.1038/nn759.

Ferando, Isabella et al. (2015). 'In vitro gamma oscillations following partial and complete ablation of δ subunit-containing GABAA receptors from parvalbumin interneurons.' In: *Neuropharmacology* 88, pp. 91–8. DOI: 10.1016/j.neuropharm.2014.09.010.

Fernández-Ruiz, Antonio et al. (2013). 'Identifying the synaptic origin of ongoing neuronal oscillations through spatial discrimination of electric fields.' In: *Frontiers in computational neuroscience* 7, p. 5. DOI: 10.3389/fncom.2013.00005.

Ferraguti, Francesco et al. (2004). 'Immunolocalization of metabotropic glutamate receptor 1a (mGluR1a) in distinct classes of interneuron in the CA1 region of the rat hippocampus'. In: *Hippocampus* 14.2, pp. 193–215. DOI: 10.1002/hipo.10163.

Ferster, D et al. (1995). 'Cracking the neuronal code.' In: *Science (New York, N.Y.)* 270.5237, pp. 756–7. DOI: 10.1126/SCIENCE.270.5237.756.

Fino, Elodie et al. (2011). 'Dense Inhibitory Connectivity in Neocortex'. In: *Neuron* 69.6, pp. 1188–1203. DOI: 10.1016/J.NEURON.2011.02.025.

Fisahn, A. et al. (1998). 'Cholinergic induction of network oscillations at 40 Hz in the hippocampus in vitro.' In: *Nature* 394.6689, pp. 186–189. DOI: 10.1038/28179.

Fisahn, A. et al. (2004). 'Distinct roles for the kainate receptor subunits GluR5 and GluR6 in kainate-induced hippocampal gamma oscillations.' In: *The Journal of neuroscience : the official journal of the Society for Neuroscience* 24.43, pp. 9658–68. DOI: 10.1523/JNEUROSCI.2973-04.2004.

French, C R et al. (1990). 'A voltage-dependent persistent sodium current in mammalian hippocampal neurons.' In: *The Journal of general physiology* 95.6, pp. 1139–57. DOI: 10.1085/JGP.95.6.1139.

Freund, T F et al. (1996). 'Interneurons of the hippocampus.' In: *Hippocampus* 6.4, pp. 347–470. DOI: 10.1002/(SICI)1098-1063(1996)6:4\<347::AID-HIPO1\>3.0.CO;2-I.

Fries, P. (2005). 'A mechanism for cognitive dynamics: neuronal communication through neuronal coherence'. In: *Trends in Cognitive Sciences* 9.10, pp. 474–480. DOI: 10.1016/J.TICS.2005.08.011.

— (2015). 'Rhythms for Cognition: Communication through Coherence'. In: *Neuron* 88.1, pp. 220–235. DOI: 10.1016/j.neuron.2015.09.034.

Fries, P. et al. (2001). 'Modulation of oscillatory neuronal synchronization by selective visual attention.' In: *Science (New York, N.Y.)* 291.5508, pp. 1560–3. DOI: 10.1126/science.291.5508.1560.

Fries, P. et al. (2007). 'The gamma cycle'. In: *Trends in Neurosciences* 30.7, pp. 309–316. DOI: 10.1016/J.TINS.2007.05.005.

Fröhlich, Flavio et al. (2010). 'Endogenous Electric Fields May Guide Neocortical Network Activity'. In: *Neuron* 67.1, pp. 129–143. DOI: 10.1016/J.NEURON.2010.06.005.

Fuchs, Elke C. et al. (2007). 'Recruitment of Parvalbumin-Positive Interneurons Determines Hippocampal Function and Associated Behavior'. In: *Neuron* 53.4, pp. 591–604. DOI: 10.1016/J.NEURON.2007.01.031.

Fukuda, Takaichi et al. (2006). 'Gap junctions among dendrites of cortical GABAergic neurons establish a dense and widespread intercolumnar network.' In: *The Journal of neuroscience : the official journal of the Society for Neuroscience* 26.13, pp. 3434–43. DOI: 10.1523/JNEUROSCI.4076-05.2006.

Fukuda, T. et al. (2003). 'Ultrastructural study of gap junctions between dendrites of parvalbumin-containing GABAergic neurons in various neocortical areas of the adult rat'. In: *Neuroscience* 120.1, pp. 5–20. DOI: 10.1016/S0306-4522(03)00328-2.

El-Gaby, Mohamady et al. (2016). 'Archaerhodopsin Selectively and Reversibly Silences Synaptic Transmission through Altered pH'. In: *Cell Reports* 16.8, pp. 2259–2268. DOI: 10.1016/J.CELREP.2016.07.057.

Galarreta, Mario et al. (2002). 'Electrical and chemical synapses among parvalbumin fast-spiking GABAergic interneurons in adult mouse neocortex.' In: *Proceedings of the National Academy of Sciences of the United States of America* 99.19, pp. 12438–43. DOI: 10.1073/pnas.192159599.

Gelman, Diego M. et al. (2010). 'Generation of interneuron diversity in the mouse cerebral cortex'. In: *European Journal of Neuroscience* 31.12, pp. 2136–2141. DOI: 10.1111/j.1460-9568.2010.07267.x.

Gentet, L J et al. (2012). 'Unique functional properties of somatostatin-expressing GABAergic neurons in mouse barrel cortex'. In: *Nat Neurosci* 15.4, pp. 607–612. DOI: 10.1038/nn.3051.

Gibson, Jay R. et al. (1999). 'Two networks of electrically coupled inhibitory neurons in neocortex'. In: *Nature* 402.6757, pp. 75–79. DOI: 10.1038/47035.

Gillespie, Anna K. et al. (2016). 'Apolipoprotein E4 Causes Age-Dependent Disruption of Slow Gamma Oscillations during Hippocampal Sharp-Wave Ripples'. In: *Neuron* 90.4, pp. 740–751. DOI: 10.1016/J.NEURON.2016.04.009.

Glickfeld, Lindsey L et al. (2009). 'Interneurons hyperpolarize pyramidal cells along their entire somatodendritic axis'. In: *Nature Neuroscience* 12.1, pp. 21–23. DOI: 10.1038/nn.2230.

Gloveli, Tengis et al. (2005). 'Differential involvement of oriens/pyramidale interneurones in hippocampal network oscillations In vitro'. In: *The Journal of Physiology* 562.1, pp. 131–147. DOI: 10.1113/jphysiol.2004.073007.

Gray, Charles M et al. (1989). *Osillatory responses in cat visual cortex exhibit inter-columnar synchronization which reflects global stimulus properties*. DOI: 10.1038/338334a0.

Gregoriou, Georgia G et al. (2009). 'High-frequency, long-range coupling between prefrontal and visual cortex during attention.' In: *Science (New York, N.Y.)* 324.5931, pp. 1207–10. DOI: 10.1126/science.1171402.

Grothe, Iris et al. (2012). 'Switching neuronal inputs by differential modulations of gamma-band phase-coherence.' In: *Journal of Neuroscience* 32.46, pp. 16172–16180. DOI: 10.1523/JNEUROSCI.0890-12.2012.

Gulyás, A. I. et al. (1999). 'Total number and ratio of excitatory and inhibitory synapses converging onto single interneurons of different types in the CA1 area of the rat hippocampus.' In: *The Journal of neuroscience : the official journal of the Society for Neuroscience* 19.22, pp. 10082–97. DOI: 10.1523/JNEUROSCI.19-22-10082.1999.

Gulyás, A. I. et al. (2010). 'Parvalbumin-containing fast-spiking basket cells generate the field potential oscillations induced by cholinergic receptor activation in the hippocampus.' In: *The Journal of neuroscience : the official journal of the Society for Neuroscience* 30.45, pp. 15134–45. DOI: 10.1523/JNEUROSCI.4104-10.2010.

Haider, Bilal et al. (2016). 'Millisecond Coupling of Local Field Potentials to Synaptic Currents in the Awake Visual Cortex.' In: *Neuron* 90.1, pp. 35–42. DOI: 10.1016/j.neuron.2016.02.034.

Hajos, N. (2004). 'Spike Timing of Distinct Types of GABAergic Interneuron during Hippocampal Gamma Oscillations In Vitro'. In: *Journal of Neuroscience* 24.41, pp. 9127–9137. DOI: 10.1523/JNEUROSCI.2113-04.2004.

Hájos, Norbert et al. (2009). 'Network mechanisms of gamma oscillations in the CA3 region of the hippocampus'. In: *Neural Networks* 22.8, pp. 1113–1119. DOI: 10.1016/j.neunet.2009.07.024.

Hardy, John et al. (2002). 'The amyloid hypothesis of Alzheimer's disease: progress and problems on the road to therapeutics.' In: *Science (New York, N.Y.)* 297.5580, pp. 353–6. DOI: 10.1126/science.1072994.

Harris, Kenneth D. et al. (2003). 'Organization of cell assemblies in the hippocampus'. In: *Nature* 424.6948, pp. 552–556. DOI: 10.1038/nature01834.

Harwell, Corey C. et al. (2015). 'Wide Dispersion and Diversity of Clonally Related Inhibitory Interneurons'. In: *Neuron* 87.5, pp. 999–1007. DOI: 10.1016/j.neuron.2015.07.030.

Hasenstaub, Andrea et al. (2005). 'Inhibitory Postsynaptic Potentials Carry Synchronized Frequency Information in Active Cortical Networks'. In: *Neuron* 47.3, pp. 423–435. DOI: 10.1016/J.NEURON.2005.06.016.

Henze, D.A et al. (2001). 'Action potential threshold of hippocampal pyramidal cells in vivo is increased by recent spiking activity'. In: *Neuroscience* 105.1, pp. 121–130. DOI: 10.1016/S0306-4522(01)00167-1.

Herman, Alexander M et al. (2014). 'Cell type-specific and time-dependent light exposure contribute to silencing in neurons expressing Channelrhodopsin-2'. In: *eLife* 3, e01481. DOI: 10.7554/eLife.01481.

Herrmann, C.S. et al. (2005). 'Human EEG gamma oscillations in neuropsychiatric disorders'. In: *Clinical Neurophysiology* 116.12, pp. 2719–2733. DOI: 10.1016/J.CLINPH.2005.07.007.

Hodgkin, A L et al. (1952). 'Currents carried by sodium and potassium ions through the membrane of the giant axon of Loligo.' In: *The Journal of physiology* 116.4, pp. 449–72.

Hofer, Sonja B et al. (2011). 'Differential connectivity and response dynamics of excitatory and inhibitory neurons in visual cortex'. In: *Nature Neuroscience* 14.8, pp. 1045–1052. DOI: 10.1038/nn.2876.

Hormuzdi, Sheriar G. et al. (2001). 'Impaired Electrical Signaling Disrupts Gamma Frequency Oscillations in Connexin 36-Deficient Mice'. In: *Neuron* 31.3, pp. 487–495. DOI: 10.1016/S0896-6273(01)00387-7.

Howard, Marc W. et al. (2003). 'Gamma Oscillations Correlate with Working Memory Load in Humans'. In: *Cerebral Cortex* 13.12, pp. 1369–1374. DOI: 10.1093/cercor/bhg084.

Howe, William M et al. (2017). 'Acetylcholine Release in Prefrontal Cortex Promotes Gamma Oscillations and Theta-Gamma Coupling during Cue Detection.' In: *The Journal of neuroscience : the official journal of the Society for Neuroscience* 37.12, pp. 3215–3230. DOI: 10.1523/JNEUROSCI.2737-16.2017.

Hu, Hang et al. (2011). 'Submillisecond firing synchrony between different subtypes of cortical interneurons connected chemically but not electrically.' In: *The Journal of neuroscience : the official journal of the Society for Neuroscience* 31.9, pp. 3351–61. DOI: 10.1523/JNEUROSCI.4881-10.2011.

Hu, Hang et al. (2013). 'Not all that glitters is gold: off-target recombination in the somatostatin–IRES-Cre mouse line labels a subset of fast-spiking interneurons'. In: *Frontiers in Neural Circuits* 7, p. 195. DOI: 10.3389/fncir.2013.00195.

Hu, Hua et al. (2014). 'Interneurons. Fast-spiking, parvalbumin+ GABAergic interneurons: from cellular design to microcircuit function.' In: *Science (New York, N.Y.)* 345.6196, p. 1255263. DOI: 10.1126/science.1255263.

Huang, Shiwei et al. (2013). 'Physiological temperature during brain slicing enhances the quality of acute slice preparations'. In: *Frontiers in Cellular Neuroscience* 7, p. 48. DOI: 10.3389/fncel.2013.00048.

Iaccarino, Hannah F. et al. (2016). 'Gamma frequency entrainment attenuates amyloid load and modifies microglia'. In: *Nature* 540.7632, pp. 230–235. DOI: 10.1038/nature20587.

Jackman, Skyler L et al. (2014). 'Achieving high-frequency optical control of synaptic transmission.' In: *The Journal of neuroscience : the official journal of the Society for Neuroscience* 34.22, pp. 7704–14. DOI: 10.1523/JNEUROSCI.4694-13.2014.

Jackson, Jesse et al. (2011). 'Fast and slow γ rhythms are intrinsically and independently generated in the subiculum.' In: *The Journal of neuroscience : the official journal of the Society for Neuroscience* 31.34, pp. 12104–17. DOI: 10.1523/JNEUROSCI.1370-11.2011.

Kametani, Hideki et al. (1990). 'Alterations in acetylcholine release in the rat hippocampus during sleep-wakefulness detected by intracerebral dialysis'. In: *Life Sciences* 47.5, pp. 421–426. DOI: 10.1016/0024-3205(90)90300-G.

Katona, I et al. (1999). 'Postsynaptic targets of somatostatin-immunoreactive interneurons in the rat hippocampus'. In: *Neuroscience* 88.1, pp. 37–55. DOI: 10.1016/S0306-4522(98)00302-9.

Kim, Dohoung et al. (2016). 'Distinct Roles of Parvalbumin- and Somatostatin-Expressing Interneurons in Working Memory'. In: *Neuron* 92.4, pp. 902–915. DOI: 10.1016/J.NEURON.2016.09.023.

Kim, Hoseok et al. (2016). 'Prefrontal Parvalbumin Neurons in Control of Attention'. In: *Cell* 164.1-2, pp. 208–218. DOI: 10.1016/J.CELL.2015.11.038.

Klausberger, Thomas et al. (2003). 'Brain-state- and cell-type-specific firing of hippocampal interneurons in vivo.' In: *Nature* 421.6925, pp. 844–848. DOI: 10.1038/nature04910.

Klausberger, Thomas et al. (2008). 'Neuronal diversity and temporal dynamics: the unity of hippocampal circuit operations.' In: *Science (New York, N.Y.)* 321.5885, pp. 53–7. DOI: 10.1126/science.1149381.

Knoferle, Johanna et al. (2014). 'Apolipoprotein E4 produced in GABAergic interneurons causes learning and memory deficits in mice.' In: *The Journal of neuroscience : the official journal of the Society for Neuroscience* 34.42, pp. 14069–78. DOI: 10.1523/JNEUROSCI.2281-14.2014.

Kohus, Z. et al. (2016). 'Properties and dynamics of inhibitory synaptic communication within the CA3 microcircuits of pyramidal cells and interneurons expressing parvalbumin or cholecystokinin'. In: *The Journal of Physiology* 594.13, pp. 3745–3774. DOI: 10.1113/JP272231.

Lacaille, J C et al. (1987). 'Local circuit interactions between oriens/alveus interneurons and CA1 pyramidal cells in hippocampal slices: electrophysiology and morphology.' In: *The Journal of neuroscience : the official journal of the*

Society for Neuroscience 7.7, pp. 1979–93. DOI: 10.1523/JNEUROSCI.07-07-01979.1987.

Lamme, Victor A. F. et al. (1998). 'Neuronal synchrony does not represent texture segregation'. In: *Nature* 396.6709, pp. 362–366. DOI: 10.1038/24608.

Lasztóczi, Bálint et al. (2014). 'Layer-Specific GABAergic Control of Distinct Gamma Oscillations in the CA1 Hippocampus'. In: *Neuron* 81.5, pp. 1126–1139. DOI: 10.1016/J.NEURON.2014.01.021.

— (2016). 'Hippocampal Place Cells Couple to Three Different Gamma Oscillations during Place Field Traversal'. In: *Neuron* 91.1, pp. 34–40. DOI: 10.1016/J.NEURON.2016.05.036.

Leão, Richardson N et al. (2012). 'OLM interneurons differentially modulate CA3 and entorhinal inputs to hippocampal CA1 neurons'. In: *Nature Neuroscience* 15.11, pp. 1524–1530. DOI: 10.1038/nn.3235.

LeBeau, Fiona E. N. et al. (2002). 'Fast network oscillations induced by potassium transients in the rat hippocampus in vitro'. In: *The Journal of Physiology* 542.1, pp. 167–179. DOI: 10.1113/jphysiol.2002.015933.

Lesh, Tyler A et al. (2011). 'Cognitive Control Deficits in Schizophrenia: Mechanisms and Meaning'. In: *Neuropsychopharmacology* 36.1, pp. 316–338. DOI: 10.1038/npp.2010.156.

Li, Jingcheng et al. (2017). 'Primary Auditory Cortex is Required for Anticipatory Motor Response'. In: *Cerebral Cortex* 27.6, pp. 3254–3271. DOI: 10.1093/cercor/bhx079.

Light, Gregory A. et al. (2006). 'Gamma Band Oscillations Reveal Neural Network Cortical Coherence Dysfunction in Schizophrenia Patients'. In: *Biological Psychiatry* 60.11, pp. 1231–1240. DOI: 10.1016/J.BIOPSYCH.2006.03.055.

Lisman, John E. et al. (2013). 'The Theta-Gamma Neural Code'. In: *Neuron* 77.6, pp. 1002–1016. DOI: 10.1016/j.neuron.2013.03.007. arXiv: NIHMS150003.

Lovett-Barron, Matthew et al. (2012). 'Regulation of neuronal input transformations by tunable dendritic inhibition'. In: *Nature Neuroscience* 15.3, pp. 423–430. DOI: 10.1038/nn.3024.

Lovett-Barron, Matthew et al. (2014). 'Dendritic inhibition in the hippocampus supports fear learning.' In: *Science (New York, N.Y.)* 343.6173, pp. 857–63. DOI: 10.1126/science.1247485.

Ma, Yunyong et al. (2006). 'Distinct subtypes of somatostatin-containing neocortical interneurons revealed in transgenic mice.' In: *The Journal of neuroscience : the official journal of the Society for Neuroscience* 26.19, pp. 5069–82. DOI: 10.1523/JNEUROSCI.0661-06.2006.

Maccaferri, Gianmaria et al. (2000). 'Cell surface domain specific postsynaptic currents evoked by identified GABAergic neurones in rat hippocampus in vitro'. In: *The Journal of Physiology* 524.1, pp. 91–116. DOI: 10.1111/j.1469-7793.2000.t01-3-00091.x.

Mahn, Mathias et al. (2016). 'Biophysical constraints of optogenetic inhibition at presynaptic terminals'. In: *Nature Neuroscience* 19.4, pp. 554–556. DOI: 10.1038/nn.4266.

Mainen, Z F et al. (1995). 'Reliability of spike timing in neocortical neurons.' In: *Science (New York, N.Y.)* 268.5216, pp. 1503–1506. DOI: 10.1126/science.7770778.

Malsburg, C von der (1999). 'The what and why of binding: the modeler's perspective.' In: *Neuron* 24.1, pp. 95–25. DOI: 10.1016/S0896-6273(00)80825-9.

Mamad, Omar et al. (2015). 'Medial septum regulates the hippocampal spatial representation'. In: *Frontiers in Behavioral Neuroscience* 9, p. 166. DOI: 10.3389/fnbeh.2015.00166.

Mann, Edward O. et al. (2005a). 'Hippocampal gamma-frequency oscillations: from interneurones to pyramidal cells, and back'. In: *The Journal of Physiology* 562.1, pp. 55–63. DOI: 10.1113/jphysiol.2004.078758.

Mann, Edward O. et al. (2005b). 'Perisomatic Feedback Inhibition Underlies Cholinergically Induced Fast Network Oscillations in the Rat Hippocampus In Vitro'. In: *Neuron* 45.1, pp. 105–117. DOI: 10.1016/j.neuron.2004.12.016.

Mann, Edward O. et al. (2007). 'Role of GABAergic inhibition in hippocampal network oscillations'. In: *Trends in Neurosciences* 30.7, pp. 343–349. DOI: 10.1016/j.tins.2007.05.003.

Mann, Edward O. et al. (2010). 'Control of hippocampal gamma oscillation frequency by tonic inhibition and excitation of interneurons'. In: *Nature Neuroscience* 13.2, pp. 205–212. DOI: 10.1038/nn.2464.

Markram, H et al. (1997). 'Regulation of synaptic efficacy by coincidence of postsynaptic APs and EPSPs.' In: *Science (New York, N.Y.)* 275.5297, pp. 213–5. DOI: 10.1126/SCIENCE.275.5297.213.

Marrosu, Francesco et al. (1995). 'Microdialysis measurement of cortical and hippocampal acetylcholine release during sleep-wake cycle in freely moving cats'. In: *Brain Research* 671.2, pp. 329–332. DOI: 10.1016/0006-8993(94)01399-3.

Martin, Kevan A C et al. (2016). 'Phase Locking of Multiple Single Neurons to the Local Field Potential in Cat V1.' In: *The Journal of neuroscience : the official journal of the Society for Neuroscience* 36.8, pp. 2494–502. DOI: 10.1523/JNEUROSCI.2547-14.2016.

Marty, Alain et al. (2005). 'Excitatory effects of GABA in established brain networks.' In: *Trends in neurosciences* 28.6, pp. 284–9. DOI: 10.1016/j.tins.2005.04.003.

Masters, Colin L. et al. (2015). 'Alzheimer's disease'. In: *Nature Reviews Disease Primers* 1, p. 15056. DOI: 10.1038/nrdp.2015.56.

McAdams, C J et al. (1999). 'Effects of attention on orientation-tuning functions of single neurons in macaque cortical area V4.' In: *The Journal of neuroscience : the official journal of the Society for Neuroscience* 19.1, pp. 431–41. DOI: 10.1523/JNEUROSCI.19-01-00431.1999.

McCormick, D A et al. (1985). 'Comparative electrophysiology of pyramidal and sparsely spiny stellate neurons of the neocortex.' In: *Journal of neurophysiology* 54.4, pp. 782–806. DOI: 10.1152/jn.1985.54.4.782.

McGuire, Barbara A. et al. (1991). 'Targets of horizontal connections in macaque primary visual cortex'. In: *The Journal of Comparative Neurology* 305.3, pp. 370–392. DOI: 10.1002/cne.903050303.

Mcilwain, H et al. (1951). 'The Inorganic Phosphate and Phosphocreatine of Brain Especially during Metabolism in vitro'. In:

Megias, M et al. (2001). 'Total number and distribution of inhibitory and excitatory synapses on hippocampal CA1 pyramidal cells'. In: *Neuroscience* 102.3, pp. 527–540. DOI: 10.1016/S0306-4522(00)00496-6.

Merker, Bjorn (2013). 'Cortical gamma oscillations: the functional key is activation, not cognition'. In: *Neuroscience & Biobehavioral Reviews* 37.3, pp. 401–417. DOI: 10.1016/J.NEUBIOREV.2013.01.013.

Meyer, Axel H et al. (2002). 'In vivo labeling of parvalbumin-positive interneurons and analysis of electrical coupling in identified neurons.' In: *The Journal of neuroscience : the official journal of the Society for Neuroscience* 22.16, pp. 7055–64. DOI: 20026742.

Miao, Chenglin et al. (2017). 'Parvalbumin and Somatostatin Interneurons Control Different Space-Coding Networks in the Medial Entorhinal Cortex'. In: *Cell* 171.3, 507–521.e17. DOI: 10.1016/J.CELL.2017.08.050.

Miles, Richard et al. (1996). 'Differences between Somatic and Dendritic Inhibition in the Hippocampus'. In: *Neuron* 16.4, pp. 815–823. DOI: 10.1016/S0896-6273(00)80101-4.

Milner, Peter M. (1974). 'A model for visual shape recognition.' In: *Psychological Review* 81.6, pp. 521–535. DOI: 10.1037/h0037149.

Minzenberg, Michael J. et al. (2012). 'Developing treatments for impaired cognition in schizophrenia'. In: *Trends in Cognitive Sciences* 16.1, pp. 35–42. DOI: 10.1016/J.TICS.2011.11.017.

Mitchell, Jude F. et al. (2007). 'Differential Attention-Dependent Response Modulation across Cell Classes in Macaque Visual Area V4'. In: *Neuron* 55.1, pp. 131–141. DOI: 10.1016/J.NEURON.2007.06.018.

Montgomery, Sean M et al. (2007). 'Gamma oscillations dynamically couple hippocampal CA3 and CA1 regions during memory task performance.' In: *Proceedings of the National Academy of Sciences of the United States of America* 104.36, pp. 14495–500. DOI: 10.1073/pnas.0701826104.

Moore, Tirin et al. (2017). 'Neural Mechanisms of Selective Visual Attention'. In: *Annual Review of Psychology* 68.1, pp. 47–72. DOI: 10.1146/annurev-psych-122414-033400.

Muller, Christina et al. (2014). 'Dendritic inhibition mediated by O-LM and bistratified interneurons in the hippocampus'. In: *Frontiers in Synaptic Neuroscience* 6, p. 23. DOI: 10.3389/fnsyn.2014.00023.

Murakoshi, Takayuki et al. (1993). 'Electrophysiological identification of horizontal synaptic connections in rat visual cortex in vitro'. In: *Neuroscience Letters* 163.2, pp. 211–214. DOI: 10.1016/0304-3940(93)90385-X.

Nagel, Georg et al. (2003). 'Channelrhodopsin-2, a directly light-gated cation-selective membrane channel.' In: *Proceedings of the National Academy of Sciences of the United States of America* 100.24, pp. 13940–5. DOI: 10.1073/pnas.1936192100.

Ni, Jianguang et al. (2016). 'Gamma-Rhythmic Gain Modulation'. In: *Neuron* 92.1, pp. 240–251. DOI: 10.1016/J.NEURON.2016.09.003.

Nicholson, C et al. (1975). 'Theory of current source-density analysis and determination of conductivity tensor for anuran cerebellum.' In: *Journal of neurophysiology* 38.2, pp. 356–68. DOI: 10.1152/jn.1975.38.2.356.

Noble, D. et al. (1966). 'The threshold conditions for initiation of action potentials by excitable cells'. In: *The Journal of Physiology* 187.1, pp. 129–162. DOI: 10.1113/jphysiol.1966.sp008079.

Oke, Olaleke O. et al. (2010). 'High-frequency gamma oscillations coexist with low-frequency gamma oscillations in the rat visual cortex in vitro'. In: *European*

Journal of Neuroscience 31.8, pp. 1435–1445. DOI: 10.1111/j.1460-9568.2010.07171.x.

Oren, Iris et al. (2006). 'Synaptic currents in anatomically identified CA3 neurons during hippocampal gamma oscillations in vitro.' In: *The Journal of neuroscience : the official journal of the Society for Neuroscience* 26.39, pp. 9923–9934. DOI: 10.1523/JNEUROSCI.1580-06.2006.

Oren, Iris et al. (2010). 'Identification of the current generator underlying cholinergically induced gamma frequency field potential oscillations in the hippocampal CA3 region'. In: *The Journal of Physiology* 588.5, pp. 785–797. DOI: 10.1113/jphysiol.2009.180851.

Packer, Adam M et al. (2011). 'Dense, unspecific connectivity of neocortical parvalbumin-positive interneurons: a canonical microcircuit for inhibition?' In: *The Journal of neuroscience : the official journal of the Society for Neuroscience* 31.37, pp. 13260–71. DOI: 10.1523/JNEUROSCI.3131-11.2011.

Pelkey, Kenneth A. et al. (2017). 'Hippocampal GABAergic Inhibitory Interneurons'. In: *Physiological Reviews* 97.4, pp. 1619–1747. DOI: 10.1152/physrev.00007.2017.

Perrenoud, Quentin et al. (2016). 'Membrane Potential Dynamics of Spontaneous and Visually Evoked Gamma Activity in V1 of Awake Mice'. In: *PLOS Biology* 14.2. Ed. by Alberto Bacci, e1002383. DOI: 10.1371/journal.pbio.1002383.

Pfeffer, Carsten K et al. (2013). 'Inhibition of inhibition in visual cortex: the logic of connections between molecularly distinct interneurons'. In: *Nature Neuroscience* 16.8, pp. 1068–1076. DOI: 10.1038/nn.3446.

Pietersen, Alexander N.J. et al. (2009). 'Comparison between spontaneous and kainate-induced gamma oscillations in the mouse hippocampus in vitro'. In: *European Journal of Neuroscience* 29.11, pp. 2145–2156. DOI: 10.1111/j.1460-9568.2009.06771.x.

Pietersen, Alexander N.J. et al. (2014). 'Transition between fast and slow gamma modes in rat hippocampus area CA1 in vitro is modulated by slow CA3 gamma oscillations'. In: *The Journal of Physiology* 592.4, pp. 605–620. DOI: 10.1113/jphysiol.2013.263889.

Pike, Fenella G. et al. (2000). 'Distinct frequency preferences of different types of rat hippocampal neurones in response to oscillatory input currents'. In: *The Journal of Physiology* 529.1, pp. 205–213. DOI: 10.1111/j.1469-7793.2000.00205.x.

Pouille, Frédéric et al. (2001). 'Enforcement of temporal fidelity in pyramidal cells by somatic feed-forward inhibition.' In: *Science (New York, N.Y.)* 293.5532, pp. 1159–1163. DOI: 10.1126/science.1060342.

— (2004). 'Routing of spike series by dynamic circuits in the hippocampus'. In: *Nature* 429.6993, pp. 717–723. DOI: 10.1038/nature02615.

Poulet, James F. A. et al. (2008). 'Internal brain state regulates membrane potential synchrony in barrel cortex of behaving mice'. In: *Nature* 454.7206, pp. 881–885. DOI: 10.1038/nature07150.

Quian Quiroga, R. (2009). 'What is the real shape of extracellular spikes?' In: *Journal of Neuroscience Methods* 177.1, pp. 194–198. DOI: 10.1016/J.JNEUMETH.2008.09.033.

Quiroga, R. Quian et al. (2004). 'Unsupervised Spike Detection and Sorting with Wavelets and Superparamagnetic Clustering'. In: *Neural Computation* 16.8, pp. 1661–1687. DOI: 10.1162/089976604774201631.

Rama, Sylvain et al. (2015). 'Presynaptic hyperpolarization induces a fast analogue modulation of spike-evoked transmission mediated by axonal sodium channels'. In: *Nature Communications* 6.1, p. 10163. DOI: 10.1038/ncomms10163.

Ramirez, Denise MO et al. (2011). 'Differential regulation of spontaneous and evoked neurotransmitter release at central synapses'. In: *Current Opinion in Neurobiology* 21.2, pp. 275–282. DOI: 10.1016/J.CONB.2011.01.007.

Rawlins, J. N. P. et al. (1979). 'Septo-hippocampal connections and the hippocampal theta rhythm'. In: *Experimental Brain Research* 37.1, pp. 49–63. DOI: 10.1007/BF01474253.

Ray, Supratim et al. (2010). 'Differences in Gamma Frequencies across Visual Cortex Restrict Their Possible Use in Computation'. In: *Neuron* 67.5, pp. 885–896. DOI: 10.1016/J.NEURON.2010.08.004.

— (2015). 'Do gamma oscillations play a role in cerebral cortex?' In: *Trends in Cognitive Sciences* 19.2, pp. 78–85. DOI: 10.1016/J.TICS.2014.12.002.

Reynolds, John H. et al. (2004). 'ATTENTIONAL MODULATION OF VISUAL PROCESSING'. In: *Annual Review of Neuroscience* 27.1, pp. 611–647. DOI: 10.1146/annurev.neuro.26.041002.131039.

Riehle, A et al. (1997). 'Spike synchronization and rate modulation differentially involved in motor cortical function.' In: *Science (New York, N.Y.)* 278.5345, pp. 1950–3. DOI: 10.1126/SCIENCE.278.5345.1950.

Rodriguez, Rosa et al. (2004). 'Short- and long-term effects of cholinergic modulation on gamma oscillations and response synchronization in the visual cortex.' In: *The Journal of neuroscience : the official journal of the Society for Neuroscience* 24.46, pp. 10369–78. DOI: 10.1523/JNEUROSCI.1839-04.2004.

Roelfsema, Pieter R et al. (2004). 'Synchrony and covariation of firing rates in the primary visual cortex during contour grouping'. In: *Nature Neuroscience* 7.9, pp. 982–991. DOI: 10.1038/nn1304.

Roskies, Adina L. (1999). 'The Binding Problem'. In: *Neuron* 24.1, pp. 7–9. DOI: 10.1016/S0896-6273(00)80817-X.

Roux, Frédéric et al. (2012). 'Gamma-band activity in human prefrontal cortex codes for the number of relevant items maintained in working memory.' In: *The Journal of neuroscience : the official journal of the Society for Neuroscience* 32.36, pp. 12411–20. DOI: 10.1523/JNEUROSCI.0421-12.2012.

Royer, S eacute bastien et al. (2012). 'Control of timing, rate and bursts of hippocampal place cells by dendritic and somatic inhibition'. In: *Nature Neuroscience* 15.5, pp. 1–10. DOI: 10.1038/nn.3077.

Sachidhanandam, Shankar et al. (2013). 'Membrane potential correlates of sensory perception in mouse barrel cortex'. In: *Nature Neuroscience* 16.11, pp. 1671–1677. DOI: 10.1038/nn.3532.

Salinas, Emilio et al. (2000). 'Gain Modulation: A Major Computational Principle of the Central Nervous System'. In: *Neuron* 27.1, pp. 15–21. DOI: 10.1016/S0896-6273(00)00004-0.

Schomburg, Erik W et al. (2014). 'Theta phase segregation of input-specific gamma patterns in entorhinal-hippocampal networks.' In: *Neuron* 84.2, pp. 470–85. DOI: 10.1016/j.neuron.2014.08.051.

Senior, T. J. et al. (2008). 'Gamma Oscillatory Firing Reveals Distinct Populations of Pyramidal Cells in the CA1 Region of the Hippocampus'. In: *Journal of Neuroscience* 28.9, pp. 2274–2286. DOI: 10.1523/JNEUROSCI.4669-07.2008.

Shute, C. C. D. et al. (1963). 'Cholinesterase-Containing Systems of the Brain of the Rat'. In: *Nature* 199.4899, pp. 1160–1164. DOI: 10.1038/1991160a0.

Siegle, Joshua H et al. (2014). 'Gamma-range synchronization of fast-spiking interneurons can enhance detection of tactile stimuli'. In: *Nature Neuroscience* 17.10, pp. 1371–1379. DOI: 10.1038/nn.3797.

Silver, R. Angus (2010). 'Neuronal arithmetic'. In: *Nature Reviews Neuroscience* 11.7, pp. 474–489. DOI: 10.1038/nrn2864.

Singer, W (1993). 'Synchronization of Cortical Activity and its Putative Role in Information Processing and Learning'. In: *Annual Review of Physiology* 55.1, pp. 349–374. DOI: 10.1146/annurev.ph.55.030193.002025.

Sohal, V. S. (2016). 'How Close Are We to Understanding What (if Anything) Oscillations Do in Cortical Circuits?' In: *Journal of Neuroscience* 36.41, pp. 10489–10495. DOI: 10.1523/JNEUROSCI.0990-16.2016.

Sohal, V. S. et al. (2009). 'Parvalbumin neurons and gamma rhythms enhance cortical circuit performance.' In: *Nature* 459.7247, pp. 698–702. DOI: 10.1038/nature07991. arXiv: NIHMS150003.

Somogyi, Peter et al. (2005). 'Defined types of cortical interneurone structure space and spike timing in the hippocampus.' In: *The Journal of physiology* 562.Pt 1, pp. 9–26. DOI: 10.1113/jphysiol.2004.078915.

Spellman, Timothy et al. (2015). 'Hippocampal–prefrontal input supports spatial encoding in working memory'. In: *Nature* 522.7556, pp. 309–314. DOI: 10.1038/nature14445.

Stein, Astrid von et al. (2000). 'Different frequencies for different scales of cortical integration: from local gamma to long range alpha/theta synchronization'. In: *International Journal of Psychophysiology* 38.3, pp. 301–313. DOI: 10.1016/S0167-8760(00)00172-0.

Stepanyants, Armen et al. (2009). 'The fractions of short- and long-range connections in the visual cortex.' In: *Proceedings of the National Academy of Sciences of the United States of America* 106.9, pp. 3555–60. DOI: 10.1073/pnas.0810390106.

Steriade, M et al. (1993). 'Thalamocortical oscillations in the sleeping and aroused brain.' In: *Science (New York, N.Y.)* 262.5134, pp. 679–685. DOI: 10.1126/science.8235588.

Suh, Junghyup et al. (2011). 'Entorhinal cortex layer III input to the hippocampus is crucial for temporal association memory.' In: *Science (New York, N.Y.)* 334.6061, pp. 1415–20. DOI: 10.1126/science.1210125.

Tallon-Baudry, C et al. (1999). 'Oscillatory gamma activity in humans and its role in object representation.' In: *Trends in cognitive sciences* 3.4, pp. 151–162. DOI: 10.1016/S1364-6613(99)01299-1.

Tamás, Gábor et al. (2000). 'Proximally targeted GABAergic synapses and gap junctions synchronize cortical interneurons'. In: *Nature Neuroscience* 3.4, pp. 366–371. DOI: 10.1038/73936.

Taniguchi, Hiroki et al. (2011). 'A Resource of Cre Driver Lines for Genetic Targeting of GABAergic Neurons in Cerebral Cortex'. In: *Neuron* 71.6, pp. 995–1013. DOI: 10.1016/J.NEURON.2011.07.026.

Teles-Grilo Ruivo, Leonor M. et al. (2017). 'Coordinated Acetylcholine Release in Prefrontal Cortex and Hippocampus Is Associated with Arousal and Reward on Distinct Timescales'. In: *Cell Reports* 18.4, pp. 905–917. DOI: 10.1016/J.CELREP.2016.12.085.

Thiele, Alexander et al. (2003). 'Neuronal synchrony does not correlate with motion coherence in cortical area MT'. In: *Nature* 421.6921, pp. 366–370. DOI: 10.1038/nature01285.

Traub, R. D. et al. (1996a). 'A mechanism for generation of long-range synchronous fast oscillations in the cortex'. In: *Nature* 383.6601, pp. 621–624. DOI: 10.1038/383621a0.

Traub, R. D. et al. (1996b). 'Analysis of gamma rhythms in the rat hippocampus in vitro and in vivo.' In: *The Journal of Physiology* 493.2, pp. 471–484. DOI: 10.1113/jphysiol.1996.sp021397.

Traub, R. D. et al. (2000). 'A model of gamma-frequency network oscillations induced in the rat CA3 region by carbachol in vitro'. In: *European Journal of Neuroscience* 12.11, pp. 4093–4106. DOI: 10.1046/j.1460-9568.2000.00300.x.

Traub, R. D. et al. (2001). 'Gap junctions between interneuron dendrites can enhance synchrony of gamma oscillations in distributed networks.' In: *The Journal of neuroscience : the official journal of the Society for Neuroscience* 21.23, pp. 9478–86.

Treisman, Anne (1996). 'The binding problem'. In: *Current Opinion in Neurobiology* 6.2, pp. 171–178. DOI: 10.1016/S0959-4388(96)80070-5.

Tukker, John J et al. (2007). 'Cell Type-Specific Tuning of Hippocampal InterneuronFiring during Gamma Oscillations'. In: 27.31, pp. 1–6. DOI: 10.1523/JNEUROSCI.1685-07.2007.

Tukker, John J et al. (2013). 'Distinct dendritic arborization and in vivo firing patterns of parvalbumin-expressing basket cells in the hippocampal area CA3.' In: *The Journal of neuroscience : the official journal of the Society for Neuroscience* 33.16, pp. 6809–25. DOI: 10.1523/JNEUROSCI.5052-12.2013.

Uhlhaas, Peter J. et al. (2006). 'Neural Synchrony in Brain Disorders: Relevance for Cognitive Dysfunctions and Pathophysiology'. In: *Neuron* 52.1, pp. 155–168. DOI: 10.1016/j.neuron.2006.09.020.

— (2010). 'Abnormal neural oscillations and synchrony in schizophrenia'. In: *Nature Reviews Neuroscience* 11.2, pp. 100–113. DOI: 10.1038/nrn2774.

Urban-Ciecko, Joanna et al. (2016). 'Somatostatin-expressing neurons in cortical networks'. In: *Nature Reviews Neuroscience* 17.7, pp. 401–409. DOI: 10.1038/nrn.2016.53.

Vaidya, Sachin P et al. (2013). 'Temporal synchrony and gamma-to-theta power conversion in the dendrites of CA1 pyramidal neurons'. In: *Nature Neuroscience* 16.12, pp. 1812–1820. DOI: 10.1038/nn.3562.

Veit, Julia et al. (2017). 'Cortical gamma band synchronization through somatostatin interneurons'. In: *Nature Neuroscience* 20.7, pp. 951–959. DOI: 10.1038/nn.4562.

Verret, Laure et al. (2012). 'Inhibitory Interneuron Deficit Links Altered Network Activity and Cognitive Dysfunction in Alzheimer Model'. In: *Cell* 149.3, pp. 708–721. DOI: 10.1016/J.CELL.2012.02.046.

Vinck, Martin et al. (2013). 'Attentional Modulation of Cell-Class-Specific Gamma-Band Synchronization in Awake Monkey Area V4'. In: *Neuron* 80.4, pp. 1077–1089. DOI: 10.1016/j.neuron.2013.08.019.

Vinck, Martin et al. (2016). 'Cell-Type and State-Dependent Synchronization among Rodent Somatosensory, Visual, Perirhinal Cortex, and Hippocampus CA1'. In: *Frontiers in Systems Neuroscience* 9, p. 187. DOI: 10.3389/fnsys.2015.00187.

Viollet, Cécile et al. (2017). 'Somatostatin-IRES-Cre Mice: Between Knockout and Wild-Type?' In: *Frontiers in endocrinology* 8, p. 131. DOI: 10.3389/fendo.2017.00131.

Vyazovskiy, Vladyslav V. et al. (2013). 'Sleep and the single neuron: The role of global slow oscillations in individual cell rest'. In: *Nature Reviews Neuroscience* 14.6, pp. 443–451. DOI: 10.1038/nrn3494.

Wang, X J (2010). 'Neurophysiological and computational principles of cortical rhythms in cognition'. In: *Physiological reviews*, pp. 1195–1268. DOI: 10.1152/physrev.00035.2008..

Wang, X J et al. (1996). 'Gamma oscillation by synaptic inhibition in a hippocampal interneuronal network model.' In: *The Journal of neuroscience : the official journal of the Society for Neuroscience* 16.20, pp. 6402–13. DOI: 10.1523/JNEUROSCI.16-20-06402.1996.

Weber, Franz et al. (2016). 'Circuit-based interrogation of sleep control'. In: *Nature* 538.7623, pp. 51–59. DOI: 10.1038/nature19773.

Whittington, M. A. et al. (1995). 'Synchronized oscillations in interneuron networks driven by metabotropic glutamate receptor activation'. In: *Nature* 373.6515, pp. 612–615. DOI: 10.1038/373612a0.

Whittington, M. A. et al. (2000). 'Inhibition-based rhythms: experimental and mathematical observations on network dynamics'. In: *International Journal of Psychophysiology* 38.3, pp. 315–336. DOI: 10.1016/S0167-8760(00)00173-2.

Whittington, M. A. et al. (2011). 'Multiple origins of the cortical gamma rhythm'. In: *Developmental Neurobiology* 71.1, pp. 92–106. DOI: 10.1002/dneu.20814.

Wierenga, C.J et al. (2003). 'Functional relation between interneuron input and population activity in the rat hippocampal cornu ammonis 1 area'. In: *Neuroscience* 118.4, pp. 1129–1139. DOI: 10.1016/S0306-4522(03)00060-5.

Wilson, Hugh R. et al. (1972). 'Excitatory and Inhibitory Interactions in Localized Populations of Model Neurons'. In: *Biophysical Journal* 12.1, pp. 1–24. DOI: 10.1016/S0006-3495(72)86068-5.

Winson, J (1978). 'Loss of hippocampal theta rhythm results in spatial memory deficit in the rat.' In: *Science (New York, N.Y.)* 201.4351, pp. 160–3. DOI: 10.1126/SCIENCE.663646.

Womelsdorf, Thilo et al. (2006). 'Gamma-band synchronization in visual cortex predicts speed of change detection'. In: *Nature* 439.7077, pp. 733–736. DOI: 10.1038/nature04258.

Womelsdorf, Thilo et al. (2014). 'Dynamic circuit motifs underlying rhythmic gain control, gating and integration'. In: *Nature Neuroscience* 17.8, pp. 1031–1039. DOI: 10.1038/nn.3764.

Womelsdorf, Thilo et al. (2015). 'Long-Range Attention Networks: Circuit Motifs Underlying Endogenously Controlled Stimulus Selection'. In: *Trends in Neurosciences* 38.11, pp. 682–700. DOI: 10.1016/J.TINS.2015.08.009.

Xu, Qing et al. (2004). 'Origins of cortical interneuron subtypes.' In: *The Journal of neuroscience : the official journal of the Society for Neuroscience* 24.11, pp. 2612–22. DOI: 10.1523/JNEUROSCI.5667-03.2004.

Yamamoto, C et al. (1966). 'Electrical activities in thin sections from the mammalian brain maintained in chemically-defined media in vitro.' In: *Journal of neurochemistry* 13.12, pp. 1333–43.

Yamamoto, Jun et al. (2014). 'Successful Execution of Working Memory Linked to Synchronized High-Frequency Gamma Oscillations'. In: *Cell* 157.4, pp. 845–857. DOI: 10.1016/J.CELL.2014.04.009.

Zhang, Li I. et al. (1998). 'A critical window for cooperation and competition among developing retinotectal synapses'. In: *Nature* 395.6697, pp. 37–44. DOI: 10.1038/25665.